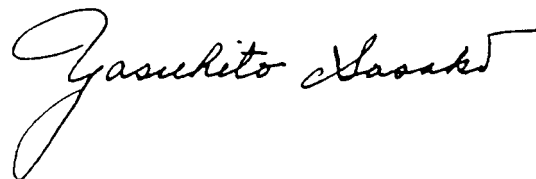# Preface

The fiscal year (FY) 2001 was an epoch-making year for National Institute of Radiological Sciences (NIRS) since NIRS re-started as an independent administrative institution(IAI) this year. This change was a part of administrative reform of Japanese government. we conducted our activities and services in accordance with the middle term (from FY 2001 to 2005) plan and the FY 2001 annual plan that submitted to the Ministry of Education, Culture, Sport, Science and Technology (MEXT) and announced for the public. In parallel we established new standards for evaluation, a high quality technical support system, a strengthened information system, etc. Public relations became more important for NIRS to increase opportunities to communicate with the general public. For this purpose we held open lectures and open exhibitions.

Results of our activities in FY 2001 were reported to MEXT in June, which included financial report. The newly established external evaluation committee will evaluate the results in mid 2002 and announce its opinion to the public.

The whole research activities smoothly progressed in accordance with the middle term plan in spite of partial influences of reorganization and relocation of laboratories on research groups. In addition to 5 major projects, a frontier type research project, 20 fundamental subjects, etc. are being conducted under the middle-term plan. Small scale funds were provided for emerging basic research to encourage young investigators, where new 48 themes were selected by President among 78 applications.

A total of 224 original papers were published and 22 patents were submitted in FY 2001. Based on clinical trials of more than 1,200 patients Heavy Ion Radiotherapy for cancers was applied in April 2002 to Ministry of Health, Welfare and Labor for a license of highly advanced medical procedures.

It is my great pleasure to publish the FY 2001 general report of NIRS activities. I welcome your comments and frank opinions including criticisms. NIRS is determined to make every effort to serve as the center of excellence in the field of radiological sciences in Japan. I sincerely hope your contituing supports and cooperation for NIRS.

Yasuhito Sasaki, M. D., Ph. D.
President

PHYSICS

1. Count Rate Analysis of GSO-DOI PET Scanners

Keishi Kitamura and Hideo Murayama

Keywords: *count rate, Monte Carlo simulation, positron emission tomography (PET), nuclear medicine*

A detector made of thick crystals with a depth-of-interaction (DOI) capability can maintain high spatial resolution while increasing system sensitivity in 3D PET scanners with high geometrical efficiency, that is small detector ring diameter and large axial field of view (FOV). Along with sensitivity and spatial resolution, count rate performance is an important factor to affect the image signal-to-noise ratio in clinical PET studies. High light yield and fast decay time properties of Gd_2SiO_5:Ce (GSO) are suitable for improving energy and time resolution, which result in the decrease in scatter and random coincidences. However, these contributions may be canceled by the dead time losses at detector modules using a large area PS-PMT placed close to the patient. We therefore investigated the count rate properties of GSO-DOI PET scanners with the large PS-PMT using a Monte Carlo simulation and event loss model.

In this work, Monte Carlo simulation programs based upon EGS4 were used to calculate photon interactions in scintillation crystals and phantoms. Photons which have escaped from the phantom were tracked within the scintillator, and their position and energy were recorded if interactions occurred. A pair of photons having the same annihilation tag was counted as a coincidence event, and single events were used to generate random events. Dead-time factors at each stage of the data acquisition system were estimated using a conventional count rate model with the product of paralyzable and non-paralyzable dead time losses for the front-end circuit and non-paralyzable dead time losses for the other circuits. Noise equivalent count rates NECR = $T^2/(T+S+fR)$ were then calculated as a function of activity concentrations, where T, S and R are the total true, scatter and random coincidence rates, respectively, and f is the ratio of the lines of response passing through the object.

The proposed detector unit consisted of four stages of 16 x 16 GSO crystal arrays with a total depth of 30 mm coupled to a 52 mm squire PS-PMT having 16 x 16 multi-anodes. The scanner consisted of 5 ring detector blocks with 24 detectors per ring with a diameter of 38.2 cm and an axial FOV of 25.8 cm. All detector elements were assumed to have the same energy resolution of 20% with a pulse integration time of 250 ns. The outputs of the front-end circuits with an energy window of 400-600 keV were grouped into buckets and presented to the

coincidence processors with a time-window of 6 ns. The relative gains of count rates by processing subset signals of the PS-PMT anodes in parallel with additional front-end electronics were also calculated. The results shown in Fig. 1 predict that the scanner will have higher sensitivity compared to current PET scanners mainly due to the high geometrical efficiency, and higher NECR despite the large size of the detector block. Using the 2x2 subdivision can increase the maximum NECR approximately 20% with a slight loss of sensitivity. However, using the 4x4 subdivision reduces sensitivity substantially because there are many escaping incident gamma rays from one segment to adjacent segments by Compton scattering in the scintillator.
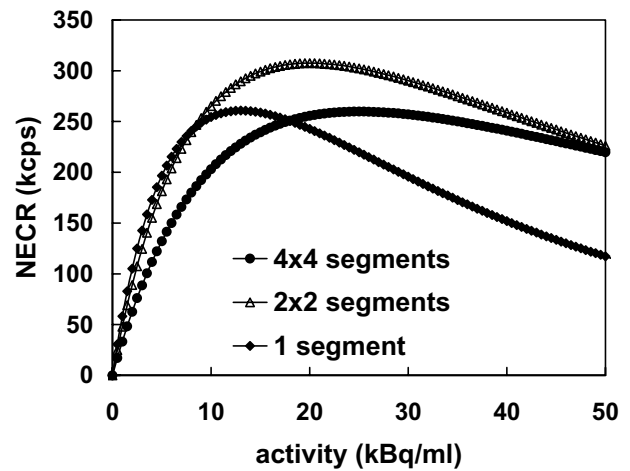

Fig.1.   NECR for the GSO-DOI PET scanner with parallel processing of PS-PMT signals divided by 1 x 1 (without subdivision), 2 x 2, and 4 x 4.

Publications:
1)   Kitamura, K., *et al.*: *KEK Proceedings 2001-11*, pp.108-114, 2001.
2)   Kitamura, K., *et al.*: *2001 IEEE NSS & MIC Conf. Rec.*, M5A-7, 2001.

2. Algebraic 2D PET Image Reconstruction Using Depth-of-Interaction Information

Taiga Yamaya, Takashi Obi*,
Masahiro Yamaguchi*,
Nagaaki Ohyama* and Hideo Murayama
(* Tokyo Institute of Technology)

Keywords: *image reconstruction, depth-of-interaction (DOI), positron emission tomography (PET), nuclear medicine*

Development of a new generation positron emission

tomography (PET) system with depth-of-interaction (DOI) capable detectors is in progress at the National Institute of Radiological Sciences. In current 3-dimensional (3D) PET scanners, the length of the detector crystals is about ten times as long as their width in order to improve detection efficiency. Therefore the PET measurement system exhibits shift-variant characteristics, such as broadened sensitivity functions of each detector pair from center to edge of field-of-view (FOV) and/or from small to large ring differences. However, using DOI information can narrow the broadened sensitivity functions while maintaining system sensitivity.

In this paper, we applied an algebraic image reconstruction method, such as natural pixel decomposition (NPD), to a 2-dimensional (2D) DOI-PET scanner, in order to evaluate the effects of using DOI information on PET image quality. Algebraic reconstruction methods have been successfully used to improve quality of PET images by accurate modeling of the measurement system, while the conventional filtered backprojection (FBP) method is based on an inaccurate system model. The measurement system model for the DOI-PET scanner was defined in consideration of geometrical arrangement and penetration of crystals. At this stage, we supposed that scatter coincidences, random coincidences and attenuation were corrected completely.

We applied NPD to simulated data for a small animal DOI-PET scanner. The scanner had a ring of 144 BGO crystals of 3.8 x 3.8 x 10 mm^3 arranged in 2 DOI layers. For comparison, a non-DOI PET scanner, which had a ring of 144 BGO crystals of 3.8 x 3.8 x 20 mm^3, was also simulated. The detector ring had a diameter of 187 mm, and the FOV had a diameter of 140 mm. Reconstructed images were obtained using NPD and FBP. Two figures of merit (FOMs), background noise and spatial resolution, were used to evaluate the image quality. The spatial resolution was measured as the average of radial and tangential full widths at half maximum (FWHM) of the point spread function at the center, and 20, 40 and 60 mm off center. A warm phantom of 100 mm diameter was used to measure the background noise as the normalized standard deviation (NSD). First the trade-off between the background noise and the spatial resolution was investigated, using NPD with different values of the regularization parameter and FBP with ramp filters of different cut-off frequencies. Plots of radial and tangential resolution at the same background noise levels (NSD=0.09) are shown in Fig. 2. Comparison between NPD and FBP shows the improvement of image quality by using the accurate system model. Also comparison between DOI-PET and non-DOI PET shows the improvement of resolution uniformity by using DOI information.

In summary, the numerical simulation results show

that accurate system modeling improves spatial resolution without noise emphasis, and that DOI information improves uniformity of spatial resolution.
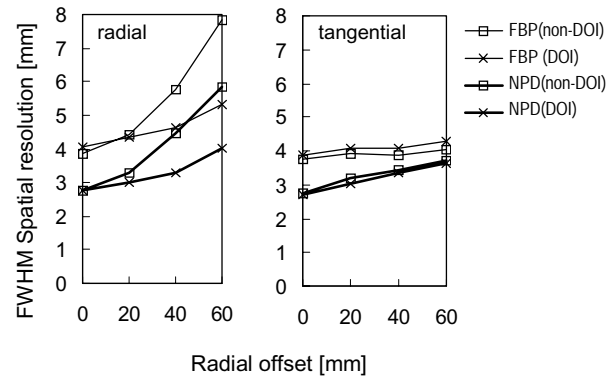

Fig. 2.   FWHM resolution of the point source image using NPD and FBP at the same background noise levels (NSD = 0.09).

3.   A Depth-of-Interaction Detector for PET with GSO Crystals Doped with Different Amounts of Ce

Naoko Inadama,
Hideo Murayama and Hideyuki Kawai

Keywords: *depth-of-interaction detector (DOI), positron emission tomography (PET), pulse shape discrimination, GSO crystal*

As one way to obtain high resolution and high sensitivity in 3D mode acquisition on PET, the concept for a depth-of-interaction (DOI) detector was proposed. In this paper, the new 4-stage DOI detector which was developed from the 3-stage DOI detector reported previously is introduced. Like the previous one, it is composed of one 16-channel (4-by-4 matrix anodes) position-sensitive photomultiplier tube (PS-PMT) and four scintillator blocks. The PS-PMT is optically coupled to the blocks by silicone oil. One block is four stage deep and one stage consists of a 2-by-2 array of rectangular Gd$_2$SiO$_5$ (GSO) crystal elements sized 2.9mm by 2.9mm by 7.5mm. Except for the fourth stage, there is a reflector between elements in the same stage; the fourth stage has an air gap instead. Each block is also wrapped in a reflector and optically isolated. Therefore scintillation light is spread over the block from the site

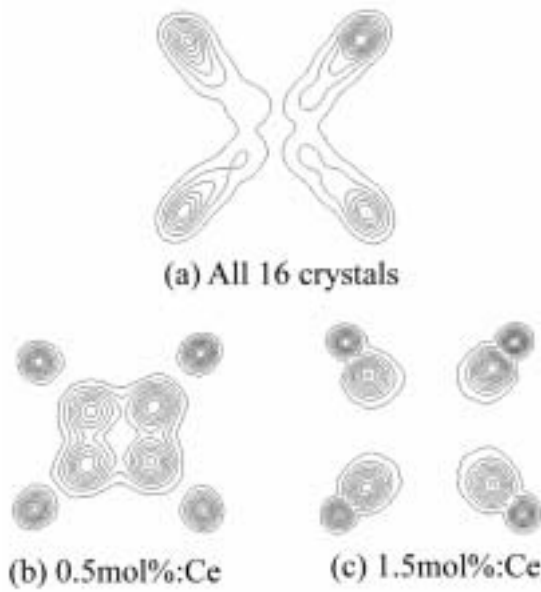(a) All 16 crystals

(b) 0.5mol%:Ce   (c) 1.5mol%:Ce

Fig.3. 2-dimensional positioning image histograms obtained in the uniform irradiation experiment of the 4-stage DOI detector with one block. The upper histogram, (a), represents all crystal data before the selection by pulse shape and height. The lower histograms express data from (b) 0.5mol% GSO crystals and (c) 1.5mol% GSO crystals.

of the interaction through the fourth stage crystals, and it enters the photo cathode of the PS- PMT. Because incident photons have a distribution corresponding to the interaction site, outputs of the four PS-PMT anode signals under the block indicate the crystal of interaction. It is identified on a 2-dimensional positioning image histogram mapped by an Anger-type position arithmetic calculation using the signals.

The 4-stage DOI detector is achieved by using two kinds of GSO crystals doped with different amounts of Ce, 0.5mol% and 1.5mol%. The scintillation decay time constant of 1.5mol% GSO crystal is 35ns and 0.5mol% GSO is 60ns. From pulse shape discrimination, it can be recognized in which kind of crystals the interaction takes place. The Anger-type position arithmetic calculation is applied to anode signals of each event data after classifying them according to the pulse shape discrimination, and two positioning contour image histograms are obtained. Setting these GSO crystal stages alternately as a 4-stage block, the performance of the detector is evaluated by irradiating a gamma ray uniformly from a 0.1mCi ^{137}Cs point source.

Fig. 3 (a) is the positioning image histogram of the measurement for 750k events before pulse shape discrimination and pulse height selection. Conducting pulse shape discrimination and setting windows on the energy spectra of each crystal, we obtain two 2-dimensional histograms as a result (Figs. 3 (b), (c)). The

crystal of interaction can be easily identified in both histograms compared to the histogram without selecting by pulse shape and height. The accuracy of crystal identification with this 4-stage block detector is checked by scanning collimated gamma rays along the detector face. The results show that there is no significant problem for crystal identification by this method.

We conclude that the performance tests verify the 4-stage DOI detector is reliable enough for crystal identification. The detector will be investigated further while changing detector parameters such as crystal surface and size, reflector arrangement, and arrangement of two kinds of crystals in order to realize a large number of reliable detectors for the next generation PET.

4. Improvement of the HIMAC Treatment System with the Layer-Stacking Conformal Irradiation Method

Nobuyuki Kanematsu, Tatsuaki Kanai, Yasuyuki Futami, Ken Yusa and Masahiro Endo

Keywords: *heavy ion radiotherapy, 3D conformal radiotherapy, dynamic multi-leaf collimation, spread-out Bragg peak*

Even though charged particles have ideal characteristics for radiotherapy, the actual particle treatments may not always be perfect in terms of dose distribution. One of the major limitations in the conventional particle therapy, where used is a range-modulation device such as a ridge filter, is that a fixed width of the spread-out Bragg peak (SOBP) has to cover the 3D target volume. Therefore, it is usually inevitable for the fixed SOBP to extend to healthy tissues. The layer-stacking method was proposed to resolve this problem by producing a variable SOBP without requiring a drastic modification of the conventional beam delivery system.

In the layer-stacking method, a target volume is virtually divided into thin layers in the depth direction and those individual layers are treated sequentially with irradiations with a common small SOBP, different beam ranges, and conformal fields. In order to deliver the sequence of irradiations automatically as a dynamic beam for daily clinical practice, the beam-monitor/device-control system was modified and an independent device-monitor/beam-interlock system was added to shut off the beam during the transition times in a sequence and in case of any control failures for safety.

In addition to the range shifter and the multi-leaf collimator, the wobbler magnets are dynamically controlled in order to keep the field uniformity during the delivery. The treatment planning system was also modified to automatically determine the control sequence of the beam. Since the conventional ridge-filter method and the layer-stacking method should flawlessly coexist on the same treatment system, great care was taken for continuity and integrity with the ongoing treatments to provide the clinical-level quality assurance.

The layer-stacking method will be routinely used at NIRS in a complementary manner with the conventional method. Furthermore, it should be a reasonable upgrade option for many other facilities with a conventional particle radiotherapy machine.
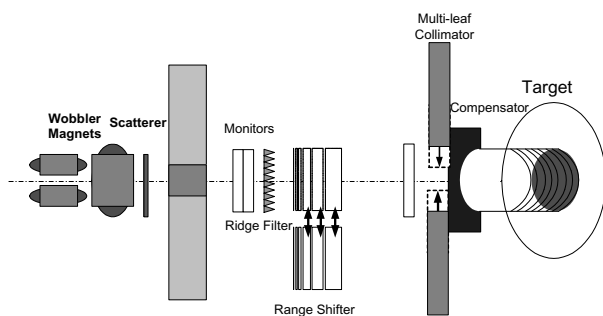

Fig. 4. Principle of the layer-stacking irradiation shown with the relevant devices and a patient: For each layer of the target, the thin ridge filter produces a small SOBP, the range shifter adjusts the beam range, and the multi-leaf collimator defines the field. The wobbling radius is always adjusted to keep the field uniformity. These devices are controled according to the integrated output of the beam monitor to coform a variable SOBP to the target volume (red region).

Publications:
1) Kanai, T., Kawachi, K. , Matsuzawa, H. and Inada, T.: *Med. Phys.*, 10, 344-346 (1983).
2) Futami, Y., Kanai, T., Fujita, M., Tomura, H., Higashi, A., Matsufuji, N., Miyahara, N., Endo, M. and Kawachi, K.: Nucl. *Instrum. Methods A*, 430, 143-153 (1999).
3) Schaffner, B., Kanai, T., Futami, Y., Shimbo, M. and Urakabe, E.: *Med. Phys.*, 27, 716-724 (2000).
4) Kanematsu, N., Endo, M., Futami, Y.,Kanai, T., Asakura, H., Oka, H. and Yusa, K.: to be published in *Med. Phys.*.
5) Kanai ,T., Yusa, K., Kanematsu, N. and Y. Futami: submitted to *Int. J. Radiat. Oncol. Biol. Phys.*.

5. Quantitative Computed Tomography Using Dual-Energy Monochromatic X-rays

Masami Torikoshi, Takanori Tsunoo, Makoto Sasaki, Masahiro Endo, Yutaka Noda, Kentaro Uesugi[1], Maoto Yagi[1] and Kazuyuki Hyodo[2]
([1]Japan Synchrotron Radiation Research Institute, Hyogo, Japan; [2]High Energy Accelerator Research Organization, Tsukuba, Japan)

Keywords: *CT, electron density, synchrotron radiation, monochromatic x-rays*

Monochromatic x-ray computed tomography (CT) at two different energies provides information about electron density of human tissue without ambiguity due to the beam hardening effect. This information makes the treatment planning for heavyion radiotherapy more accurate. We have started a feasibility study on the dual energy x-ray CT by using synchrotron radiation. The first goal of this study was measurement of the electron density with precision of less than one percent. A translate-rotate scanning mode CT system was developed for quantitative measurement in order to clarify what precision in the measurement was achieved in the dual energy x-ray CT.

A photon attenuation coefficient is approximately described by the following equation:

$$\mu(k) = \rho_e \sigma_T Z^4 4\sqrt{2}\alpha^4 \left(\frac{m_e c^2}{k}\right)^{\frac{7}{2}} \phi_0 \sum_{nll'} f_{nl} + \rho_e \left(\Phi_{KN} + \left(1 - Z^{b-1}\right)\frac{Z}{Z'^2}\Phi_{coh}\left(Z',k'\right)\right),$$

where the first term denotes a photoelectric effect, the second term denotes a scattering effect and ρ_e denotes the electron density of an object. Solving simultaneous equations with respect to $\mu(k_1)$ and $\mu(k_2)$ with the aid of an iterative calculation gives an atomic number Z (we call it an effective atomic number) and the electron density ρ_e.

Experiments were carried out at BL20B2 of SPring-8 by using high intensity x-rays of 40 keV and 70 keV that were obtained by monochromatizing synchrotron radiation. The translate-rotate scanning mode CT system consisted of an x-ray detector with a plastic scintillator, a rotating table and a sliding stage. An ionization chamber, upstream from the rotating table, counted the number of the incident photons. The plastic scintillator was connected with a photo-multiplier (Hamamatsu Photonics R3550). The output current of the detector was proved to be proportional to the x-ray intensity from 10^4 ph/s to about 10^9 ph/s. The rotating table on which a sample was set was moved horizontally in a step of 1 mm. Data were taken every step by being exposed to the x-rays for a few hundred ms. At the end of the stroke, the object was rotated by 0.8º. This motion was repeated until the rotation angle became 180º.

Several samples were used: phantoms equivalent to human tissue produced by Kyoto-kagaku Co. (1) soft tissue (SZ207), (2) adipose tissue (SZ49), (3) cartilage bone (SZ160) and (4) compact bone (BE-T), and aqueous solutions of dipotassium hydrophosphate K_2HPO_4. An ellipsoidal vessel with the dimensions of 16 cm × 12 cm filled with water that contained smaller vessels filled with the solutions was used for simulation of a human head.

In order to verify the electron densities measured with the dual energy x-ray CT, (i) we compared them with the theoretical values for the solutions of the head phantom, and (ii) we measured the electron densities of the tissue phantoms by a different method using carbon ions for a second comparison. The carbon ions entered a water column after they penetrated a sample, they have a range in water. The range was measured, both with and without the sample in the front of the water column. The difference of the ranges gave information on the stopping power of the sample for carbon ions. Therefore, the electron density of the sample can be derived from the difference of the range using the Bethe-Bloch formula. The mean excitation energy for water was 75 eV quoted from ICRU 37, and it was used for the tissue phantoms except for BE-T. The mean excitation energy for BE-T was calculated from values listed in the catalogue of Kyoto-kagaku Co. and was 108 eV. In addition, aluminum samples were used to evaluate the precision of this method. Comparison of the aluminum electron density with the theoretical one suggests that the precision of this method is less than 0.5%.

The images of the head phantom reconstructed based on the electron density and the effective atomic number are shown in Figs. 5(a) and 5(b), respectively. There are noticeable differences between these images. The acrylic plastic of the vessel wall has a high electron density, but its effective atomic number is relatively small. This shows that the acrylic plastic has the highest density among materials of the head phantom, and it consists of relatively light elements. The K_2HPO_4 solutions have less electron density than the acrylic plastic but their effective atomic numbers are higher due to the existence of heavier elements such as potassium and phosphate. For the K_2HPO_4 solutions, the average ratio of the difference between the electron density and the theoretical value to the theoretical value is 0.25 %. In the case of the tissue phantoms, the ratio is 0.97 %. The results of the comparison are summarized in Fig. 6.

We conclude that:
(1) the first goal of this study has been almost achieved: electron density measurement with the precision of less than 1 %;
(2) the image of electron density and the image of effective atomic number describe different features of the material.

The information on the electron density and on the effective atomic number of a human tissue may open an avenue for new medical diagnoses.
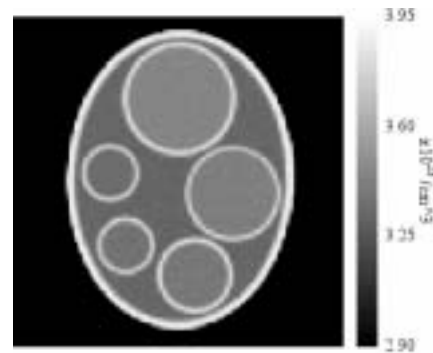

Fig. 5(a). The image of the head phantom based on the electron density. As the color becomes lighter, the electron density becomes higher.
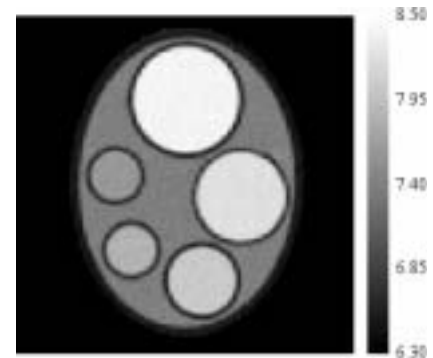

Fig. 5(b). The image of the head phantom based on the effective atomic number. As the color becomes lighter, the atomic number becomes larger.
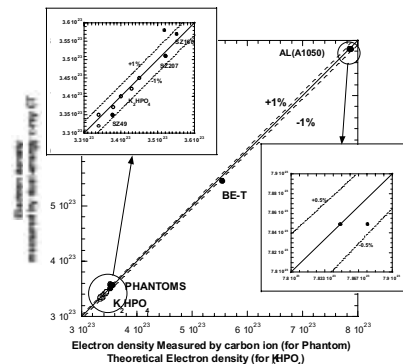

Fig. 6   Comparison of the electron densities with the theoretical values for the K_2HPO_4 solutions and with the values measured in the method of stopping powers for the tissue phantoms.

6. Fast Beam Cut-Off Method in RF-knockout Extraction For Spot Scanning

Takuji Furukawa, Koji Noda, Shinji Shibuya,
Masayuki Muramatsu, Mitsutaka Kanazawa,
Eiichi Takada and Satoru Yamada

Keywords: *RF-knockout slow extraction, synchrotron, heavy ion therapy, dose management, spot scanning*

Beam scanning methods, such as spot and raster scanning, have been developed in order to achieve a high irradiation accuracy, even for an irregular-shaped target. Early studies indicated that to significantly reduce any unwanted dose in these irradiation methods, the time structure of an extracted beam (spill) should have a ripple of less than ±20%, and the response time to beam-off should be less than 1% of the shortest irradiation time of one spot, because the extracted particles after the cut-off signal considerably affect the dose management for irradiation.

At the HIMAC synchrotron, the RF-knockout extraction has utilized a bunched beam to reduce the beam-spill ripple. Therefore, particles near the resonance can be spilled out from the separatrices by the synchrotron oscillation as well as by a transverse RF field. From this viewpoint, a fast beam cut-off method, turning off the transverse and longitudinal RF fields at the same time, has been proposed and verified by both simulations and experiments. The delay from the beam cut-off signal to beam-off has been improved to around 60 μs from 700 μs by turning off only the transverse RF field. Unwanted dose has been considerably reduced by around a factor of 10 compared with that by the usual method.

The delay of 700 μs corresponds to one period of the synchrotron oscillation. In the synchrotron, the delay is limited by the excursion time from the position just outside the separatrix to the extraction channel. The delay of 60 μs, obtained by the new method, is in good agreement with the analytical solution of this excursion time. Therefore, our proposal is one of the best methods to minimize the unwanted dose. The proposed method will play an important role for precise dose management in spot scanning.
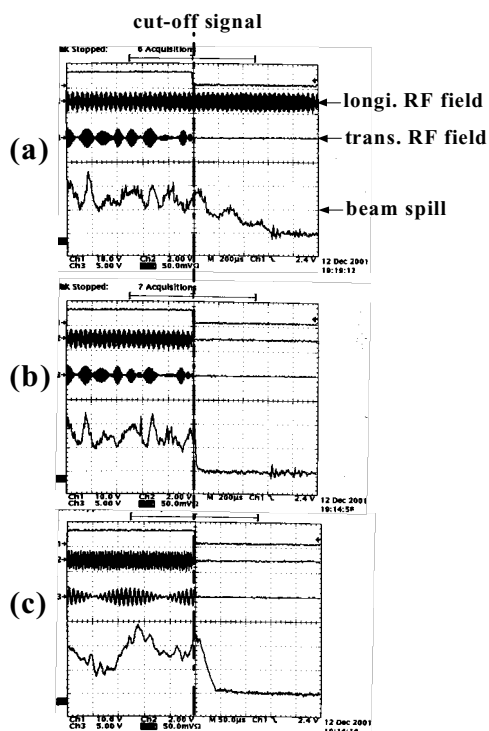
Fig. 7. Typical experimental results. (a) Turning off only the transverse RF field; and (b) in the fast beam cut-off method with a time scale of 200 μs/div. (c) An enlarged view using the fast beam cut-off method with a time scale of 40μs/div.

7. The Scanning Micro-Beam PIXE Analysis Facility at the Electrostatic Accelerator Building

Hitoshi Imaseki, Masae Yukawa,
Takahiro Ishikawa, Frank Watt[1] and Hiroyuki Iso[2]
([1]National University of Singapore; [2]Neos Tech, Chiba)

Keywords: *PIXE, micro-beam scanning, mapping, elemental distribution*

In March 1999, a HVEE Tandetron was installed in the Electrostatic Accelerator Building for PIXE (Particle Induced X-ray Emission) analysis. The specifications of the Tandetron accelerator system operating at NIRS are as follows: The accelerating voltage is 0.4 to 1.7MV, and the maximum beam current is 5 A at 3.4MeV. The accelerator facility incorporates three beam lines for conventional, in-air and microbeam PIXE analysis. The conventional beam line has two types of X-ray detecting devices, Si (Li) and CdZnTe detectors, and elements from Na (Z=11) to U (Z=92) are detectable. Fifteen samples can semi automatically be measured at one time using a proton beam of optical beam size from 0.5 to 2.0 mm at 100 nA beam current. The in-air beam line is used for irradiation of wet sample using a proton beam of optical beam size from 2 mm Φ. The proton beam, thru out of Kapton film, is introduced into a chamber filled with helium gas of 1 atmosphere.

The scanning microbeam PIXE analysis line is based around an Oxford Microbeams OM2000 nuclear microscope endstage. This system provides the ability of multi-elemental mapping over sample areas up to 2× 2mm area with spatial resolutions routinely at 1µm× 1µm. The scheduled operation of this facility started in April 2000. The results of beam resolution tests carried out in 2001 are as follows: For Scanning Transmission Ion Microscopy (STIM), the estimated beam size is 100 x 200 nm, measured using a 2.6 MeV proton beam scanned over a 12.5µm repeat distance copper grid (Fig.8). For Particle Induced X-ray Analysis (PIXE) operation at 50 pA beam current, the estimated best spot size is 0.4 x 0.6 microns (Fig.9). The micro-beam facility apparatus is being used for research into the elemental distribution of small biological samples such as biological cells and tissue.

The operation of this machine is controlled by the Technical Service and Development Section.

Publications:

1) Imaseki, H., Yukawa, M.: *International Journal of PIXE*, **10**[3-4], 77-90, 2001.
2) Imaseki, H., Yukawa, M.: *Tandem kasokuki oyobi sono syuhengijyutu no kenkyukai* (in Japanese), **14**, 105-107, 2001.

8. Development of Very Strong Magnet by New Techniques

Masayuki Kumada

Keywords: permanent magnets, magnetic circuit

The author has been developing a very strong magnet based on a new type of magnetic circuit of permanent magnet material. The strongest magnetic material was invented by Dr. Sagawa of Sumitomo Special Metal(SMMC) many years ago. It was an ingenious material. Although its patent is going to expire this year, no new material has been invented since then. Instead its performance has been improved by the continuing efforts of Dr. Sagawa's successors at SMMC. The permanent magnet has been used to produce a relatively low field magnet in many applications as volume is less. The applications go from hard disk in computers to MRI (Magnetic Resonance Imaging). The weight of MRI magnet is more than one metric ton. The market share of MRI magnets is 1/3 where that of superconducting magnets is 2/3. Electric MRI magnets are almost unused. This is a field which requires extremely high uniformity and stability. Another high tech application is in the filed of synchrotron radiation of light by a high energy electron beam. Permanent magnet wiggler/undulator is an example of this. Main development of this kind of advanced magnet was exploited by Halbach of Laurence Berkley laboratory(LBL). He developed the magnetic circuit of the strongest PM undulator magnet. The strongest undulator magnet was constructed by a Japanese researcher based on Halbach's idea. It was about 3 Tesla and represented a great achievement, as it is stronger that the residual field of a material itself which is about 1.3 Tesla

The author produced a 4.45Tesla dipole filed last year using a permanent magnet which was only possible by a superconducting magnet or pulsed field in collaboration with SSMC http://www.cerncourier.com/main/article/41 /7/5/1 (*CERN Courier* September 2001 p9). This is shown in Figure 8. This is the world's strongest PM magnet ever manufactured. The key point was to use saturated iron as part of the pole and cool it down to -50 degree C. This world record was broken by other researchers this year at ESRF(European Synchrotron
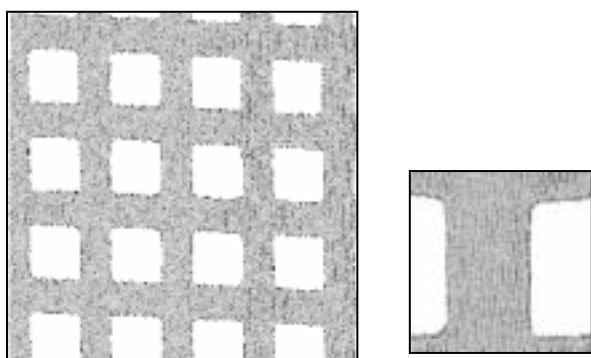

Fig. 8. STIM tests using 2000 lines per inch Cu grid. Proton energy 2.6 MeV protons; scan sizes 50 microns; resolution estimated visually approximately 100 nm (horizontal) and 200 nm (vertical).
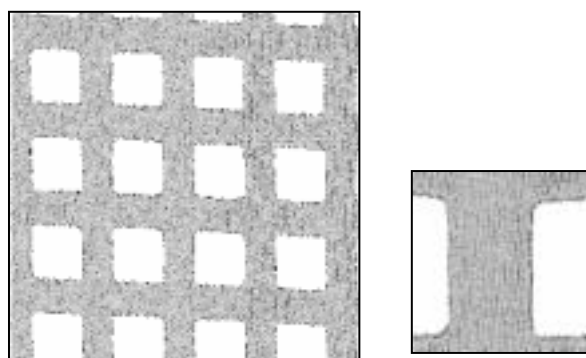

Fig. 9. PIXE scan of 2000 lines per inch mesh gold grid. Proton energy 3 MeV protons; scan size 50 microns; estimated beam size 0.4x0.6 microns.
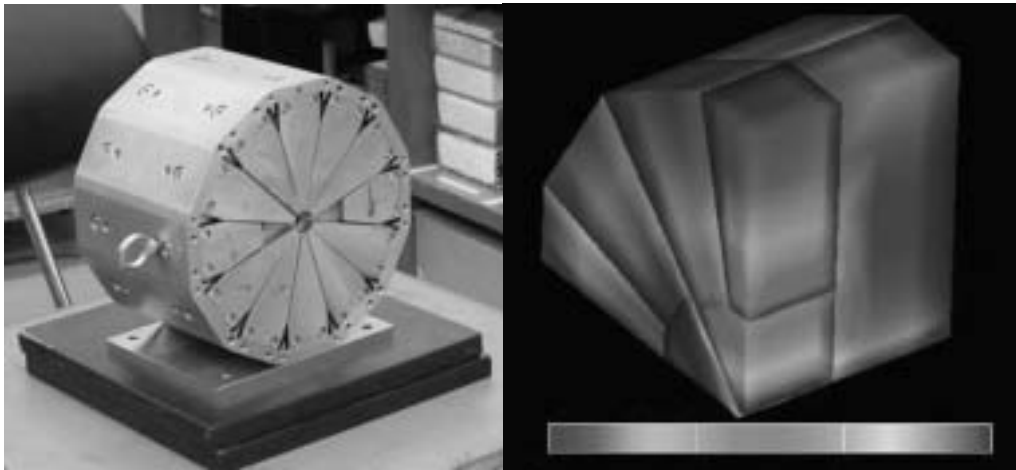
Fig. 10.   Photo of 4 Tesla PM dipole(left) and flux distribution(right)

Radiation Facility) in Grenoble, France(http://cerncourier.com/main/article/42/3/5/1). They generated 5 Tesla in a tiny submicron gap. The author uses a 6 mm gap.

The author has started to invent a variable field magnet, using PM material. It is named MiM, Magnet -in-Magnet, and is a combination of PM magnet and electro magnet. The author made a proof of principle demonstration and manufactured a 3 Tesla variable filed model magnet. There are many variations of this concept. After a successful model experiment, funding was granted from the Japan Science and Technology Corporation(JST) as a 3 years project. The author is collaborating with Prof.Iwashita of Kyoto Univ. for application of a quadrupole magnet system to get a nano-size beam. This is the application for a linear collider for high energy physics in future. Other projects for the MiM or PM cyclotron are going to be started.

many kinds of martial arts as a pair for 40 years performed a remote action in an experiment. They had mainly trained in a martial art that lets a person foresee an attack from an attacker. The experiment was performed in Rooms 201, 202 (central control room) and 203 for Various Simultaneous Measurements in the Multipurpose Facility at NIRS on March 30-31, 2000. In the experiment, the subjects were placed in separate rooms with normal communication deprivation. One of them acted as a sender (male, 58 years old) who was seated in Room 201and the other acted as a receiver (male, 64 years old) who was seated in an electromagnetic shielding cage in Room 203.

The experiment was designed on double blinded and randomized conditions. The start and the end time of the trial was announced automatically to subjects by the multistem stimulator which was in the central control room. Before the experiment, the specific sending time was set by a pseudo random number generation program
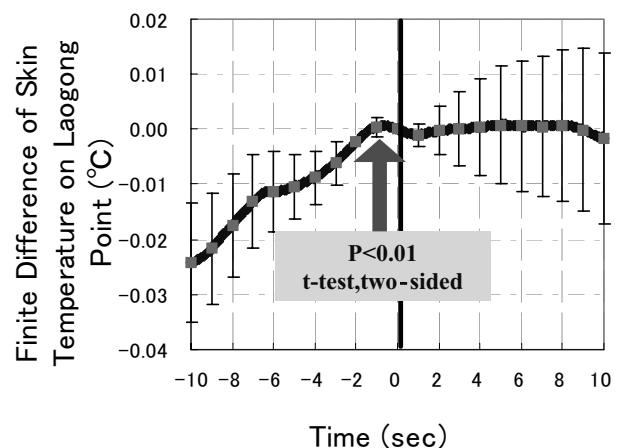
9. Skin Temperature Changes in Remote Action Experiment

Weizhong Chen,
Hideyuki Kokubo, Tomoko Kokado,
Tong Zhang, Suzue Haraguchi,
Mikio Yamamoto and Kimiko Kawano*
(*Nippon Medical School , Tokyo)

Keywords: average skin temperature change, remote action, laogong point, thermistor, hand surface

A series of remote action experiments were performed in sense shielded conditions with paired subjects. One pair has previously shown statistical significant coincidences of the time of their apparent motions.

In this study, two other subjects who had trained in

Fig.11.   Skin temperature changes of receiver's laogong on the left hand before and after transmission (±10.0sec) (22 trials). Error bars show standard errors.

and prepared in a file by someone who did not participate in the experiment. After seeing a light signal to send, the sender attempted to give "remote influence" only once to the receiver in a short time. And as soon as the sender emitted "qi" and the receiver felt it, each pushed an event marker switch.

One trial was 80 seconds and was performed with a 10-second stand-by before the next one. Three continuous trials made one run (260 seconds). A break and feedback of results of the experiment were given between runs, and subjects could talk about how to do better.

Physiological changes of the receiver were measured such as skin surface temperature of the left laogong (middle of the palm), photoplethysmogram (PPG), respiration (Resp), electrodermal activity (EDA), microvibrations (MV) and brain waves (EEG).

The receiver's skin temperature was analyzed to find if there is any change when the sender attempted to give "remote influence" to the receiver. For the period of 10 seconds before and after sending time, the average temperature was analyzed and is shown in Fig.11. It can be seen that the average temperature of 22 trials changes from increasing to constant one second before the sending time. The difference of average temperature between 2 seconds before and after that time is statistically significant and 1% or less.

In conclusion, a significant difference of average temperature change was observed 1 second before the sending time in the period of [±2.0] seconds. It was possible to consider that this was an expression of the characteristics of this martial art that trains foreseeing of a partner's attack sign.

Publications:
1) Yamamoto, M., Hirasawa, M. , Kawano, K. , Yasuda, N. and Furukawa, A.: *J. Intl. Soc. Life Info. Sci.*, 14(1): 97-101, 1996.
2) Yamamoto, M. , Hirasawa, M. , Kawano, K. , Kokubo, H. , Kokado, T. , Hirata, T. , Yasuda, N. , Furukawa, A. and Fukuda, N.: *J. Intl. Soc. Life Info. Sci.*, 14(2): 228-248, 1996.
3) Kokubo, H., Yamamoto, M. , Hirasawa, M. , Kawano, K. , Kokado, T. , Hirata, T. , Yasuda, N. and Furukawa, A.: *Proceedings of 29th Annual Convention of Japanese Society for Parapsychology*, 20-23, 1996 [in Japanese].
4) Yamamoto, M., Hirasawa, M., Kokado, T., Kokubo, H., Yamada, T., Taniguchi, J., Kawano, K. and Fukuda, N.: *J. Intl. Soc. Life Info. Sci.*, 17(1): 191-197, 1999.
5) Kokubo, H., Yamamoto, M., Hirasawa, M., Kawano, K., Kokado, T., Taniguchi, J. and Fukuda, N.: *J. Intl. Soc. Life Info. Sci.*, 18(1): 127-133, 2000.
6) Kawano, K., Yamamoto, M., Kokubo, H., Tanaka, M., Zhang, T., Parkhomtchouk, D. V., Kokado, T., Nakamura, H.   and Soma, T.: *J. Intl. Soc. Life Info. Sci.*, 18(2): 395-399, 2000.
7) Chen, W., Kokubo, H., Nakamura, H., Tanaka, M., Haraguchi S., Zhang T., Kokado T., Yamamoto M., Kawano K. and Souma T.: *J. Intl. Soc. Life Info. Sci.*, 19(1): 179-186, 2001.
8) Yamamoto, M., Kokubo, H., Kokado, T., Haraguchi, S., Tanaka, M., Parkhomtchouk D.V., Soma, T. and Kawano, K.: *J. Intl. Soc. Life Info. Sc.*, 19(2): 437-453, 2001.
9) Chen, W., Kokubo, K., Kokado, T., Zhang, T., Haraguchi, S., Kawano, K. and Yamamoto, M.,: *J. Intl. Soc. Life Info. Sci.*, 19(2): 473-479, 2001.

10. New Gamma-Ray Directional Detectors with Different Types of Scintillators

Yoshiyuki Shirakawa

The tandem detector, which positively increases directional sensitivity to incident gamma rays, mainly consists of two different types of scintillators, a photomultiplier tube and electronic devices such as a preamplifier. In the detector, a cylindrical front scintillator A, the same-sized back scintillator B and a photomultiplier tube fitted with scintillators are combined optically in this order in tandem. Since path length of gamma rays through each scintillator is dependent on incident directions, the probability of photoelectric absorption events occurring in each scintillator will also be changed. Hence the photopeak counts in a spectrum collected by the front scintillator A, and those by the back scintillator B have some relations with the incident direction θ. One indicator to express these relations is proposed here. It is the ratio R which is defined as the quotient, i.e. photopeak counts by B / photopeak counts by A. They are apparently proportional to probability of photoelectric absorption:

R = photopeak counts by B / those by A = P_b / P_f (1)
where Pb and Pf mean the probability of photoelectric absorption in the B scintillator and that in the A scintillator, respectively. We expect that R(θ) has a value in the range between R(0) and R(90), and the value monotonously increases with θ. Here requirements for both scintillators A and B should be considered. The most important characteristic is that scintillation efficiencies of both scintillators are sufficiently apart to distinguish photopeaks completely

for stable counting. Another desired feature is that each scintillator has a high density to detect gamma rays efficiently for a short counting time. From these considerations, it is reasonable to chose a NaI(Tl) scintillator as the front one of A and a BGO scintillator as the back one of B. There tandem detectors were designed and made for experiments. They have 1) the diameter of 50 mm and thickness of 25 mm for the NaI(Tl) scintillator and the BGO scintillator; 2) the diameter of 50 mm and thickness of 50 mm for the NaI(Tl) scintillator and the BGO scintillator; and 3) the diameter of 25 mm and thickness of 50 mm NaI(Tl) scintillator and the BGO scintillator. Using these detectors, we carried out experiments to confirm the measurement principle and to examine the performance. A ^{137}Cs source of 3.7 MBq was selected as representative of gamma ray sources because of its widespread use. Experimental procedure is described with reference to Fig. 12. The source was set 100 cm in front of the detector (θ =0). Gamma rays coming from the source and reaching the detector were counted for 60 seconds and the ratio R was calculated from observation of photopeaks in the spectrum. Then the source was moved in 10-degree intervals towards the side of the detector (θ =90) and the same procedure was repeated. These curves were expressed by

$$R(\theta)=-4.42 \times 10^{-6}\theta^{3}+5.86 \times 10^{-4}\theta^{2}-3.53 \times 10^{-2}\theta+1.620 \tag{2}$$

$$R(\theta)=-4.26 \times 10^{-6}\theta^{3}+3.82 \times 10^{-4}\theta^{2}+2.31 \times 10^{-2}\theta+0.491 \tag{3}$$

$$R(\theta)=-2.70 \times 10^{-6}\theta^{3}+7.20 \times 10^{-4}\theta^{2}+7.20 \times 10^{-2}\theta+0.633 \tag{4}$$

where eq.(2), eq.(3) and eq.(4) were applied for experimental data by the detectors with the 50 mm x 25 mm scintillators, the 50 mm x 50 mm scintillators, and the 25 mm x 50 mm scintillators, respectively. These fitting curves agree well with experimental data points and the curve for the detector with the 25 mm x 50 mm

scintillators is more sensitive to the change of θ than curves for the other detectors. In practical applications, R(θ) is given by calculation using photopeak count data after measurements and then the direction θ, which is an objective parameter, must be solved. From this viewpoint, the third order polynomial is suitable for this application because the equation can be solved analytically and we can regularly obtain the result θ. Characteristics of other parameters, i.e. energies and counts are confirmed to be the same as those by conventional NaI(Tl) and BGO scintillation detectors. Hence the simulations and experiments show that the proposed detectors have a potential for measuring three parameters simultaneously.

Publications:

1) Shirakawa, Y.: *Radioisotopes*, **50** [4], 117-122 (2001).
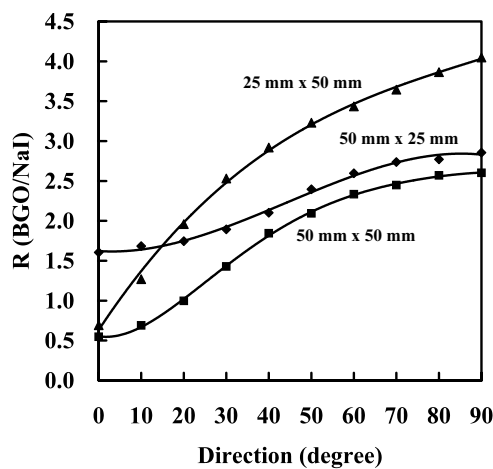2) Shirakawa, Y.: *JASP, Radiation Science*, **26** [4], 67-73 (2001).

Fig. 12. Relations between the indicator R and the incident direction θ.

CHEMISTRY

11. DMPO-mediated Conversion of Singlet Oxygen to Hydroxyl Radical in the Presence of Phenolic Compounds

Jun-ichi Ueda, Keizo Takeshita and Toshihiko Ozawa

Skin is a defensive barrier and constantly exposed to certain kinds of oxidative stress such as ultraviolet and ionizing irradiation. Singlet oxygen ($^1O_2$) is produced through the interaction of the ultraviolet-A component (UVA) of sunlight with endogenous photosensitizers such as porphyrins and flavins in the skin. Since phenolic compounds are widely used for the production of pharmaceuticals as well as cosmetic and food flavoring goods, skin is inevitably exposed to phenolic compounds. Therefore, it is considered that a phenolic compound, which is a potent electron donor, may cause the conversion of $^1O_2$ to another reactive oxygen species. Then, we intend to elucidate whether oxygen radicals are produced from $^1O_2$ in the presence of phenolic compounds.

In this study, $^1O_2$ was generated by the irradiation with UVA-visible light ($\lambda > 330$ nm) of hematoporphyrin (HP), a model compound for endogenous porphyrins in the skin and the assignment of oxygen radicals was performed by the ESR spin-trapping method using a spin trap, 5,5-dimethyl-1-pyrroline *N*-oxide (DMPO). The reaction of $^1O_2$ generated by UVA-visible light ($\lambda > 330$ nm) irradiation of air-saturated solutions of HP with phenolic compounds in the presence of DMPO gave an electron spin resonance (ESR) spectrum characteristic of the DMPO-hydroxyl radical spin adduct (DMPO/·OH). In contrast, the ESR signal of 5,5-dimethyl-2-pyrrolidone-*N*-oxyl (DMPOX), an oxidative product of DMPO, was observed in the absence of phenolic compounds. The ESR signal of DMPO/·OH decreased in the presence of ·OH scavengers, ethanol and sodium formate, and disappeared completely in the presence of sodium azide, a quencher of $^1O_2$, indicating the $^1O_2$-mediated formation of free ·OH during the reaction. A linear correlation between the amounts of DMPO/·OH produced and oxidation potentials of phenolic compounds was observed. When DMPO was replaced with 5-(diethoxyphosphoryl)-5-methyl-1-pyrroline *N*-oxide (DEPMPO), no DEPMPO adduct of oxygen radical species was obtained. These results indicate that $^1O_2$ reacts at first with DMPO, and the resulting DMPO-$^1O_2$ adduct is immediately decomposed/reduced to form ·OH. Phenolic compounds should participate in this reaction as electron donors.

12. Dose- and Time- Dependence of Radiation-Induced Nitric Oxide Formation in Mice as Quantified with Electron Paramagnetic Resonance

Hidehiko Nakagawa, Nobuo Ikota and Toshihiko Ozawa

Nitric oxide (NO) has been shown to be an important messenger molecule in various physiological activities in animals and humans. A large amount of NO is produced in some pathological states such as sepsis, arthritis, and diabetes. There have been studies that indicate that exposing living animals to ionizing radiation caused NO formation in various organs. In cellular systems, ionizing radiation induced NO synthase in the presence of exogenous interferon-gamma. In contrast, exogenous NO has been shown to be radio-protective *in vivo*. The initial response of living systems to radiation exposure is damage in cellular components. In addition to acute damage, ionizing radiation also results in the expression of early phase inflammatory genes, although the mechanism of this gene induction is not understood. The resulting production of inflammatory cytokines is believed to cause the induction of the inducible isoform of NO synthase (iNOS) and NO formation. Free radicals that are produced by ionizing radiation are believed to act as signaling molecules to initiate inflammation. The initial step involving a inflammatory transcription factor such as nuclear factor κB (NF-κB), is followed by the expression of inflammatory cytokines and enzymes.

Although quantitative determination of radiation-induced NO in living systems it important in the evaluation of radiation trauma, is has been hampered by the unstable and elusive nature of the molecule NO. For the measurement of NO level in organs of animal models, the NO trapping method combined with electron paramagnetic resonance (EPR) spectroscopy is unique. This method utilizes the *in vivo* reaction of NO with an administered iron-sulfur cmplex that results in the formation of a stable EPR-active NO-iron complex. This complex is relatively stable in living animals and can be detected by EPR using whole-body EPR spectroscopy. But the sensitivity of the whole-body EPR spectroscopy is limited. Therefore, when the concentration of NO in the tissue is low, an organ section is subjected to *ex vivo* EPR analyses. By using this method, Voevodskaya and Vanin were the first to show that NO is produced in multiple organs in mice after whole-body gamma-ray irradiation. A lipophilic iron complex, iron-diethyl dithiocarbamate (Fe-DETC) was used as a trapping compound and the EPR measurement was made at liquid
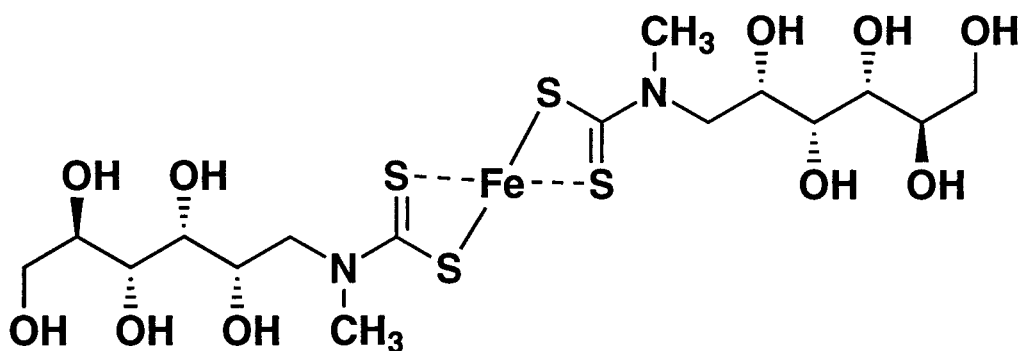
Fig. 13. Structure of Fe-MGD complex as an NO spin trap.

nitrogen temperature. Because the iron-DETC complex is not water soluble, iron and DETC had to be separately administered to the animal by different routes, thus the *in vivo* concentration of the iron-DETC complex was difficult to estimate. In this study, we used a water soluble iron complex of D-N-methyl glucamine dithiocarbamate (Fe-MGD). EPR signals from the trapped NO (NO-iron-MGD complex) were recorded in mouse liver tissue at room temperature, which allowed us to determine the accurate time course of NO formation after irradiation and the dependence of NO levels on the radiation dose. *In vivo* NO formation was quantified in mice after exposure to high-dose whole-body X-ray irradiation, ranging from 0 to 100 Gy. NO produced and accumulated in the livers of irradiated mice was determined. When mice were irradiated with 50 Gy X-rays, NO formation peaked in approximately 3 to 5 h after the irradiation was terminated. A dose-dependence study indicated that NO formation measured 5 h after irradiation leveled off for doses higher than 50 Gy. Administration of NO synthase inhibitor, N(G)-monomethyl L-arginine (L-NMMA) shortly after irradiation completely eliminated the NO signal, indicating that radiation-induced NO is produced through L-arginine-dependent NO synthase pathways. These results suggest that X-ray irradiation initiates inflammation processes, resulting in delayed NO synthase expression and NO formation.

Publication:
Nakagawa, H., Ikota, N., Ozawa, T. and Kotake, Y.: *Nitric Oxide*, **5**, 47-52, 2001.

13. Functional Modification of Cytochrome c by Peroxynitrite in an Electron Transfer Reaction

Hidehiko Nakagawa,
Yukiko Ohshima, Mitsuko Takusagawa,
Nobuo Ikota and Toshihiko Ozawa

Reactive oxygen species (ROS) such as superoxide and reactive nitrogen species such as nitric oxide are suggested to be involved in the pathogenesis of various diseases. Although nitric oxide and superoxide are both endogenous and important compounds for physiological responses, they become toxic and pathogenic when overproduced. Peroxynitrite, which is derived from nitric oxide and superoxide by a diffusion rate-limiting reaction, is one of the toxic intermediates produced under the ROS and RNS overproduction conditions. A typical reaction of peroxynitrite for the biological components is the nitration of protein tyrosine residues. In various diseases associated with oxidative stress, nitrotyrosine formation has been reported, suggesting the involvement of peroxynitrite in the pathogenesis. The effect of the nitration of tyrosine residue in proteins, however, is not clear. In this report, we investigated the effect of tyrosine nitration in cytochrome c on its electron transfer reaction in the mitochondrial energy production. Cytochrome c was treated with a bolus of synthetic peroxynitrite at a sub-millimolar concentration under physiological conditions, and then subjected to reduction by superoxide and oxidation by hydrogen peroxide, that is the redox reaction of cytochrome c. The ability for the membrane potential formation in the mitochondrial respiratory chain was also evaluated. After the treatment with peroxynitrite, it was revealed that the cytochrome c molecule was mono-nitrated mainly at a tyrosine residue, by liquid chromatography-electrospray ionizing mass spectrometry (LC-ESIMS) and HPLC analysis. No obvious changes were observed in the circular dichromism (CD) spectra and the absorption spectra from peroxynitrite-treated cytochrome c. These results suggest that the sub-millimolar peroxynitrite treatment did not obviously affect the cytochrome c molecule except for mono-nitration of the protein. Although the redox capacity of cytochrome c

was not changed by the treatment under the conditions in this study, it was found that the oxidation of ferrocytochrome c to ferricytochrome c by hydrogen peroxide was accelerated depending on the concentration of peroxynitrite used. When cytochrome c was treated with peroxynitrite in the presence of 5-methoxytrypta-mine, a selective inhibitor for the tyrosine nitration by peroxynitrite, the acceleration of hydrogen peroxide-mediated oxidation was suppressed. This result suggests that the tyrosine nitration induced the acceleration of the oxidation mediated by hydrogen peroxide, which is a non-physiological oxidation pathway of cytochrome c. Furthermore, it was also found that the formation of membrane potential in the rat liver mitochondria was suppressed when peroxynitrite-treated cytochrome c was used instead of the intact cytochrome c *in vitro*. From these results, we concluded that the sub-millimolar peroxynitrite treatment induced nitration of cytochrome c at a tyrosine residue, and that the resulting mono-nitrated cytochrome c became more susceptible to oxidation by hydrogen peroxide, concomitantly losing the ability to transfer electrons in the mitochondrial respiratory chain. We would suggest that the peroxynitrite-induced modification of cytochrome c increases the susceptibility to non-physiological oxidants, and may cause dysfunction of mitochondria by suppressing membrane potential.

Publication:
Nakagawa, H., Ohshima, Y., Takusagawa, M., Ikota, N., Takahashi, Y., Shimizu, S. and Ozawa, T.: *Chem. Pharm. Bull.* (Tokyo), **49**, 1547-1554, 2001.
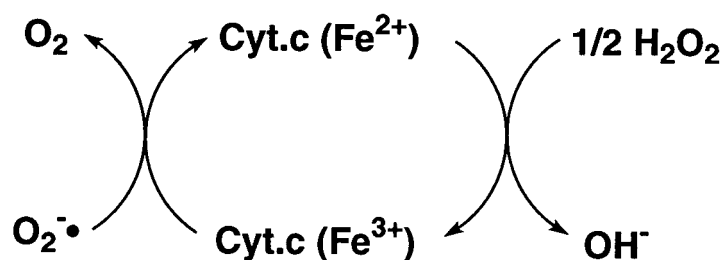
(a)
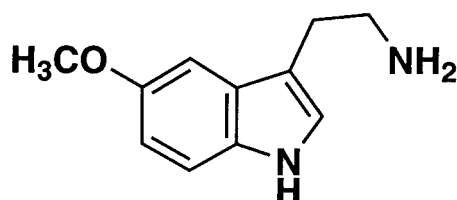
(b)

Fig. 14. (a) The structure of 5-methoxytryptamine (5MT), a nitration-selective inihibitor for peroxynitrite reaction.
(b) The redox reaction scheme for cytochrome c coupling with superoxide and hydrogen peroxide.

BIO-MEDICAL SCIENCES

Biochemistry and Biophysics

14. Enhancement of Early Retrotransposon (ETn) RNA in Myeloid Leukemia Cells from C3H/He Mice

Hiroshi Ishihara and Izumi Tanaka

Keywords: retrotransposon, gene expression, early-transposon, VL30, intracisternal A-particle, DNA-protein binding

Acute myeloid leukemia (AML) cells from C3H/He mice induced by radiation have an active retrovirus-like retrotransposon, the intracisternal A-particle (IAP) element. Examples of an accumulation of IAP RNA and genomic aberration by the IAP-mediated retrotransposition in AML cells were reported previously. Since the function of the retrotransposon is inhibited in normal and most tumor cells, the AML cells may lack mechanisms to repress the retrotransposons. To confirm this possibility, we analyzed the transcription of other mouse retrotransposons, the early retrotransposon (ETn) and virus-like 30S (VL30) particle elements in the AML cells.

All the AML lines from different mice commonly overexpressed the ETn RNA (Fig. 15 (a)). The ETn is known as an inactive transposon since the expression is limited to only early embryonic cells. As with other tumor cells, only faint levels of ETn RNA were detected in the cells from other tumors including hepatoma and lymphoma from C3H mouse. By structural analyses of ETn cDNA clones, it was revealed that the ETn RNA molecules overexpressed in AML cells had complete forms except for a larger variation in the polyadenylation sites at the 3'-end of the molecule.

To determine the nucleotide sequence that contributes to the transcription of ETn, electrophoretic mobility-shift assay using the long-teminal repeat sequence of ETn and the nuclear extract of the AML cells was performed. The target sequence against the nuclear protein was the C-rich nucleotide sequence positioned 30 nucleotides upstream from the transcriptinal start site (Fig. 15 (b)). The C-rich sequence did not have any similarity with previously reported target motifs for enhancers.

Since ETn does not have any open-reading frame, a biological effect due to the overexpression can be ignored in AML cells. However, this finding shows that the cells of all the leukemia lines are activated by a common mechanism that simultaneously transcribes ETn. The activation of this mechanism is probably necessary for the leukemic transformation. Thus the ETn LTR function is useful to study the leukemogenetic process in myloid cells.
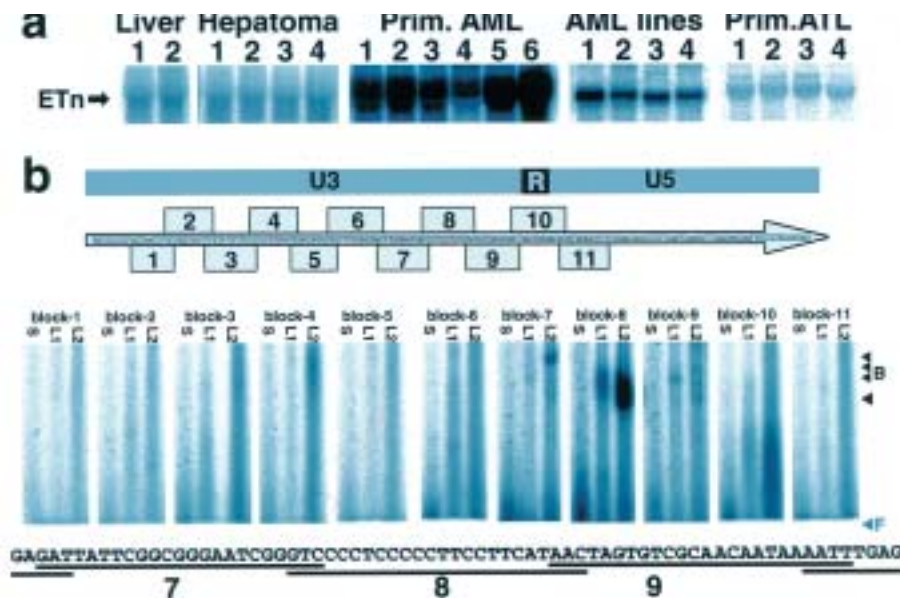
Fig. 15. Overexpression of ETn in AML cells and binding of ETn LTR sequence to nuclear extracts. (a). RNAs from normal liver cell from 2 different mice, 4 lines of primary hepatic tumor cells, 6 lines of primary AML cells, 4 lines of AML strain cells and 4 lines of primary thymyc lymphoma cell were used in northern analysis probing ETn. (b). Mixtures of the end-labeled double-stranded oligonucleotides (block-1 to 11, shown in numbered boxes on both sides of the arrow) corresponding to ETn LTR (arrow) and nuclear extract from spleen (S) or leukemia lines (L1 or L2) were used for the EMSA assay until free DNAs (F) were overrun from the gel. Areas of gels where bands are retarded are shown as (B). Nucleotide sequence that can bind to the nuclear protein (corresponding to block-7 to 9) is indicated at the bottom.

15. *In Vivo* Radioprotection of Stable Free Radical Nitoxides, Carbamoyl- and Methoxycarbonyl-PROXYL against Whole Body X-Ray Irradiation of Mice

Kazunori Anzai, Masako Furuse,
Hiroshi Ishihara and Nobuo Ikota

Keywords: *radioprotection, stable nitroxide radical, X-ray irradiation, mice*

Radiation induced biological damages are thought to be initiated and propagated via free radical reactions. Therefore, antioxidants are possible candidates for the radiation protection agents. Among these antioxidants, stable nitroxide radicals are interesting because they have superoxide dismutase-like activity. In addition, the radiation protection activity of stable nitroxide radicals has been reported. Methoxycarbonyl-PROXYL (MC-PROXYL) is one of the stable nitroxide radicals. It has a unique property; it is moderately lipophilic and blood-brain-barrier permeable. Previously, we have demonstrated the distribution of MC-PROXYL to mouse brain using autoradiography and *in vivo* ESR. In the present study, we examined in vivo radiation protection activity of MC-PROXYL against whole body X-ray irradiation of mice in comparison with carbamoyl-PROXYL, a similar but more hydrophilic stable nitroxide radical.

Mice (C3H, male, 10 weeks old) were placed in a chamber after the *i.p.* administration of MC-PROXYL (450 mg/kg body wt.) and were X-ray irradiated (8.0 Gy, 0.6 Gy/min) at 5 min after the administration of MC-PROXYL. MC-PROXYL increased the survival rate from 0% to 40-50%, showing radiation protection activity. The survival rate was dependent on the timing of the administration and the dose of MC-PROXYL. The condition of *i.p.* administration at 5 min before the X-irradiation and 450 mg/kg body wt. was the best. A higher dose of MC-PROXYL than 450 mg/kg body wt. caused acute toxicity. MC-PROXYL (450 mg/kg body wt.) increased the $LD_{50/30}$ from 6.7 Gy to 8.0 Gy, yielding the dose reduction factor (DRF) of 1.2. This radiation protection activity of MC-PROXYL was larger than that of carbamoyl-PROXYL (DRF = 1.1). The distribution of carbamoyl- and MC-PROXYL to the bone marrow was measured by using ESR. At 5 min after the *i.p.* administration of carbamoyl- or MC-PROXYL, the mice were killed and bone marrow cells were collected from the thigh bones. ESR spectra of the cell suspensions after oxidation by 1 mM $K_3Fe(CN)_6$ showed that the distribution of MC-PROXYL in the bone marrow was similar for MC-PROXYL and carbamoyl-PROXYL. Therefore, the difference in radioprotection was not due to any difference in distribution of the chemicals to the bone marrow. A combined administration of MC-

PROXYL with heat-killed *Lactobacillus casei* preparation (LBC) further increased the radiation protection activity. Since the concentration of LBC used in this experiment was in the range showing saturation effect, this finding suggested that the radio-protection mechanism of MC-PROXYL was different from that of LBC.

16. Hydroxyl Radical Formation Mediated by Spin Trapping Agent, DMPO, in Uroporphyrin Photodynamic Reaction in the Presence of Biological Reductants

Keizo Takeshita,
Chiho Nishizawa*, Jun-ichi Ueda,
Kazuo T. Suzuki* and Toshihiko Ozawa
(* Graduate School of Medical and Pharmaceutical
Sciences, Chiba University)

Keywords: *hydroxyl radical, singlet oxygen, spin trapping, DMPO, DEPMPO*

The photodynamic reaction has been actively used for the treatment of malignant disease (photodynamic therapy, PDT). The oxidation of biomaterials caused by reactive oxygen species (ROS) is believed to be one of the potent mechanisms of PDT. The spin trapping/ESR technique with 5,5-dimethyl-1-pyrroline N-oxide (DMPO) has been commonly used to detect oxygen radicals. However, the reaction of DMPO in photosensitization has not been characterized enough. We observed that the presence of reducing agents such as NADPH, glutathione and Trolox (a water-soluble tocopherol derivative) remarkably increased the ESR signal of hydroxyl radical (·OH) adduct of DMPO (DMPO/·OH) in the uroporphyrin photosensitizing reaction with visible light. The inhibition experiments with ROS scavengers indicated that the formation of DMPO/·OH results from singlet oxygen ($^1O_2$)-mediated generation of free ·OH. When DMPO was replaced with 5-(diethoxyphosphoryl)-5-methyl-1-pyrroline N-oxide (DEPMPO), neither NADPH, gluthathione nor Trolox increased the ESR signal of ·OH adduct of DEPMPO (DEPMPO/·OH). However, the addition of DMPO to the reaction mixture together with DEPMPO remarkably increased the signal of DEPMPO/·OH regardless of the presence of the reducing agents, accompanying a distinct DMPO/·OH signal only in the presence of the reducing agents. The production of ·OH was also determined with hydroxylation of salicylic acid. The presence of DMPO increased the amount of 2,3-dihydrobenzoic acid (a product of ·OH reaction with salicylic acid). The increase in the presence of the reducing agent was

almost the same as that in the absence of the reducing agent. These results indicated that the $^1O_2$-mediated $\cdot OH$ formation occurs DMPO-dependently to form DMPO/$\cdot OH$ regardless of the presence of the reducing agents, and that the DMPO/$\cdot OH$ declines in the absence of reducing agent.

17. Acute Induction of Heme Oxygenase-1 in Rat Liver by a Whole-body X-ray Irradiation

Keiko Suzuki, Masahiko Mori,
Fumihiko Kugawa* and Hiroshi Ishihara
(*Nihon Univ.)

Keywords: *heme oxygenase, X-rays, liver*

The transcription of the heme oxygenase-1 (HO-1) gene is enhanced by various stimuli, such as oxidative stress, UVA radiation and heat shock, and a considerable body of evidence has confirmed that the HO-1 gene is cytoprotective against numerous stresses. The HO-1 gene is also commonly called Hsp (heat shock protein) 32. In mammals, biliverdin, which is one of the products of an enzyme reaction by heme oxygenase, is subsequently converted to bilirubin by biliverdin reductase. Both biliverdin and bilirubin are powerful antioxidants. Another product of the enzyme reaction by heme oxygenase is carbon monoxide, which is considered to be a promising and significant messenger molecule in the soluble guanylate cyclase (sGC)-cGMP system.

No immediate early effect of radiation upon the induction of HO-1 enzyme has been characterized, yet. Now, in the present study we have provided evidence that the heme oxygenase-1 enzyme is induced by ionizing radiation in rat liver within a few hours.

When male Wistar MS strain rats (8 weeks) received


Fig. 16.   * P < 0.02

whole-body X-ray irradiation of 17.0 Gy, the activity of heme oxygenase in the liver was significantly enhanced (2.5 times) 7 h later (Fig.16). Western blotting of the irradiated liver demonstrated a significant increase in the level of HO-1 protein. The level increased 2 h after the irradiation, reached a peak at 4 h, and then decreased gradually until 10 h, when it was still higher than the control level. Thus, X-rays were confirmed to be stressors that induce acute HO-1 expression transiently in the liver.

18. Involvement of Protein Kinase C in Radiation-Induced Apoptosis Signaling Pathways in Murine Thymic Lymphoma Cells (3SBH5 Cells)

Tetsuo Nakajima, Osami Yukawa,
Chihiro Azuma*, Harumi Ohyama,
Bing Wang, Shuji Kojima*,
Isamu Hayata and Hiroko Hama-Inaba
(*Science University of Tokyo)

Keywords: *murine thymic lymphoma, protein kinase C, apoptosis, radiosensitivity, Raf-1*

Radiation-induced apoptosis is known to be important for understanding the mechanism of radiosensitivity. It is widely accepted that protein kinase C (PKC) participates in the regulation of radiation-induced apoptosis. However, the PKC function remains obscure in the mechanism of radiosensitivity. Using 3SBH5 cells, one of the radiation sensitive murine thymic lymphoma cells were used to assess involvement of PKC in radiation-induced apoptosis regulation. 3SBH5 cells are quite sensitive to X-rays and undergo apoptosis shortly after X-ray-irradiation. PMA (phorbol 12-myristate 13-acetate), an activator of PKC, blocked the radiation-induced apoptosis in 3SBH5 cells. In contrast, chelerythrine, a PKC inhibitor, enhanced the radiation-induced apoptosis, as did Gö6976, a classical PKC (cPKC) specific inhibitor, for irradiation with 0.5Gy. These results imply that cPKC contributes to the balance between cell survival and death through radiation-induced activation of cPKC. Furthermore, irradiation alone had no effect on the distribution of PKC subtypes in 3SBH5 cells. This suggests that the radiation-induced cPKC activation is not caused by translocation of PKC molecules. On the other hand, although it was demonstrated that cPKC is associated with an anti-Raf-1 antibody-recognized protein in 3SBH5 cells, Raf1 Kinase Inhibitor I, one of the Raf1 kinase inhibitors, had no effect on the radiation-induced apoptosis. The anti-apoptotic function of cPKC in the radiation-induced
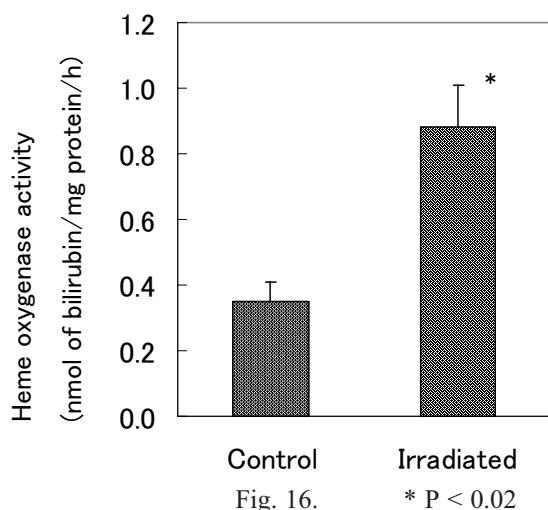
apoptosis is under investigation by exploring cPKC-associated proteins. This function of cPKC may offer a clue to understanding radiosensitivity and radiation-induced adaptive response.

19. Difference among Heavy Ion Beams in Cell Killing and Mutation Induction

Yoshiya Furusawa, Tatsuaki Kanai,
Naoyuki Shigematsu[1], Noriko Ihara[1],
Tetsuya Kawata[1], Osamu Kawaguchi[1],
Atsuya Takeda[1], Ryoichi Ishibashi[1],
Shoji Kutsuki[1], Atsushi Kubo[1],
Koichi Isobe[2], Takashi Uno[2] and Hisao Ito[2]
([1]Keio Univ.; [2]Chiba Univ.)

In this study, human cancer cell lines were used to attempt to clarify the radiobiological effects of heavy ion beams on carbon beam radiotherapy. Killing efficiency was determined by the usual colony forming method, and mutation was observed as the induction of 6-thioguanine resistant colony. Cells were irradiated by HIMAC carbon ion beams with LET value at 20 or 80 keV/μm, or neon ion beams at 80 keV/μm. Carbon beams of 80 keV/μm had an enhanced cytotoxic effect compared with those of 20 keV/μm. The carbon beams of 80 keV/μm showed almost the same efficiency in cell killing compared with neon beams even though they had the same LET value. Efficiencies of induction of mutation for all heavy ion beams tested were significantly higher than that for X-rays for all cell lines used. The efficiency for 80 keV/μm carbon beams was higher than that for 20 keV/μm beams. The efficiency was, however, lower for neon ion beams then carbon beams at 80 keV/μm, even though they had the same LET value. Split dose irradiation of carbon beams showed no effect on cell killing but the mutation efficiency was lowered. Neon beams might be more appropriate for cancer therapy with heavy ion beams, and the fractionated dose might be appropriate to reduce the mutation frequency in heavy ion radiotherapy.

Publication:
Shigematsu, N., Ihara, N., Kawata, T., Kawaguchi, O., Takeda, A., Ishibashi, R., Kutsuki, S., Kubo, A., Kanai, T., Furusawa Y., Isobe, K., Uno, T., and Ito, H.: *Int. J. Mol. Med.* **7**, 509-513, 2001.

20. Medium-Mediated Bystander Effects on HSG Cells Co-Cultivated with Carbon Beam-Irradiated Cells

Yoshiya Furusawa, Chunlin Shao and Mizuho Aoki

The mechanisms of medium-mediated bystander effects on cell survival and micronucleus (MN) induction were investigated by co-cultivating unirradiated HSG cells with cells irradiated by X-rays or 290 MeV/u carbon beams. It was found that the survival of the irradiated cells exponentially decreased along with the dose, and that the plating efficiency (PE) of the unirradiated recipient cells was clearly more enhanced than that of the control cells. Moreover, MN was induced in the unirradiated recipient cells and its yield had a maximum distribution corresponding to the donor dose, which was different from the linear-quadratic dose response of the yield of MN in the irradiated cells. The treatment of PTIO, a scavenger of nitric oxide (NO), decreased both PE and MN of the unirradiated recipient cells to control levels. Moreover, nitrite was detected in the co-culture medium, and its concentration was related to the donor dose. These results indicated that NO was involved in the above mentioned medium-mediated bystander effects. In addition, an equation was deduced which well fit the induction of MN of the unirradiated recipient cells.

Publication:
Shao, C., Aoki, M. and Furusawa, Y.: *J. Radiat. Res.* **42**, 305-316, 2001.

Cell Biology

21. Expression, Subcellular Localization and Chromosome Localization of Hamster Ku70 and Ku80

Manabu Koike, Asato Kuroiwa*, Yoichi Matsuda* and Aki Koike.
(*Hokkaido Univ.)

Keywords: Ku70, Ku80, hamster, mapping, GFP

Ku, a heterodimer of Ku70 and Ku80, plays a key role in multiple nuclear processes, e.g. DNA repair, chromosome maintenance, and transcription regulation. To understand the fundamental characteristics of Ku proteins, we examined the electrophoretic mobility, subcellular localization and expression of hamster Ku70 and Ku80 and determined the chromosome locations of their genes. When transfected into hamster cells, exogenous Ku70 and Ku80 tagged with green fluorescent protein (GFP) accumulated in the nucleus, indicating that both Ku proteins can localize in the nucleus of hamster cells. The electrophoretic mobility of hamster Ku proteins is different from that of human Ku proteins. No significant changes in the quantity of Ku proteins were observed in CHO-K1 cells treated with 10 Gy of ionizing radiation, suggesting that both proteins are expressed constitutively in amounts adequate to repair DNA DSBs. The chromosome locations of the Ku genes were determined by direct R-banding fluorescence in situ hybridization. The Ku70 gene was localized to Syrian hamster chromosome 4qa4.1 →qa4.2 and Chinese hamster chromosome 2p3.1, and the Ku80 gene was localized to Syrian hamster chromosome 4qb5 →qb6.1 and Chinese hamster chromosome 2p3.5 →p3.6. These results provide clues to the biological functions of Ku, as well as useful information for constructing comparative chromosome maps between hamsters and other mammalian species, including human, mouse, and rat.

Publications:
1) Koike, M., Kuroiwa, A., Koike, A., Shiomi, T., and Matsuda, Y. : Cytogenetics and Cell Genetics. 93, 52-56, 2001.
2) Koike, M., Shiomi, T., and Koike, A.: J. Biol. Chem. 276, 11167-11173, 2001.

22. Endothelins Control the Proliferation and Differentiation of Murine Melanocytes from UVB-induced Pigmented Spots

Tomohisa Hirobe

Keywords: melanocyte, keratinocyte, UVB, proliferation, differentiation

Long-term exposure to ultraviolet radiation B (UVB) is known to induce pigmented spots in the dorsal skin of hairless mice. By using a serum-free culture medium supplemented with dibutyryl adenosine 3':5'-cyclic monophosphate and basic fibroblast growth factor, it has been shown that the proliferation of epidermal melanoblasts and melanocytes from UVB-induced pigmented spots is greatly stimulated, and the stimulation is regulated by keratinocytes rather than melanocytes. In this study, we tried to understand what factors derived from keratinocytes were involved in regulating the proliferation and differentiation of epidermal melanoblasts and melanocytes from UVB-induced pigmented spots. For the purpose, antibodies towards growth factors and cytokines were added to the serum-free culture medium in the presence of keratinocytes. Results showed that antibodies towards endothelin (ET)-1, ET-2 and ET-3 inhibited the proliferation and differentiation of cultured epidermal melanoblasts/melanocytes from UVB-induced pigmented spots of hairless mice, but not from non-irradiated mice. In contrast, antibodies towards hepatocyte growth factor and leukemia growth factor failed to affect the proliferation and differentiation of cultured epidermal melanoblasts/melanocytes from both control and irradiated mice. These results suggest that ETs are keratinocyte-derived factors which are involved in regulating the proliferation and differentiation of epidermal melanoblasts/melanocytes from UVB-induced pigmented spots in the dorsal skin of hairless mice.

Publication:
Hirobe, T.: *J. Invest. Dermatol. Symp. Proc.*, **6**, 25-31, 2001.

23. Effect of Nitric Oxide on Sertoli Cell Tight Junction-Associated Proteins

Makoto Onoda, Takanori Katsube and Hiroshi Inano

Keywords: Sertoli cell, nitric oxide, tight junction, occludin, ZO-1, cortactin, NOC18

Nitric oxide (NO) is an important biological molecule with a wide variety of functions. NO appears to be present in all parts of the male reproductive system and to play diverse roles in testicular, epididymal and vas deferent functions. We, therefore, undertook clarification of the effects of NO on the Sertoli cells (SC) tight junction (TJ)-associated proteins by using a culture
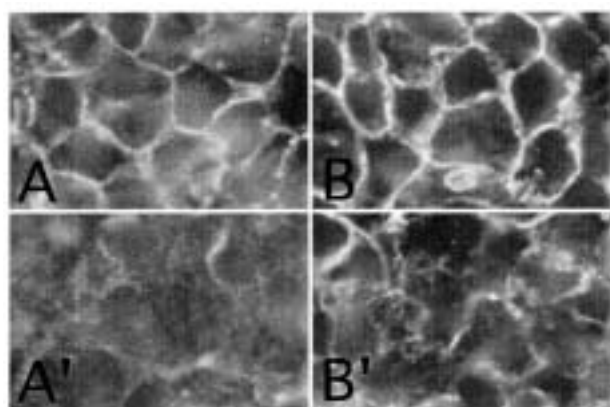
Fig. 17. Immunocytochemistry of tight junction-associated proteins in cultured rat Sertoli cells. Sertoli cells (1.5×10^6 cells/well) were isolated and cultured on Matrigel coated-cover glass in serum free defined medium with (A' and B') or without (A and B) NOC18 (400 μM). Sertoli cells were subjected to immunocytochemistry with specific antibodies. A and A': Cultures stained with anti-occludin antiserum, B and B': Cultures stained with anti-ZO-1 antiserum.

Fig. 18. Effect of NOC18 on the expression of occludin in rat Sertoli cells. Sertoli cell -lysates (15 μg/lane) were loaded onto SDS-PAGE mini-gel system, and immunoblotting with a specific antibody was carried out. Values presented at the bottom of lanes are percentage of non-treated control. Std: standard rainbow marker proteins, (1): serum free defined medium alone, (2): with 200 μM NOC 18, (3): with 400 μM NOC 18.

system.

SC were isolated from 16-day-old immature rat testes by a three-step sequential enzyme digestion procedure, and cultured on 15-mm round glass cover slides coated with reconstituted extracellular matrix (Matrigel) in the well of a 24-multiwell plate. The cultures were maintained in serum free defined medium throughout the experimental period. 2,2'-(Hydroxynitrosohydrazino) bis-ethanamine (NOC 18), a NO donor, was added to the cultures, and the distribution and expression of the TJ-associated proteins, such as occludin, ZO-1 and actin cytoskeleton, were determined by immunocytochemistry and Western blot analysis, respectively, with specific antibodies. Cortactin (p80/85), a prominent substrate for Src protein tyrosine kinase, was also examined.

The amount of NO produced by SC in culture was 3.4 ±1.4 nmol/ml and 7.3 ± 0.9 nmol/ml for 24 hr- and 48 hr-incubation periods, respectively. This suggests that SC produce NO spontaneously under the culture condition, although the amount is relatively minute. On the other hand, the exogenously released NO from an NO donor into the medium was 147.8 ± 2.7 nmol/ml and 333.9 ±10.1 nmol/ml in the cultures with 200 μM and 400 μM of NOC 18, respectively, in a 24 hr-culture period. These values are in agreement with the theoretical values based on the half-life time (21 hr) of NOC 18. Immunostaining for occludin, ZO-1 and cortactin in untreated-SC showed continuous labeling around the cell periphery in the region of the cell-cel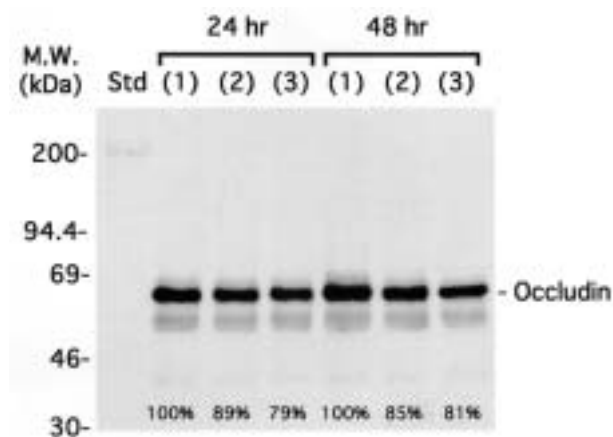l junctional complex, and these colocalized with TJ-associated F-actin filaments. However, incubation with NOC 18 (200 μM and 400 μM) caused complete disorganization of occludin staining and partial disruption of ZO-1 staining within 48 hr (Fig. 17), while, alteration in the immunolabeling pattern for cortactin and F-actin was inconclusive in NOC 18 treated SC. Furthermore, Western blotting of occludin, ZO-1 and cortactin exhibited descending expressions of these TJ-associated proteins in a dose-dependent manner of NOC 18 in the NO donor treated SC (Fig. 18). These results suggest that excessive production of NO within testis during acute or chronic pathophysiological conditions disrupts TJ-associated proteins of SC and that NO may perturb blood-testis barrier formation and then, in turn, the regulation of normal spermatogenesis.

24. Chemically Induced Premature Chromosome Condensation in Human Fibroblast Cell Lines: Fundamental Study for Applications to the Biodosimetry of Local Exposure

Reiko Kanda, Yoko Yamagishi,
Hiromi Ohuchi, Kiyomi Eguchi-Kasai,
Hiromi Itsukaichi, Masahiko Mori and Isamu Hayata

Keywords: *cell cycle, human fibroblasts, premature*

chromosome condensation (PCC), phosphatase inhibitors, X-rays

The premature chromosome condensation (PCC) of human peripheral lymphocytes treated with inhibitors of protein phosphatase has been demonstrated to be an excellent tool for the estimation of high dose whole-body exposure. To develop a new biodosimetry for local exposure, the cytogenetical reaction of human fibroblast lines to PCC inducers was examined and compared with that of lymphocytes.

The efficiency of the induction by calyculin A was greater than that by okadaic acid in both lymphocytes and fibroblasts. Calyculin A induced PCC in 5 Gy-irradiated and unirradiated samples at almost the same frequency in the lymphocytes, whereas the efficacy was considerably lower in irradiated fibroblasts than unirradiated ones.   Calcium ionophore enhanced the induction of PCC in irradiated fibroblasts, although PCC frequencies were still much lower than those in the lymphocytes.

Fig. 19(a) shows the time-course of the induction of PCC when fibroblasts were irradiated, cultured and treated with calcium ionophore and calyculin A. The proliferative cycle of 2 Gy-irradiated fibroblasts seemed to be synchronous so that a wave of PCC reactions was evident. However, no synchrony was observed in 5 and 10 Gy-irradiated samples, presumably due to a difference in the fractions of the cells in cycling states after exposure. The frequency of ring chromosomes observed in 2 and 5 Gy-irradiated fibroblasts was too low to be used as a marker for cytogenetic dosimetry, but that of excess fragments, scored as the observed chromosome number minus 46, might be substituted.

The frequency of excess fragments for 2, 5 and 10 Gy-irradiated fibroblasts was less than 0.75, about 1 and a few per cell, respectively, although these values changed with the culture period (Fig. 19(b)).   As for cultured fibroblasts, the frequencies of PCC and excess fragments for the period of Day 2 to Day 5 could give a very rough estimation of exposed doses *in vitro.*

To apply PCC techniques to fibroblasts for cytogenetic dosimetry, there are two major problems: First the *in vitro* cell cycle of fibroblasts is more difficult to control than that of lymphocytes. This may be solved by the analysis of PCC in a non-cycling phase but preliminary attempts have not been successful. Second, human fibroblasts are refractory to PCC induction by calyculin A compared with tumor cell lines. On the other hand, our PCC method has an advantage for cytogenetic analysis of fibroblasts: in the process of PCC induction, okadaic acid and calyculin A detached cells from culture plates as well, and the trypsin treatment was skipped.   The trypsin treatment is necessary for conventional cytogenetic analysis of adhesive cells, although it affects cell membranes so to make chromosome preparation difficult.

Publication:
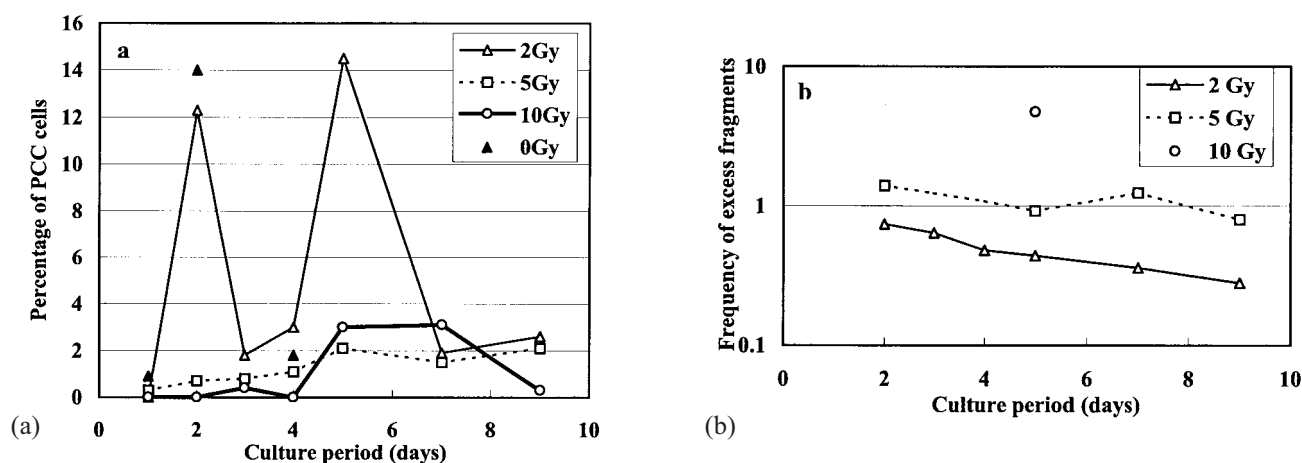Kanda, R., Eguchi-Kasai, K., Itsukaichi, H., Mori, M. and Hayata, I.: *Somat. Cell Mol. Genet*. (in press)

Fig. 19: Time-course of the PCC induction in hTERT-BJ1 human fibroblasts. After fibroblasts in the confluent phase were irradiated at 0 (▲), 2 (△), 5 (□) and 10 Gy (○) and held at 37℃ for 3 hours, they were trypsinized, plated and cultured for 1-9 days. At 5 hours and 30 minutes before harvesting, 1 M A23187 and 250 nM calyculin A were added to the cultures, respectively. (a) The percentage of cells having prematurely condensed chromosomes (PCC cells). (b) The frequency of excess fragments per cell, scored as the observed chromosome number minus 46.

25. Targeted Disruption of *Np95* Gene Renders Murine ES Cells Hypersensitive to DNA Damaging Agents and DNA Replication Blocks

Masahiro Muto,
Yasuyoshi Kanari[1], Eiko Kubo,
Tamami Takabe, Takayuki Kurihara[2],
Akira Fujimori and Kouichi Tatsumi
([1]Kinki Univ. School of Medicine;
[2]Medical Research Institute,
Kanazawa Medical Univ.)

Keywords: *X-rays, UV, MNNG, SCE, cell cycle, hydroxyurea, replication fork*

NP95, which contains a ubiquitin-like domain, a cyclin A/E-Cdk2 phosphorylation site, Rb binding motif and ring finger domain, has been shown to be colocalized as foci with PCNA in early and mid-S phase nuclei. We established *Np95* nulligous ES cells by replacing the exons 2-7 of the *Np95* gene with a neo cassette and by selecting out a spontaneously occurring homologous chromosome crossing-over with a higher concentration of neomycin. *Np95*-null cells were more sensitive to X-rays, ultraviolet light (UV), N-methyl-N"-nitro-N-nitrosoguanidine (MNNG) and hydroxyurea (HU) than ES wild type (*Np95*+/+) or heterozygously inactivated (*Np95*+/-) cells. Expression of transfected *Np95* cDNA in *Np95*-null cells restored the resistance to X-rays, UV, MNNG or HU concurrently to a level similar to that of *Np95*+/- cells, though slightly below that of wild type (*Np95*+/+) cells. These findings suggested that NP95 played a role in the repair process for DNA damages incurred by these agents. The frequency of spontaneous sister chromatid exchange was significantly higher for *Np95*-null cells than for *Np95*+/+ cells or *Np95*+/- cells (P < 0.001). We inferred that NP95 functioned as a common component in the multiple response pathways against DNA damages and replication arrest and thereby contributed to the genomic stability.

Publications:
1) Muto, M., Kanari, Y., Kubo, E., Takabe, T., Kurihara, T., Fujimori, A., and Tatsumi, K.: *J. Biol. Chem.*(*in press.* Published online June 25, 2002., 10.1074/jbc.M205189200).
2) Miura, M., Watanabe, H., Sasaki, T., Tatsumi, K.,Muto, M.: *Exp Cell Res.*, 263, 202-208, 2001.
3) Uemura, T., Kubo, E., Kanari, Y., Ikemura, T., Tatsumi, K., Muto, M.: *Cell Struct. Funct.*, 25, 149-159, 2000.
4) Fujimori, A., Matsuda, Y., Takemoto, Y., Hashi-moto, Y., Kubo, E., Araki, R., Fukumura, R., Mita, K., Tatsumi, K., Muto, M.: *Mamm. Genome*, 9, 1032-1035, 1998.

26. Significance of Fractionated Irradiation for the Biological Therapeutic Gain of Carbon Ions

Koichi Ando, Sachiko Koike, Akiko Uzawa,
Nobuhiko Takai, Takeshi Fukawa,
Yoshiya Furusawa, Mizuho Aoki,
Chisa Oohira, Manami Monobe,
Ryonfa Lee, Masao Suzuki and Kumie Nojima

Keywords: *relative biological effectiveness, mouse, tumor, skin*

It is well established that the RBE (relative biological effectiveness) for cell killing depends on LET (linear energy transfer), and that a maximum RBE is observed at ~150 keV/μm. However, the therapeutic gain depends on the ratio of the RBEs for the effects on the cancer cell population and the effects on normal tissues. The RBE of a given radiation quality depends on LET but also on dose, biological system and effect, and irradiation conditions. There are no data available to answer the question: which LET is suitable to improve the biological therapeutic gain of carbon ions? Here, we selected 3 different LET values of 290 MeV/u carbon ions, and compared the relative biological effectiveness between tumor growth retardation and skin damage using a murine transplantable tumor. Larger RBE values for tumors than the skin type were obtained when carbon ions of intermediate LET were delivered daily for 2 through 5 fractions (Fig. 20). The biological therapeutic gain would be high for the carbon ion SOBP when the number of fractions has been correctly selected in clinical trials.

Publication:
1) Koike, S., Ando, K., Uzawa, A., Takai, N., Fukawa, T., Furusawa, Y., Oohira, C., Aoki, M., Lee, R., Suzuki M. and Nojima, K. *Radiation Protection Dosimetry* **99**, 405-408, 2002.
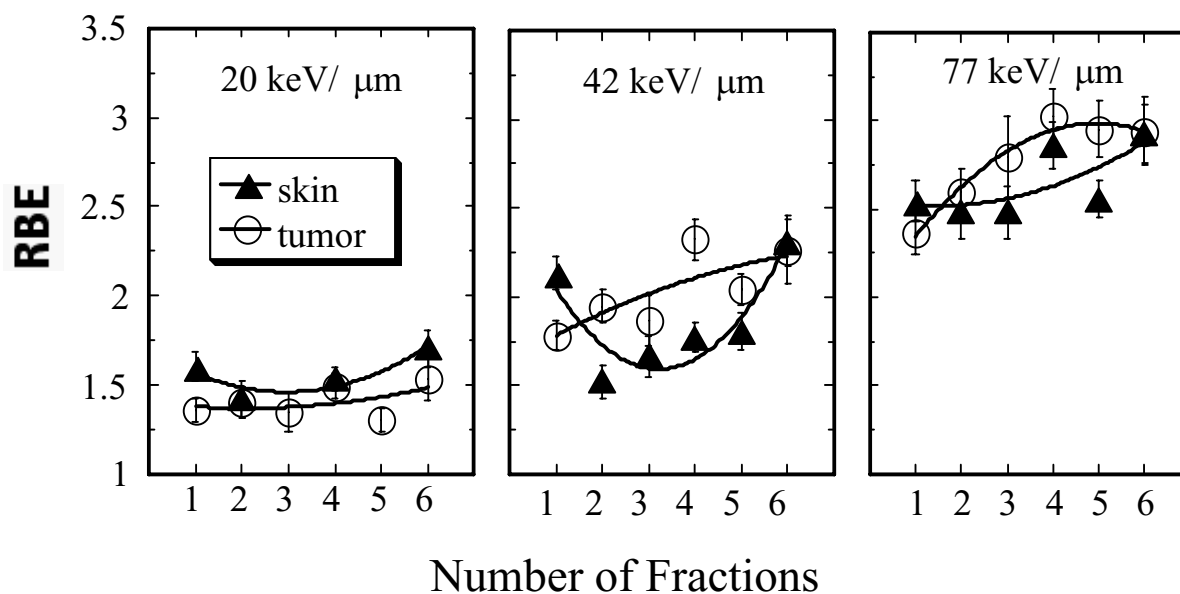
Fig. 20. RBE values of carbon ions for tumors and skin.   The RBE value is calculated by comparing the isoeffect dose
of carbon ions with that of   rays for the corresponding number of fractions.   The open circles and closed trian-
gles represent tumors and skin, respectively.

27. Time-Course of Reoxygenation in Experimental Murine Tumors after Carbon-Beam and X-Ray Irradiation

Sachiko Koike, Kumie Nojima,
Yoshiya Furusawa, Koichi Ando,
Natsuo Oya[1], Keisuke Sasai[1],
Toru Shibata[1], Takehisa Takagi[1],
Keiko Shibuya[1] and Masahiro Hiraoka[1]
([1]Kyoto Univ.)

Keywords: high-LET radiation, reoxygenation, SCCVII, EMT6

We compared the tumor reoxyge nation patterns in three different murine tumor cell lines after X-ray irradiation with those after carbon beam irradiation using the heavy ion medical accelerator (HIMAC) system. The tumors of the cell lines SCCVII, SCCVII-variant-1 and EMT6 on the hind legs of mice received local priming irradiation with a carbon beam (8 Gy, 73 keV/ μm in LET, 290 MeV/u, 6 cm SOBP) or X-rays (13 Gy, 250 kVp). After various intervals, the mice were given whole-body test irradiation (16 Gy, 250 kVp X-rays) either in air or after they were killed. The hypoxic fractions were estimated as the proportions of the surviving fractions of the tumors in killed mice to those in air-breathing mice. In the SCCVII tumors, the hypoxic fractions at 0.5 h were 50% and 21% (p < 0.05) after the priming X-ray irradiation and carbon beam irradiation, respectively. In   the   SCCVII-variant-1

tumors, the hypoxic fractions were 85% and 82% at 0.5 h, 84% and 20% at 12 h (p < 0.01), and 21% and 31% at 24 h after X-ray irradiation and after carbon beam irradiation, respectively. In the EMT6 tumors, the reoxygenation patterns after X-irradiation and carbon beam irradiation were similar. We concluded that the reoxygenation pattern differed among the three tumor cell lines, and that reoxygenation tended to occur more rapidly after carbon beam irradiation than after X-ray irradiation for SCCVII and SCCVII-variant-1 tumors.

Publication:
Oya, N., Sasai, K., Shibata, T., Takagi, T., Shibuya, K., Koike, S,. Nojima, K., Furusawa, Y., Ando, K., and Hiraoka, M.: *J. Radiat. Res*. **42**, 131-141, 2001.

28. Chromatid Breaks Induced in Normal Human Cells by Heavy Ions at Initial, Metaphase and Interphase States

Yoshiya Furusawa, Tetsuya Kawata[12],
Kerry George[2], Durante Marco[3],
Honglu Wu[2], Veronica Willingham[2],
Hisao Ito[1] and Francis A. Cucinotta[2]
([1]Chiba Univ.; [2]Johnson Space Center, NASA;
[3]Univ. Fedellico II)

Keywords: chromosome aberrations, high-LET radiations, initial breaks, cell-cycle, PCC-FISH

To investigate initial chromatid breaks and how cell-cycle delays in human cells affect the expression of complex chromosome damage in metaphase following high- and low-LET radiations, we irradiated whole blood or exponentially growing human fibroblast cells AG1522 *in vitro* with a low and a high dose of iron, neon, carbon, and silicon particles or γ-rays. Lymphocytes were cultured and meta-phase cells were collected at different time points after 48-84 h in culture. Interphase chromosomes were prematurely condensed using calyculin-A, either 48 or 72 h after exposure to iron particles or γ-rays. Cells in the first division were analyzed using a combination of FISH whole-chromo-some painting and DAPI/Hoechst 33258 harlequin staining. Chromosomes of AG1522 cells were prematurely condensed using calyculin-A. Initial chromatid-type and isochromatid breaks in G2 cells were scored.

The dose-response for total chromatid breaks was linear regardless of radiation type. The relative biological effectiveness (RBE) increased with LET, and showed a maximum at 55-80 keV/μm, then decreased at higher LET. Induction of isochromatid-type breaks was linear to dose for high-LET radiations, but linear-quadratic for γ-rays or 13 keV/μm carbon beams. The RBE for the induction of isochromatid breaks obtained from linear components increased rapidly between 13 keV/μm and 80 keV/μm carbon beams and decreased gradually for higher LET beams. High-LET radiations were more effective in induction of isochromatid breaks, while low-LET radiations were more effective in induction of chromatid-type breaks. The densely ionizing track structures of high-LET radiation and the geometry of sister chromatids in G2 cells resulted in an increase in isochromatid breaks.

The delay of chromosome damage expression in metaphase was LET- and dose-dependant. This delay was mostly related to the late emergence of complex-type damage into metaphase. Yields of damage in PCC collected 48 h after irradiation with iron particles were similar to that obtained from cells undergoing mitosis after prolonged incubation. The yield of high-LET radiation-induced complex chromosome damage could be underestimated when analyzing metaphase cells collected at one time point after irradiation. Chemically induced PCC method might be a more accurate technique, because the problems with complicated cell-cycle delays would be avoided.

Publications:
1)   George, K., Wu, H., Willingham, V., Furusawa, Y., Kawata, T. and Cucinotta F. A.: *Int. J. Radiat. Biol*. **77**, 175-183, 2001.
2)   Kawata, T., Durante, M., Furusawa, Y., George, K., Takai, N., Wu, H. and Cucinotta F.A.: *Int. J. Radiat. Biol*. **77**, 165-174, 2001.
3)   Kawata, T., Durante, M., Furusawa, Y., George, K., Ito, H., Wu, H and Cucinotta F. A.: *Radiat. Res*. 156, 598-602, 2001.

29. Hsp25 Regulates the Expression of p21 [Waf1/Cip1/Sdi1] through Multiple Mechanisms

Park Sang-Hee, Toshiyasu Hirama,
Naoyuki Anzai, Yoshiko Kawase,
Misao Hachiya, Hisayoshi Kondo,
Saori Kawamura, Yasunari Takada,
Daisaku Takai and Makoto Akashi

Exposure of cells to external stresses leads to the induction or activation of certain proteins. Expression of heat shock proteins (Hsps) is induced in response to these stresses. Hsps are known to have molecular chaperone activities; but recent studies have shown that Hsps have a variety of functions such as triggering proliferation, differentiation, and apoptosis of cells. Previously, we found that overexpression of a 25 kDa Hsp (Hsp25) induced the expression of the cell cycle inhibitory protein p21 (WAF1/Cip1/Sdi1) in murine fibroblastoid L929 cells. However, the mechanisms for the induction of p21 by Hsp25 are unknown. In the present study, we have investigated the mechanisms of the regulation of p21 expression by Hsp25 in these cells. The introduction of Hsp25 cDNA stimulated the accumulation of p21 transcripts through transcriptional but not posttranscriptional regulation in these cells. We also found that overexpression of Hsp25 markedly increased the translational rate of p21 and stabilized the protein. Studies using proteasome inhibitors and Western blot analysis for ubiquitination of p21 have demon-strated that the stabilization of p21 is regulated through a ubiquitin-independent pathway. However, no direct association of Hsp25 with p21 was observed. These findings suggest that Hsp25 induces p21 expression through multiple mechanisms and that transcriptional, translational, and post-translational regulations are important in the regulation of p21.

Immunology and Hematology

30. Analysis of the Receiver's EEG in Remote Perception Task

Tong Zhang, Mikio Yamamoto,
Hideyuki Kokubo, Kimiko Kawano*,
Masataka Tanaka and Tomoko Kokado
(* Nippon Medical School)

Keywords: *EEG, alpha activity, theta activity, frontal lobes, mental concentration, martial arts*

In the present experiment, two experienced practitioners of a Japanese martial art were subjects. One acted as a sender while the other acted as a receiver. They were put in separate rooms with communication deprivation to perform a task of "remote action and perception". One run was made up of three successive 80-second trials during which only one 'sending' was performed in double-blinded and randomized conditions. Both physiological changes of the sender and the receiver were measured during the experiment. In this paper, changes of the mean power of α and θ waves of the receiver during a period of 10 seconds around the sending time were analyzed at a 1-second interval.

Compared with values of the resting state (analysis 1), statistically significant decreases of θ activity were found in C_4 and T_6 areas, while statistically significant increases of the α wave were found in Fp_1, Fp_2 and T_5 areas ($p<0.05$). However when compared to values during the period of non-sending (analysis 2), statistically significant changes ($p<0.05$) of α wave were found in T_5, T_6, O_1 and O_2 areas (Fig .21).

In analysis 1 when compared with the resting state, a significant increase of the α wave in the frontal area and a decrease of θ activity in the sensory-motor areas suggest the receiver is in a mental state of concentration on the task. However, the increase of α activity in T_5 area before sending time shown in analysis 2, and the decrease of α activity in occipital areas and α activity

and θ activity in T_6 area after sending time shown in analysis 1 and analysis 2 suggest the possibility of physiological changes related to the action of the sender or perception of the action of sending.

The analyses in this study are based on part of a series of experiments with the same subjects. Not only more sensitive analyzing methods and more data, but also comparison with ordinary people doing the same task is essential to confirm the possibility of "remote action and perception" in further studies. Meanwhile, physiological and psychological differences before and after receiving time also need to be analyzed.

Publications:
1) Zhang, T., Yamamoto, M., Kokubo, H., Kawano, K., Tanaka, M., and Kokado, T.: *J. Intl. Soc. Life Info. Sci.*, **20 (1)**: 458-465, 2001.
2) Yamamoto, M., Kokubo, H., Kokado, T., Haraguchi, S., Zhang, T., Tanaka, M., Park-homtchouk, DV., Soma, T., and Kawano, K.: *J. Intl. Soc. Life Info. Sci.*, **19 (2)**: 437-452, 2001.
3) Kawano, K., Yamamoto, M., Kokubo, H., Tanaka, M., Zhang, T., Kokado, T., and Soma, T.: *J. Intl. Soc. Life Info. Sci.*, **20 (1)**: 453-457, 2001.
4) Tanaka, M., Yamamoto, M., Kokubo, H., Kokado, T., Zhang, T., Tanaka, M., Parkhomtchouk, DV., Kawano, K., and Soma, T.: *J. Intl. Soc. Life Info. Sci.*, **20 (1)**: 466-473, 2001.
5) Chen, W., Kokubo, H., Kokado, T., Zhang, T., Haraguchi, S., Kawano, K., and Yamamoto, M.: *J. Intl. Soc. Life Info. Sci.*, **20 (1)**: 473-479, 2001.
6) Kokubo, H., Yamamoto, M., Yamada, K., Kawano, K., Soma, T., Tanaka, M., Zhang, T., and Fukuda, N.: *J. Intl. Soc. Life Info. Sci.*, **20(1)**: 480-487, 2001.

31. Age-Related Changes in Bone Mineral Density, Cross-Sectional Area and Strength at Different Skeletal Sites in Male Rats

Haruzo Iida and Satoshi Fukuda

Keywords: *age change, bone mineral density, male rat, peak bone mass, peripheral quantitative computed tomography (pQCT)*

Age-related changes in bone mineral density (BMD), cross-sectional area and strength strain index (SSI) of the long bones in the limbs and first lumbar vertebra of male Wistar rats were measured by peripheral quantitative computed tomography (pQCT). One hundred and ten rats aged 2-30 months were used. The results indicate that the total (cortical + trabecular), cortical and trabecular BMD values of the metaphysis and cortical
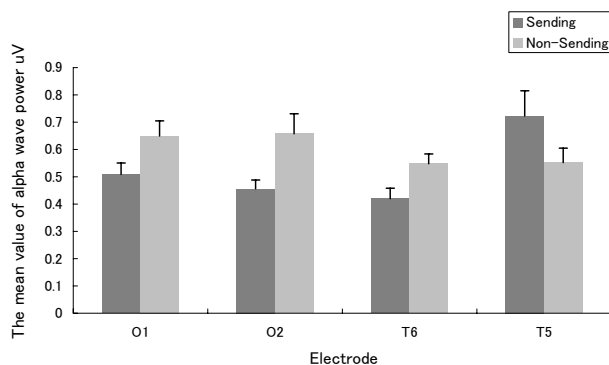

Fig.21. Results of alpha wave power analysis 2.
S: sending period ; NS: non-sending period Welch-test, two-tailed, p<0.05

BMD values of the diaphysis in the long bones varied
for each bone and differed from those of the first lumbar
vertebra. The total BMD of long bones showed high
values at 6-21 months and then decreased, but these did
not always coincide with cortical and trabecular BMD.
The values of SSI in the long bones varied. The values
of total and cortical BMD and SSI of lumbar vertebra
increased for 6-12 months and then decreased, but the
trabecular BMD increased after 12 months. The total
area in both the long bones and the first lumbar vertebra
increased with the decrease in cortical area and the
increase in the trabecular area with increasing age. It was
concluded that age-related changes in bones, similar to
those observed in humans, could be observed in some
bones and parameters, although the age in rats when the
so-called peak bone mass appears in the whole skeleton
could not be clearly determined.

Pathology and Physiology

32. Reduced Sensitivity and ras Mutation Spectrum of N-Ethyl-N-Nitrosourea-Induced Thymic Lymphomas in Adult C.B-17 *Scid* Mice

Mayumi Nishimura, Shizuko Kakinuma, Shigeharu Wakana, Aya Mukaigawara, Kazuei Mita, Toshihiko Sado, Toshiaki Ogiu and Yoshiya Shimada

Keywords: *K-ras, ENU, thymic lymphoma, scid mouse*

Scid mice are defective in their ability to repair DNA double strand breaks and, as a consequence, their cells are radiosensitive. Further, they have been shown to be prone to develop thymic lymphomas (TL) after small doses of ionizing radiation. Little is known, however, about the role of *scid* mutation in chemical carcinogenesis. To determine if scid mutation increased predisposition to chemical carcinogenesis, we examined both the susceptibility of *scid* mice to *N*-ethyl-*N*-nitrosourea (ENU)-induced lymphomagenesis and the involvement of *ras* gene activation. Adult female mice at 8 weeks of age were given ENU (400ppm) in their drinking water for 2-10 weeks. Contrary to expectations, we observed a two to three-fold reduction in TL development in the scid mice. The highest incidence was achieved by ENU treatment for 8 weeks for *scid* and wild-type C.B-17 mice, of 42 and 85%, respectively (P<0.05). We investigated whether this was attributable to the usage of the *ras* mutation pathway. There was, however, no significant difference in the frequency and spectrum of K-*ras* mutation between the *scid* and wild-type C.B-17 mice. Most of the K-*ras* mutations were either GGT to GAT transition in codon 12 (11/23: 48%) or CAA to CCA transversion in codon 61 (8/23: 35%) which were independent of *scid* background. The incidence of N-*ras* mutation was very low. These results indicate that *scid* mice are less susceptible to ENU-induced lymphomagenesis and *ras* gene mutation frequently occurs in both *scid* and wild-type C.B-17 mice.

33. Characteristic Association between K-ras Gene Mutation with Loss of Heterozygosity in X-ray-Induced Thymic Lymphomas of the B6C3F1 Mouse

Yoshiya Shimada, Mayumi Nishimura, Shizuko Kakinuma, Takeshi Takeuchi, Toshiaki Ogiu, Gen Suzuki, Yukiko Nakata, Shun-ichi Sasanuma, kazuei Mita and Toshihiko Sado

Keywords: *T-cell lymphoma, LOH, K-ras*

PURPOSE: To elucidate the characteristics of radiation carcinogenesis, the spectra of K- and N-*ras* oncogene mutations, loss of heterozygosity (LOH) and their association in X-ray-induced thymic lymphomas (TL) were determined by comparing with those of *N*-ethyl-*N*-nitrosourea (ENU)-induced and spontaneously occurring TL.
MATERIALS AND METHODS: TL that arose in untreated, X-ray-irradiated and ENU-treated B6C3F1 mice were examined both for K- and N-*ras* mutations by PCR-SSCP and DNA sequencing and for LOH by PCR with polymorphic microsatellite markers.
RESULTS: (1) *ras* gene mutations were found in some TL from X-ray-exposed (approximately 20%) and ENU-treated (30-40%) mice while no *ras* gene mutations were found in spontaneous TL. N-*ras* mutations were rare. (2) The spectrum of *ras* gene mutations was diverse and seemed to differ a little between X-ray-induced and ENU-induced TL, even though there was a higher frequency of *ras* mutations in ENU-induced TL that clustered to K-*ras* codon 12. (3) The X-ray-induced TL showing K-*ras* mutation were associated with LOH on chromosome 6, while those showing no K-*ras* mutation were associated with high frequency of LOH on chromosomes 4, 11 and 12.
CONCLUSION: These results demonstrate that, in the B6C3F1mouse TL, X-ray-induced lymphomagenesis showed both co-expression, with low occurrence of allelic imbalance on chromosome 6 and K-*ras* mutation, and exclusive expression of frequent allelic imbalance on chromosomes 4, 11 and 12 and K-*ras* mutation.

34. Incidence of Pyometra in Colony-raised Beagle Dogs

Satoshi Fukuda

Keywords: *beagle dogs, clinical findings, pyometra*

Incidence of pyometra observed in our colony-raised beagle dogs over a 12-year period is described. Pyometra was observed in 25 female dogs aged over 4 years, and was frequent at 8-11 years, with the average age of onset 9.36±0.38 years (Fig. 22). The incidence of the disease was 15.2 % for female dogs (n=165) more than 4 years old. Clinical findings useful in the diagnosis of this disease included an excretion of pus from the cervix, rapid increase in leukocyte count, and enlarged uterus as revealed by radiography. The relationships of delivery, and estrus cycles to this disease are discussed.
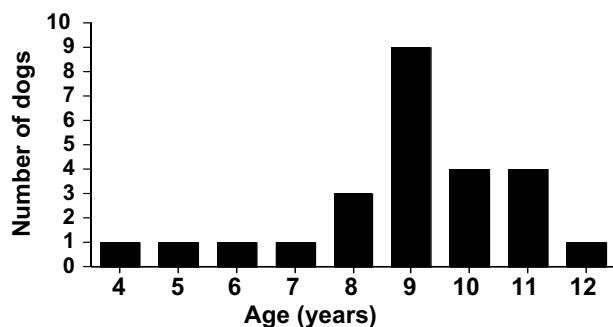
Fig. 22. Age distribution and incidence of pyometra observed in 25 female beagle dogs.

Ovariohysterectomy or uterectomy was the only effective treatment for this disease. In conclusion, the results indicated that pyometra might be an age-related disease because it occurred particularly in aged dogs.

35. Production of Virus-Specific Antiserum Corresponding to Sequences in the Lactate Dehydrogenase-Elevating Virus ORF6 Protein

Hiromi Takahashi-Omoe,
Satoru Matsushita and Akihiro Kawano

The *Arteriviridae* are enveloped positive-stranded RNA viruses comprised of a variety of animal pathogens including lactate dehydrogenase-elevating virus (LDV), equine arteritis virus (EAV), simian hemorrhagic fever virus (SHFV), and porcine reproductive and respiratory syndrome virus (PRRSV). The ability to replicate in a variety of cell lines is characteristic of EAV, SHFV, and PRRSV but not of LDV, which has a strict host cell specificity. To date, no LDV receptors responsible for cell tropism have been identified. Thus, as a first step toward understanding the underlying mechanism of the restriction of LDV susceptibility, a system for the analysis of LDV envelope protein in mammalian cells was developed.

LDV possesses two major envelope proteins. The smaller is an 18- to 19-kDa nonglycosylated protein (M/VP-2; encoded by ORF6), and the other protein is a primary envelope glycoprotein (VP-3; encoded by ORF5). It has been shown that M/VP-2 and VP-3 of LDV are present in virions as heterodimers that are covalently linked by disulfide bond(s). Since breakage of the disulfide bond(s) in virions resulted in a loss of viral infectivity, the linkage between M/VP-2 and VP-3 seems to be required for host cell entry, perhaps by generating the virion receptor attachment site. Further analysis of the interaction between VP-3 -VP-2/M heterodimer envelope proteins of LDV and host cells will require antibodies directed specifically against each envelope protein. Although several specific antibodies against LDV VP-3 have been generated, despite much effort, no antibodies that react consistently with virion M/VP-2 have been generated. As a first step to examine the biological and functional properties of LDV M/VP-2, we prepared a newly generated specific antibody and analyzed the expression of ORF6 protein in mammalian cells.

A synthetic polypeptide corresponding to the C-terminal region of lactate dehydrogenase-elevating virus strain C (LDV-C) ORF6 which encodes virion structural protein M/VP-2 was chemically synthesized and coupled to keyhole limpet hemocyanin. The peptide was immunogenic in rabbits and induced antibody specific for viral protein. Western blotting and immunofluores-cence analysis of virion M/VP-2 in infected macro-phages or ORF6 protein in transfected COS-7 cells showed that the antibody was able to react with both authentic and expressed proteins. The immunoreactive antibody against both LDV M/VP-2 and expressed ORF6 protein described in this study provides the experimental basis for further studies of interaction between LDV envelope proteins and receptive host cells.

36. Development of Purkinje Cells in the Cerebellum of xpg-Deficient Mice

Xue-Zhi Sun, Yoshi-Nobu Harada,
Sentaro Takahashi, Naoko Shiomi and Tadahiro Shiomi

A mutant mouse carrying nonfunctional xeroderma pigmentosum group G gene (the mouse counterpart of the human *XPG* gene) alleles has been generated by using gene-targeting and embryonic stem cell technol-ogy. Homozygote animals of this autosomal recessive disease exhibited signs and symptoms, such as postnatal growth retardation, reduced levels of activity, progres-sive ataxia and premature death, similar to the clinical manifestations of Cockayne syndrome (CS). Histological analysis of the cerebellum revealed multiple pyknotic cells in the Purkinje cell layer of the *xpg* homozygotes,

which had atrophic cell bodies and shrunken nuclei. Further examination by immunohistochemistry for calbindin-D 28k (CaBP) showed that a large number of immunoreactive Purkinje cells were atrophic and their dendritic trees were smaller and shorter than in wild-type littermates. These results indicated a marked degeneration of Purkinje cells in the *xpg* mutant cerebellum. Study by *in situ* detection of DNA fragmentation in the cerebellar cortex demonstrated that some TUNEL-positive cells appeared in the granule layer of the mutant mice, but few cell deaths were confirmed in the Purkinje layer. These results suggested Purkinje cell degeneration in the mutant cerebellum was underway, in which many Purkinje cell deaths had not appeared, and the appearance of some abnormal cerebellar symptoms in the *xpg*-deficient mice was not only due to a marked Purkinje cell degeneration, but also to damage to other cells.

37. Histogenesis of Heterotopic Gray Matter in the Brain of the Mouse Prenatal Exposed to X-Ray Irradiation

Xue-Zhi Sun, Sentaro Takahashi,
Yoshihisa Kubota, Hiroshi Sato,
Chun Cui*, Rui Zhang* and Yoshihiro Fukui*
(*Univ. of Tokushima, School of Medicine)

Keywords: *cerebral cortex, pregnancy, X-rays*

Histogenesis of heterotopic gray matter in the brain of the mouse prenatally exposed to X-ray irradiation at embryonic day 13 (E13) was studied immunohistochemically. Bromodeoxyuridine (BrdU) as a marker to label the migrating position of neuroblasts generated at various embryonic stages showed that no "inside-out" pattern of neuronal migration occurred in the heterotopic cell mass similar to that seen in the laminated cortex. Further results in which midkind (MK) immunoreactive radial glial fibers did not appear in the heterotopic cell mass demonstrated that heterotopia formed in the absence of radial glia system. Different types of cells (pyramidal and nonpyramidal neurons) in the heterotopic cell mass were identified with immunoreactivity for anti-parvalbumin and anti-calbindin D-28K antibodies in addition to current histological methods. Two major types of neurons were mixed together with random distribution in the heterotopic cell mass. This finding indicates that irradiation might have no selective effects on the precursors of pyramidal and nonpyramidal neurons. Moreover, anti-glial fibrillary acidic protein (GFAP) immunostaining showed that numerous astrocytes were present in the heterotopic cell mass. The fact that astrocytes appeared in the heterotopia without the transition from classic radial glial cells to astrocytes suggests that astrocytes might be generated directly from a separate astroglial precursor.

Genetics

38. Dose-dependent Increase of Spi⁻ Mutations in the Spleen and Liver of Atm-disrupted Mice Following X-ray Irradiation

Ikuko Furuno-Fukushi, Yuko Noda, Takeshi Furuse, Yuko Hoki, Masahiko Takahagi, Ken-ichi Masumura[1], Hiroshi Suzuki[2], Takehiko Nohmi[1] and Kouichi Tatsumi ([1]Nat. Inst. Health. Sci.; [2]Chugai Pharmaceutical Co. Ltd.)

Keywords: Atm, Spi-, mutation, in vivo, X-rays

We have studied X-ray-induced mutations in *Atm* deficient (-/-) mice. The *gpt*-delta transgenic mice with *Atm* deficiency were generated for *in vivo* mutation assay. After X-irradiation, the transgenic mice were sacrificed and genomic DNA containing an inserted lambda shuttle vector was isolated from the liver and spleen. The DNA was packaged *in vitro*, and the phage was subjected to Spi⁻ (sensitive to P2 interference) selection. When both Red and Gam functions were inactivated, deletion mutants were positively selected as Spi⁻ plaques. Both the spontaneous mutant frequencies of the liver and spleen in *Atm* homozygously disrupted (-/-) mice were the same for those in *Atm* wild-type (+/+) mice. A linear increase in mutant frequency was observed as the dose of X-rays increased in *Atm* (-/-) mice and *Atm* (+/+) mice. The induced mutant frequency in the liver of *Atm* (-/-) mice exhibited no significant difference from that in *Atm* (+/+) mice. The induced mutant frequency in the spleen of *Atm* (-/-) mice was significantly higher than that in the spleen of *Atm* (+/+) mice. PCR analysis of the Spi⁻ mutants obtained from irradiated mice liver and spleen revealed that deletion mutants prevailed. However, no difference was observed in the proportion of mutants with deletions between the *Atm* (-/-) mice and *Atm* (+/+) mice. These results indicate that effects of *Atm* deficiency on mutation induction in the spleen are different from those in the liver. The liver cells do not divide regularly and are relatively resistant to radiation. The lymphoid tissues such as spleen are very sensitive and depleted of cells by rather small radiation doses. *Atm*-mediated repair mechanisms of mutagenic damage after irradiation may be different depending on the organ.

39. Expression Profile Using HiCEP

Masumi Abe, Ryutaro Fukumura, Tatsuya Ohhata, Ryoko Araki, Yuki Miyamoto, Can Ismail, Hajime Ohkaze, Hirokazu Takahashi, Yoko Tsutsumi, Yuko Hoki, Akira Fujimori and Toshiyuki Saito

Keywords: transcripts, expression profile, mouse embryonic fibroblast, X-ray irradiation

Cells save themselves and/or their hosts under stressful conditions through various mechanisms, one of which is programmed expression of a subset of genes. A novel technique exhibiting all transcriptional events in a cell would provide a great tool to understand such important mechanisms in life as differentiation and apoptosis. We have previously developed an expression profile system that can detect approximately 80% of the entire transcripts from a minimal size of cell or tissue samples (HiCEP).

This year, we investigated the sensitivity and the reproducibility of this novel strategy. (1) Different amounts of synthesized poly(A)RNA were added to total RNA from budding yeast and a test for detection by HiCEP was performed. The result showed that HiCEP is so sensitive as to be able to detect one copy per cell of the contaminated poly(A)RNA. (2) We performed HiCEP analyses for mouse embryonic fibroblast (MEF) cell samples, which were harvested at 0, 3, 6 and 24 hr after X-ray irradiation (7Gy). More than 200 transcripts exhibited altered levels of expression among approx. 20,000 transcripts detected in the HiCEP analysis. Those included p21 gene, for which expression increased 2-fold in the first 3 hrs after irradiation. Quantitative RT-PCR targeting each individual transcript verified that alteration of expression level by 1.3-fold was reliable in the HiCEP analyses.

We also performed expression analysis with MEF's of mice that were deficient in p53 or in ATM. Among 200 of the X-ray associated transcripts, only a subset of the genes was altered in both types of knockout mice, while the majority of them appeared to depend on either p53 or ATM.

Recent development of extensive genome resources is facilitating establishment of a database for the HiCEP analysis. We are now developing software to handle a great amount of HiCEP data more efficiently in order to realize bioinformatics on the HiCEP database. In the future, our HiCEP database should greatly contribute to medical, pharmaceutical and agricultural applications.

40. Comparison Study on Genome Coding DNA-dependent Protein Kinase between Chickens and Mice

Masumi Abe, Akira Fujimori, Ryutaro Fukumura, Tatsuya Ohhata, Ryoko Araki, Toshiyuki Saito, Hirokazu Takahashi and Yoko Tsutsumi

Keywords: *chickens, mice, DNA-PKcs gene*

The gene of catalytic subunit of DNA dependent protein kinase is responsible gene for SCID mice. The molecules play a critical role in non-homologous end joining including the V(D)J recombination. Contribution of the molecules to the difference of radiosensitivity and the susceptibility to cancer has been suggested. Here we show the entire nucleotide sequence of approximately 193 kbp and 84 kbp genomic regions encoding the entire DNA-PKcs gene in the mouse and chicken, respectively. Retroposon was found in intron 51 of mouse genomic DNA-PKcs gene but not in human and chicken. Comparative analysis of these two species strongly suggested that only two genes, DNA-PKcs and MCM4, exist in the region of both species. Several conserved sequences and cis elements, however, were predicted.

Publications:
1) Fujimori, A., Hashimoto, H., Araki, R., Saito, T., Kasama, Y., Mori, M., Fukumura, R., Ohhata, T., Tatsumi, K. and Abe, M. *Rad. Res*. **157**, 298-305, 2002.

2) Ohhata T., Araki R., Fukumura R., Kuroiwa A., Matsuda Y. and Abe M. *Gene*. **280**, 59-66, 2001.

3) Fukushima T., Takata M., Morrison C., Araki R., Fujimori A., Abe M., Tatsumi K., Jasin M., Dhar P.K., Sonoda E., Chiba T. and Takeda S. *J. Biol. Chem*. **276**, 44413-44418, 2001.

41. Disruption of *Xpg* Increases Spontaneous Mutation Frequency, Particularly A:T to-C:G Transversion

Tadahiro Shiomi, Naoko Shiomi, Emiko Hayashi*, Shun-ichi Sasanuma and Kazuei Mita
(*Chiba University)

Keyword: *xeroderma pigmentosum, Xpg, supF, mutation assay, transversion*

Cells isolated from *Xpg* (the mouse counterpart of human XPG)-deficient mice underwent premature senescence and showed early onset of immortalization, suggesting that *Xpg* might be involved in genetic stability. Recent studies showed that human XPG, in addition to the nucleotide excision repair (NER) protein, was involved in repair of oxidative base such as thymine glycol and 8-oxo-guanine, and this may explain the genetic instability observed in *Xpg*-deficient cells. To clarify this point, we determined spontaneous mutation frequencies and the type of spontaneous base substitution mutations in cells obtained from normal and *Xpg*-deficient mice using the *supF* shuttle vector(pNY200) for mutation assay. The spontaneous mutation frequency of the *supF* gene in pNY200 propagated in the *Xpg*-deficient cells was about three times higher than that in normal cells, indicating the importance of *Xpg* in reducing the frequency of spontaneous mutations. The frequency of spontaneous base substitution mutations at A:T sites, particularly that of the A:T-to-C:G transversion, increased markedly in the *Xpg*-deficient cells.

Publication:
Shiomi, N., Hayashi, E., Sasanuma, S., Mita, K., Shiomi, T.: *Mutat.Res.*, **487**, 127-135, 2001.

42. A New Technique to Prevent Self-Ligation of DNA

Hideki Ukai[1], Maki Ukai-Tadenuma[2], Toshiaki Ogiu and Hideo Tsuji
([1]Domestic Postdoctoral Fellow; [2]Japan Science and Technology Corporation)

Keywords: *gene cloning, self-ligation, molecular technique*

Ligation of DNA fragments by DNA ligase is an essential step in many molecular biology techniques, including gene cloning and messenger RNA (mRNA) fingerprinting. Efficient ligation requires the DNA strands to be prevented from self-ligating (self-circularization and concatenation). Here, we describe a technique to prevent self-ligation of the DNA ligation-partner of 5'-dephosphorylated DNA.

Some techniques to prevent self-ligation are already known, including standard dephosphorylation of the 5' ends by alkaline phosphatase. Because DNA ligase catalyzes the formation of the phosphodiester bond between the 5'-phosphate group (5'-P) and the 3'-hydroxyl group (3'-OH), 5'-dephosphorylated DNA can not self-ligate. The 5'-dephosphorylated DNA still contains a 3'-OH, however, allowing ligation with untreated DNA that contains a 5'-phosphate group (5'-P).

The untreated DNA ligation-partner remains capable of self-ligation, e.g., concatenated DNA fragments could insert into the 5'-dephosphorylated vector DNA molecule.

Another technique used to prevent self-ligation is partial filling-in. In this technique, the two DNA species are digested with different restriction enzymes that form 3'-recessed ends. The ends are then partially filled-in using Klenow DNA polymerase with deoxy-nucleotides (dNTPs). The resulting ends are unable to self-ligate but ligate with partner DNA via the complementary 5'-overhang sequence. Although this technique simultaneously prevents self-ligation of both DNA species, it cannot be applied to 5'-recessed or blunt ends. Moreover, only restriction enzymes that produce complementary overhang sequences after partial filling-in can be used, further reducing the flexibility of this technique.

The ligation reaction catalyzed by DNA-ligase is similar to the polymerization of nucleotides by DNA polymerase. DNA polymerase catalyzes the formation of the phosphodiester bond between the 5'-P of a mononucleotide and the 3'-OH of a polynucleotide. A standard technique to inhibit the extension of DNA by DNA polymerase employs dideoxyribonucleotides (ddNTPs). When DNA has a ddNTP incorporated at its 3'-end, the lack of a 3'-OH prevents DNA polymerase from extending the DNA.

In the present study, we replaced the 3'-dNTP of DNA with ddNTP to prevent self-ligation by DNA ligase (Fig. 23). The resulting 3'-H DNA fragment, denoted here as a 3'-replaced DNA fragment, was unable to self-ligate in the presence of DNA ligase. Moreover, because the 3'-replaced fragment still contained a 5'-P, the fragment remained capable of ligating with the 3'-OH of the partner DNA. By combining this 3'-replacement technique with the 5'-dephosphorylation technique, self-ligation of both species of DNA involved in a given ligation was simultaneously prevented, while the 5'-phosphate remaining at the 5'-end permitted ligation with the 3'-hydroxyl end of the 5'-dephosphorylated DNA strand. We successfully applied this 3'-replacement technique to gene cloning, adapter-mediated polymerase chain reaction, and messenger RNA fingerprinting. The 3'-replacement technique is simple and not restricted by sequence or conformation of the DNA termini, and is thus applicable to a wide variety of methods involving ligation.
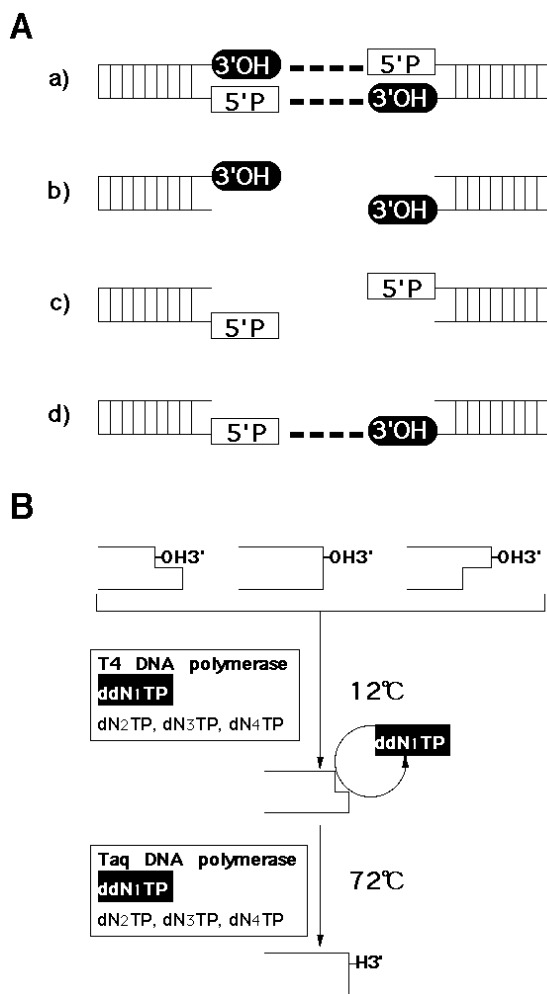

Fig. 23. Prevention of DNA ligation by 3'-replacement. (A) Patterns of DNA ligation. DNA ligase catalyzes the phosphodiester bond (dotted lines) between a 5'-phosphate group (5'-P) and a 3'-hydroxyl group (3'-OH). (a) When DNA contains both the 5'-phosphate and 3'-hydroxyl groups, both strands of DNA are ligated. DNA that does not contain a (b) 5'-phosphate group or a (c) 3'-hydroxyl group cannot self-ligate. (d) 3'-replaced DNA contained a 5'-P, which would be able to ligate with the 3'-OH of the partner DNA, even though the partner was 5'-dephosphorylated. (B) Scheme of the 3'-replacement method. Restriction enzyme-digested DNA was blunt-ended by T4 DNA polymerase and a ddNTP mix that contained one type of ddNTP and three types of dNTPs. The ddNTP was the complementary nucleoside to the 5'-end of the restriction enzyme-digested strand. Immediately after incorporation of the ddNTP, it was removed via the 3'-5' exonuclease activity of T4 DNA polymerase. Thus, incorporation and removal of the ddNTP were repeated at the DNA terminus. The DNA was then incubated with Taq DNA polymerase, which lacks 3'-5' exonuclease activity, at 72 C. Under these conditions, T4 DNA polymerase was completely inactivated, and the Taq DNA polymerase filled the recessed 3' terminus with ddNTP without a 3'-dAMP overhang.

43. The Trial Study for Establishment of New Mutant Rat Strains Using the Chemical Mutagen

Yoshi-nobu Harada, Aya Sugyo,
Atsushi Tsuji and Takashi Imai

The rat is an experimental animal which has been widely studied in medicine, pharmaceutical sciences, and biology. A method, however, is not available to establish model animals which have lost a specific gene function in rats. Mutagenesis is a good way to produce gene deletion model animals. The aim of our study is to establish a method for making gene deletion models of rats by chemical mutagenesis. It has been reported that chlorambucil could induce deletion mutation in mouse spermatid DNA. The same effect for chlorambucil can be expected it in rats.

A mating experiment was carried out by the following method. Male 12-week-old Brown Norway rats were given 1.0 mg/Kg, 2.5 mg/Kg, 5.0 mg/Kg, 10.0 mg/Kg or 15.0 mg/Kg of chlorambucil intracelially. Each male rat, after injection in with chiorambucil was mated with two normal F344 females at an interval of one week. Then the number of offspring born from F344 female was counted. The litter size observed in 1.0mg/Kg and 2.5mg/Kg injected groups was not different from the control group. However, in 5.0 mg/Kg, 10.0 mg/Kg and 15.0 mg/Kg injected groups, the litter size got from matings 3-4 and 4-5 weeks post-injection significantly decreased. The decrease of the litter size may be caused by dominant lethal mutation induced in the spermatid of the male rats. These results suggested that 5.0 mg/Kg or more chlorambucil could cause some mutations in the spermatid of male rats.

44. Characterization of Genes in Response to Irradiation though Systematic Transcriptome Analysis

Kumiko Saegusa, Masao Suzuki,
Kennichi Ishikawa, Yoshimi Ohtsuka,
Tomo Kimura, Atsuko Ishikawa and Takashi Imai

To predict unusual response to clinical radiations, identifying molecular markers and understanding the variation in radio sensitivity at a molecular level are required. Microarray technology can be used for simultaneously detecting expression of thousands of genes in different cell types in a single hybridization experiment. Microarray technology has also proved to be a powerful tool for comparing gene expression in normal and disease states and/or for analyzing the response of cells exposed to drugs or unknown physiological conditions. We have studied gene expression profiles of two normal fibroblast cell lines (NB1RGB, HFLIII) and 13 cancer cell lines (A549, C32TG, Marcus, U-251MG (KO), SK-MG-1, KNS89, KS-1, A-172, KNS-76, KNS-60, Becker, T98G, SF126) with different radio sensitivities using an oligonucleotide microarray before/after exposure to ionizing radiation.

All cell lines were cultured in Eagle's minimum essential medium (MEM) supplemented with 10% fetal bovine serum in a 5% C02 incubator at 37 ℃. The plating efficiencies of cell lines used varied from 20% to 90% in each cell line. Total RNA was purified from the cells at zero, one or three hours after X-ray irradiation. Fluorescent complementary RNA was prepared by reverse transcription and in vitro RNA synthesis with Cy3- or Cy5- labeled nucleotides. Hybridization was performed with the custom-made oligonucleotide microarray containing 22,500 probes (representing 14,000 unique genes). Cells were irradiated with X-rays at room temperature. The dose rate was 0.87Gy/min. We performed mutation analysis spanning p53 exons 5-8 in 15 cell lines by Denaturing High Pressure Liquid Chromatography (DHPLC) using a Wave Fragment Analysis System (Transgenomics). Expression profiles were analyzed using a custom-made oligonucleotide microarray (Agilent Technologies, CA). After hybridization, slides were washed and scanned using a confocal laser scammer (Agilent Technologies, CA). Gene expression analysis was performed using RESOLVER (Rosetta Inpharmatics, WA.)

We compared gene expression profiles of 15 cell lines whose radio sensitivities were quite different. The two-dimensional cluster analysis indicated that the radio-resistant cell lines such as Becker, KNS60, T98G and A549, were clearly separated from the radiosensitive ones. The genes classified by this analysis may be useful to predict radio-resistant cells that were clarified by D10 value.

It has been well documented that p53 is activated in response to DNA-damaging agents including ionizing radiations. We, therefore, examined the relationships between radiation sensitivity and p53 status in the cell lines and found that the D10 values were not correlated with the p53 status. The two-dimensional cluster analysis also indicated that there were at least two groups of genes for classifying the cell lines by D10 values. One group of the genes was useful for clustering the cell lines with wild-type p53 while the other was advantageous for clustering the cell lines with p53

mutants. These results suggest that p53 plays a critical role in the radiation-induced signal transduction in both radiosensitive and resistant cells and that the cells may contain a p53 independent-pathway for determining radiation sensitivity.

Publications:
1) Suzuki M, Kase Y, Yamaguchi H, et al. Relative biological effectiveness for cell-killing effect on various human cell lines irradiated with heavy-ion medical accelerator in Chiba (HIMAC) carbon-ion beams. Int. J. Radiation Oncology Biol. Phys, 2000; 48: 241-250
2) Suzuki M, Kase Y, Kanai T, and Ando K. Correlation between cell killing and residual chromatin breaks measured by PCC in six human cell lines irradiated with different radiation types. Int. J. Radiat. Biol, 2000; 76: 1189-1196

45. Analysis of Genetic Differences in Radiation Sensitivity Using Animal Models.

Mayumi Iwakawa, Ryonfa Lee,
Miyako Goto, Chisa Ohira,
Toshie Ohta, Shuhei Noda,
Yoshinobu Harada and Takashi Imai

Keywords: strain difference, radiosensitivity, mouse, jejunal crypt, skin reaction

Analysis of 5 murine strain differences were demonstrated by examining the extent of normal tissue damage from irradiation for several endpoints used in experimental animals. Levels of radiation-induced normal tissue damage were compared in A/J, C57BL, C3H, C3H-scid and C.B-scid mice. Jejunal Crypt Assay: whole body irradiated mice were sacrificed 3.5 days later and the number of regenerating crypts of the sectioned jejunum was scored. Endogenous spleen colony assay: whole body irradiated mice were sacrificed 9 days later and their spleens were removed and the colonies were counted. Acute Skin Reaction: One hind leg of each mouse was irradiated and the skin response was observed. Leg Contracture Assay: The length of irradiated leg and unirradiated leg to the ankle were measured. Early and Late Response of the Lung: the thorax of mice was irradiated. Pathological changes of the lung were observed and fibrogenetic cytokines were measured. C3H mice showed the highest resistance against radiation in most of the assays, while the scid mice were found to be the most sensitive among the four strains analyzed. The inter-strain difference of radiation sensitivity revealed in this study strongly supports the hypothesis that genetic factors are an important determinant for the response against irradiation. A macroarray assay for gene expression is now under investigation.

46. A Large-scale Gene Expression Analysis of Radiosensitive and Radioresistant Rats Exposed to Ionizing Radiation

Atsushi Tsuji, Aya Sugyo,
Sagara Masashi, Toshiaki Ogiu,
Hiroshi Aburatani, Takashi Imai and Yoshinobu Harada

Keywords: rat, X-ray,s microarray

The LEC rat is an X-ray hypersensitive animal characterized by radiation-induced bone marrow death, intestinal death, and an impaired ability to repair DNA double-strand breaks. This radiosensitivity is controlled by the responsible gene, mapped on rat chromosome 4 by Agui et al. in 2000. LEC rat is useful for investigating a molecular mechanism of radiation-induced responses in vivo. To identify the radiation-induced LEC-specific gene expression, we performed a large-scale gene expression analysis using microarrays between LEC and F344 rats.

We extracted mRNAs of LEC and F344 tails before exposure and 6 hours after whole-body irradiation at 4.5Gy. These mRNAs were labeled and hybridized three types of rat GeneChip microarrays (RGU34A¥B¥C, Affymetrix, Santa Clara, CA) according to the recommendations of Affymetrix. We normalized fluorescence intensities and performed comparative analysis of gene expressions of 26,379 probe-sets (24,681 genes or ESTs) using GeneChip 3.1 software, and excluded 11,855 probe-sets, which were undetected expression in all samples. An increase or decrease of 2-fold was chosen as a criterion for changes in gene expression.

We found 223 genes/ESTs increased or decreased in LEC rat, but not in F344 rat. By contrast, we identified 303 genes/ESTs increased or decreased in F344 rat, but not in LEC rat. In addition, 85 genes/ESTs had 2-fold different expression levels between LEC and F344 rats after irradiation. This result suggests these genes/ESTs could be associated with radiosensitivity in LEC rat. Gadd45, known for cell cycle regulation and DNA repair, was induced 5-fold in LEC rat, but was unchanged in F344 rat. Gadd45 expression is known to be increased by irradiation in normal susceptible tissues and cells. We, however, mapped Gadd45 near the responsible locus on rat chromosome 4. Then, we compared the Gadd45 cording sequence of LEC rat with

that of F344 rat, and we found no difference, resulting that another gene was associated with radiosensitivity in LEC rat.

In the present study we detected approximately 600 genes/ESTs, which were shown to have different expression manners between radiosensitive and radioresistant rats exposed to ionizing radiation. This finding shouls be useful for investigating a molecular mechanism of radiation-induced response.

47. Radiation Sensitivity of 49 Cultured Human Cancer Cell Lines

Sadayuki Ban, Hitomi Sudo, Masashi Sagara,
Yuichi Michikawa, Kumiko Saegusa,
Yoshinobu Harada, Yoshiya Shimada, Masami Arai,
Yutaka Shimada, Jhoji Inazawa and Takashi Imai

Keywords: radiation sensitivity, clonogenic assay, human cancer cells

Classification of cells with different radiosensitivities provides the base for a genome-wide search for radiation-responsible genes by using cDNA microarray technology.

A clonogenic assay was used to determine the cellular radiosensitivity of 49 cultured human cancer cell lines, of which five were established from breast cancer, 3, from pancreas cancer, 31, from esophageal cancer, 4, from cervical cancer, and 6, from colon/rectum cancer. One breast cancer cell line had a homologous mutation in BRCA11, one pancreas cancer cell line, in BRCA2 (1), 3 colon/rectum cancer cell lines, in APC and 3 colon/rectum cancer cell lines, in mismatch-repair genes. Alpha MEM supplemented with 10 % FCS was used for maintenance and subculture for all experiments. Actively growing cells were harvested and suspended in growth medium, after which cells were put into plastic test tubes and exposed to various doses of X rays with a dose rate of 1 Gy/min. Immediately after irradiation, appropriate known numbers of cells were seeded into plastic culture dishes and cultured for 10 - 14 days in 95 % air plus 5 % CO_2 at 37 ℃. The dose responses were analyzed using a multitarget model, $S/S0 = 100[1-(1-e-D/Do)n]$ (2,3). Chromosomal radiosensitivity of six colon/rectum cancer cell lines was also determined with a micronucleus assay (1,4,5).

There was a wide variation in each of the three dose-survival parameters among 49 cell lines (D0 = 0.77 - 2.37 Gy, D10 = 2.06 - 7.34 Gy, Dq = 0.16 - 2.71 Gy). Dq was not correlated with D10, or D0, although there was a weak correlation between D0 and D10. These results suggested that the repair pathway in the sublethal dose range was different from that in the lethal

dose range. The BRCA1-defective cell line had the highest radiosensitivity (D0 = 0.77 Gy, D10 = 2.06 Gy, Dq = 0.29 Gy) among cell lines tested. BRCA2-defective cells also showed unusual radiation sensitivity (D0 = 1.43 Gy, D10 = 3.92 Gy, Dq = 0.62 Gy). Cells with mutation in mismatch repair genes had a slightly higher radiosensitivity (D0 = 0.80 - 0.81 Gy, D10 = 2.23 - 4.31 Gy, Dq = 0.35 - 2.45 Gy) than APC-defective cells (D0 = 1.23 - 1.59 Gy, D10 = 5.00 - 5.86 Gy, Dq = 2.15 - 2.19 Gy), but the chromosomal radiosensitivity of APC-defective cells was higher than that of the others. For other cell lines, genes involved in the heterogeneity in radiation sensitivity remained unknown. Our cancer cell collection is characteristic of the number of esophageal cancer cell lines (31 among 49 lines) (6). One of the worst diagnoses is given to esophageal cancer, because most patients do not feel any symptoms in an early stage and they are not diagnosed till the disease has progressed to an advanced stage (7). A wide variation was also observed in each of three dose-survival parameters of esophageal cancer cell lines. D0 values were 0.96 - 2.37 Gy, D10, 2.81 - 7.34 Gy, and Dq, 0.16 - 2.71 Gy. Preliminary study demonstrated that some cell lines lost the G1- or G2/M- checkpoint, others did not.

Detection and identification of radiation-related genes in various types of cells are urgently needed to deliver radiation effectively to tumor tissues, and to minimize the side effects on normal tissues. We are planning a genome-wide search of the genes involved in heterogeneous radiation susceptibility and the cell-cycle checkpoint in various types of cultured human cells. Our studies are extremely useful to design radiation-therapy protocols for advanced cancers with heterogeneous radiation sensitivities.

Publications:
1) Ban, S., Shinohara, T., Hirai, Y., Moritaku, Y., Cologne, J.B., MacPhee, D.G.: Mutation Research 474, 15-23, 2001.
2) Ban, S., Setlow, R.B., Bender, M.A., Ezaki, H., Hiraoka, T., Yamane, M., Nishiki, M., Dohi, K., Awa, A.A., Miller, R.C., Parry, Mulvihill, D.M., J.J., Beebe, J.W.: Cancer Res. 50, 4050-4055, 1990.
3) Ban, S., Setlow, R.B., Ezaki, H., Hiraoka, T., Yamane, M., Nishiki, M., Dohi, K.: J. Radiat. Res. (Suppl.) 32, 330-338, 1991.
4) Ban, S., Cologne, J.B., Radiat. Res. 131, 60-65, 1992.
5) Ban, S., Cologne, J.B., Fujita, S., Awa, A.A.: Radiat. Res. 134, 170-178, 1993.
6) Shimada, Y., Imamura, M., Wagata, T.,Yamaguchi, N., Tobe, T.: Cancer 69, 277-284, 1992.
7) Kan, T., Shimada, Y., Sato, F., Maeda, M., Kawabe, A., Kaganoi, J., Itami, A., Yamasaki, S., Imamura,

M.: Biochem. Biophys. Res. Commun. 286, 792-801, 2001.

48. Relationship between Cellular Radiosensitivity and DNA Damage Measured by Come Assay

Miyako Goto, Yoshimi Ohtsuka,
Mayumi Iwakawa, Kumiko Saegusa,
Kaori Yasuda, Ryonfa Lee,
Atsuko Ishikawa, Yoshinobu Harada and Takashi Imai

Keywords: *comet assay, radiosensitivity, microarray*

The purpose of this investigation was to determine whether comet assay and expression analysis of genes would predict the radiosensitivity of human cancer cell lines which showed differences in D10 or Dq values. Two human cancer cell lines were investigated. For comet assay, cells were irradiated with X-rays ato dose of 4 or 8Gy and DNA damage was assessed under alkali conditions. For expression analysis of genes, cells of each cell lines were exposed to X-rays at a dose of 2 Gy. The gene expression profiles of the two cell lines after irradiation using cDNA microarray analysis of 14,000 genes were clustered. The survival curve after X-ray irradiation for each cell lines introduced each D10 value. Comet assay was used as an index of induced DNA damage after irradiation. The value of the mean tail moment in each cell line was observed. A correlation between the D10 value of each cell line and the mean tail moment by the comet assay in each cell line was obtained. Cell lines could be separated as two groups a radiosensitive group and a radioresisitant group, depending on the comet assay and D10 values. Expression analysis of the microarray reveled several genes were induced in the radiosensitive cell line and suppressed in the radioresistant cell lines. These results suggest that the comet assay and gene expression analysis would promising for predicting the radiosensitivity of tumor tissue.

49. Amino Acid Substitution of the Largest Subunit of Yeast RNA Polymerase II: Effect of a Temperature-sensitive Mutation Related to G1 Cell Cycle Arrest

Kimihiko Sugaya

Keywords: *RPB1, site-directed mutagenesis, temperature sensitivity, distribution*

A temperature-sensitive mutant, tsAF8, of the BHK21 Syrian hamster cell line shows cell cycle arrest at nonpermissive temperatures in mid-G_1 phase. DNA sequence comparison of the largest subunit of RNA polymerase II (Rpb1) from the wild type and the mutant shows that the mutant phenotype results from a (hemizygous) C-to-A variation at nucleotide 944 in one *rpb1* allele; this gives rise to an Ala-to-Asp substitution at residue 315 in the protein. To examine this hemizygous mutation in the *rpb1* gene and to determine the molecular mechanism underlying the temperature-sensitive defects, this amino acid substitution was introduced into the *Schizosaccharomyces pombe rpb1* gene. Whereas tsAF8 cells showed growth defects and an altered distribution of Rpb1 at nonpermissive temperatures, yeast cells harboring this amino acid substitution did not show any temperature sensitivity. Distribution of Rpb1 in yeast cells appeared normal at permissive and nonpermissive temperatures. The additive or subtractive effect of another temperature-sensitive Rpb1 mutation was also very little. These results suggest that mutation of the *rpb1* gene, which is critical in mammalian cells, may not be deleterious in yeast cells.

50. Rederivation of Infected Mice by Embryo Transfer Technique

Masanori Okamoto

Keywords: *embryo transfer, germfree mice, infected mice, rederivation*

This introduces a reproductive biotechnology, mainly an embryo manipulation technique, for the purposes of strain maintenance, transport, rederivation of infected mice, etc. in management laboratory mice. We developed a strain maintenance system using the embryo cryopreservation method on inbred mice which were produced in our facilities, which includes rederivation of HVJ (hemagglutinating virus of Japan) infected mice and production of germfree mice using an embryo transfer technique.

This study was undertaken to determine whether HVJ infected mice at inoculation were rederived by the embryo transfer technique. The embryos were collected from donor mice, all HVJ positive, and were transferred to the uteri of pseudopregnant recipients that were HVJ-free SPF mice. All the recipients and live young obtained after transferred were negative to testing by HVJ antibody. These results indicate that the embryo transfer technique is useful for rederivation of HVJ infected mice. Besides, conventionally, in preparing

germfree (GF) mice, the uterus is removed from animals immediately before delivery; the fetus is taken out, and nursed by a GF foster mother. With this technique, it is difficult to determine the optimum time to remove the uterus. The resuscitation rate of offspring can be reduced if natural delivery occurs earlier than expected or if surgical delivery is too early. Furthermore, foster nursing requires skill. To increase the efficiency of GF mouse production, we examined the embryo transfer technique. The embryos were collected from conventional donor mice in a clean bench, and were transferred to the uteri of pseudopregnant recipients, which were GF mice reared in a flexible vinyl isolator. All the recipients and live young delivered after transfer were negative when examined for sterility. The results indicated that GF mice could be produced by embryo transfer, in addition to the conventional techniques of hysterectomy and cesarotomy. Furthermore, we developed new aseptic techniques for producing vasectomized sterile males from GF mice and for manipulating embryos. These methods of producing GF and clean mice by the embryo transfer technique, in combination with reproductive biotechnology such as techniques for storing frozen embryos, should be useful for strain maintenance, transportation of mice, and *in vitro* fertilization.

Radiotoxicology

51. Effects of D-penicillamine and Ca-DTPA on Removal of Radiocobalt in Rats

Satoshi Fukuda, Haruzo Iida,
Yumi Abe* and Hiroki Yoshida*
(*Tokyo Nuclear Service Co. Ltd.)

Keywords: D-penicillamine, Ca-DTPA, removal, radiocobalt, daily recommended human dose

Based on a medical treatment schedule for humans, the effects of D-penicillamine and Ca-DTPA on the removal of radiocobalt were examined in rats. Rats were pre-injected with radiocobalt and then treated with D-penicillamine alone via an oral route, Ca-DTPA alone via an intraperitoneal injection, or both compounds at the same time at doses equivalent to the daily recommended human dose. The compounds were administered for 3 days, beginning with or 1h after radiocobalt injection on the first day. The radioactivity levels of the whole body of rat, urine and feces were measured at intervals of 24 h. On day 4, the rats were sacrificed in order to obtain blood and organs. When D-penicillamine was administered with and 1 h after injection of radiocobalt, the whole body activity was reduced to 9.6 and 79.0% of that of the control, respectively, in the Ca-DTPA-alone groups and to 54.8% in the group in which both compounds were administered 1 h after radiocobalt. In the D-penicillamine-alone groups, the activity levels were reduced to 33.6 and 56.6% with and 1h after radiocobalt injection, respectively (Fig. 24). In conclusion, the results of this study indicate that D-penicillamine is useful in treating a person contaminated with radiocobalt in an accident.
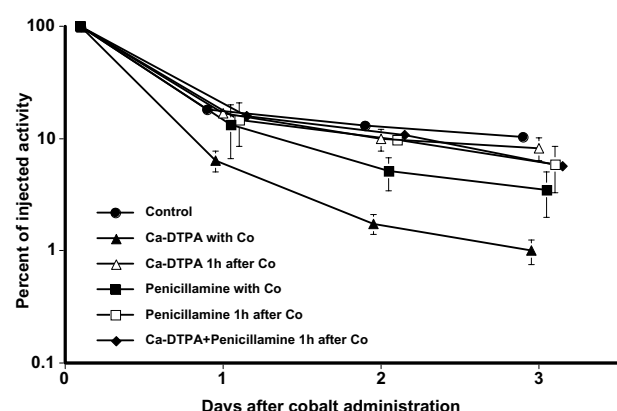
Fig.24. Whole-body retention of radio-cobalt after administration of Ca-DTPA and D-Penicillamine. Values are mean and bars are standard deviation.

52. Effects of CBMIDA on Removal of Uranium in Rats

Satoshi Fukuda, Haruzo Iida,
Xueming Yan* and Yuyuan Xie*
(*Shanghai Institute of Materia Medica, China)

Keywords: CBMIDA, uranium, rat

The effects of a chelating agent, CBMIDA, on the removal of uranium in rats were determined. Thirty rats were divided into six groups. Group 1(G1): rats injected intraperitonially with uranium in a solution of pH 3.2 and injected with sodium bicarbonate 30 min later; Group 2 (G2): uranium compounded with CBMIDA before injection; Group 3 (G3): uranium in a pH 3.2 solution; Group 4 (G4): uranium in a pH 3.2 solution and injection of 1200 μmol/kg CBMIDA 30 min later, Group 5: uranium in a pH 6.8 solution; and Group 6: uranium in a pH 6.8 and injection of 1200 μmol/kg CBMIDA. The uranium activities in the excreta and organs in rats 24 hrs after injection were measured.

The rates of uranium excreted were 1.05 % of the injected dose in group G1, 1.00% in G3, and 0.24% in G5, whereas they were 11.26% in group G2, 9.49% in G4, and 10.13% in G6, respectively (Table 1). The amount of activity in excreta (urine and feces) was highest in group G2. A significant difference of activity in the excreta between groups G 5 and G6 was found. The retention rates in the liver, femur, and spleen in groups G2, G4, and G6, except for the value of spleen in G4, decreased more than those of the corresponding G1, G3 and G5 groups, respectively. However, the retention

Table 1. The rates of uranium activity excreted in urine and feces 24 hr after injection of uranium; the values are presented as percentages of injected doses.

Group	Excreted rate in urine (%)	Excreted rate in feces (%)	Total rate in excreta (%)
G1:U pH 3.2 and NaHCO3	1.05±0.20	2.06±1.27	3.11
G2: compound CBMIDA and U	11.26±3.29	12.65±3.00	23.92
G3: U pH 3.2	1.00±0.16	15.69±4.02	16.69
G4: U pH 3.2 and CBMIDA	9.49±3.21	6.13±2.34	15.62
G5: U pH 6.8	0.24±0.11	0.13±0.03	0.37
G6: U pH6.8 and CBMIDA	10.13±2.70	1.69±0.22	11.72

rate in the kidney in groups G2 and G4 was higher than that in groups G1 and G3 respectively, but the rate in the G6 group was lower than that of G5.

In conclusion, the results indicate that CBMIDA can remove uranium at pH6.8 from the body, while its has no effect for uranium at pH3.2 solution and shows undesirable characteristic of accumulating uranium in the kidney. Further study of the analogues of CBMIDA will be necessary in order to enhance its removal effects and reduce the associated accumulation of radioactive materials from the kidney.

53. DTPA Treatment for Removal of Inhaled Plutonium Nitrate in Rats.

Satoshi Fukuda and Haruzo Iida

This study was performed in order to determine the maximum removal rate of plutonium by DTPA treatment. Aerosols of a complex of plutonium-239 and DTPA (Pu-DTPA) and plutonium nitrate were inhaled by 40 female 3-month-old Wistar rats. Ten rats from the inhaled Pu-DTPA and Pu nitrate group were sacrificed in groups of five at 3 and 7 days. Subsequently, in the period from 7 to 28 days after inhalation, five rats in each group were orally administered Zn-DTPA via their drinking water. The activity of plutonium which was

Fig.25. Daily activities of plutonium excretion in urine of rats in the plutonium-nitrate inhalation groups observed for 28 days after inhalation.

retained in the urine and feces collected at 24 hr-intervals and in all organs was measured. The body retention rates of plutonium in the plutonium-nitrate and plutonium-nitrate + Zn-DTPA groups observed for 28 days were 30.4%, and 23.5%, respectively, of total intake, while those in the Pu-DTPA and Pu-DTPA + Zn-DTPA groups were reduced to 2.3%, and 1.5%, respectively. The administration of Zn-DTPA in the plutonium-nitrate group enhanced the excretion of plutonium in the excreta (Fig. 25), whereas such increases in the Pu-DTPA group were not observed. The greater part of the plutonium retained in the bodies of rats in the plutonium-nitrate group was deposited in the lung. The results indicate that DTPA essentially has the effect of reducing the amount of plutonium in the body, up to about 2% of intake. The problem might be that the effects of DTPA treatment might actually be low if DTPA were administered to persons contaminated with plutonium in an accident. In conclusion, attempts to enhance the effects of DTPA and the development of new chelating agents will be necessary to adequately reduce the risk of plutonium inhalation in the future.

54. Immunohistochemical Study on Cellular Origins of Rat Lung Tumors Induced by Inhalation Exposure to Plutonium Dioxide and by X-ray Irradiation

Yoichi Oghiso and Yutaka Yamada

Immunohistochemical examinations were done on rat lung tumors induced by inhalation exposures to plutonium or by X-ray irradiation to identify and compare cellular origins or, in turn, target cells at risk for radiation carcinogenesis. Female Wistar (W/M) strain rats were either exposed to submicron-sized $^{239}PuO_2$ aerosols, or irradiated locally or systemically by X-rays at 100 to 120 days after birth. Primary lung tumor specimens were selected for the present examinations from 135 plutonium-exposed and 41 X-ray irradiated rats. All of those lung tumors appeared to occur from the lower respiratory tract epithelium through bronchioles into alveoli and were histopathologically diagnosed as adenoma, adenocarcinoma, adenosquamous carcinoma, and squamous cell carcinoma. Immunohistochemical staining of neoplastic lesions using rabbit
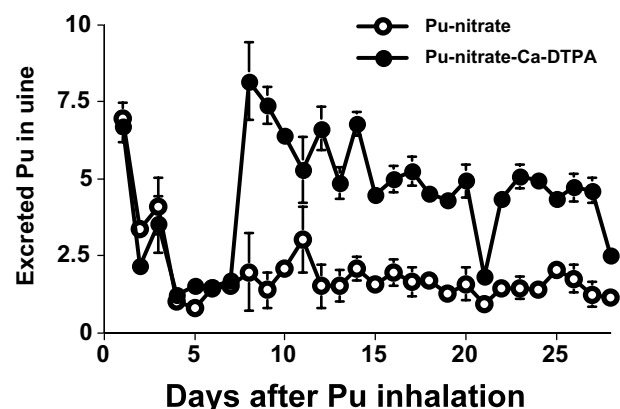
polyclonal antibodies to rat surfactant apoprotein A specific for alveolar type II pneumocytes and Clara cell antigen specific for nonciliated bronchiolar Clara cells, showed that most adenomatous and adenocarcinomatous lesions from plutonium-exposed or X-ray irradiated rats were positive for either or both antigens, while in contrast, adenosquamous and squamous lesions were mostly negative for both antigens. Even though there were some differences in the proportions and distributions of immunoreactive cells between plutonium- and X-ray-induced tumors and among neoplastic lesions, the results indicated that radiation-induced pulmonary adenomas and adenocarcinomas mostly originate from either alveolar type II pneumo-cytes or bronchiolar Clara cells, while adenosquamous and squamous carcinomas may be derived from other epithelial cell components, or might have lost specific antigenicity during their transforming differentiation.

55. Induction of Micronuclei in Rat Alveolar Epithelial Cell Line by Alpha Particle Irradiation

Yutaka Yamada, Yoichi Oghiso,
Hiroko Enomoto and Nobuhito Ishigure

Keywords: *micronucleus, alpha particle, rat, alveolar type II cell line, biodosimetry*

A life-span study has been conducted on rats that inhaled plutonium dioxide aerosols and it was observed that plutonium deposited in lung induces lung tumors in a dose-dependent manner. The absorbed dose in lung was calculated from radioactivity in thorax by whole body counting procedure, but the absorbed dose in target cells' level remains unclear. The lung model of ICRP publication 66 describes cells at risk of respiratory tract tissues as secretory and basal cells in bronchial airways, and Clara and Type II cells in the alveolar interstitial region. Therefore, dose estimations in the tissue layers containing the target cells are required in the model. Recently, a biodosimetric approach has been developed and applied to estimate absorbed dose in respiratory cells. In the biodosimetry, responses of isolated cells that have been previously exposed to alpha emitters *in vivo* are compared to the responses obtained from similar populations of cells that were irradiated *in vitro* using alpha sources. As a preliminary experiment for biodosimetry in respiratory epithelial cells of rat, the dose-response relationships of radiation-induced micro-nucleus formation were investigated utilizing an immortalized rat alveolar Type II cell line (SV40T2).

The SV40T2 cells were exposed to either alpha particles (^{241}Am: 3.2 MeV, 128 keV/μm, 0.093 Gy/min at cell-Mylar interface) or X-rays (200 kVp, 1 Gy/min). The frequency of micronucleus formation was 1.6 - 3.0% for unirradiated subjects but increased for irradiated ones in a dose-dependent manner. A linear relationship between the dose and the micronucleus formation was observed until 1 Gy for alpha particles and 4 Gy for X-rays. The linear slope for alpha particles was 28.5 % per Gy and the relative biological effectiveness (RBE) was 4.3, as calculated from the slopes. The slope for alpha particles was dependent on the energy of the alpha particles. These results indicate that the micronucleus assay is available for biodosimetry of alpha particle irradiation in the rat alveolar epithelial cells.

56. Involvement of p53-Dependent Apoptosis in Radiation Teratogenesis and in the Radioadaptive Response in the Late Organogenesis of Mice

Bing Wang, Harumi Ohyama,
Masako Nose, Kaoru Tanaka,
Tetsuo Nakajiama, Osami Yukawa,
Takeshi Yamada, Shirou Aizawa and Isamu Hayata

Keywords: *apoptosis, p53, teratogenesis, adaptive response, organogenesis*

The irradiation of fetuses at the late period of organogenesis has been known to induce a dramatic increase in malformations. The mechanisms involved, however, have remained unclear. Using the mouse limb bud system, we first found that radiation-induced apoptosis is involved in the malformation, namely, radiation-induced apoptosis in the predigital regions of embryonic limb buds is responsible for digital defects in mice. An examination of embryonic C57BL/6J mice with different p53 (trp53) status enabled us to further find that susceptibility to radiation-induced apoptosis in the predigital regions and digital defects depend on both the p53 status and the radiation dose; p53 wild-type mice appeared to be the most sensitive, while p53 knockout mice were the most resistant. These results indicate that p53-dependent apoptosis mediates radiation-induced digital defects in the later organogenesis period. The existence of a radioadaptive response in embryonic mice, which has not been reported so far, was found by irradiating embryos with either 5 cGy or 30 cGy on

embryonic day 11 prior to a challenging irradiation at 3 Gy on embryonic day 12. p53-heterozygous embryos did not show the radioadaptive response, indicating the involvement of p53 in the radioadaptive response in embryogenesis.

Publications:

1) Wang, B., Ohyama, H., Haginoya, K., Odaka, T., Itsukaichi, H., Yukawa, O., Yamada, T. and Hayata, I.: *Radiat. Res.*, **154**, 277-282, 2000.

2) Wang, B., Ohyama, H., Haginoya, K., Odaka, T., Yamada, T. and Hayata, I.: *Radiat. Res.*, **154**, 673-679, 2000.

3) Wang, B.: *Radiol. Sci.*, **43**, 343-347, 2000 (in Japanese).

4) Wang, B.: *J. Radiat. Res.*, **42**, 1-10, 2001.

CLINICAL RESEARCH

57. Experiences of Carbon Ion Radiotherapy at NIRS

Hirohiko Tsujii, Shinroku Morita,
Tadaaki Miyamoto, Jun-etsu Mizoe,
Tadashi Kamada, Hirotoshi Kato,
Hiroshi Tsuji, Shigeru Yamada,
Naotaka Yamamoto and Hajime Murata

Functional and cosmetic preservation is of paramount importance in cancer therapy. For this purpose, heavy ion therapy is an advantageous modality over megavoltage x-ray therapy in terms of safely delivering high doses coupled with increased cell-killing ability. Heavy ions have the beneficial property of superior physical dose localization due to exhibiting the Bragg peak in the body, as well as greater biological effectiveness than low-LET radiation (protons and photons). Thus, heavy ions are expected to be effective against locally advanced radio-resistant tumors and those located near critical structures. In 1993, construction and installation of the Heavy Ion Medical Accelerator in Chiba (HIMAC), the world's first heavy ion accelerator complex dedicated to medical use in a hospital

Table 2. Patient Distribution registered in Carbon Ion Therapy at NIRS
(Treatment: June 1994 to August 2001)

Sites	1994	1995	1996	1997	1998	1999	2000	2001	Total	
Head and neck	9	10	19	31	22	38	29	20	178	(17.1)
Brain	6	8	10	6	9	7	15	4	65	(6.2)
Base of skull	-	-	-	6	4	2	2	2	16	(1.5)
Lung	6	11	27	17	28	33	45	20	187	(17.9)
Liver	-	12	13	19	25	17	22	11	119	(11.4)
Prostate	-	9	18	10	30	30	31	16	144	(13.8)
Uterus	-	9	13	11	10	11	13	2	69	(6.6)
Bone/ soft tissue	-	-	9	13	19	18	25	7	91	(8.7)
Esophagus	-	-	1	16	4	-	2	-	23	(2.2)
Pancreas (pre-op RT)	-	-	-	-	-	-	3	3	6	(0.6)
Rectum (Pelvic rec)	-	-	-	-	-	-	-	2	2	(0.2)
Eye(advanced)	-	-	-	-	-	-	-	4	4	(0.4)
Miscellaneous	-	24	16	30	17	32	14	5	138	(13.2)
Total	21	83	126	159	168	188	201	96	1042	(%)

Table 3. Normal tissue morbidity in carbon ion therapy at NIRS
(Treatment: June 1994 to August 2001)

Site	Early (<3mo)							Late (>3mo)						
	No	0	1	2	3	4	5	No	0	1	2	3	4	5
Skin														
Scalp	77	22	38	14	1	0	0	77	71	6	0	0	0	0
Head & neck	180	2	71	86	21	0	0	172	66	96	10	0	0	0
Chest	206	0	191	14	1	0	0	200	0	198	2	0	0	0
Upper abdomen	128	10	95	22	1	0	0	128	11	113	4	0	0	0
Lower abdomen	212	154	58	0	0	0	0	211	186	25	0	0	0	0
Others	243	14	134	82	13	0	0	230	31	167	22	9	1	0
Total	1046	204	587	218	37	0	0	1018	365	605	38	9	1	0
(%)	(100)	(20)	(56)	(21)	(4)	(0)	(0)	(100)	(36)	(59)	(4)	(0.9)	(0.1)	(0)
Mucosa	168	24	67	64	13	0	0	161	126	28	7	0	0	0
Lung	252	234	8	7	3	0	0	244	59	178	7	0	0	0
Intestine	512	431	66	13	2	0	0	486	413	42	16	7	8	0
Bladder/Urethra	235	194	37	4	0	0	0	234	178	40	9	7	0	0

environment, was completed at NIRS. The HIMAC project was initiated as part of the Japanese government's 10-year plan to combat cancer. In June 1994, clinical research for the treatment of malignant tumors was begun using carbon ions generated by the HIMAC. Since then more than 1,000 patients have been treated with carbon ions, in which both the phase I/II dose escalation study and phase II study were performed.

Tables 2-5 summarize the results of carbon ion radiotherapy including the radiation-induced morbidity, local control, and survival rates for patients with various types of tumors.

Table 4. Results of carbon ion radiotherapy at NIRS (Treatment: June 1994 to August 2001)

Protocol	Phase	Material	Treatment (fractions/week)	No. of patients	Response rate a)	2yr local control b)	3yr survival
H&N-1	I/II	Locally advanced	18/6	17	73%	80%	44%
H&N-2	I/II	Locally advanced	16/4	19	68%	71%	44%
H&N-3	II	Locally advanced	16/4	134	52%	61%	42%
Lung-1	I/II	Stage I (peripheral)	18/6	47(+1)	54%	62%	88%
Lung-2	I/II	Stage I (peripheral)	9/3	34	85%	86%	65%
Lung-3	I/II	Stage I (Hilar)	9/3	10	90%	100%	-
Lung-4	II	Stage I (peripheral)	9/3	50(+1)	65%	100%	73%
Lung-6	I/II	Stage I (peripheral)	4/1	18	67%	-	-
Liver-1	I/II	T2〜4 MONO	15/5	24(+1)	75%	79%	50%
Liver-2	I/II	T2〜4 MONO	4〜12/1〜3	82(+4)	72%	83%	45%
Liver-3	II	T2〜4 MONO	4/1	11	55%	-	-
Prostate-1	I/II	B2〜C	C ion+Hormone	35	-	100%	94%
Prostate-2	I/II	A2〜C	C ion+Hormone	61	-	100%	97%
Prostate-3	II	T1C〜C	C ion+Hormone	47	-	-	-
Uterus-1	I/II	III-Iva(ACC)	24/6	30	100%	50%	40%
Uterus-2	I/II	Iib-Iva(SCC)	24/6	14	100%	67%	36%
Uterus-3	I/II	Iib-Iva(SCC)	20/5	11	100%	-	-
Uterus	I/II	Advanced(Adenoca)	20/5	12	100%	38%	39%
Bone/Soft-1	I/II	un-resectable	16/4	57(+7)	36%	77%	50%
Bone/Soft-2	II	un-resectable	16/4	30(+1)	57%	-	-

a) Response rate : Percent of tumors with >50% reduction in size.
b) Local control rate : Percent of tumors with no evidence of local recurrence or relapse.

Table 5. Clinical studies for Stage I NSCLC

Protocol No.	Lung-1 (9303)	Lung-2 (9701)	Lung-3 (9801)	Lung-4 (9802)	Lung-6 (0001)
Phase	I/II	I/II	I/II	II	I/II
Period of the study	10/'94 to 9/'97	9/'97 to 2/'99	4/'98 to present	4/'99 to 12/'00	12/'00 to present
Tumor Type	All type*	Peripheral	Central	Peripheral	Peripheral
Total Dose (GyE)	59.4〜95.4	68.4〜79.2	57.6〜64.8	72	54 or 60
Fraction / wks (fixed)	18f / 6w	9f / 3w	9f / 3w	9f / 3w	4f / 1w
# Pats (# Tumors)	47(48)	34(34)	15(15)	50(51)	35(35)
Adenoca / SCC / Large cellca	26/22/0	18/15/1	13/2/0	32/19/0	23/11/1

* All type includes both peripheral and central type of tumor.

58. The Dose - Volume Histogram Analysis for Pelvic Tumor Using Carbon Ion Radiotherapy

Takeshi Yanagi, Tadashi Kamada, Hiroshi Tsuji, Shigeru Yamada and Hirohiko Tsujii

Keywords: carbon ion radiotherapy, pelvic tumor

It is important to conform an irradiation beam only to a tumor, and to minimize the dose to the normal tissues around it. International interests exist in the use of charged particles in cancer radiotherapy, because of its good dose distribution. The aim of this study is to confirm the merits of the dose distribution of carbon ion beams compared to photon beams by simulating treatment planning analyzed by dose volume histograms (DVHs).

In comparative treatment planning, two types of pelvic tumor were selected; case 1/sacrum chordoma (volume: 701ml) and case 2/ recurrent rectal cancer (2267ml). Plans for of carbon and conventional photon beams were simulated using CT scans for each pelvic tumor, and the results were analyzed using DVH. In standard photon planning, 3,4,5,7 ports were used in case 1, and 2,3,4,5,6 ports in case 2, and the margin for the planning target volume (PTV) was given to cover the clinical target volume (CTV) with 80 - 100% of the prescribed dose. In carbon planning, 3 ports were used, and the minimum target dose given was at least 90% of the prescribed dose.

As a result, for the target volume, the carbon plans provided good coverage with a homogeneous dose around the maximum dose in both cases. Volumes of both bowels and bladders could be reduced at any dose levels in the carbon plans. Whole irradiated volumes of each case were less at low or middle dose level for carbon ion beams than for photons. Significantly higher dose could be given to 95% of the target with carbon beams than in photons for the bowel dose <50GyE. The use of carbon ion beams provided improved target dose homogeneity and reduced doses to critical structures compared to conventional photon beams.

The use of carbon ion beams provides superior dose localization characteristics to those of photons.

59. Second Cancer Following Radiation Therapy for Uterine Cervical Carcinoma.

Tatsuya Ohno, Hirohiko Tsujii, Kenjiro Fukuhisa, Shinroku Morita, Reiko Imai, Takashi Nakano[1] and Tatsuo Arai[2] ([1] Gunma Univ. School of Medicine; [2] Motojima General Hospital)

Key words: second cancer, radiation therapy, cervical carcinoma

Purpose: To examine the incidence and clinical feature of second cancer following radiation therapy.

Materials and methods: Between 1961 and 1990, 1877 patients with uterine cervical squamous cell carcinoma were treated radically with radiation therapy alone at NIRS. Patients were followed up intensively; 10 years after radiation therapy the follow up rate was more than 90%. We diagnosed a radiation-associated second cancer using the following criteria: (1) difference of histologic type from the primary cancer (except for vagina); (2) latency period of at least 2 years after radiation therapy (RT); and (3) development site in the irradiated field.

Results: Twenty-nine of 1877 (1.54%) patients developed second cancer. The sites of second cancer were rectum in 8 patients, bladder in 3, uterus in 6, ovary in 5, vagina in 2, and bone and soft tissue in 5. Patient age at diagnosis of cervical carcinoma was 40 to 75 years, with a median of 58 years and at diagnosis of second cancer was 49 to 95 years, with a median of 72 years. Latency period from RT to the development of second cancer ranged from 3 to 27 years, with a median of 16 years. Treatment of second cancer consisted of surgery in 12 patients (41%), RT in 4 (14%), and chemotherapy in 1 (3%). Median survival from the diagnosis of second cancer was 7 months.

Conclusion: Radiation therapy for cervical carcinoma results in large numbers of long term survivors who can develop second cancers very late in life. The advantage of radiation therapy may be considered large enough to compensate for the risk of radiation-associated cancer.

60. Usefulness of 3D Ultrasonography in Diagnosis of Hepatocellular Carcinoma and Its Invasively Growing Lesion: Deciding a Precise Target Volume in Radiation Therapy

Hirotoshi Kato, Shuji Yamada, Masao Ohto and Hirohiko Tsujii

Keywords: hepatocellular carcinoma, ultrasonography, Fusion 3D, contrast-enhanced Fusion 3D, contrast-enhanced CT scan

One half of local recurrences of hepatocellular carcinomas (HCC) treated with carbon ion therapy occurred in the tumors that had invasively growing parts in themselves. Vascular invasion is one of the most clinically problematic findings in HCC treatment.

Therefore, more precise examination of invasively growing lesions is essential to advance clinical results in HCC treatment.

Ultrasonography (US) is an examination offering easy observation of the local environment and providing vascular information around the HCC. So, in 1995 we started the study of US for diagnosis of HCC, especially for diagnosis of both tumors and vascular structures with ultrasonographic three-dimensional images (Fusion 3D). We also started a study of Fusion 3D using a contrast agent (contrast-enhanced Fusion 3D). The US machine we used was an Aplio (Toshiba Medical Systems Co., Ltd.) and contrast agent was Levovist (Nihon Schering KK).

We investigated the characteristic features of HCC, including the usefulness of contrast -enhanced Fusion 3D in diagnosis of invasively growing lesions of HCC.

Study 1: Characteristic features of HCC in contrast-enhanced Fusion 3D

We performed contrast-enhanced Fusion 3D on 22 patients with histologically proven HCC (40mm or less in diameter) and 5 with metastatic liver cancer. The results were as follows. 1. We recognized a Network Pattern and Flush Sign as characteristic features of HCC that were thought to be contrast-enhanced vascular images (Figure and Table). None of these features were detected in the metastatic liver cancers. 2. All five HCCs 15mm or less in diameter had the Network Pattern and Flush Sign, 60% of which had early staining and 40% had late washout in the contrast-enhanced CT scan
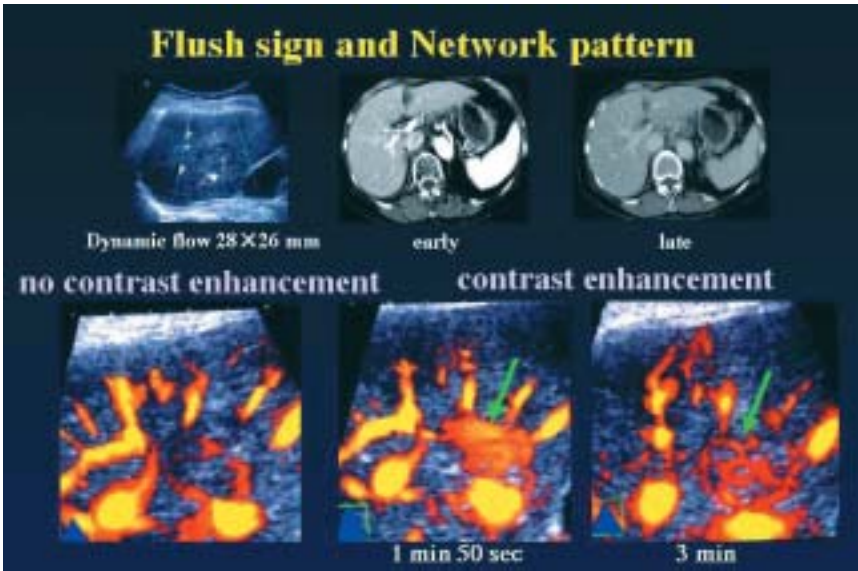
Fig. 26.

Table. 6.

Diameter (mm)	Features	
	Flush	Network
≦15	5 / 5	5 / 5
15＜～≦30	11 / 12	11 / 12
30＜～≦40	5 / 5	5 / 5

with bolus injection of a contrast agent.

Study 2: Diagnosis of invasively growing lesions of HCC with contrast-enhanced Fusion 3D

We performed contrast-enhanced Fusion 3D on 41 patients with histologically proven HCC. The results were as follows. 1. All the invasively growing lesions of HCC had the Network Pattern and Flush Sign. 2. We could detect the invasively growing lesions of HCC with contrast-enhanced Fusion 3D more easily than simple US for both 2D and 3D. 3. HCCs 15mm or less in diameter had no invasively growing lesions, 74% of HCCs more than 15mm in diameter had the lesions. 4. Sixty-seven percent of the invasively growing lesions detected with Contrast-Enhanced Fusion 3D could not be diagnosed by contrast-enhanced CT scan.

In conclusion, contrast-enhanced Fusion 3D may allow the diagnosis of HCC and its invasively growing lesions by such characteristic features as the Network Pattern and Flush Sign, and it may be superior to the contrast-enhanced CT scan especially in small HCC.

61. Cytokine Responses Detected in Blood from Cancer Patients Given X-ray or Carbon Ion Therapy

Shigeru Yamada, Tadashi Kamada and Hiroshi Tsuji.

Ionizing radiation induces an acute inflammatory response in many normal cells and tissues. Exposure of cells to irradiation induces some cytokines such as tumor necrosis factor-alpha (TNF-α) and interleukin-6 (IL-6). Heavy ions are reported to have several advantages compared to conventional photon therapy, including a better physical dose distribution and a higher biological efficiency in tumor cell killing. However there are few data on biological responses in patients treated with heavy ions compared to photon therapy. In this study we examined cytokine responses induced by carbon ions and X-ray irradiation. We measured inflammatory cytokines such as IL-4, IL-6, IL-8, TNF-α and INF-γ. Blood samples from patients with esophageal cancer were obtained before and after treatment. No significant differences in the response of these cytokines from the patients treated with X-rays were detected. On the other hand IL-4, IL-8 and TNF-α displayed similar response with X-rays, however the secretion of IL-6 and INF-γ was induced by the carbon ions. These results suggested cytokine responses differ between X-rays and carbon

ions.

62. Objective Assessment of Cranial Nerve Neuropathy by Heavy Ions

Azusa Hasegawa, Jun-etsu Mizoe, Hitoshi Miyachi, Shogo Hasegawa, Atsushi Mizota and Hirohiko Tsujii

Purpose: In radiation therapy of head and neck cancers, preservation of the Quality Of Life (QOL) is important for patients. Therefore, we evaluated the late effects of carbon ions on the cranial nerve neuropathy as the start for an investigation on safe doses for the cranial nerves. These results are a clinical indicator of the QOL.

Patients and Methods: We selected patients whose trigeminal and/or optic nerves were included in Planning Target Volume (PTV), and we recorded somatosensory evoked potentials before and after carbon ion radiotherapy.

1. Visual Evoked Potential (VEP)
The time-course VEP recording and examination of visual acuity were performed for patients who developed a loss of visual acuity due to tumor invasion. We objectively investigated nerve stimulation using VEP during carbon ion irradiation, and we reconsidered the treatment plan if the nerve pathway is included the in irradiation field.

2. Trigeminal Somatosensory Evoked Potential (TSEP)
TSEP was recorded to examine the clinical availability for patients with/without paresthesia at the time of carbon ion radiotherapy. The stimulating electrodes were composed of a spring clip with upper and lower lips. For patients who were expected to show nerve impairment after irradiation, we recorded the time-course TSEP, and analyzed paresthesia grade.

Results: We are currently still collecting data. This study will be helpful in evaluation of the cranial nerve neuropathy. We present one example case of trigeminal nerve included in PTV. A twenty year-old man was treated using carbon ion radiotherapy. After six months, the early components corresponded with the latency of the normal TSEP (Fig. 27).

| Superior Lip Stimulation | Inferior Lip Stimulation |
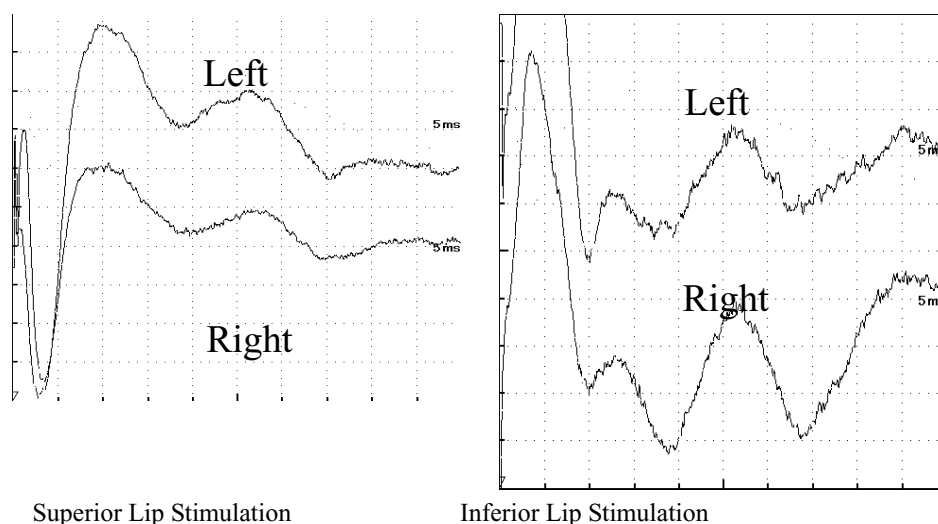
Fig. 27. TSEPs obtained from a subject with undifferentiated carcinoma of left maxillary sinus. The recorded and the stimulated sites are shown in the figure. These waves do not show the impairment of the 5th left cranial nerve.

63. Allelic Loss of Chromosome 2 in Human Oral Squamous Cell Carcinoma: Correlation with Lymph Node Metastasis

Nobuharu Yamamoto[1], Jun-etsu Mizoe,
Hideyuki Numasawa[2], Hidetaka Yokoe[3],
Katsuhiro Uzawa[4], Takahiko Shibahara[2],
Hirohiko Tsujii, Hiroyasu Noma[2] and Hideki Tanzawa[3, 4]
([1]NIRS and Tokyo Dental College;
[2]Tokyo Dental College;
[3]Chiba Univ. Hospital;
[4]Chiba Univ.)

Keywords: tumor, oral squamous cell carcinoma

To evaluate the role of chromosome 2 deletions in human oral squamous cell carcinoma (SCC) progression and to define the precise location of putative tumor suppressor genes, we examined 40 primary tumors and seven lymph node metastatic tumors from 40 patients with oral SCC by the polymerase chain reaction (PCR)-loss of heterozygosity (LOH) assay, using 10 different polymorphic loci on the long arm of chromosome 2. LOH was observed in 67.5% of the patients at one or more loci on the chromosome 2q. Two commonly deleted regions with high frequency of LOH, D2S1327 region at 2q32-35 (31.6%) and D2S206 region at 2q36 (36.7%), were identified by the deletion mapping of chromosome 2q, suggesting the presence of putative tumor suppressor genes associated with oral SCC. Examination of seven metastatic tumors also revealed four commonly deleted regions, D2S436, D2S1327, D2S155 and D2S164. Of these four regions D2S1327 region had no significant increase in the frequency of LOH between in primary tumors and in metastatic tumors. However, for the other three regions, the frequencies were much increased in metastatic tumors, compared to the results in primary tumors. In particular, very high frequencies of LOH in metastatic tumors were detected at two regions on 2q35, 100.0% at D2S155 and 57.1% at D2S164, suggesting a significant relationship between lymph node metastasis and LOH at these two regions. Our results indicate that LOH on chromosome 2q is a common event in oncogenesis and/or progression of oral SCC, and they also suggest that LOH at 2q35 plays a significant role in the lymph node metastasis.

64. Clinical Application of Autoactivation PET Imaging Derived from C-12 Ion Radiotherapy and Its Fusion Imaging with Therapy Planning CT.

Kyosan Yoshikawa, Takehiro Tomitani,
Mitsutaka Kanazawa, Tatsuaki Kanai,
Katsumi Tamura, Takashi Tomemori,
Susumu Kandatsu, Junetsu Mizoe,
Fumio Shishido, Hiroshi Fukuda and Hirohiko Tsujii.

Keywords: autoactivation, carbon ion radiotherapy, HIMAC, PET, CT, fusion imaging

Clinical application of PET imaging of auto activation derived from C-12 ion radiotherapy (HIMAC) was studied. It is very important to perform the PET measurements under exactly the same patient positioning as in HIMAC therapy to compare RI distributions. We performed some clinical PET measurements and got superimposed images of PET and CT planning of

HIMAC therapy patients. We tried to use a fitting method, the automatic multi modality image registration method (AMIR method) of the Dr. View applications. In this method, we fitted the transmission images of PET to planning CT images at the start, and then superimposed emission images on the planning CT images. Our fitting results were relatively good. But some problems were identified. The most important one was due to the difference in patients breathing phases between PET examination and CT imaging. The difference of patients breathing phases should cause fitting errors of the fusion images of PET and CT especially in chest and abdominal regions. To confirm this, we investigated a lung cancer patient who received HIMAC therapy with 15.0 GyE dose per fraction, totally 4 fractions (60 GyE). A PET measurement was done immediately after an irradiation. Two sets of CT images were also taken in both expiration phase and inhalation phase. PET fusion images with the two sets of CT images were calculated and compared with each fusion image. The PET fusion image with CT image in the expiration phase resulted in better quality compared to that in the inhalation phase. We think that the breathing phases of PET and CT should be in phase with each other to perform precise fitting of the two modalities.

between methionine uptake in the tumor and patient survival rate, and of the relation between the changing rate of tumor methionine uptake and tumor local control rate. Tumor methionine high uptake state before HIMAC therapy seemed to suggest tumor malignancy and high risk of occurring metastasis, i.e. prognosis poor. When tumor uptake decreased a lot after HIMAC therapy, it suggested good tumor local control. In study (2), 38 cases with hepatocellular carcinoma were studied by FDG-PET. We found that when the liver function was more damaged, liver tissue showed higher FDG accumulation. There was no relationship between tumor differentiation level and FDG uptake, and between the change of FDG uptake after HIMAC therapy and the reduction rate of tumor size. Cases that showed high reduction of tumor FDG uptake after HIMAC therapy tended to show reduced AFP level. In study (3), 9 cases with breast tumor were studied by methionine PET. All breast carcinoma showed positive accumulation of methionine. There was no relationship between methionine uptake level and FDG uptake level. We think that methionine PET gives different information about breast tumor, about differentiation between benignancy and malignancy, and about prognosis after treatment etc., in comparison with FDG-PET.

65. Functional Diagnosis of Cancer Using PET

Kyosan Yoshikawa, Katsumi Tamura, Takashi Tomemori, Noriyo Matsuno, Masahisa Koga, Susumu Kandatsu, Tetsuya Suhara, Kazutoshi Suzuki, Hirotoshi Kato, Junetsu Mizoe, Osamu Inoue, Fumio Shishido, Hiroshi Fukuda and Hirohiko Tsujii

Keywords: Positron emission tomography (PET), C-11 methionine, head and neck cancer, hepatocellular carcinoma, breast tumor

Positron emission tomography (PET) can demonstrate increased metabolic demand as visual images, and it provides alternative information for diagnosis that can be used to complement morphological observations. This year, we carried out three studies on (1) the usefulness of methionine PET for evaluation of the therapeutic effect and prognosis in head and neck cancer, (2) the imaging ability of FDG-PET for hepatocellular carcinoma, and (3) the imaging ability of methionine PET for breast tumor. In study (1), 22 cases with head and neck cancer were followed long term (70.3 months maximum) after HIMAC therapy. Kaplan-Maier methods were applied for evaluation of the relation

66. The Cancer Functional Diagnosis and the Evaluation of Therapeutic Effects Using Magnetic Resonance Imaging and Spectroscopy

Masahisa Koga, Kyosan Yoshikawa, Takayuki Obata, Jun-etsu Mizoe and Hiroo Ikehira

Keywords: magnetic resonance spectroscopy(MRS), positron emission tomography(PET).

Thirty seven patients with abnormal T2-elongated space showing a brain lesion in magnetic resonance imaging were studied with multi-slice proton magnetic resonance spectroscopic imaging (multi-slice ^{1}H-MRSI) and positron emission tomography(PET). MRS images were obtained by combining volume-selective excitation with phase encoded acquisition. Choline maps were created and compared with PET maps of methionine metabolism. Choline signal elevation seen in brain neoplasms was associated with increased cellular proliferation. Elevation of choline signal seemed most cases of regrowth of brain tumor, whereas loss of choline signal showed brain necrosis (Figs. 28-30).
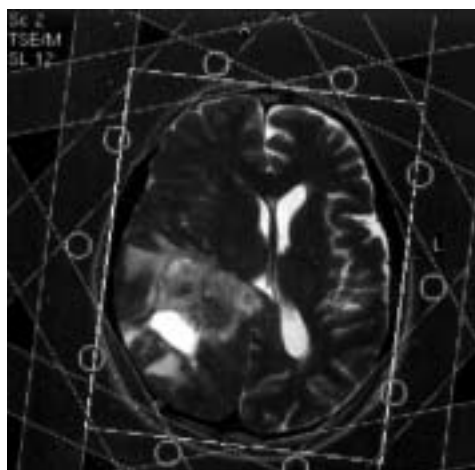
Fig.28. MRI: glioblastoma multiforme
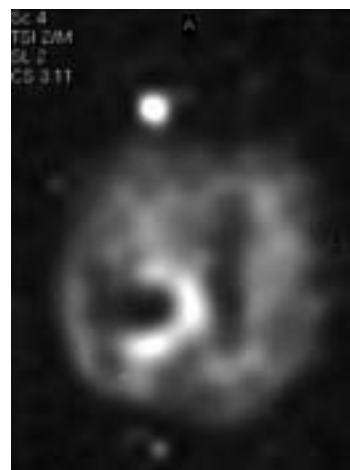
Fig.29. MRSI choline imaging
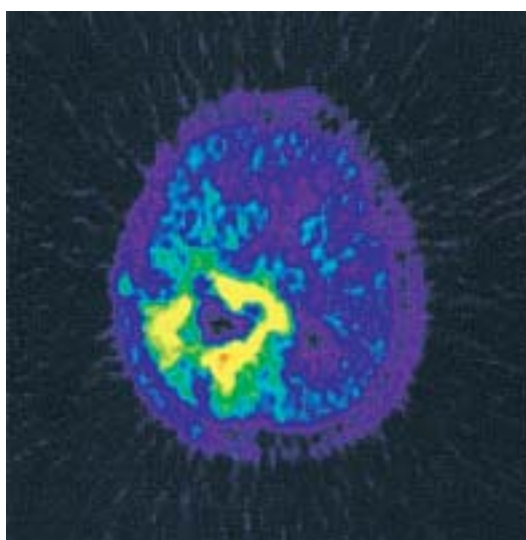
Fig. 30. PET: C-11 Methionine

67. Synthesis and Preliminary Evaluation of [¹⁸F]FEtP4A, a Promising PET Tracer for Mapping Acetylcholinesterase *in vivo*

Ming-Rong Zhang, Akio Tsuchiyama,
Terushi Haradahira, Kenji Furutsuka,
Yuichiro Yoshida, Takayo Kida,
Junko Noguchi, Toshiaki Irie and Kazutoshi Suzuki

Postmortem studies on patients with Alzheimer's disease showed a reduction in the activity of acetylcholinesterase (AchE) in the neocortex and hippocampus, compared with normal subjects.   To measure brain AchE activity and further elucidate the relationship between AchE and Alzheimer's disease, *N*-F-18-fluoroethyl-4-piperidyl acetate ([¹⁸F]FEtP4A), a F-18 analog of [¹¹C]→MP4A, was designed, synthesized and evaluated as a PET tracer for imaging AchE *in vivo*. Since this tracer, possessing aminoalkyl acetate moiety, is an acetylcholine derivative, [¹⁸F]FEtP4A may readily enter the brain and be specifically metabolized by AchE into the hydroxy product ([¹⁸F]FEtP4OH) which can be retained at the site of the hydrolysis enzyme in the brain. Moreover, the longer half-life of ¹⁸F offers the advantage to get more precise AchE activity information in the PET measurement, and to deliver the tracer to other facilities.   Based on these considerations, [¹⁸F]FEtP4A is expected to become a useful PET tracer for measurement of AchE activity *in vivo*.

[¹⁸F]FEtP4A was prepared by reacting 4-piperidyl acetate (P4A) with 2-[¹⁸F]fluoroethyl bromide ([¹⁸F]FEtBr) using a newly developed automated system with 76 ± 4 min of total synthesis time from the end of

bombardment. At the end of the synthesis (EOS), 380 ±120 MBq (n = 3) of [^{18}F]FEtP4A were obtained after 15-25 min proton bombardment at a beam current of 15 μA with 49 ± 18% of radiochemical yield (based on [^{18}F]FEtBr, corrected for decay). The radiochemical purity and specific activity of [^{18}F]FEtP4A were 97 ±1.9% and 270 ± 45 GBq/μmol at EOS. In the final product solution (10 mL), the contamination of P4A was quantified using LC/MS and determined to be 0.06-0.2 ppm. Preliminary evaluation showed that the initial uptake of [^{18}F]FEtP4A into mouse brain was > 8% injected dose/g tissue. The radioactivity washout of [^{18}F]FEtP4A from all regions examined on the stationary phase (10-120 min after *iv* injection) followed monoexponential curves with similar elimination rates with half-lives of about 30 min. The rank of uptake of [^{18}F]FEtP4A in these regions on the stationary phase agreed with that of AchE in the brain: striatum > cerebral cortex > cerebellum. The chemical analysis of *in vivo* radioactive metabolites indicated 83% of [^{18}F]FEtP4A was hydrolyzed to [^{18}F]FEtP4OH at 1 min postinjection, suggesting that this hydrolysis process was mediated by AchE. Therefore, this tracer may be useful as an imaging agent for mapping the AchE activity *in vivo* and assessing the extent of cholinergic neuronal damage in Alzheimer's disease.

Publications:

1) Zhang M-R., Tsuchiyama A., Haradahira T., Furutuka K., Yoshida Y., Kida T., Noguchi J., Irie T. and Suzuki K.: *Nuclear Medicine and Biology*, **29**, 463-468, 2002.
2) Zhang M-R., Tsuchiyama A., Haradahira T., Yoshida Y., Irie T. and Suzuki K. : *J. Labelled Compds and Radiopharm*., **44**, s883 - s885, 2001.

68. Effect of Donepezil on Brain AChE Activity in Patients with Alzheimer's Disease Measured by PET

Hitoshi Shinotoh, Kiyoshi Fukushi,
Shin-Ichiro Nagatsuka, Hiroki Namba,
Akiyo Aotsuka, Noriko Tanaka,
Tsuneyoshi Ota, Shuji Tanada and Toshiaki Irie

Keywords: *positron emission tomography (PET), acetylcholinesterase, ^{11}C-MP4A, Alzheimer's Disease, donepezil*

Acetylcholinesterase (AChE) inhibitors such as donepezil have been used for the treatment of Alzheimer's disease (AD). The recent development of carbon-11 labeled acetylcholine analogues such as *N-*[^{11}C]methylpiperidin-4-yl acetate ([^{11}C]MP4A) and propionate([^{11}C]MP4P) has made it possible to determine brain AChE activity by PET. We have measured the effect of donepezil on brain AChE activity in patients with AD. For the quantification of AChE activity, two methods of kinetic analysis were used: a standard non-linear least square (NLS) analysis using arterial input function and a simple method for direct estimation of AChE activity without the use of an arterial input function, namely "shape analysis".

Nine patients with probable AD (three men and six women, 60±7 years) participated in this study. Patients with AD were scanned once before and once during donepezil therapy (5 mg/day in 8 patients and 3mg/day in one patient). A sequence of 16 PET scans was acquired covering 60 minutes after intravenous injection of [^{11}C]MP4A (approximately 740 MBq) in each subject. Arterial blood samples were collected 24 times in 15 minutes after intravenous tracer injection for measurement of total radioactivity and metabolite analysis. A standard NLS analysis was performed to yield estimates of K_1 (transport into tissue), k_2 (tissue clearance of unchanged tracer into blood), and k_3 (hydrolysis rate of [^{11}C]MP4A by AChE, i.e. AChE activity) using metabolite corrected arterial plasma input function. In the shape analysis, k_3 values were estimated in the following formula; $C_M(n) - C_M(n-1) = k_3 \times C_S(n-1) \times DT(n)$, where $C_M(n)$ is concentration of metabolic product at frame n, $C_S(n-1)$ is concentration of authentic tracer at frame n-1, and $DT(n)$ is duration of the scan at frame *n*. The PET data consisting of observed (from 0 to 3min) and fitted (from 3 to 50min) data points were interpolated to yield an eight-fold increase in the number of data points prior to shape analysis calculation.

Authentic tracer was remarkably increased by factors of 1.5 at the peak and 3.5 at 15 minutes after tracer injection during donepezil therapy compared with the baseline study. In the NLS analysis, k_3 values in the cerebral cortex were 0.061±0.004 min^{-1} (mean±SD, n=9) in the baseline study and 0.038±0.005 min^{-1} (n=9) during donepezil therapy. The % inhibition of cortical k_3 values by donepezil therapy was 37.5±7.1% (n=9) in the NLLS analysis. In the shape analysis, cortical k_3 values were 0.056±0.006 min^{-1} (n=9) in the baseline study and 0.039±0.005 min^{-1} (n=9) during donepezil therapy. The % inhibition of k_3 by donepezil therapy was 30.3±9.4% (n=9) in the shape analysis. In both methods, cortical k_3 values were highly significantly reduced by donepezil (n=9, p<0.0001 in paired t-test). There was a trend toward linear correlation between % inhibition in the NLLS analysis and the shape analysis.

The present results suggest the feasibility of measuring the effect of clinical doses of donepezil by PET for both methods of kinetic analysis with [^{11}C]MP4A. These techniques may be useful for

monitoring therapeutic effect of AChE inhibitors in AD.

69. Reference Tissue-based Kinetic Analysis of [^{11}C]MP4A PET Data without Arterial Input Function

Shin-ichiro Nagatsuka, Kiyoshi Fukushi,
Hitoshi Shinotoh, Noriko Tanaka,
Akiyo Aotsuka, Tsuneyoshi Ota,
Hiroki Namba, Shuji Tanada and Toshiaki Irie

Keywords: *positron emission tomography (PET), acetylcholinesterase, ^{11}C-MP4A, kinetic analysis*

N-[^{11}C]Methylpiperidin-4-yl acetate ([^{11}C]MP4A) has been used for positron emission tomography (PET) to determine cerebral regional acetylcholinesterase (AChE) activity quantitatively. The arterial input function is required in the conventional kinetic analysis of [^{11}C]MP4A PET data using nonlinear least squares optimization. We have evaluated a simplified kinetic analysis based on a reference tissue without using an arterial input function.

The kinetics of irreversible radiotracers has been analyzed by a linear algorithm involving tissue radioactivity C(t), arterial input function Ca(t), and kinetic parameters of K_1(transport into tissue), k_2(tissue clearance of tracer into blood) and k_3(irreversible transfer rate):

$$C(t) = K_1 \int Ca(t)dt + K_1 k_3 \iint Ca(t)dt - (k_2 + k_3) \int C(t)dt$$

Because [^{11}C]MP4A showed flow-dependent kinetics in regions with very high AChE activity such as striatum or cerebellum, we assumed that the time-courses of radioactivity in these reference tissues were equivalent to the integral of arterial input function, and derived the following operational function:

$$C(t) = K_r Cr(t) + K_r k_3 \int Cr(t)dt - (k_2 + k_3) \int C(t)dt$$

where Cr(t) is radioactivity of reference tissue and Kr is the ratio of K_1 between target and reference tissues.

[^{11}C]MP4A PET data obtained from 10 normal subjects and 20 patients with Alzheimer's disease (AD) were analyzed by the linear least squares analysis (LLS)

using a reference tissue and the nonlinear least squares analysis (NLS) using the arterial input function to obtain regional k_3, an index of AChE activity. When the cerebellum was used as the reference tissue, LLS gave an almost identical neocortical k_3 as NLS ([LLS k_3]=0.99[NLS k_3], r=0.95, p<0.001). Meanwhile, LLS using the striatum was susceptible to head motion of subjects because of smaller ROI size. Reduced neocortical AChE activity in AD patients as compared with normal subjects was shown by LLS of 21.4% (average of 5 regions), which was also comparable with the result from NLS (24.3%). Additionally a Monte-Carlo simulation study showed both LLS and NLS gave stable k_3 estimates (bias within ±5%, CV less than 10%) for regions with k_3/k_2 ratio of up to 2.0, covering the regions with low (cortex) to moderate (thalamus) AChE activity.

The present LLS using a reference tissue was almost equivalent to NLS in determining regional AChE activity in cortex and thalamus. We conclude that this non-invasive method is practical and useful for quantitative measurement of cortical AChE activity with [^{11}C]MP4A.

70. Brain N-acetylaspartate Is Elevated in Pelizaeus-Merzbacher Disease with PLP1 Duplication

Jun-ichi Takanashi, Mika Tomita, Hiroo Ikehira,
Shuji Tanada, Eiji Yoshitome and Youichi Kohno

Keywords: *Pelizaeus-Merzbacher disease, proteolipid protein gene 1, proton MRS*

We assessed alterations in brain metabolites of patients with Pelizaeus-Merzbacher disease (PMD) with the proteolipid protein gene 1 (PLP1) duplications using quantitative proton MRS. Five unrelated male Japanese patients with PMI and PLPl duplications were analyzed by an automated proton brain examination with the point resolved spectroscopy technique (repetition and echo time of 5,000 and 30 msec). Localized spectra in the posterior portion of the centrum semiovale were acquired, and absolute metabolite concentrations were calculated using the LCModel. Absolute concentrations of N-acetylaspartate (NAA), creatine (Cr), and myoinositol (MI) were increased by 16% (p < 0.01,),

43% (p < 0.001), and 31% (p < 0.01) in patients with PMD as compared with age-matched controls. There was no statistical difference in choline concentration. The increased concentration of NAA, which could not be detected by previous relative quantitation methods, suggests two possibilities: axonal involvement secondary to dysmyelirlation, or increased cell population of oligdendrocyte progenitors. Elevated Cr and MI concentrations may reflect reactive astrocytic gliosis. Our study thus emphasizes the importance of absolute quantitation of metabolites to investigate the disease mechanism of the dysmyelinating disorders of the central nervous system.

71. The Measurement of the Electrical Properties of Human Skin and the Variation among Subjects with Certain Skin Conditions

Takahiro Sunaga, Hiroo Ikehira,
Shigeo Furukawa, Hiroshi Shinkai,
Eiji Yoshitome, Takayuki Obata,
Shuji Tanada, Hajime Murata and Yasuhito Sasaki

Keywords: *dielectric constant, human skin, skin conditions, MRI*

In this study the dielectric properties are reported for human skin tissues over the frequency range 1-450MHz at 36 ℃. Healthy volunteers, collagen disease patients and dialysis patients are studied in order to investigate, primarily, the variability among (1) different regions of one individual, (2) the same region among different individuals and (3) skin conditions due to diseases. Considerable differences exist among skin dielectric properties obtained from different regions of one individual body. Although region dependence is observed, larger variability is found even in the same skin region among individuals.

The results indicate that considerable differences exist between the skin dielectric properties obtained from different regions of one individual body. These wide range distributions reflect variations in tissue composition. Biological tissues are inhomogeneous and have considerable variability in structure and composition and hence in dielectric properties. In addition, differences between subjects are also revealed. The variability of mean values at higher frequencies is 20, 5, 8 and 3% in palm, temple, neck, and abdomen regions, respectively.

Although results from some regions such as the abdomen agree, it is found that dielectric constant values of the same regions can have a difference of more than 20% over the entire range of frequencies between two subjects. Conductivity values are obtained from the expression $\sigma = 2\pi f\, \xi_0\, \xi^{11}$, where ξ^{11} is the loss factor of complex permittivity, ξ_0 is the dielectric constant of free space and f is the frequency of the applied electromagnetic field. The experimental data points shown at each frequency are the average set of three to five measurements on this region of each subject, and in all cases the inaccuracy of measurement is never greater than 5%. This inaccuracy can be attributed to a combination of experimental error and the natural heterogeneity of the tissue. Measurement on distilled water produces both relative dielectric constant and conductivity values within 1.5% of the literature values at the lower frequencies and more accurate values (less than 1%) at higher frequencies. Thus, this decreased accuracy has evidently arisen from heterogeneity in the skin tissue rather than from experimental errors. The spectrum of the relative dielectric constant ξ^1 displays a high frequency tail and frequency dependence decreases generally as ξ^1 dispersion up to about 200 MHz. At frequencies above around 200 MHz, the value of ξ^1 decreases very slightly with frequency while the conductivity σ increases gradually. The total spreads from the mean values among the five subjects are estimated to be about 19% and 12% in the dielectric constant and 27% and 24% in conductivity values at 64 MHz and 420 MHz, respectively.

No remarkable change is detected in the dielectric constant among the three groups. Region dependence of dielectric properties is observed. The spreads at lower frequency on the tail of dispersion are larger than at higher frequency. This tendency is generally observed in both dielectric constant and conductivity.

From our study and other previous reports, it is acknowledged that most of the relative dielectric constant values of the human skin are distributed in the range 20-50, while the conductivity values are in the range 0.1-0.8 at frequencies higher than 200 MHz.

72. Decreased Dopamine D2 Receptor Binding in the Anterior Cingulate Cortex in Schizophrenia

Tetsuya Suhara, Yoshiro Okubo, Fumihiko Yasuno,
Yasuhiko Sudo, Makoto Inoue, Tetsuya Ichimiya,
Yoshifumi Nakashima, Kazuhiko Nakayama,
Shuji Tanada, Kazutoshi Suzuki,
Christer Halldin and Lars Farde

The clinical efficacy of dopamine D2 receptor antagonism on the psychotic symptoms of schizophrenia has been widely demonstrated. However, most in vivo imaging studies have not been able to detect significant changes in striatal D2 receptors in schizophrenia. On the other hand, a number of studies have reported abnormalities in the cerebral cortex of schizophrenia. The aim of this study was to examine the extrastriatal D2 receptors of patients with schizophrenia.

Eleven drug-naïve male patients with schizophrenia were examined with positron emission tomography using [^{11}C]FLB 457. Symptoms were assessed using the brief psychiatric rating scale (BPRS). Eighteen healthy controls were used for comparison. Region of interest analysis was performed using the reference tissue method and binding potential (BP) was used for the index of dopamine D2 receptor binding. The BP value was significantly lower, by about 12.5 %, in the anterior cingulate cortex in drug-naïve patients with schizophrenia than in normal controls. A significant negative correlation was observed between BP in the anterior cingulate cortex and the positive symptom score on BPRS. It was concluded that lower BP values indicate fewer D2 receptors in the anterior cingulate cortex in patients with schizophrenia. Alterations in D2 receptor function in the extrastriatal region may underlie the positive symptoms of schizophrenia.

73. Development of an ECR Ion Source for Carbon Ion Therapy

Masayuki Muramatsu, Atsushi Kitagawa,
Yukio Sato and Satoru Yamada

Ion sources for medical facilities should have characteristics of easy maintenance, low electric power, good stability and long lifetime (on the order of one year). A compact ECR ion source with all permanent magnets is one of the best types for these purposes.

A tentative goal of the source performance has been set at around those of existing 10 GHz NIRS-ECR ion source. The size of the magnets and their arrangement were determined in a way that both the peak and minimum values in the mirror field become close to those of the 10 GHz ion source. The magnetic field was calculated using the POISSON/SUPERFISH code. We measured the magnetic field to confirm the difference between the calculated and measured values by using a Hall generator. The results showed a small reduction compared to the designed value; 10% in the maximum mirror field and 5% in the sextupole field, though these reductions should be acceptable.

Based on previous experience with the ECR ion source, we modified the structure for the present source regarding three points. First, the length of the sextupole magnet was extended to cover the full mirror field region, aiming at good confinement of electrons. Second, the extraction electrode was cooled by water. This modification was very effective to reduce outgassing from the chamber wall and to keep a good vacuum around the extraction region, even for cw operation. Third, the Einzel lens was moved 150 mm away from the ion source, which enabled us to suppress the PIG discharge due presumably to the leakage of magnetic flux. These modifications raised reliability of the source. A schematic view of the modified source is shown in Fig. 31.

Tuning parameters of the source are only three; gas-flow rate, microwave power and frequency, which ensure easy operation. The microwave frequency is changeable between 9 and 18 GHz, with the maximum power of 300 W. A traveling-wave-tube (TWT) amplifier was employed in order to find the optimum frequency for the fixed and uncontrollable magnetic field.

The ion source has been operated both under pulse and cw modes with the TWT amplifier. In the case of low-duty pulsed mode operation (2 Hz, 3.5 ms), the source can produce the intensity of 180 eμA for C^{4+}, which is close to our goal of 200 eμA. In this case, the microwave frequency is 10.524 GHz, the microwave power is 300 W and the extraction voltage is 25 kV. Our best record for C^{4+} is 220 eμA. In the case of high-duty pulsed mode operation (300 Hz, 1 ms), the beam intensity of 100 eμA is obtained for C^{4+} with good stability. Our best record under this mode is 140 eμA, which is somewhat smaller than the required value. The poor intensity under the high-duty mode seems to be due to outgassing from the heated plasma chamber; the yield of highly charged ions generally decreases as the vacuum becomes worse.

The emittance is one of the most important information to judge beam qualities. The horizontal
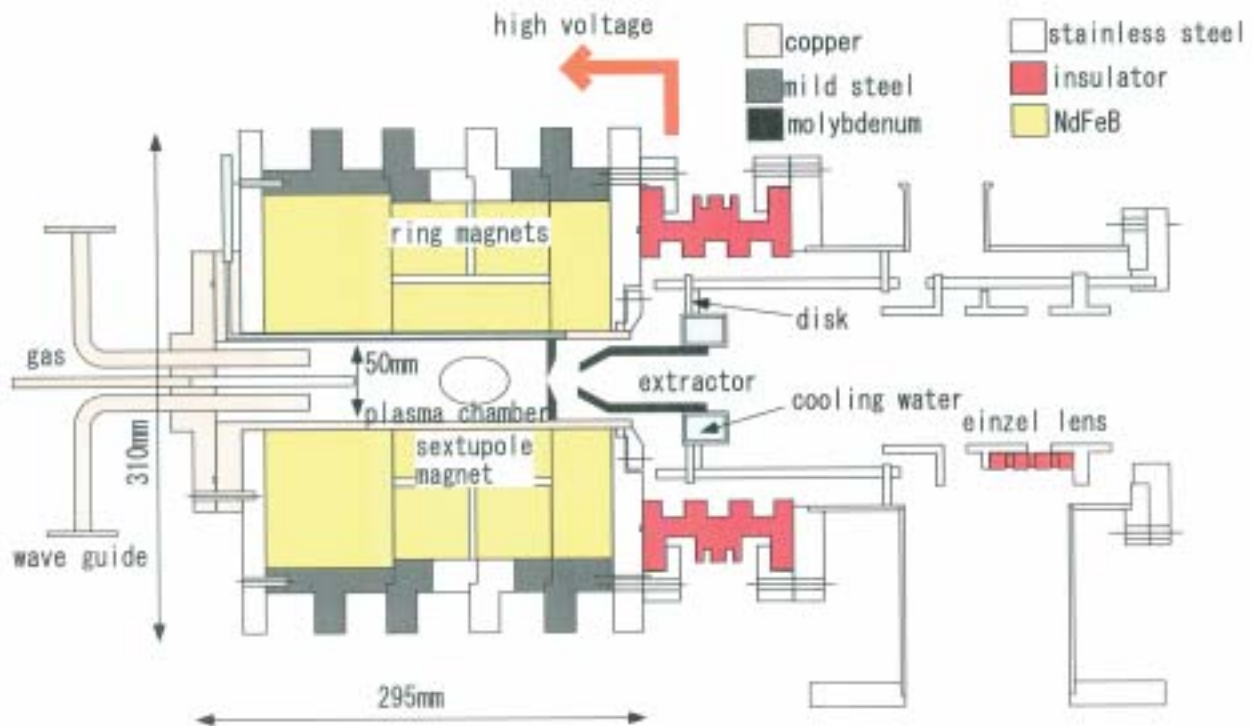
Fig. 31. Schematic view of our modified ion source.

emittance of C^{4+} ions with CH_4 gas was measured using a multi-slit and a scanner. The multi-slit has 13 slits with a spacing of 6 mm and a width of 0.4 mm. The scanner is located 80 mm downstream from the multi-slit. Parameters of the source are optimized to the production of C^{4+} and the beam intensity is 140 eμA in cw operation. The 90% emittance of C^{4+} is 240 π mm mrad (unnormalized), which is 3 times larger than the expected value (80 π mm mrad). We believe that this is due to non-optimization of the extraction scheme.

In the case of the high-duty pulsed mode, the beam intensity of 140 eμA for C^{4+} is obtained which does not reach the required value (200 eμA). The ion source will, therefore, be systematically tested by using a double-frequency heating technique and a biased disk method in order to increase the beam intensity. The horizontal emittance is quite large (240 π mm mrad). In order to improve this, optimization of the extraction configuration will also be necessary.

Publications:
1) Muramatsu M. et al., *Rev. Sci. Instrum.* **71[2]**, 984-986, 2000.
2) Muramatsu M. et al., *Rev. Sci. Instrum.* **73[2]**, 573-575, 2002.

74. Evaluation of Functional Changes in the Cerebral Cortex with Clustering:Multi-functional PET Images Taken Pre- and Post Operation

Hinako Toyama, Kazuhiro Takazawa[1],
Tadashi Nariai[2], Koji Uemura[1],
Kenji Ishii[3], Keiichi Oda[3] and Michio Senda[3]
([1]Waseda Univ.; [2]Tokyo Medical and Dental Univ.;
[3]Tokyo Metropolitan Institute of Gerontology)

Keywords: *positron emission tomography(PET), hemodynamic deficiency*

We developed a method of clustering the brain pixels on the basis of different stages of hemodynamic deficiency using three sets of PET images and applied it to evaluate the regional vasodilative and vasoconstrictive reactivity before and after revascularized surgery in chronic occlusive cerebrovascular disease.(Fig.32). The 3D brain surface, representing the cortical rim in the transaxial images, was projected on a 2D plane by utilizing a Mollweide projection because of the advantages of treating the cortical rim once and saving computation time. Four anatomically and pathophysiologically different areas were delineated with four clusters in these two cases with cerebrovascular disease. (Figs.33-35). Functional changes in the revasvularized region are depicted on the clustered brain images.
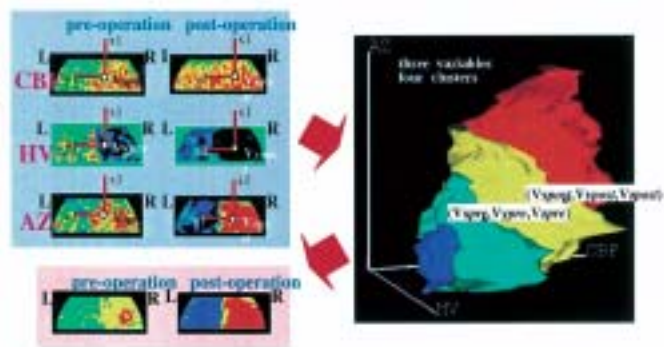
Fig. 32. Three- variable correlation map, in which the pixel values of resting CBF, the hyperventilatory (HV) response, and the acetazolamide (AZ) response was plotted on X-, Y-, and Z-coordinates, respectively. The clustered correlation maps of three variables by means of agglomerative hierarchical method (left-lower).
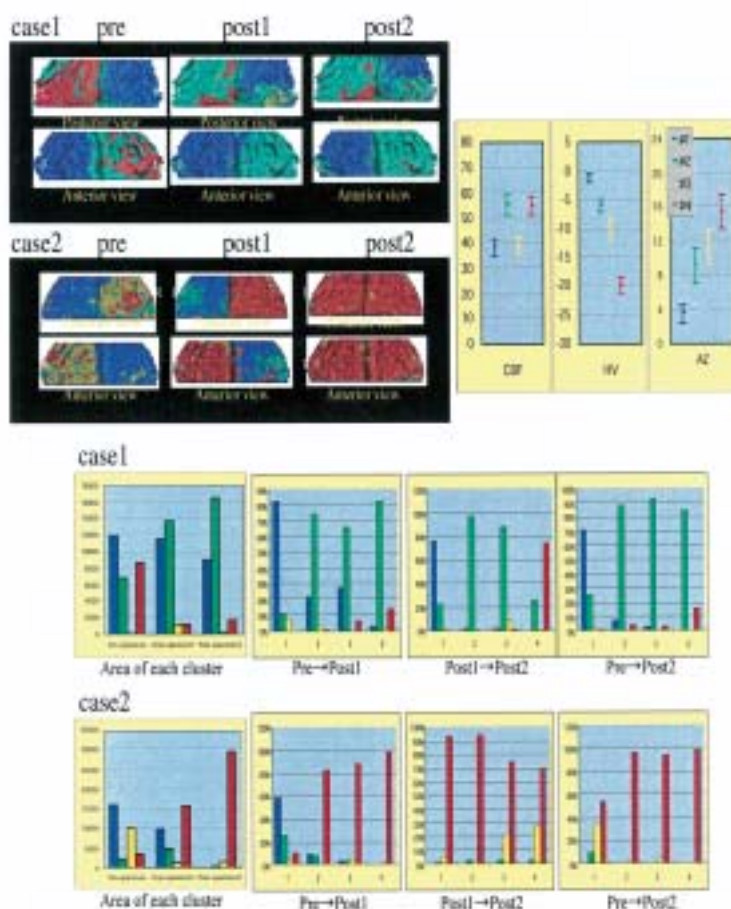
Fig. 33. Two cases with ICA occlusion (case 1 and case 2) were analyzed together by using a correlation map. **Case 1:** A 60-year-old male with occlusion of the right cervical ICA . The territories of the right anterior cerebral artery (ACA) and middle cerebral artery (MCA) were only fed by a poorly developed anterior communicating artery from the left side. Since the right posterior cerebral artery (PCA) was not visualized by vertebral angiography, the occluded right ICA was thought to have had a fetal-type posterior communicating artery. The patient once presented transient left side weakness and was found to have multiple cerebral infarctions on MRI. The superficial temporal artery (STA)-MCA anastomosis was performed on the right side. PET studies were performed before and three and eleven months after the surgery. **Case 2:** A 53 year old male with severe (> 95%) stenosis of bilateral cervical internal carotid and bilateral intracranial vertebral artery. He presented transient weakness on right extremities and small infarction was detected on left parietal subcortical area. Staged cervical endoarterectomy was performed at first on the right side and hal year later on the left side. Before, during and after the operation, he did not present any ishchemic symptom again. PET measurement was performed before the operation, 2 months after the first and the second operations.
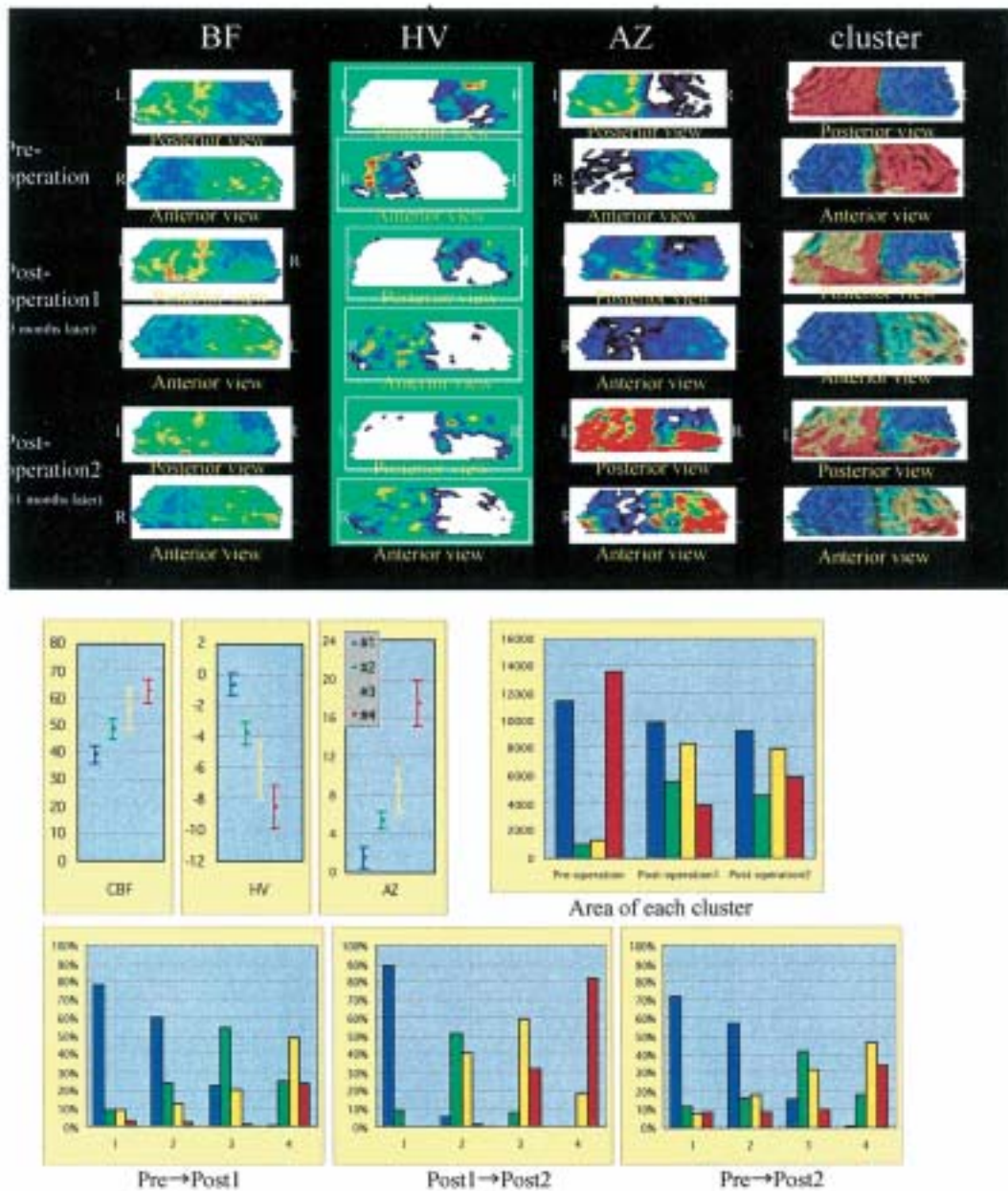
Fig. 34. (Case 1: ICA occlusion) The upper row shows 2D-projection images of pre- and post-operative CBF, HV, AZ and clustered maps. The mean and SD values are shown in the middle row; #4 (red) = cortex with hyper CBF and hyper responses to AZ and to HV, #3 (yellow)= normal, #2(green)= cortex with impaired vasodilative response to AZ and less vasoconstrictive response to HVand #1 (blue) = cortex with abnormal value in all three variables. In the patient with the occlusion of ICA, the area of segment #1 located at the operated region in the pre-operative image became into segment #3 (normal) with revascularization in the post-operative (the STA-MCA anastomosis) image. The areas of each segment in three scans are shown on the right side of middle row. The % changes of area of each segment between two scans are shown in the lower row.
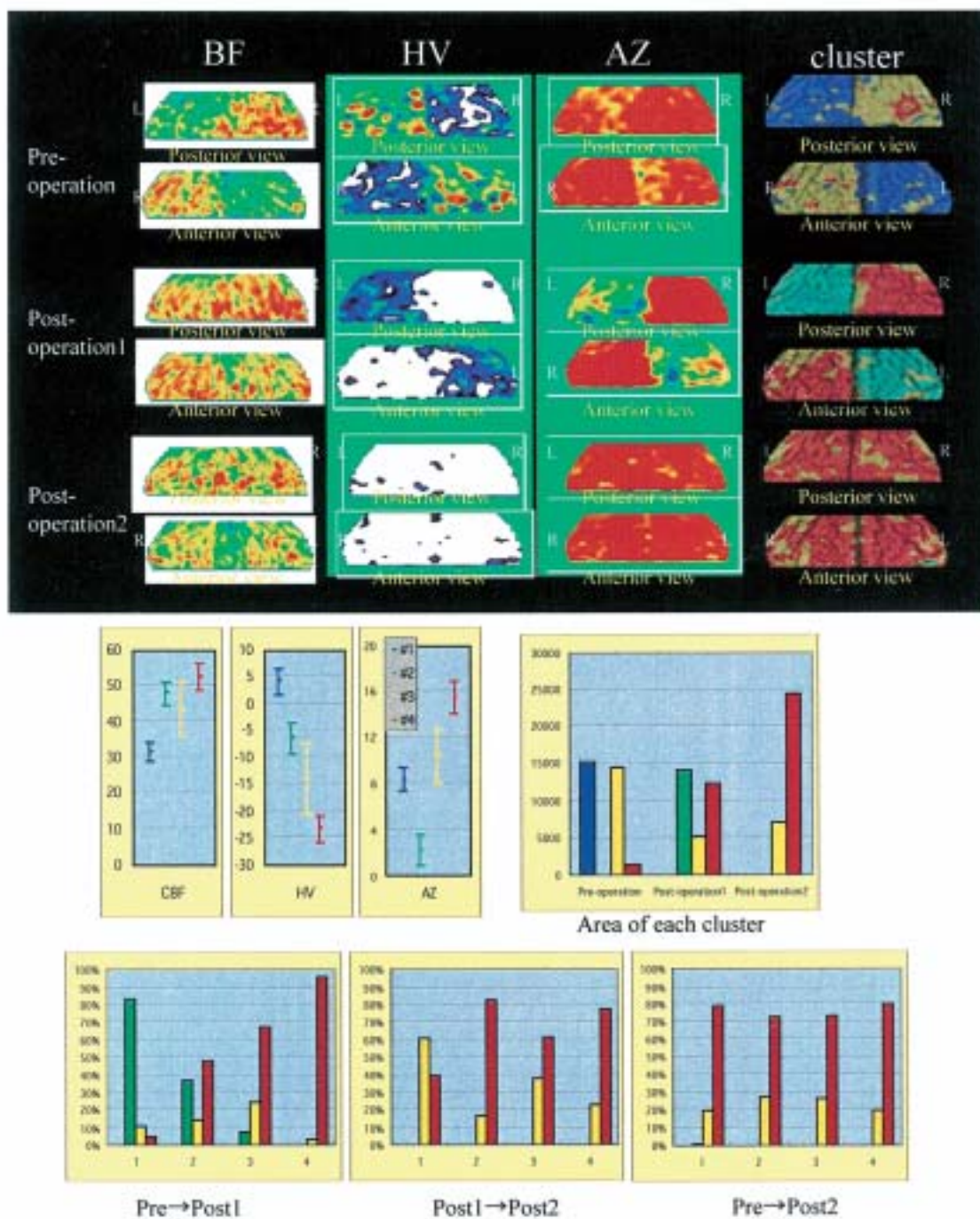
Fig. 35. (Case 2: ICA occlusion) The upper row shows 2D-projection images of pre- and post-operative CBF, HV, AZ
and clustered maps. The mean and SD values are shown in the middle row; #4 (red) = cortex with hyper CBF
and hyper responses to AZ and to HV, #3 (yellow)= normal, #2(green)= cortex with impaired vasodilative
response to AZ and less vasoconstrictive response to HV and #1 (blue) = cortex with abnormal value in all three
variables.

This clustering was considered to be useful for multivariate staging of hemodynamic deficiency in obstructive cerebrovascular disease and that it is suitable for objective representation of multiple PET parameters obtained in the activation study as well as in a study with ^{15}O labeled CO_2, O_2 and CO gases. Two more cases involved Moyamoya disease(Fig.36 and 37) and results with the method were satisfactory.
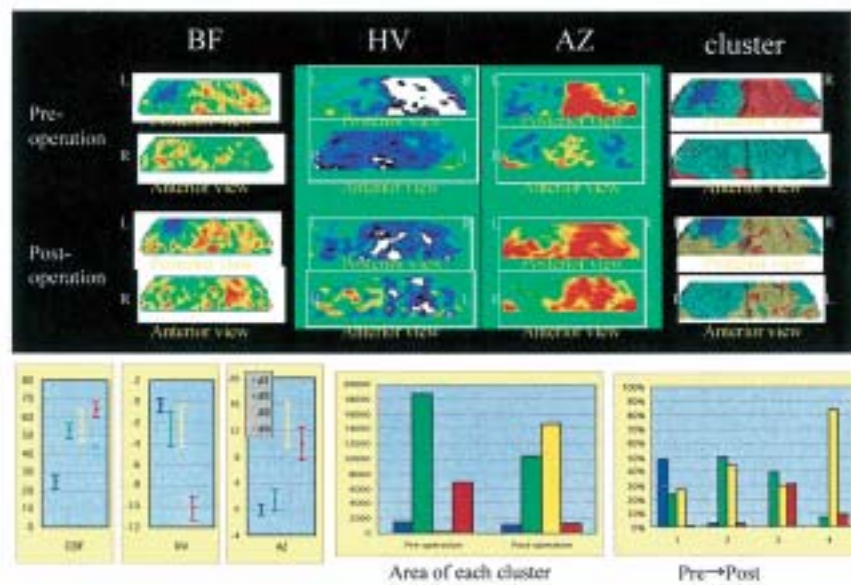
Fig. 36. (Case 3: Moyamoya disease) The upper row shows 2D-projection images of pre- and post-operative CBF, HV, AZ and clustered maps. The mean and SD values are shown in the left side of the lower; #4 (red) = normal cortex, #3 (yellow)= cortex with less vasoconstrictive response to HV and, #2(green)= cortex with impaired vasodilative response to AZ and less vasoconstrictive response to HV and #1 (blue) = cortex with abnormal value in all three variables. **Case 3:** A 40 year old male with moyamoya disease presented right hemianopsia and aphasia with left temporoparietal infarction. His aphasia recovered well but had been suffering from transient aphasia and right hemiparesis. Indirect bypass surgery (EDAS) was performed on bilateral side. His transient symptom completely disappeared after operation. PET measurement was performed before and one year after the operation.
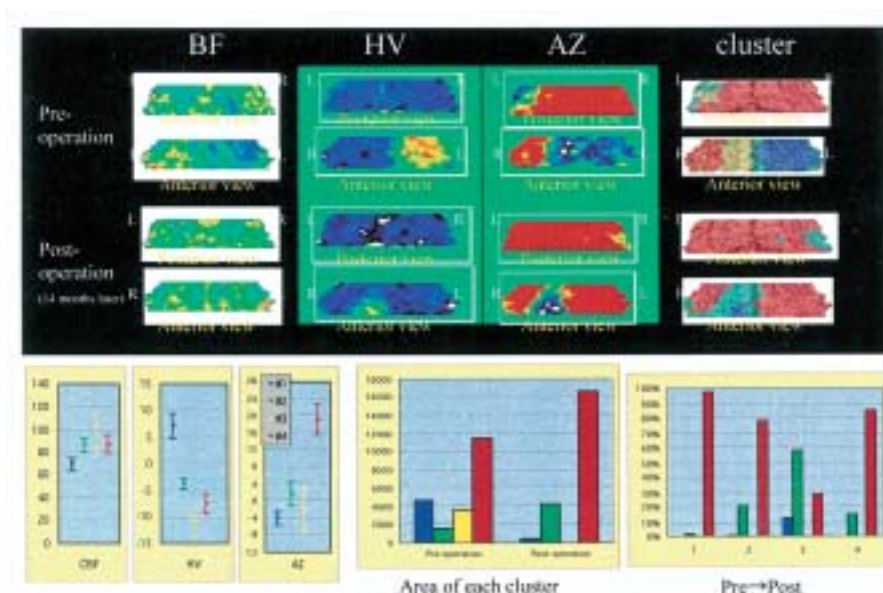
Fig. 37. (Case 4: Moyamoya disease) The upper row shows 2D-projection images of pre- and post-operative CBF, HV, AZ and clustered maps. The mean and SD values are shown in the left side of the lower; #4 (red) = normal cortex, #3 (yellow) and #2(green) = cortex with normal vasoconstrictive response to HV and with impaired vasodilative response to AZ and #1 (blue) = cortex with abnormal value in all three variables. **Case 4:** A 14-year-old girl with occlusion of bilateral ICA (Moyamoya disease). The left MCA had poorer antegrade perfusion than the right MCA. The territories of bilateral MCA and ACA were also perfused from PCA through leptomeningeal collateral flow. The patient complained about transient weakness of left or right extremities. MRI showed no abnormality. The patient was treated by indirect bypass surgery (encephalo-duro-arterio-synangiosis, EDAS), in which the anterior and posterior branches of left STA, and the posterior branch of right STA were intracranially implanted. After the operation, she did not show transient weakness any more. Angiography one year after the operation demonstrated markedly improved collateral flow in the whole territory of the left anterior circulation through implanted vessels. It was demonstrated that the posterior part of the right anterior circulation was well fed by the external carotid artery. However, as the stage of the disease progressed during the follow-up period, the anterior part of right frontal lobe, where vessel was not surgically implanted, showed increasingly poor perfusion. An additional PET study was performed 14 months after the operation.

75. A Medical Image and the Database Archiving System at Research Center for Heavy Ion Therapy in NIRS

Hinako Toyama, Yoko Ikoma,
Koji Uemura, Eiko Takeda and Shinnichirou Satou

Keywords: *heavy ion therapy, DICOM3, PACS, HIS, WEB viewer, relational database*

To assess clinical trials of carbon ion therapy, an archiving system of medical images and clinical records for performed radiotherapy has been developed in our institute. The characteristics of this " A Medical Image and Database Archiving System (AMIDAS)" are :

1.to use WEB tools for the man-machine interface;

2.to connect organically to other systems such as HIS and the radiotherapy planning system in our hospital; and

3.to include data processing and statistical analyzing system.

Archiving all examined clinical data (images, biochemical data, pathological data and so on) and treatment history together make it possible to get information necessary to evaluate carbon ion therapy and related treatment for patients. This system consists of the image acquisition terminals connected into the imaging devices (CT, MR, PET), an image server, an image data backup device, a central information management system with database, a WEB server, a server for data analysis and image referring devices.(Fig.38). Basic personal information for a patient and results for a biochemical study which are registered and are managed at first in a hospital information system (HIS) are transferred into the central information management system in AMIDAS on the network.(Fig.39). Privacy of a patient is guarded with a security system such as a firewall and an access control system.

We show a clinical application of this system.(Fig.40).

Studies of SPECT, PET and CT were performed for a patient with lung cancer who received pre- and post-therapy with carbon ions. A method for co-registration among images of three modalities has been developed. Functional changes in perfusion, ventilation and V/Q ratio of the lung and especially around the tumor were evaluated. Relation between these functional changes and radiation dose was also studied by using the data in the server system. Changes in the tumor size and radiotracer accumulation after the radiotherapy were investigated by using CT and PET images. The data analysis is considered to offer a new concept for evaluation of tumor effect of the therapy.

The results of the clinical trial for a heavy ion therapy have to be distributed to other institutes in Japan and worldwide. Standardization of the database and the communication tool is desired. We are planning to extend our system while keeping it secure.
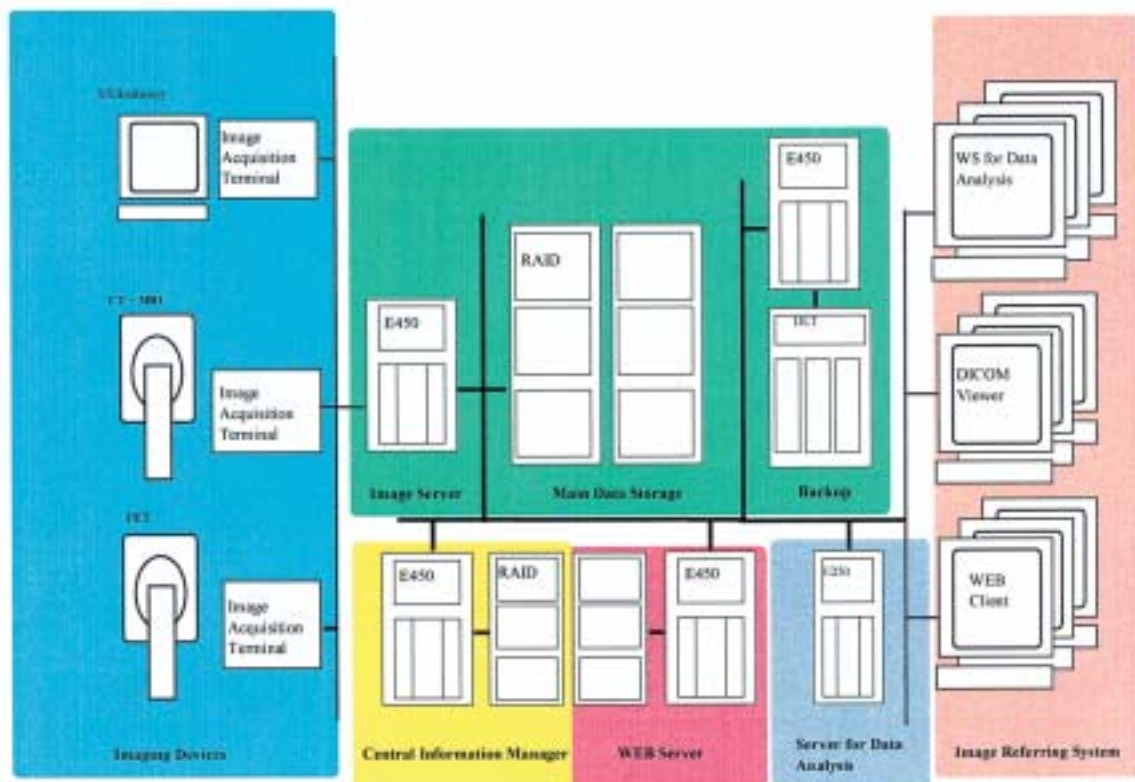
Fig.38. A Medical Image and Database Archiving System in NIRS
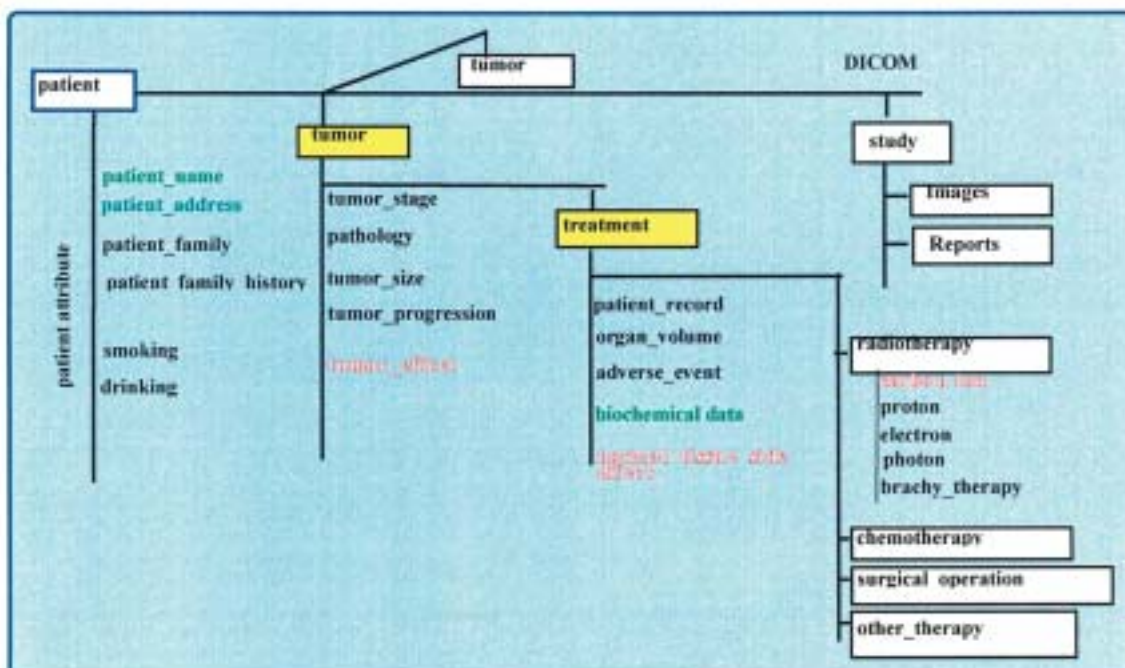
Fig.39. Schema for the records in the database system System in NIRS
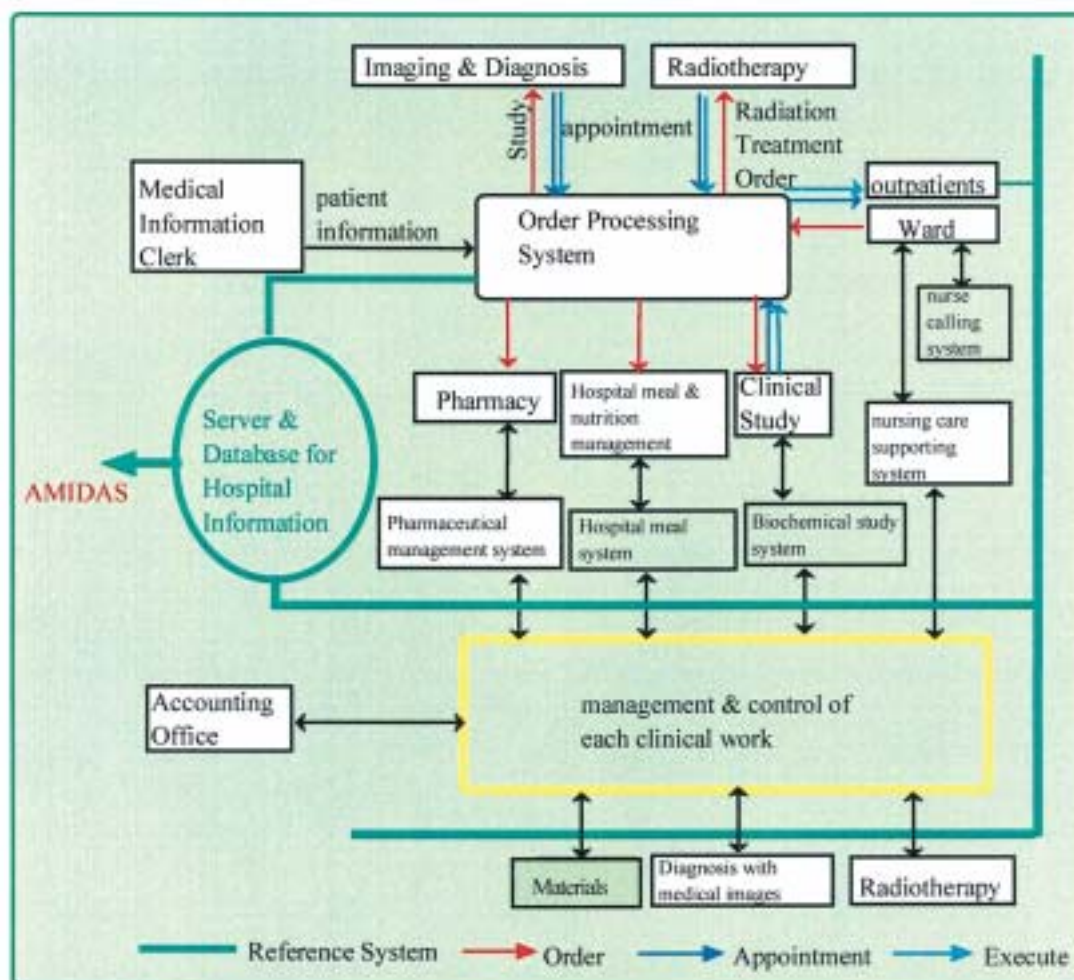
Fig.40.   A hospital information system connected to AMIDAS

ENVIRONMENTAL SCIENCE

76. Final Report on Dose Estimation for Three Victims of JCO Accident

Kenzo Fujimoto and
the Dose Estimation Working Group

Keywords: criticality accident, dose estimation, Na-24

The English version final report of the Dose Estimation Working Group for Three Victims was published in April 2002 and the Japanese version in February 2002. Those are the reports of the Working Group that was established at NIRS just after the accident to estimate the doses of the three JCO workers who were severely exposed to radiation in the criticality accident. Within a few days after the accident, the Working Group provided the estimated dose, required for the treatment of these three workers, and then published the results of the group activities in various formats, such as the interim report on February 29, 2000. The issue of the interim report did not mark the end of the activities of the Working Group: the Group has continued its studies to obtain as much knowledge as possible from the disaster. These studies include 1) dose measurements of samples provided in the latter stage, 2) computational simulation analyses to derive more precise dose distribution within the human body, and 3) experiments using Transient Experiment Critical Facility in JAERI. The final reports detail the dose estimation experiments carried out by the Group, including the measurements and analyses conducted after the interim report was published. They supersede the entire content of the interim report and cover the dose estimation of the three workers who were severely exposed during the JCO criticality accident.

The data in those reports are presented for academic purposes with the consent of the three severely exposed workers and/or their families. We would like to express our deep condolences to the families who lost loved ones due to the accident.

On September 30, 1999, at about 10:35 in the morning, a criticality accident occurred in a uranium conversion test plant at JCO in Tokai-mura. Three workers who were purifying uranium were severely exposed to radiation. NIRS, which is a Tertiary Radiological Emergency Facility, agreed to admit the workers, established a Countermeasure Headquarters and a Dose Estimation Working Group for Three Victims and started preparing to receive the workers. The procedures implemented by all parts of NIRS concerning this accident are summarized in the "The report of the criticality accident in a uranium conversion test plant in Tokai-mura" NIRS-M-154. The final reports mentioned here describe the response of the Dose Estimation Working Group.

To inform readers of the principal methodology that was used to estimate the dose, the key details directly related to dose estimation are all covered at first. The secondary details of methods and measurement data are covered in the following chapter. The various problems encountered during the dose estimation process are also discussed. The initial actions and chemical analyses are described in the Appendices.

For the JCO criticality accident, the radiation dose was estimated using three main methods: lymphocyte counting, chromosome analysis, and measurements of the specific activity of ^{24}Na in blood samples. At the time of publication of the Interim Report, the doses of the three workers were estimated by these three methods to be 1-4.5, 6-10, and 16-20+ GyEq. At the latter stage more precise analyses estimated doses of 1-5, 6-8, and 16-23 GyEq by lymphocyte counting; doses of 2.8-3.2, 6.9-10, and 16-30+ GyEq by chromosome analyses; and doses of 0.81, 2.9, and 5.4 Gy with respect to neutrons and 1.5, 4.1 and 9.9 Gy with respect to gamma radiation by means of ^{24}Na specific activity measurements. These values fall within the estimations in the Interim Report but are more precise. Of these estimated doses, the methods based on counting the numbers of lymphocytes in the peripheral blood or which examined chromosomal abnormalities could not distinguish the dose contribution of neutrons from that of gamma rays; these doses were estimated by comparing the previous results based on gamma ray effects. Therefore, we could not use radiation dose units such as Gy or Sv but used another unit: GyEq. On the other hand, the method used to estimate the doses from the specific activity of ^{24}Na in the blood can only derive doses attributable to neutrons. Therefore, the doses of gamma rays had to be estimated using other methods, such as investigating the readings from radiation monitors during the accident and performing computational simulations. At the initial stage, the total dose was estimated in GyEq units using an RBE of 1.7 and the dose estimated by the specific activity of ^{24}Na in the blood. However, after further investigation, we concluded that the best method for expressing dose estimations was to express them in units of Gy for each component, neutron and gamma rays. For the temporary evaluation of health effects on the entire body and comparison with the results derived from other dose estimation methods, we judged it was necessary to assume an appropriate RBE and derive the sum of the neutron and gamma ray doses. For these purposes, the doses of the three workers estimated from the specific activity of ^{24}Na in the blood and using a RBE of 1.7 were 2.9, 9.0, and 19 GyEq, respectively for the three workers.

Taking these inaccuracies into account, we compared the results of these dose estimation methods and derived

overall doses to be 2-3, 6-9 and 16-25 GyEq for the three workers. The ranges do not reflect the uneven dose distribution in the bodies; rather, they show the ranges of estimation by various methods.

Publications:

1) National Institute of Radiological Sciences: Final Report on Dose Estimation for Three Victims of JCO Accident. Edited by K. Fujimoto, NIRS-R-147 (2002).
2) National Institute of Radiological Sciences: Final Report on Dose Estimation for Three Victims of JCO Accident. Edited by K. Fujimoto, NIRS-M-153 in Japanese (2002).
3) National Institute of Radiological Sciences: Interim Report on Dose Estimation for Three Victims of JCO Accident. Edited by K. Kawachi and K. Fujimoto NIRS-M-138, in Japanese (2000).

77. Sensitivity to Thoron on Passive Radon Detectors

Shinji Tokonami, Weihai Zhuo,
Masahide Furukawa and Yuji Yamada

Keywords: *radon, thoron, passive detector*

Although a lot of studies on radon have been done, there are few reports on thoron. It was considered that the effect of thoron would be negligible because of its small quantity compared to that of radon. However, recent studies have shown high thoron levels in living environment. In particular, high thoron concentrations have been occasionally observed in some areas of Japan. This fact made it clear that some passive radon detectors were sensitive to the presence of thoron. They are commonly used for indoor radon surveys. It is possible that such detectors will give false values unless they are placed properly. Therefore, it is important to understand the detector response to thoron before practical use. A compact thoron chamber system was set up for the purpose. In this study, the following items are shown: configuration of the thoron chamber and sensitivity to thoron of several passive radon detectors.

The thoron chamber system consists of two parts: an exposure chamber and a thoron gas generator. They are connected through an inline filter holder, a flow meter and an external pump. Fig. 41 illustrates a sectional view of the thoron chamber system when thoron exposure tests are carried out for passive radon detectors. The exposure chamber is a 150-liter cylindrical vessel (565 mm diameter and 600 mm height), made of stainless steel. Four metal tubes are attached to the lid of the

chamber. They are used to supply/exhaust thoron/radon gas and to take air samples. A fan is mounted on the lid to make the internal concentration uniform. The generator is a 10-liter stainless steel cylindrical vessel (240 mm diameter and 240 mm height). The vessel is filled with thorium-rich ceramics as the solid source. The ceramics were crushed into small pieces so as to promote thoron diffusion. After connecting the exposure chamber and generator, thoron gas is circulated through the system by the external pump. The thoron concentration in the exposure chamber depends on the flow rate of the circulation. The flow rate is set at around 20 L/min in this system. Thoron and radon concentrations are measured with scintillation cells after taking an air sample through the metal tube. The measurement technique is based on two measurements using the difference of the half life between radon and thoron.

Thoron and radon concentrations in the exposure chamber were measured after connecting the exposure chamber with the thoron gas generator through the external pump, as shown in Fig. 41. Air samples were occasionally taken while the thoron gas circulated through the system at the flow rate of 19.5 L/min. This performance test lasted 4 days. The average thoron and radon concentrations during the period were estimated to be 2530 Bq/m^3 and 230 Bq/m^3, respectively.

In the present study, the following passive radon detectors were actually examined: German monitors (CR-39 installed), RADTRAK, R-T discriminative dosimeters and electrostatic integrating radon monitors (EIRM). The results of the conversion factor on the radon and thoron concentration are shown in Table 7. The radon conversion factors of the RADTRAK and R-T discriminative dosimeter were determined with the authorized facilities in advance. In terms of the RADTRAK, the conversion factors have changed compared to the previous result. The German monitor and the RADTRAK were highly sensitive to thoron. The R-T discriminative dosimeter consists of two radon detectors with two different ventilation rates. Since the upper hemisphere has a high ventilation rate, thoron concentrations are mainly measured. The lower hemisphere is designed to detect radon only. However, it was found that even this lower hemisphere was affected by thoron in this exposure test. On the other hand, the EIRM had no sensitivity to thoron. Although most passive radon detectors are designed to minimize the entry of thoron, it can be seen that they are sensitive to the presence of thoron except for one device in the present study.

In order to check the sensitivity to thoron on passive radon detectors, the thoron chamber system has been set up. Subsequently, performance tests of the chamber system were carried out so as to confirm its stability and

reliability. Although some passive radon detectors were examined, most of them were sensitive to thoron. Although the presence of thoron may be negligible in the environment, it is important to check the sensitivity to thoron with the proposed test before practical use.

Publications:

1) Tokonami, S., et al.: *Health Phys*., **80**, 612-615, 2001.
2) Tokonami, S., et al.: *Sci. Total Environ*., **272**, 247-248, 2001.
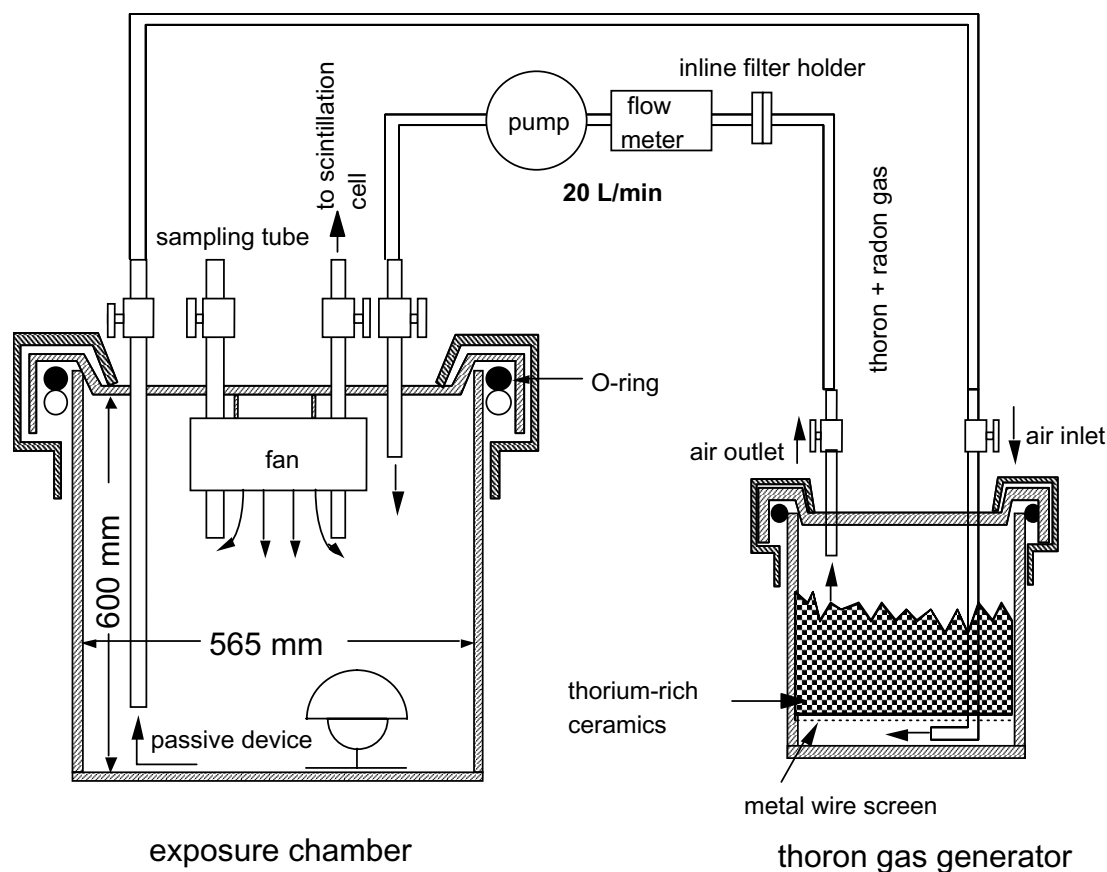
Fig. 41.   A sectional view of the thoron chamber system when thoron exposure tests are carried out for passive radon detectors.

Table 7   Conversion factors of radon and thoron concentrations.

Measuring device	Radon	Thoron
German monitor (CR-39)	10.14 x 10^{-4}	10.17 x 10^{-4}
RADTRAK	6.74 x 10^{-4}	4.51 x 10^{-4}
Radon-Thoron discriminative dosimeter (upper hemisphere)	2.40 x 10^{-4}	1.22 x 10^{-4}
Radon-Thoron discriminative dosimeter (lower hemisphere)	2.82 x 10^{-4}	0.26 x 10^{-4}
Electrostatic integrating radon-222 monitor	189.4 x 10^{-4}	No sensitivity

unit: tracks/mm^2/(Bq/m^3-d)

78. Am-241 as a Metabolic Tracer for Inhaled Plutonium Nitrate in External Chest Counting

Nobuhito Ishigure,
Takashi Nakano and Hiroko Enomoto

The most difficult radionuclides to measure accurately by external chest counting are the isotopes of plutonium (Pu). They are detected through weak emission of low energy L X-rays; in the case of ^{239}Pu, 11-20 keV L X-rays are emitted with the total emission rate of 0.0417 per disintegration. These photons are severely attenuated by overlying tissue; typically about 0.1 % of the photons, that is, only 0.00004 photon per unit α-disintegration will escape from the human thorax.

The Pu treated in the nuclear fuel cycle is usually accompanied with ^{241}Am produced from ^{241}Pu by β disintegration, which emits γ-rays of 60 keV with the emission rate of 0.36, being more penetrable than the L X-rays from Pu. The ^{241}Am could improve the detection limit of chest counting of Pu, if it were used as a metabolic tracer for Pu in lungs.

Young adult male Wistar rats were exposed to polydisperse aerosols of Pu(NO$_3$)$_4$ with an Activity Median Aerodynamic Diameter of 0.6 μm. Their initial lung burdens were between 900 Bq and 2400 Bq. These exposed rats were periodically sacrificed and the radioactivity of ^{241}Am and $^{238/239/240}$Pu in the autopsied lungs was measured with a NaI/CsI phoswich detector system.

The results (Fig.42) show that the activity ratio of ^{241}Am vs. $^{238/239/240}$Pu in the autopsied lungs, (2.37±0.04) % at the exposure, slowly decreased to (2.07±0.05) % at 4 weeks, (2.02±0.03) % at 12 weeks and (2.00±0.04) % at 24 weeks. However, from a practical point of view, it could be concluded that ^{241}Am would be a valid metabolic tracer for inhaled Pu nitrate at least for half a year post inhalation, considering the detection limit for Pu in chest counting, which is much greater than the ALI (annual limit on intake) of Pu and the large uncertainties due to the estimation of chest wall thickness, the change in the distribution of particles within the lungs, etc.

Fig. 42. Ratio of lung burdens of ^{241}Am and $^{238/239240}$Pu.

79. Isotope Ratios of Uranium in Soil Samples Using Thermal Ionisation Mass Spectrometry Equipped with a WARP filter

Sarata Kumar Sahoo

Uranium consists of three natural isotopes viz. ^{234}U, ^{235}U, and ^{238}U with relative isotopic abundances of 0.0054%, 0.720% and 99.275%, respectively . Both ^{238}U and ^{235}U isotopes are of primordial origin. The ^{238}U isotope, upon radioactive decay, produces long-lived daughter products, ^{234}U and ^{230}Th. ^{234}U is present, approximately in radioactive equilibrium with ^{238}U. Anthropogenic uranium also contains trace quantity of ^{236}U produced by neutron capture of ^{235}U in nuclear industrial processes. Therefore, ^{236}U can be used as a "fingerprint" for the presence of uranium in the environment which originates from a nuclear reactor. In this regard, it has substantial advantages relative to anthropogenic ^{238}U and ^{235}U since both isotopes are quickly diluted by the natural background in soils and sediment making then unsuitable markers for the spent uranium released into the environment. Thus uranium isotope ratios may have small variations depending on the geological origin of the sample, due to natural isotopic fractionation, nuclear reactions or anthropogenic contamination. Uranium ores, which have a relatively high neutron flux, are expected to have a measured ^{236}U/^{238}U ratio of about 10^{-10} which is higher than elsewhere in nature.

Two NBS standards, namely NBS U005 and NBS U010 were used to check the accuracy of the calibration and optimisation of procedures. Two uranium ores and three soil samples were chosen for this study: sediment reference material supplied by Geological Survey of Japan (JLK-1) and two surface soil samples from the

Table 8 Isotope ratios of uranium measured from soil samples

Sample Name	$^{234}U/^{238}U$	$^{235}U/^{238}U$	$^{236}U/^{238}U$
Faraday Mine (Canada, Bancroff)	0.0000544 (51)	0.0072560(32)	$1.59136(67) \times 10^{-8}$
Mistamisk (Canada, Labrador)	0.0000544(46)	0.0072553(39)	$8.145183(59) \times 10^{-9}$
JLK-1	0.0000544 (51)	0.0072560(32)	Not detectable
Chernobyl A	0.000090(46)	0.008194(39)	0.000325(45)
Chernobyl B	0.000117(74)	0.00993(43)	0.000972(44)

Analytical uncertainties are expressed as $2\sigma_m$.

Ukraine obtained in the 30 km exclusion zone affected by the Chernobyl accident (A and B). Sediment sample, JLK-1 and soil samples were dried at 60±5 C. After homogenisation, 250 mg of soil sample were digested using a closed vessel (PTFE vessel) microwave unit (MLS 1200 mega, Italy) .

A chemical procedure for isolation of uranium is based on extraction chromatography and anion exchange resins. Precise determination of uranium isotopic composition ($^{234}U/^{238}U$, $^{235}U/^{238}U$ and $^{236}U/^{238}U$) was carried out in uranium ores and soils from the Chernobyl accident zone using a single focussing VG (Micromass) Sector 54-30 thermal ionization mass spectrometer (TIMS) equipped with nine new bucket type Faraday collectors and a Daly ion-counting system detector positioned behind the axial Faraday and wide aperture retardation potential (WARP) energy filter. Under the optimal conditions, five replicate analyses of NBS U005 yielded an average value of $^{235}U/^{238}U$ as 0.005089 against certified value of 0.00509001. The measurements of the isotopic ratio in the reference materials demonstrate that isotopic fractionation, if occurring in the system, is less than the uncertainty in the measurement. The measured isotope ratios, $^{234}U/^{238}U$, $^{235}U/^{238}U$ and $^{236}U/^{238}U$, of two uranium ore samples, representative duplicate set of samples from standard and soil samples from the Chernobyl exclusion zone are given in Table 8.

Samples collected from the Chernobyl exclusion zone showed a spread in uranium isotope ratio well outside the 99.7% confidence limit, having $^{235}U/^{238}U$ in the range of 0.008194 to 0.009934. Enrichment of ^{234}U was also noticeable from the $^{234}U/^{238}U$ ratio and the presence of radioactive disequilibrium between ^{234}U and ^{238}U. These results showed the heterogeneity in the distribution of isotopically enriched material within the soil. Duplicate runs of each sample confirmed that such deviations from natural ratios were readily reproducible at statistical levels predicted by standard measurements.

Publications:
1) Sahoo, S.K., Yonehara, H., Kurotaki, K., Fujimoto, K., and Nakamura, Y.: *J. Radioanal. Nucl. Chem*., **252**, 241-245, 2002.
2) Sahoo, S.K., Shiraishi, K., Kimura, S., Masuda, A., Los, I.P. and Zamostyan, P.V.: *Radioprotection-Colloques*, **37**, C1-951-955, 2002.

80. Cell-Specific Distribution of Trace Elements in Rat Testis

Shino Homma-Takeda, Yoshikazu Nishimura, Yoshito Watanabe and Masae Yukawa

Keywords: *PIXE, imaging, trace elements, seminiferous tubules*

Testis is known to be very sensitive to radiation as well as endocrine disruptors. Testis is an ideal subject to study the effect of environmental stresses. Spermatogenesis is a complex process in which germ cells within the seminiferous epithelium of testis progress through mitosis, meiosis, and cellular differentiation to become spermatozoa. The three types of germ cells, such as spermatogonia, spermatocytes, and spermatids, undergo a development series, which is further classified into several stages of senimiferous epithelium cycles. Trace elements are known to have a pivotal role in the spermatogenesis. The presence of copper, manganese, selenium, and zinc, for example, plays an important role in the self defense mechanism in the body with the antioxidant metalloenzymes. It has been demonstrated that the localization of the metalloenzymes are varied in

stages of the seminiferous tubules and the germ cells at different stages of the seminiferous tubules respond differently to exogenous stimuli. However, the detailed distribution of the trace elements in each type of germ cells has been poorly understood. Micro-beam scanning PIXE (particle induced X-ray emission) analysis, which provides a multi-elemental imaging for small biological samples, is one of the most promising techniques to resolve the problem. In this study, we attempt to make a two-dimensional distribution of the trace elements in rat testis by the analytical method.

A 50 μm-thickness of rat testicular cryosection was subjected to micro-PIXE analysis (estimated beam size, 0.4 μm x 0.65 μm). Corresponding to PIXE imaging with scanning transmission ion microscopy, it enables us to obtain the stage- and cell-identified distributions of trace elements of the testicular section. Manganese, copper, zinc, and selenium were detected in the germ cells and their localizations were varied in each stage of germ cell development. For instance, zinc was higher in the central area of seminiferous tubules, where spermatozoa localize, than the periphery of the tubules, which contains spermatogonia. In contrast, iron was detected in the interstitial cells rather than the germ cells. These results suggest that micro-PIXE analysis is a promising technique for investigation of trace element dynamics in spermatogenesis.

81. Estimation of Dietary ^{232}Th, ^{238}U, Cesium and Strontium in Vietnamese People from Different Geological Regions

Kunio Shiraishi, Shinzo Kimura,
Hideki Arae, Nyuen Giang*,
Nguyen M. Sinh*, and Nguyen N. Tuan*
(* Nuclear Research Institute, Dalat, Vietnam)

Qualitative information about the daily intake of naturally occurring radioactive nuclides and related elements in diet samples is important for estimating metabolic parameters and concentrations in the human body. However, data on dietary element intakes for Vietnamese subjects are scarce. In this report, diet samples were collected to estimate Vietnamese element intakes from several main regions of Vietnam. Concentrations of two radionuclides (^{232}Th and ^{238}U) and two stable elements (cesium and strontium), were determined using inductively coupled plasma mass spectrometry (ICP-MS).

Two kinds of assessment methods such as a market basket study (MBS) and a duplicate portion study (DPS) were applied for collection of food samples during 1996-1998. The whole country was divided into three areas according to their geological position and food habits as follows: 1) the northern area consisting of Hanoi, Haiphong, Hoabinh, and Namdinh; 2) the middle area consisting of Vinh, Danang, and Phuyen; and 3) the southern area consisting of Ho Chi Minh City. The diet sample was digested with a mixture of nitric acid, perchloric acid , and hydrofluoric acid in a Teflon vessel. The sample solution obtained was measured with ICP-MS.

The geometric mean and standard deviation (SD) of daily ^{232}Th intake were found to be 0.99 and 2.60μg per person from 18 diet samples. Daily intakes of ^{232}Th in northern Vietnam and middle-1 (Vinh and Danang) were relatively higher than those in middle-2 (Phuyen) and southern Vietnam. Then the three areas were combined into two groups, i.e. group-1 (northern and middle-1) and group-2 (middle-2 and southern). Daily ^{232}Th intakes of group-1 and group-2 were 1.91 and 0.44μg per person, respectively. Daily ^{238}U intakes of group-1 and group-2 were 1.09 and 0.35μg per person, respectively. Daily cesium intakes of group-1 and group-2 were 7.8 and 14.2μg per person, respectively. There were statistically significant differences (p<0.01) in intakes of ^{232}Th, ^{238}U and cesium between the two groups in a non-parametric test. The difference in ^{232}Th and ^{238}U between group-1 and group-2 could be due to a geological factor because the heavy mineral, monazite, which has higher contents of ^{232}Th and ^{238}U is mined in the north and a part of middle regions of Vietnam. For cesium, the difference between the two groups could be due to the consumption rate of fishes and meats. Daily strontium intakes per person in three areas of Vietnam were as follows: 0.54-7.15 mg (northern); 0.37-1.63 mg (middle); and 0.13- 4.21 mg (southern). Daily strontium intakes were not statistically different between the three areas and the two groups. The geometric mean and S.D. of daily strontium intake were found to be 1.18 and 2.40 mg per person from 18 diet samples (Table 9).

In conclusion, the daily intakes of ^{232}Th, ^{238}U, cesium and strontium for Vietnamese subjects were estimated using ICP-MS. Daily intakes of ^{238}U, ^{232}Th, and cesium differed between northern and southern areas of Vietnam. Concentrations of ^{232}Th and ^{238}U in Vietnamese foods were similar to the global averages.

Publication:
Giang, N., Shiraishi, K., Sinh, N. M., Kimura, S., Tuan, N.N., and Arae, H. *Health Physics*, **80**, 605-611, 2001

Table 9. Daily intakes ^{232}Th, ^{238}U, cesium and strontium for a Vietnamese adult.

Sampling area	Sampling region[a]	Sampling time		Sampling method[b]	Daily intake per person			
					^{232}Th(μg)	^{238}U(μg)	Cs(μg)	Sr(mg)
North of Vietnam	Hanoi-1	Dec	1997	DPS	5.71±0.48 [a]	2.33±0.18 [a]	7.09±0.33 [a]	0.54±0.04 [a]
	Hanoi-2	Dec	1997	DPS	4.30±0.48	2.14±0.18	9.27±0.91	7.15±0.40
	Hanoi-3	Dec	1997	DPS	2.06±0.04	1.17±0.02	12.8±0.62	0.94±0.06
	Hanoi-4	Dec	1997	DPS	1.85±0.01	0.84±0.01	7.77±0.09	1.07±0.01
	Hanoi-5	May	1998	MBS	1.60±0.06	1.03±0.04	8.07±0.13	1.68±0.03
	Haiphong	May	1998	MBS	1.35±0.01	0.98±0.11	8.62±0.15	1.63±0.08
	Hoabinh	May	1998	MBS	0.76±0.02	0.62±0.03	5.86±0.10	1.99±0.05
	Namdinh	May	1998	MBS	0.69±0.09	0.66±0.07	6.32±0.07	0.78±0.02
Middle of Vietnam	Vinh(middle-1)	May	1998	MBS	2.85±0.08	1.50±0.12	7.30±0.09	1.63±0.02
	Danang(middle-1)	May	1998	MBS	2.08±0.42	0.80±0.01	6.79±0.10	1.40±0.06
	Phuyen-1(middle-2)	July	1997	DPS	0.85±0.07	0.30±0.01	17.3±0.7	1.23±0.09
	Phuyen-2(middle-2)	July	1997	DPS	0.38±0.03	0.27±0.04	28.1±0.5	0.37±0.01
South of Vietnam	Ho Chi Minh City-1	Mar	1996	DPS	1.23±0.40	0.54±0.19	11.4±0.2	1.74±0.15
	Ho Chi Minh City-2	Mar	1996	DPS	0.49±0.01	0.54±0.01	13.6±0.3	1.36±0.05
	Ho Chi Minh City-3	Mar	1996	DPS	0.27±0.05	0.31±0.02	12.3±0.4	0.49±0.04
	Ho Chi Minh City-4	Jun	1996	DPS	0.27±0.05	0.33±0.02	12.2±0.1	4.21±0.09
	Ho Chi Minh City-5	Jun	1996	DPS	0.56±0.06	0.98±0.04	20.3±0.3	1.80±0.07
	Ho Chi Minh City-6	Jun	1996	DPS	0.18±0.03	0.09±0.01	7.11±0.28	0.13±0.01
	Group-1				1.91 (1.89)	1.09 (1.54)	7.80 (1.23)	1.43 (1.93)
	Group-2				0.44 (1.81)	0.35 (1.92)	14.2 (1.5)	0.92 (2.80)
	Total mean[c]				0.99 (2.60)	0.66 (2.19)	10.2 (1.5)	1.18 (2.40)

[a]Group 1 consists of northern area and middle-1 area ; Group 2 consists of middle-2 and southern area .

[b]DPS: duplicate portion study, MBS: market basket study.

[c]Geometric mean and geometric standard deviation in parentheses.

82. Determination of Rhenium in Rock Samples by ICP-MS

Keiko Tagami and Shigeo Uchida

The long-lived radioisotope ^{99}Tc is of potential long-term importance in the environment for safety assessments of reprocessing plants and underground disposal of radioactive waste. To understand Tc behavior in environments, we have measured Re as a chemical analogue of Tc due to their physico-chemical similarities. However, no data are available for environmental samples, because Re is one of the rarest elements in the earth's crust. We developed a Re separation method from rock and soil samples using alkaline fusion and an extraction chromatographic resin (TEVA Spec resin, Eichrom Industry Inc.), providing almost constant recoveries with the average of 94±3% for rock and soil samples. The resin extraction step can satisfactorily separate Re from sample matrices and trace elements that cause isobaric interference during ICP-MS measurements.

Four standard igneous rock samples were subjected for Re measurement in this study. The rocks originated in Japan and were prepared by the Geological Survey of Japan. Their code numbers were, JB-1, JB-3, JG-1 and JR-2. Although there is no available standard rock or soil for Re worldwide, these rock samples were useful for data comparison because their provisional concentrations had previously been measured by RNAA.

The developed separation method was used to measure Re contents in these rock samples without addition of Re spike because of the steady recovery of the method. The average recovery, 94±3%, applied to these samples. Sample amounts used were 0.5 - 1 g. The strip solution (5mL of 8M HNO$_3$) from the TEVA resin was evaporated to dryness on a hot plate at ca. 90°C to reduce HNO$_3$ contents. No Re loss was found during this evaporation step. Then, the residue was dissolved into 5

Table 10. Rhenium concentrations in standard Japanese igneous rock samples.

Sample	Re contents (ng/g)			Provisional value*
JG-1	0.079	±	0.013	
	0.072	±	0.013	
	0.080	±	0.014	0.098
	0.081	±	0.007	
	0.070	±	0.006	
JB-1	4.04	±	0.69	
	3.94	±	0.68	
	3.58	±	0.20	4.8
	3.40	±	0.25	
JB-3	0.345	±	0.056	
	0.271	±	0.046	0.24
JR-2	0.051	±	0.009	
	0.067	±	0.010	0.023

* The data are obtained by RNAA (Imai, *et al*, 1995).

± Values show standard deviation (1s).

ml of 0.1M HNO_3 to measure Re by ICP-MS.

The results are listed in Table 10. The observed Re values in this study ranged from 0.05 to 4.0 ng/g. Each sample was analyzed at least 2 times; the results of these replicates indicated a good agreement with each other. This fact provided evidence of the reproducibility of the method. The values obtained in this study were compared with literature values determined by RNAA. The observed values were of the same order as the literature values. This suggested that the accuracy of our method was reasonable. No systematic differences were found between the determination methods, ICP-MS and RNAA across the various samples. One of the reasons for the discrepancies could be ascribed to matrix components in rock samples. According to a private communication with the researcher who reported the Re provisional data, only 1-2 values were included for each sample, hence they are clearly provisional. More data are required for discussion on the slight differences between the two methods.

Publication:
Tagami, K. and Uchida, S.: *J. Anal. At. Spectrom.*, **16**, 669-671, 2001.

83. Low-level Technetium-99 Determination in Soil Samples by ICP-MS

Shigeo Uchida and Keiko Tagami

Key words: Technetium-99, soil, ICP-MS, volatilization

The quantity of ^{99}Tc in the environment may increase in the future due to releases from uranium enrichment facilities, reprocessing plants or nuclear fuel waste disposal vaults. Thus, ^{99}Tc deserves special consideration in environmental dose assessment to humans and analysis data of ^{99}Tc in soil samples should give useful information for predicting the nuclide behavior. However, the ^{99}Tc must be separated and concentrated prior to determination because of its low concentration.

A simple separation method was developed for ^{99}Tc in soil samples as follows. After incineration, Tc in a soil sample was volatilized in a combustion apparatus for 3 h at 1000ºC and trapped in deionized water. After heating was completed, this sample was replaced with another 50 g batch of the same incinerated soil sample and the combustion procedure was repeated until the accumulated weight of incinerated soil samples was 200 to 300 g. The trap solution was passed through an extraction chromatographic resin (TEVA resin, Eichrom Ind. Inc.) and the resin was washed with 2M HNO_3. Technetium was eluted with 5mL of 8M HNO_3 and this fraction was

evaporated to dryness at <70ºC. The residue was dissolved in 5mL of 2% HNO_3 solution and the ^{99}Tc concentration was measured by inductively coupled plasma mass spectrometry (ICP-MS). The numbers of separation steps were less than those of acid leaching methods and the recoveries were usually higher than 60%. However, for the case of a carbonate rich soil sample, the recovery decreased remarkably because the sample matrix fixed Tc in itself during the volatilization step.

The concentrations of ^{99}Tc, ^{137}Cs and the activity ratios of ^{99}Tc/^{137}Cs in environmental soil samples are shown in Fig.43. Generally, global fallout ^{99}Tc was the main source for Japanese soil samples. The concentration was usually on the order of mBq/kg. Interestingly, the levels in paddy field soils were slightly higher than other soil types collected in Japan. This can be explained by low redox potential conditions when the paddies are flooded for rice plant cultivation. Technetium might be fixed in the paddy field soil because of the chemical form change due to reduction. When Tc is transformed to a reduced form, the solubility is lower than that of TcO_4^-. The contents in the soils collected in Germany are almost the same level as those of the Japanese one. The place where the former were collected is known to have been affected by Chernobyl fallout; because the release of the ^{99}Tc was one order of magnitude lower than that of ^{137}Cs and most of the ^{99}Tc was deposited near the Chernobyl site, the ^{99}Tc addition to the soil by the accident was not remarkable. These results give us an idea how Tc behaves in the environment, however, the data are still limited. Further studies are needed to obtain the definitive behavior of Tc in the environment.
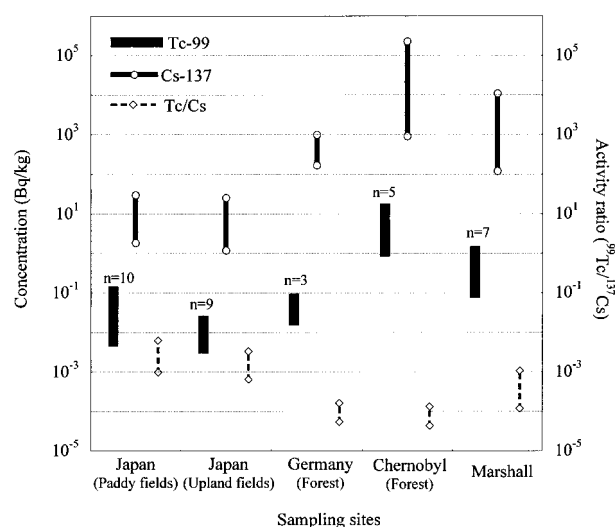
Fig. 43. Concentrations of ^{99}Tc and ^{137}Cs, and the activity ratio of ^{99}Tc to ^{137}Cs in surface soil samples.

84. Effects of Ionizing Radiation on Movement Behavior of *Euglena gracilis*

Tetsuya Sakashita, Masahiro Doi,
Hiroshi Yasuda, Shoichi Fuma,
Hiroshi Takeda, Yuji Nakamura and Donat-P. Häder*
(* Friedrich-Alexander Universitat, Germany)

Keywords: *Euglena gracilis, swimming velocity, negative gravitaxis, ^{60}Co gamma-rays, 290MeV/amu carbon ion*

Introduction: Accidental release to the environment of artificial radioactive nuclides may cause harmful effects on various organisms constituting an ecosystem. In recent years, there is an international trend in the field of toxic evaluation of chemical substances to consider effects on well-being of various organisms, e.g. lethality, mobility, reproductive success. Therefore, it is important to consider effects on well-being in the field of protection of the environment against ionizing irradiation. Movement behavior is one measure of well being of an organism and an important physiological factor since moving to an optimal position allows an organism to avoid harmful environmental conditions. In the present study, our aim is to investigate effects of ionizing irradiation on the primitive movement behavior, swimming velocity[1] and negative gravitaxis[2] of *Euglena gracilis*[3], focusing on dose-effect relationship and the difference in radiation quality.

Materials and methods: Cells in the stationary phase older than 15 days were exposed to ^{60}Co gamma-rays and 290 MeV/amu carbon ions obtained from the Heavy Ion Medical Accelerator in Chiba (HIMAC) at the doses of 0 - 200 Gy for water. Swimming velocity and negative gravitaxis were measured using a biomonitoring system ECOTOX developed by Tahedl and Häder. The r-value[4] was used to quantify negative gravitaxis. Inhibitions[5] of swimming velocity and r-value by gamma-rays and carobon ion irradiation were evaluated. 50% effective doses (*ED$_{50}$*) were calculated from these inhibitions using Emmens's equation[6].

Results: Inhibitions of the swimming velocity in *Euglena gracilis* cells irradiated with gamma-rays (15±2 h after the irradiation) and carbon ions (18±2 h after the irradiation) are shown in Fig. 44(a). There were significant differences in swimming velocities of irradiated cells between gamma-rays and carbon ions in the dose range of 10 - 20 Gy. Carbon ions had a relative higher impact at a lower dose (10 - 20 Gy) than the gamma-rays. No significant difference between gamma-rays and carbon ions was observed in swimming velocity of cells irradiated at doses of 100 and 200 Gy. Fig. 44(b) shows the dose response of inhibitions of r-value. In the same dose range (10 - 20 Gy), significant differences between gamma-rays and carbon ions were observed in r-value of irradiated cells. Table 11 shows *ED$_{50}$* of swimming velocity and r-value of *Euglena gracilis* cells exposed to both radiations. Our results indicated that irradiation of gamma-rays and carbon ions inhibited swimming velocity and negative gravitaxis of *Euglena gracilis*, and significant differences between both radiations were observed in the dose range of 10 - 20 Gy.

————————————————————

Note:

[1] Swimming velocity is defined by $Velocity = \dfrac{d}{\Delta t} f_s$, where d is the length of a movement vector [pixel], Δt =160 ms, and f_s is the scaling factor [µm/pixel]. Mean and standard deviation (SD) of swimming velocity of non-irradiated cells were 113 ±6 (Gamma) and 96 ±4 (Carbon), respectively.

[2] Negative gravitaxis means that *Euglena gracilis* swims upward in the water column, in the absence of light. This behavior is observed in swimming cells.

[3] Flagellate algae *Euglena gracilis* broadly inhabit freshwater ecosystems, e.g. ponds or lakes, all over the world. Movement behavior (swimming velocity and negative gravitaxis[1]) of this organism is highly-sensitive and has a short-term response to chemical toxins. It is therefore considered that *Euglena* is one of the most important organisms for ecotoxicity evaluation.

[4] r-value is calculated by $r = \dfrac{\sqrt{\left(\sum \sin\alpha\right)^2 + \left(\sum \cos\alpha\right)^2}}{n}$, where n is the number of movement vectors and α the deviation from the stimulus direction (gravity). In general and non-irradiated cells, around 70-80% of all *Euglena* swim upward in the water column, and the r-values are 0.45 ±0.05 (Gamma) and 0.46 ±0.08(Carbon), respectively. If the 'negative gravitaxis' is lost, around 50% of all Euglena swim upward, and the r-value decreases to 0.1, empirically.

[5] $Inhibition = \dfrac{P_{nonirradiated} - P_{irradiated}}{P_{nonirradiated}} \cdot 100\%$, P is the parameter of movement behavior.

[6] $y = \dfrac{y_0}{1 + \left(D/ED_{50}\right)^a}$, y is the response variable, D the
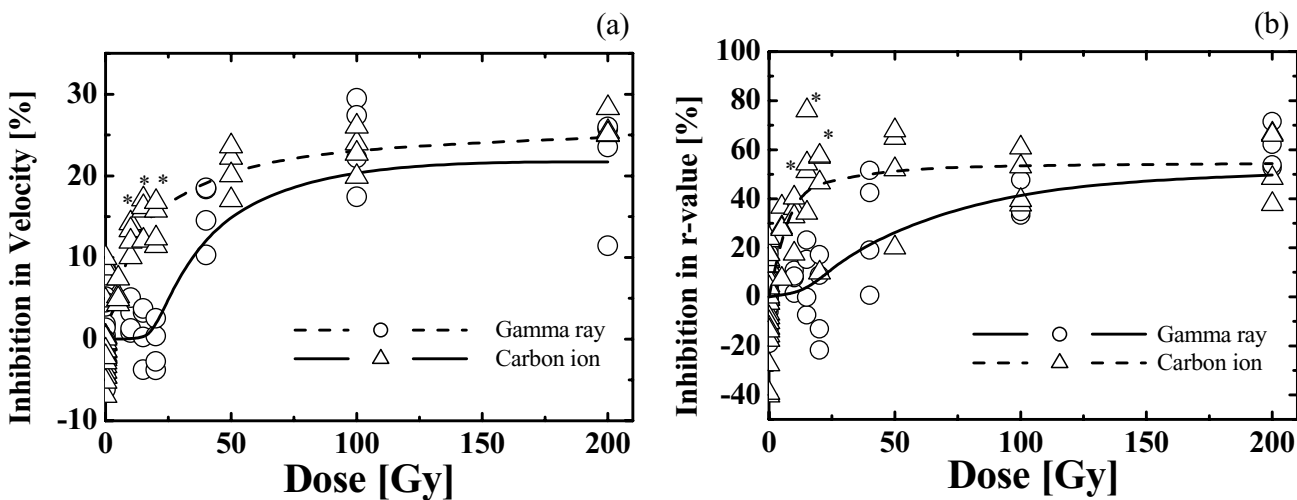
Fig. 44. Inhibition in the swimming velocity of *Euglena gracilis* cells exposed to gamma-rays and carbon ions from HIMAC. The dose response curves were calculated from Emmens's equation. The scale parameters of *a* are -5.6 ±3.0 (Gamma, velocity), -1.1 ±0.1 (Carbon, velocity), -2.5 ±1.0 (Gamma, r-value), and -1.4 ±0.7 (Carbon), respectively. Asterisks indicate statistically significant differences between cells exposed to gamma-rays and carbon ions (p < 0.05, Student's *t*-test).

Table 11. ED_{50} for swimming velocity and r-value of *Euglena* cells exposed to ^{60}Co gamma-rays and 290MeV/amu carbon ions. ED_{50} was evaluated 15±2 h after ^{60}Co gamma-ray irradiation and 18±2 h after 290MeV/amu carbon ion irradiation, respectively. The error indicate the standard error estimated from the non-linear regression.

Movement behavior	^{60}Co gamma-rays	290MeV/amu carbon ions
Swimming velocity	34±4 Gy	13±1 Gy
r-value	42±9 Gy	6±2 Gy

irradiation dose, ED_{50} the 50% effective dose, y_0 the value of y at $D\rightarrow\infty$ and *a* (<0) the scale parameter.

Publications:
1) Sakashita, T., Doi, M., Yasuda, H., Fuma, S. and Häder, D. -P.: *Adv. Space Res*., in press.
2) Sakashita, T., Doi, M., Yasuda, H., Takeda, H., Fuma, S., Nakamura, Y. and Häder, D. -P.: *Int. J. Radiat. Biol*., in press.
3) Sakashita, T., Doi, M., Yasuda, H., Takeda, H., Fuma, S., Nakamura, Y. and Häder, D. -P.: *J. Plant Physiol*., in press.
4) Streb, C., Richter, P., Sakashita, T. and Häder, D. -P.: *Res. Trends*, in press.

85. Determination of U and Pu Isotopes in Environmental Samples by Inductively Coupled Plasma Mass Spectrometry

Satoshi Yoshida and Yasuyuki Muramatsu

Keywords: *ICP-MS, uranium, plutonium, isotope ratio, soil*

Determination of isotopic composition gives useful information on the source term and the behavior of radionuclides including U and Pu in the environment. In recent years, inductively coupled plasma mass spectrometry (ICP-MS) has been increasingly applied for the analyses of long-lived U and Pu isotopes, although the precision of the isotope ratios is poorer compared with thermal ionization mass spectrometry. Compared with radioactivity measurements, the ICP-MS

method has advantages in terms of its simple analytical procedures, prompt measurement time, and capability of determining the isotope ratio such as ^{240}Pu/^{239}Pu, which can not be separated by radiation. This work focuses on the application of quadrupole ICP-MS (Q-ICP-MS) and high resolution ICP-MS (HR-ICP-MS) on the determination of U and Pu isotopes in environmental samples. Uranium isotopes were determined for samples collected on the JCO grounds after the 1999 criticality accident in Tokai-mura, and Pu isotopes were determined for samples contaminated by different sources.

In order to evaluate the impact of the criticality accident on the U isotope composition in soils, U isotopes (^{235}U and ^{238}U) were determined with ICP-MS for soil core samples collected on the JCO grounds after the accident. The soil samples were oven-dried at 80ºC and ground into powder. Then 0.1 or 0.2 g of sample were digested with acids. Q-ICP-MS (Yokogawa PMS-2000) or HR-ICP-MS (Finnigan MAT ELEMENT) was used for the analysis of ^{235}U and ^{238}U. The detection limits of U calculated for the standard solution were 0.1pg/ml for the Q-ICP-MS and 0.01 pg/ml for the HR-ICP-MS. The precisions of ^{235}U/^{238}U atom ratio were 0.6% relative standard deviation (RSD) for the Q-ICP-MS with 1.6 ng/ml of U, and 0.7% RSD for the HR-ICP-MS with 0.16 ng/ml of U.

The ^{235}U/^{238}U ratios were higher than the natural ratio in most samples. The highest ratio observed was 0.0262. Although vertical profiles of the ^{235}U/^{238}U ratio differed among the soil cores, the ratios tended to be high at the surface and decreased with depth. The U concentration also changed with depth. The percentages of ^{235}U in the excess U, estimated from the positive correlation between U concentration and the ^{235}U/^{238}U ratio in soil samples, were less than 4 % by mass (mostly 1 - 3 %), and were much lower than the enrichment of the U used in the uranium conversion building at the time of the criticality accident (18.8 %). These findings indicate that enriched U had been released before the criticality accident during the U processing at JCO in connection with the reconversion of light water reactor fuel.

The isotope composition of Pu (^{240}Pu/^{239}Pu ratio) is related to the source of the contamination. However, there is only a limited volume of quality data available on the levels and distributions of ^{239}Pu and ^{240}Pu isotopes in the environment. Samples (1 - 20 g) were mixed with a known amount of ^{242}Pu and digested with nitric acid. To the filtered leachate, $NaNO_2$ was added to convert chemical form of Pu to Pu (IV). Pu was separated with anion exchange resin (Dowex 1X8). Finally, NH_4I (5%) - 10 M HCl solution (40 ml) was added to the column to elute Pu from the resin as Pu (III). The concentrations of ^{239}Pu, ^{240}Pu and ^{242}Pu and their isotope ratios were measured with the same ICP-MS mentioned above. The detection limits of Pu by Q-ICP-MS and HR-ICP-MS were about 0.02 pg/ml and 0.001 pg/ml, respectively. The precision of ^{240}Pu/^{239}Pu atom ratio was less than 1% RSD at the concentration of > 2 pg/ml of Pu.

Analytical results of $^{239+240}$Pu in standard reference materials (IAEA-134, -135, -367, -368 and -SOIL-6) indicated that the accuracy of the method was satisfactory. Data on the ^{240}Pu/^{239}Pu atom ratios in these reference materials, which are scarce in the literature, were also obtained. Analytical results for samples originating from different places worldwide (including contaminated areas such as Chernobyl, Marshall Islands etc.) showed a wide range of the ^{240}Pu/^{239}Pu atom ratio (0.037- 0.41) according to the source of the Pu (see Fig. 45). The highest ratio was found in soils collected from the Chernobyl area. The ^{240}Pu/^{239}Pu atom ratios observed in 20 Japanese soils were usually in the range 0.17-0.19, except for one very low ratio (0.037) found in the Nagasaki area.

Publications:
1) Yoshida, S., Muramatsu, Y. and Tagami, K.: Environ. *Sci. Technol.*, **35**, 4174-4179, 2001.
2) Muramatsu, Y., Hamilton, T., Uchida, S., Tagami, K., Yoshida, S. and Robison, W.: *Sci. Total Environ.*, **278**, 151-159, 2001.
3) Muramatsu, Y., Yoshida, S., Tagami, K., Uchida, S. and Rühm, W.: In: *Plutonium in the Environment* (A. Kudo, ed.), Elsevier Science, 63-77, 2001.
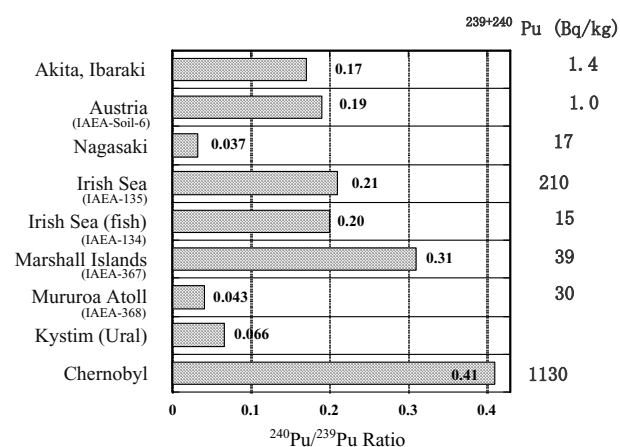
Fig. 45. The ^{240}Pu/^{239}Pu atom ratio and $^{239+240}$Pu concentration in soils, sediments and fish contaminated by different sources.

86. Trace and Natural Radioactive Elements Contents in the Bangladeshi Soils near Industrial Area of Dhaka

M. S. Sultana,
Yasuyuki Muramatsu and Satoshi Yoshida

Keywords: trace and natural radioactive elements, Bangladeshi soils, depletion, enrichment, ICP-MS

Bangladesh, a country of south Asia, is located between 20º 43' and 26º 36' N and longitude 88º 3' to 92º 42' E, and has a tropical climate. The climate can be characterized as tropical monsoon with alternating hot-wet and cool-dry seasons. Annual rainfall is 2200 mm, and varies from 1250 mm in the west to 5000 mm in the northeast. Soils of Bangladesh have been formed mostly from the ocean sediments where sandstone, siltstone, shale and clay stones are the major rock types existing all over the country.

In recent years, environmental pollution has been increasing rapidly with increasing industrial development in Bangladesh. Savar, which is the largest industrial belt near Dhaka has more than 100 local and foreign industries. The industries of Savar generate large amounts of effluents everyday which are being directly discharged into the surrounding land, agricultural fields, irrigation channels, surface water and finally rivers. For this reason, a large number of villages in Savar are now being threatened by environmental degradation. Although the levels of a few selected heavy metals in the soils of Bangladesh have found in the literatures, no information exists on the concentrations of a wide range of trace and natural radioactive elements specially halogens, Br and I and natural radionuclides, Th and U in the soils. This lack is due to the absence of proper measurement facilities. In general, contamination of the cultivated soils is often related to fertilizer use and irrigation, while uncultivated or forest soils are normally contaminated from atmospheric deposition only. Hence, it is better to measure forest soils or uncultivated soils to know the background level of elements. So, in the present study, we analyzed a wide range of trace elements and natural radionuclides, Th and U in mostly forest and open field soils near industrial areas of Bangladesh by the Inductively Coupled Plasma Mass Spectrometer (ICP-MS). We wanted to know the background levels and also to identify the environmental aspects which play the major roles in the soil of this region.

Twenty five surface soil (0-5 cm) samples were collected from the industrial areas around Savar, Dhaka, Bangladesh in the rainy season, 2001. The sampling sites selected for this study were forests located in industrial and remote rural areas around a five kilometer distances from the boundaries of DEPZ. The soil samples were air dried, sieved (1mm), oven dried at 80ºC before being ground to powder. After acid digestion (HNO₃, HF, HClO₄), the residue was dissolved in 2% HNO₃ to yield the sample solutions. However, the bromine and iodine in soils were separated by the combustion technique (phyrohydrolysis). Finally, the soil samples were analyzed by Inductively Coupled Plasma - Mass Spectrometer (Agilent 7500 ICP -MS, Yokogawa Analytical Systems Inc. Japan) for 20 trace elements (Li, Sc, V, Cr, Co, Ni, Cu, Zn, Ga, Br, As, Rb, Sr, Cd, I, Cs, Ba, Pb, Th and U). The standard solutions were prepared from SPEX Multi- Element Plasma Standards (XSTC-1 and 13), which were also used to get calibration curves. The standard solutions of halogens (Br & I) were prepared using commercially available stock standard solutions. The validity of the analytical technique was examined by analyzing standard references samples JB-1 (basalt), NIST-2704 (river sediment), GBW-07312 (stream sediment) and GSS-3&6 (soils) provided by the Geological Survey of Japan, National Institute of Standards and Technology, USA and the National Research Center for Certified Reference Materials, China respectively.

Total contents of the trace and natural radioactive elements found in the Bangladeshi soils are shown in Table-12. Although the concentrations of the trace elements varied slightly with the sampling sites, no systematic trend was observed with distance or directions around several kilometer distances. While these samples were taken from industrial and remote rural areas respectively, it was likely that the concentrations of the trace elements were derived from the natural sources. Further, the observed heavy metal contents were within the permissible limit recommended by WHO which also indicated that the effect of anthropogenic activities in this region was extremely low. The elemental concentrations in soils were further compared with the worldwide average data for soils
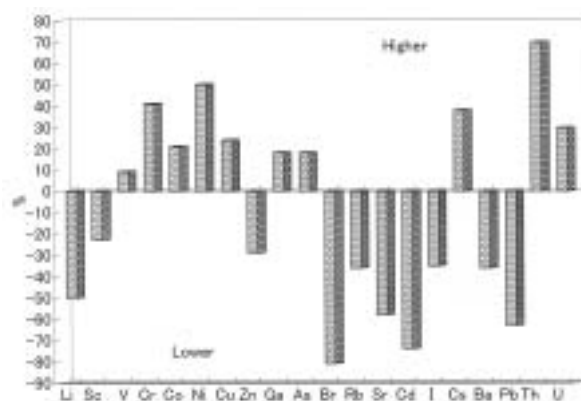
fig.46   The trace and natural radioactive elements in Bangladeshi soils in comparison to worldwide average data for soils.

(Fig. 46). The soils were enriched (10-70%) in V, Cr, Co, Ni, Cu, As, Cs, Th and U above the world wide average value which indicated that these elements were probably accumulated in the soil from the parent materials. Further, the high concentrations of these elements observed in the soils might be controlled by the strong affinity of these metals to organic matter, oxides of Fe, Al, Mn and clay minerals. A good correlation among the heavy metals with correlation coefficients (r^2) 0.94, 0.81, 0.88, 0.80 and 0.76 was also observed for V - Cr, Cr - Ni, Ni - Cu and Cu - As respectively.

In addition, the natural radionuclides, Th and U in Bangladeshi soils were enriched about 70% and 30%, respectively, above the worldwide average for soils. Further, it is interesting to see that Bangladeshi soils have relatively higher average concentrations of Th (16.5 mg/kg) than U (3.0mg/kg) with the ratio of Th/U is 5.5. It is reported that in the lithosphere the Th/U ratio is close to 3, whereas in soils this ratio ranges from 2.5-5. A marked enrichment of Th (30mg/kg) and U (4mg/kg) relative to the abundance in chondrites with high Th/U ratio 7 was observed in clay stone from which the soil in this area was originated. Therefore, the relatively high Th and U concentrations and Th/U ratio in the Bangladeshi soils of this area were accumulated from the parent rock during the soil formation process.

On the contrary, the soils of this area were heavily depleted (20-80%) in Li, Sc, Ga, Zn, Br, Rb, Sr, Cd, I, Ba and Pb compared to the world wide average value. The depletion of these elements relative to the worldwide average data was probably due to leaching. This area receives a large amount (2000 mm/yr) of precipitation. Further, the relatively lower levels of these elements in the soil than the worldwide value indicated

that the contents of these elements might be originally low in the parent material. Although, Zn showed very poor correlation with other heavy metals, it showed better correlation with Cd (r^2:0.64) for similar geochemistry. It was found that, the heavy metal contents of the study region were comparable to the data for the soils of the same geological region (Mainamoti) of Bangladesh.

Generally, the halogen contents (Br & I) of soils is considerably higher than their parent materials. The major supplier of soil bromine and iodine is the atmosphere, by way of wet and dry precipitations. Therefore, as might be expected the soils in this region were enriched in bromine and iodine due to enhanced rainfall and consequent precipitation. But, their content also depends on the ability of the soils of the region to retain them. So, in the present study area bromine and iodine were mobilized from the soil and depleted due to leaching. Since this is the first precise result for trace and natural radioactive elements contents in Bangladeshi soils, it should be useful in understanding the background level and characteristics of these elements in the nation's soils.

Table.12 Trace and natural radioactive elements contents (mg/kg) of Bangladeshi soils.

Elements	Mean	Std (±)	Median	Minimum	Maximum
Li	25.1	6.2	24.2	16.7	39.4
Sc	7.7	2.6	7.6	3.8	12
V	97.9	6.3	98.5	82.9	109
Cr	77.5	10.1	76.8	59.5	95.4
Co	12	3.9	11.5	4.6	22.2
Ni	33	9.6	31.7	17.7	50.6
Cu	21.1	7.1	21.1	10.9	38.3
Zn	60.6	28.5	52.6	26.4	164.3
Ga	14	3	13.4	9.6	19.9
As	7	0.9	7.2	5.3	8.7
Br	2	0.9	0.8	2.2	3.7
Rb	96.3	19.9	96.4	56.4	133.8
Sr	62.6	41.4	42.7	24.9	145.9
Cd	0.2	0.2	0.2	0.1	1.2
I	3.5	2.6	2.7	0.8	8.5
Cs	5.4	1.3	5.3	3.5	8.5
Ba	319.3	59.1	303.7	222.6	432.3
Pb	20.5	3.9	20.1	14.5	30.7
Th	16.5	2.8	16.6	12.4	22.4
U	3.0	0.4	2.9	2.1	3.5

87. Epidemiological Investigations of the Residents Nearby Nuclear Power Plants in Japan: Progress and Future

Yasuhiko Yoshimoto and Shinji Yoshinaga

It is easy to look at descriptive results from epidemiological research, but also easy to misunderstand their meanings. Misunderstanding occurs mainly from insufficient scientific knowledge, but also sometimes from distorted interpretation. We must be aware that our research activities generate unnecessary fears among the public, either as an inflated risk or from disregard of all but one positive aspect of a study; we must not hang onto observed small risks or dwell on large negative observations, only.

Japanese nuclear power plants (NPPs) have been designed to limit the quantity of radioactive effluents (the routine effective dose of the public is 50 μSv or less per year). The operating organizations have monitored effluents before being discharged as well as monitored radiation of the on-site environment. At present there has been no radioecology study of routine releases of radioactive materials from Japanese NPPs for epidemiologic investigations of the residents near the installations

except a system for emergency use developed after the 1979 accident at Three Mile Island, USA. The radiation monitoring of off-site environments which local governments have carried out shows dose range of the annual average of gamma rays in air is 344 to 842 μSv based on monitoring data provided by Japan Chemical Analysis Center. This variation reflects that of natural radiation mainly by geological distribution of granite and volcanic rocks. The usual doses of the public attributable to nuclear sites (10-20μSv for typical model sites) are considerably lower than the dose due to natural exposure.

Of course incidence data can provide better estimates of risk than mortality data because of differing survival rates and inadequate specification of death by individual sites or subtype of cancer. Japan also has no comprehensive national cancer registry program although continuous efforts by a research group for a population-based cancer registry have been made since 1975. Iwasaki et al in 1995 reported on mortality from leukemia and malignant lymphoma in the vicinity of NPPs in Japan. They concluded that the mortality from these two causes in the Japanese municipalities with NPPs is not significantly different from those in the control areas. But Hoffman et al have claimed that the data published by Iwasaki et al are compatible with the hypothesis of a leukemogenic impact of NPPs in Japan. We have analyzed the extended mortality data of these causes using a Poisson regression model. The results indicate that the overall relative risk of leukemia for all ages is about 1.2 and statistically significant at the 5% level when the systematic difference between 20 municipalities with NPPs and 80 selected control areas are assumed. But no clear evidence of increase is observed in childhood in contrast to a leukemia cluster argument near the Sellafield reprocessing plant in England. Although the inherent limitation of a geographical correlation study exists, our results might be influenced by a different time lag behind general temporal change of mortality in the selected areas and a drastic change of mortality in a specific area, as well as randomness. No such difference is indicated for malignant lymphoma.

A multi-site study to get composite inference of all NPPs in Japan is expected to offer more comprehensive interpretation of the findings than a local site study. There are two possible approaches for a geographical correlation study; a) usage of administrative units and b) GIS (geographic information systems) with small areas. The former approach is based on the routine health statistics of municipalities with NPPs. But it is almost impossible to select ideal comparative control administrative municipalities. The later approach is based on the individual location of cases in a defined area. But individual identification of the population at risk is not always easy in the case of a large exposed population distributed in wide areas such as thyroid cancer risk after the Chernobyl accident. The usefulness of GIS was examined for the information on the basis of small area units of the population. Instead of administrative areas where the size of area is sometimes very different, mesh units or circle areas can provide a better expression of risk for different purposes. Understanding the inherent limitation of geographical correlation study is necessary to find correct interpretations from the results for either approach.

A review of associated recent radiation experiences in the other countries as well as in Japan can give some clues for our new challenge to conduct epidemiological research in this field. At least it should be able to distinguish the difference between cases of NPP routine operation and cases of NPP accident. In the former it is important to describe complex issues of the risk of low-dose and low-dose-rate radiation without being misleading. The situation is a pendulum which swings back and forth but stays in its position. It is important to decrease uncertainties as much as possible when informing the public about what a serious problem is and what is not.

Publication:

Yoshimoto, Y: Invited talk at the 2002 International Symposium on Health Effects of Ionizing Radiation, Gwangiu, Korea, 2002.

SPACE SCIENCE

88. Genomic Instability in Mutation Induction on Normal Human Cells Exposed to Chronic Low-dose Radiation in Heavy Ion Radiation Field

Masao Suzuki, Chizuru Yamaguchi, Yukio Uchihori, Kumie Nojima, Hiroshi Yasuda and Kazunobu Fujitaka

Keywords: *genomic instability, hprt locus, low-dose scattered radiation, heavy ion radiation field*

We have been studying cellular responses in normal human fibroblasts exposed to chronically low-dose scattered radiations in a heavy ion radiation field. Cells were cultured in a CO_2 incubator, which was set in the irradiation room for heavy ions in the HIMAC. This year, we examined the induction of genomic instability in cellular effects, such as cell killing and mutation, as a function of accumulated doses of scattered low-dose irradiation. Cell-killing effect was detected as a reproductive death using a colony-formation assay. Mutation was measured as the induction of a 6-thioguanie resistant clone focused on *hprt* locus. Genomic instability in cellular responses was examined to measure either cell surviving fraction or mutation frequency in low-dose exposed cell populations irradiated with X-ray challenging doses. The preliminary results showed that there was no enhanced effect on cell killing between the low-dose accumulated and non-irradiated cell populations irradiated with defined challenging doses of X rays. On the contrary, the mutation frequency of the low-dose accumulated cell population was much higher than that of non-irradiated cell population, when irradiated with defined challenging doses of X rays. There is evidence that genomic instability was induced in mutagenesis by the chronically low-dose irradiation in the heavy ion radiation field.

89. LET and Ion Species Dependence of Cell Killing and Chromosome Damage on Normal Human Fibroblasts

Chizuru Yamaguchi, Masao Suzuki and Kazunobu Fujitaka

Keywords: *LET & ion species dependence, HZE particles, chromatin breaks, premature chromosome condensation (PCC)*

We have been studying the RBE values of either LET or ion species dependence in different biological endpoints. This year, we focused on cell-killing effect dependence upon LET using carbon, neon, argon, silicon and iron ions produced by the HIMAC and the Alternating Gradient Synchrotron (AGS) at Brookhaven National Laboratory (BNL).

The RBE-LET curves for cell killing effect showed a peak in the LET range of 100-150 keV/μm for carbon ion beams. On the other hand it showed a broad peak from 150keV/μm to 250keV/μm for silicon ion beams. There is evidence that the RBE-LET relationship for cell killing is not the same with different ion species.

The survival curves for high-energy Fe ion beams plated 1 hr after irradiation (IP) showed little or no shoulder. However, the survival curves plated 24 hr after irradiation (DP) had a small initial shoulder. RBE values compared to ^{137}Cs γ rays were 1.99 for IP and 2.73 for DP at D_{10}. The repair ratio (DP/IP) was 1.67 for γ rays and 1.22 for Fe ions. The dose-response curves for initially measured and residual chromatid fragments detected by the Calyculin A-mediated PCC technique showed a linear response. The results indicated that the induction frequency for initially measured fragments was the same between γ rays and Fe ions. On the other hand, ~85% of the fragments induced by γ rays rejoined after 24hr of post-irradiation incubation, while only 37% of the fragments induced by Fe ions did. Furthermore, the frequency of chromatid exchanges induced by γ rays measured 24 hr after irradiation was higher than that of Fe ions. No difference in chromatid exchanges induced by the two types of radiations was detected when assayed 1 hr after irradiation. The results suggest that high-energy Fe ions induce a higher frequency of complex, unrepairable damage at both the cellular and chromosomal levels than ^{137}Cs γ rays.

90. Conservative Evaluation of Space Radiation Dose Equivalent Using the Glow Curve of $^7LiF:Mg,Ti$ (TLD-700)

Hiroshi Yasuda

Keywords: *space radiation, conservative dosimetry, dose equivalent, International Space Station, low Earth orbit*

Long-term human activities in the International Space Station (ISS) require acceptance of radiation risk. A primary concern in a long stay in the ISS is stochastic effects, i.e. cancer and hereditary risk. An index of the stochastic effects (dose equivalent or equivalent dose) needs to be measured and controlled for each astronaut.

For personal dosimetry in a spacecraft, solid-state integrating detectors such as thermoluminescent dosemeters (TLD) are advantageous with respect to their small scale, long term stability, and simplicity in handling. As a simple approach for conservative evaluation of dose equivalent in space, we have proposed a new approach using the glow curve of TLD-700. This approach is superior to the previous one using a two-peak ratio, in terms of following the revised Q-LET relationship in the 1990 ICRP recommendation. The dependence of each peak on LET was confirmed using relativistic heavy ion beams (He, C, Ne, Ar, and Kr) at NIRS-HIMAC. TL values of both peak areas on the γ-ray absorbed-dose basis were additionally combined to conservatively estimate a dose equivalent over a range of LET of 0.5 - 440 keV μm^{-1}. This method was tested in an 8.8-day Shuttle-Mir mission (STS-89) at 400km×51.65º. The dose-equivalent rates obtained at two positions in the Spacehab module were about 0.9 mSv d^{-1}; this result is reasonable in a conservative sense.

Publications:
1) Yasuda, H.: *Health Phys*., **80**, 576-582, 2001.
2) Yasuda, H. and Fujitaka, K.: *Radiat. Prot. Dosim*., **94**, 275-280, 2001.
3) Yasuda, H. and Fujitaka, K.: *J. Radiat. Res*., **42**, 57-68, 2001.
4) Yasuda, H.: *J. Radiat. Res*., **42**, 69-78, 2001.
5) Yasuda, H. and Kobayashi, I.: *Radiat. Prot. Dosim*., **95**, 339-343, 2001.
6) Yasuda, H.: *Radiat. Res*., **156**, 805-808, 2001.

APPENDIX

Publications

List of Keywords

Author Index

Organization and Staff

APPENDIX

PUBLICATIONS

This list includes publications by the staff members issued during
the period form April 1, 2001 to March 31, 2002

Training School

Shirakawa, Y.: Basic Study on Simultaneously Measurement of Coming Direction and Energy Of Gamma Ray Using a Tandem Detector, Radioisotopes, **50** [4], 117-122 (2001).

Shirakawa, Y.: Simaltaneous Measurement of Both Coming Directions and Energies of Gamma Rays Using a NaI/BGO Tandem Detector, The 38th Annual Meeting on Radioisotopes and Radiation in the Physical Sciences and Industries,1a-III- 6 (2001).

Shirakawa, Y.: Development of a Scintillation Detector for Simultaneous Measurement of Coming Directions and Energies of Gamma Rays, SICE2001, 102C-1 (2001).

Division of Technical Support and Development

Yukawa, M., Imaseki, H. and Aoki, K.: Elemental Distribution in Organs of Medaka, Oryzias Laptipes, Burdened with X-ray Irradiation and Salty Water, *Int. J. PIXE*, 10, 121-125, 2000.

Imaseki, H. and Yukawa, M.: Introduction of PIXE Analysis System in NIRS, *Int. J. PIXE*, 10, 77-90, 2000.

Yukawa, M.: Bio-PIXE, Theory and Applications. Chapter 8. Application to Food Science-Application of Particle Induced X-ray Emission (PIXE) Analysis to Food Science, *Radioisotopes*, 50,12-21, 2001.

Yukawa, M.: Application of Particle Induced X-ray Emission (PIXE) Analysis to Determination of Trace Element in Biological Samples, *Biomedical Research on Trace Elements*, 12,62-70, 2001.

Yukawa, M.: Determination of Elemental Distribution in Small Area of Biological Samples Using PIXE Analysis, *Ferum*, 6, 9-14, 2001.

Yoshinaga, J., Morita, M., Yukawa, M., Shiraishi, K., Kawamura, H.: Certified Reference Material for Analytical Quality Assurance of Minor and Trace Elements in Food and Related Matrixes Based on a Typical Japanese Diet: Interlaboratory Study, *Journal of AOAC International*, 84, 1202-1208, 2001.

Low Dose Radiation Effects Research Project

Shimada, Y., Nishimura, M., Kakinuma, S., Takeuchi, T., Ogiu, T., Suzuki, G., Nakata, Y., Sasanuma, S., Mita, K. and Sado, T.: Characteristic association of K-ras gene mutation with loss of heterozygosity in X-ray-induced thymic lymphomas of B6C3F1 mice. Int. J. Radiat. Biol., 77, 465-473, 2001.

Watanabe, N., Okochi, E., Hirayama, Y., Shimada, Y., Yanagihara, K., Yoshida, M., Takahashi, S., Mochizuki, M., Sugimura, T., Nagao, M., Ushijima, T.: Single nucleotide instability without microsatellite instability in rat mammary carcinomas. Cancer Res., 61, 2632-2640, 2001.

Motoori, S., Majima, HJ., Ebara, M., Kato, H., Hirai, F., Kakinuma, S., Yamaguchi, C., Ozawa, T., Nagano, T., Tsujii, H., Saisho, H.: Overexpression of mitochondrial manganese protests against radiation-induced cell death in the human hepatocellular carcinoma cell line HLE. Cancer Res., 61, 5382-5388, 2001.

Nishimura, M., Kakinuma, S., Wakana, S., Mukaigawara, A., Mita, K., Sado, T., Ogiu, T., Shimada, Y.: Reduced sensitivity to and ras mutation spectrum of N-ethyl-N-nitorsourea-induced thymic lymphomas in adult C.B-17 scid mice. Mutat. Res., 486, 275-283, 2001.

Kakinuma, S., Nishimura, M., Sasanuma, S., Mita, K., Suzuki, G., Katsura, Y., Sado, T., Shimada, Y.: Spectrum of Ikaros inactivation and its association with loss of heterozygosity in radiogenic T-cell lymphomas in susceptible B6C3F1 mice. Radiat. Res., (in press)

Yamashita, A., Katsube T., Hashimoto N., Tomita K., Takahashi M., Ueda R., Togashi S.: Identification of *Xenopus* cortactin: two isoforms of the transcript and multiple forms of the protein. Zool. Sci., 18, 331-336,

2001.

Hirai, Y., Hayashi, T., Kubo, Y., Hoki, Y., Arita, I., Tatsumi, K., Seyama, T.: X-irradiation induces up-regulation of ATM gene expression in wild-type lymphoblastoid cell lines, but not in their heterozygous or homozygous ataxia-telangiectasia counterparts. Jpn. J. Cancer Res., 92, 710-717, 2001.

Miura, M., Watanabe, H., Sasaki, T., Tatsumi, K., Muto, M.: Dynamic changes in subnuclear NP95 location during the cell cycle and its spatial relationship with DNA replication foci. Exp. Cell Res., 263, 202-208, 2001.

Tachibana, A., Furuno-Fukushi, I., Tatsumi, K., Sasaki, M.S.: High frequency of deletions at the hypoxanthine-guanine phosphoribosyltransferase locus in an ataxia-telangiectasia lymphoblastoid cell line irradiated with gamma-rays. Jpn. J Cancer Res., 92, 1190-1198, 2001.

Shiomi, N., Hayashi, E., Sasanuma, S., Mita, K., Shiomi, T.: Disruption of Xpg increases spontaneous mutation frequency, particularly A:T-to-C:G transversion. Mutat. Res., 487, 127-135, 2001.

Koike, M., Kuroiwa, A., Koike, A., Shiomi, T., Matsuda, Y.: Expression and chromosome mapping of hamster Ku70 and Ku80. Cytogenet. Cell Genet., 93, 52-56, 2001.

Sun, X.- Z., Harada, Y.- N., Takahashi, S., Shiomi, N., Shiomi, T.: Purkinje cell degeneration in mice lacking the xeroderma pigmentosum group G gene. J. Neurosci. Res., 64, 348-354, 2001.

Koike, M., Shiomi, T., Koike, A.: Dimerization and nuclear localization of Ku proteins. J. Biol. Chem., 276, 11167-11173, 2001.

International Space Radiation Laboratory
Fukuda, S.: Incidence of pyometra in colony-raised beagle dogs, Exp. Anim. 50, 325-329, 2001.

Iida, H. and Fukuda, S.: Age-related changes in bone mineral density, cross sectional area and strength at different skeletal site in male rat, J. Vet. Med. Sci., 64, 29-34, 2001.

Yasuda, H., Suzuki, M., Ando, K. and Fujitaka, K.: Simulation of the low-earth-orbit dose rates using secondary radiations from HZE particles in NIRS-HIMAC, Phsyica Medica, 17, 135-139, 2001.

Yasuda, H., Komiyama, T. and Fujitaka, K.: Probability

of hippocampus cell hits by high-LET space radiation in a low-Earth-orbit mission (STS-91), Phsyica Medica, 17, 168-171, 2001.

Yasuda, H. and Fujitaka, K.: Responses of TLD-BeO:Na (UD-170A) to heavy ions and space radiation, Radiat. Prot. Dosim., 94, 275-280, 2001.

Yasuda, H. and Fujitaka, K.: Cosmic radiation protection dosimetry using the Electronic Personal Dosemeter (EPD) in selected international flights, J. Radiat. Res., 42, 57-68, 2001.

Yasuda, H.: Glow peak stability in ^{6}LiF:Mg,Ti (TLD-600) exposed to Fe-ion beam, J. Radiat. Res., 42, 69-78, 2001.

Yasuda, H.: Conservative evaluation of space radiation dose equivalent using the glow curve of ^{7}LiF:Mg,Ti (TLD700), Health Phys., 80, 576-582, 2001.

Yasuda, H. and Kobayashi, I.: Optically stimulated luminescence from Al_2O_3:C irradiated with relativistic heavy ions, Radiat. Prot. Dosim., 95, 339-343, 2001.

Yasuda, H.: Responses of Direct Ion Storage dosimeter (DIS-1) to heavy charged particles, Radiat. Res., 156, 805-808, 2001.

Yasuda, H.: A simple dosimetry method for biological experiments on the international space station, Japanese Journal of Aerospace and Environmental Medicine (in Japanese), 38, 1-7, 2001.

Yasuda, N., Uchikawa, K., Amemiya, K., Watanabe, N., Takahashi, H., Nakazawa, M., Yamamoto, M. and Ogura, K.: Estimation of the latent track size of CR-39 using atomic force microscope, Radiation Measurements 34,45-49,2001.

Golovchenko, A.N., Skvarc, J., Yasuda, N., Ilic, R., Tretyakova, S.P., Ogura, K. and Murakami, T.: Total charge-changing and partial cross-section measurements in the reaction of 110 MeV/u ^{12}C with paraffin, Radiation Measurements 34, 297-300, 2001.

Kuge, K., Yasuda, N., Kumagai, H., Nakazawa, K., Aoki, N. and Hasegawa, A.: Detection of colored tracks of heavy ion particles using photographic color film, Radiation Measurements 34, 203-206,2001.

Saad, A.F., Atwa, S.T., Yasuda, N. and Fujii, M.: Study on the structure of latent tracks in CR-39 and SR-90 track detectors by FT-IR spectroscopy, Radiation Measurements, 34, 51-54, 2001.

Ichikawa, A., Yasuda, N. and KEK-PS E373 collaboration: Production of twin Λ-hypernuclei from Ξ^- hyperon capture at rest, *Phys. Lett*, B500, 37-46, 2001.

Takahashi, H., Yasuda, N., et. al. and KEK-PS E373 collaboration: Observation of a (Lambda Lambda)He-6 double hypernucleus, Phys. Rev. Lett. 87(2001)212502-1 - 212502-5.

Ogura, K., Asano, M., Yasuda, N. and Yoshida, M.: Properties of TNF-1 track etch detector, Nucl. Inst. and Meth., B185, 222-227, 2001.

Yasuda, N., Kuge, K., Kobayashi, T., Aoki, N., Hasegawa, A., Kumagai, H.: Application of nuclear emulsion in particle physics and development of multi-layered color nuclear emulsion (in Japanese), *J. Soc. of Photogr Sci.*, 64(2), 87-91, 2001.

Suzuki, M., Piao, C. Q., Hall, E. J. and Hei, T. K.: Cell killing and chromatid damage in primary human bronchial epithelial cells irradiated with accelerated 56Fe ions, *Radiation Research*, 155, 432-439 , 2001.

Suzuki, M., Piao, C. Q., Zhao, Y. L. and Hei, T. K.: Karyotype analysis of tumorigenic human bronchial epithelial cells transformed by chrysolite asbestos using chemically induced premature chromosome condensation technique, *International Journal of Molecular Medicine* , 8, 43-47 (2001).

Zhou, H., Suzuki, M., Randers-Pehrson, G., Vannais, D., Chen, G., Trosko, J. E., Waldren, A. C., and Hei, T. K.: Radiation risk to low fluences of a particles may be greater than we thought, *Proc. Natl. Acad. Sci.UAS*, 98, 14410-14415 (2001).

Takada, M., Taniguchi, S., Nakamura, T., Nakao, N., Uwamino, Y., Shibata, T. and Fujitaka, K.: Neutron spectrometry in a mixed field of neutrons and protons with a phoswich neutron detector, Part 1: response functions for photons and neutrons of the phoswich neutron detector. *Nucl. Instrum. Meth.,* A465, 498-511, 2001.

Takada, M., Taniguchi, S., Nakamura, T. and Fujitaka, K.: Neutron spectrometry in a mixed field of neutrons and protons with a phoswich neutron detector, Part 2: application of the phoswich neutron detector to neutron spectrum measurements, *Nucl. Instrum. Meth.*, A465, 512-524, 2001.

Takada, M., Taniguchi, S., Nakamura, T., Nakao, N., Uwamino, Y., Shibata, T. and Fujitaka, K.:

Characteristics of a Phoswich Detector to Measure Neutron Spectrum in a Mixed Field of Neutrons and Charged Particles, Nuclear Instruments and Methods in Physics Research, A476 (2002) 332-336.

Takada, M., Yamaguchi, H., Uchihori, Y., Kitamura, H. and Fujitaka, K.: Differential Dosimetry in a Neutron-Proton Mixed Field with Low-pressure Proportional Couters, *Radiat. Prot. Dosim.*, 97, 213-222, 2001

Taniguchi, S., Takada, M., Nakamura, T.: Development of multi-moderator neutron spectrometer using a pair of 6Li and 7Li glass scintillators, Nuclear Instruments and Methods in Physics research, A460(2001) 368-373.

Koi, T., Muraki, Y., Masuda, K., et al.: Attenuation of neutrons in the atmosphere and a thick carbon target, *Nucl. Instrum. Meth*. A469, 63-69, 2001.

Ando, K. Furusawa, Y., Suzuki, M., Nojima, K., Majima, H., et al.: Relative Biological Effectiveness of the 235Mev Proton Beams at the National Cancer Center Hospital East, J.Rad. Res., 42, 2001

Motoori, S., Majima, H. J., Ebara, M., Kato, H., Hirai, F., Kakinuma, S., Yamaguchi, C., Ando, K., Ozawa, T., Nagano, T., Tsujii, H. and Saisho, H.: Overexpression of mitochondrial manganese superox-ide dismutase protects against radiation-induced cell death in the human hepatocellular carcinoma cell line, HLE. Cancer Res., 61, 5382-5388, 2001.

Yunfeng, Zhao, Yi, Xue, Terry, D. Oberley, Kelley Kiningham, K., Shu-mei, Lin., Hsiu-Chuan, Yen., Majima, H., Judy, Hines. and Daret, St. Clair.: Overexpression of MnSOD suppresses tumor formation by modulation of AP-1 signaling in a multistage skin carcinogenesis model. Cancer Res. 61: 6082-6088, 2001.

Dachev, Ts., Tomov, B., Matviichuk, Yu., Dimitrov, Pl., Lemaire, J., Gregoire, Gh., Cyamukungu, M., Schmitz, H., Fujitaka, K., Uchihori, Y., Kitamura, H., Reitz, G., Beaujean, R., Petrov, V., Shurshakov, V., Benghin, V.: Calibration Results Obtained With Liulin-4 Type Dosimeters, Adv. Space Reas. (in press)

Yamaguchi, H., G. Siebers, J., Furukawa, A., Otagiri, N., Osman, R.: Molecular Dynamics Simulation of a DNA Containing a Single Strand Break, *Radiat. Prot. Dosim.*, in press.

Amemiya, K., Takahashi, H., Nakazawa, M., Shimizu, H., Majima, T., Nakagawa, Y., Yasuda, N.,

Yamamoto, M., Kageji, T., Nakaichi, M., Hasegawa, T., Kobayashi, T., Sakurai, Y., Ogura, K.: Soft X-ray imaging using CR-39 plastics with AFM readout., *Nucl. Instrum. Meth. B*, in press.

Kuge, K., Yasuda, N., Kumagai, H., Nakazawa, K., Aoki, N. and Hasegawa, A.: Colored tracks of heavy ion particles using photographic color film, *Nucl. Instrum Meth.* in press.

Ogura, K., Asano, M., Yasuda, N. and Yoshida, M.: Properties of TNF-1 track etch detector, *Nucl. Inst. and Meth.* in press.

Environmental Radiation Protection Research

Sahoo, S. K., Yonehara, H., Kurotaki, K., Ramzaev, V. and Barkovski, A.: Determination of rare earth elements, thorium, and uranium by inductively coupled plasma mass spectrometry and strontium isotopes by thermal ionization mass spectrometry in soil samples of Bryansk region contaminated due to Chernobyl accident. *Journal of Radioanalytical and Nuclear Chemistr*y,247(2),341-345,2001.

Giang, N., Shiraishi, K., Sinh, N. M., Kimura, S., Tuan, N. N. and Arae, H.: Estimation of dietary 232Th,238U,cesium,and strontium intakes in Vietnamese people from different geographical regions. *Health Phys.*, 80(6), 605-11, 2001.

Kimura, S., Kurasaki, M., Saito, T., Ito, K., Hosokawa, T., Okabe, M., Shiraishi, K. and Niioka, T.: Effects of synthetic dopamine-melanin on oxygen radical formation induced by metal ions with dopamine. *Neurosci. Res. Commun.* 29(1),31-40,2001.

Ueno, S., Kishimoto, T., Susa, N., Furukawa, Y., Ishii, M., Yokoi, K., Yasuno, M., Sasaki, Y., Ueda, J., Nishimura, Y., Sugiyama, M.: Detection of cichromate(IV)-induced DNA strand breaks and formation of paramagnetic chromium in multiple mouse organs. *Toxicology and Applied Pharmacology*, 170, 56-62, 2001.

Nishimura, Y., Takeda, H., Miyamoto, K., Watanabe, Y., Kouno, F., Kuroda, N., Kim, H. S., Yukawa, M.: Determination of ^{32}P in urine for early estimation of neutron exposure level for three victims in the JCO criticality accident. *J. Radiological Protection* 22,25-29, 2002.

Yoshinaga, J., Morita, M., Yukawa, M., Shiraishi, K., Kasamura, H.: Certified Reference Material for Analytical Quality Assurance of Minor and Trace Elements in Food and Related Matrixes Based on a Typical Japanese Diet; Interlaboratory Study. *Journal of AOAC International* Vol. 84, No. 4(2001).

Homma-Takeda, S., Kugenuma, Y., Iwamuro, T., Kumagai, Y., and Shimojo, N.: Impairment of spermatogenesis by methylmercury in rats. *Toxicology*, 169, 25-35, 2001.

Ishigure, N., Endo, A., Yamaguchi, Y. and Kawachi, K.: Calculation of absorbed does for the overexposed patients at the criticality accident in Tokai-mura. *J. Radiat. Res*. 42: suppl., S137-S148, 2001.

Ishigure, N., Nakano, T. and Enomoto, H.: Am-241 as a metabolic tracer for inhaled plutonium nitrate in external chest counting. *Radiat. Prot. Dosimetry*, 97, 271-273, 2001.

Yamada, M. and T. Aono.: Large particle flux of $^{239+240}$Pu on the continental margin of the East China Sea. *The Science of the Total Environment* 287, 97-105, 2002.

Miyazaki, T., Nakahara, M., Ishii, T., Aoki, K. and Watabe, T.: Accumulation of cobalt in newly hatched octopus Octopus Vulgaris. *Fisheries Science*, 67, 170-172. 2001.

Miyazaki, T., Iwami, T., Yamauchi, M. and Somiya, H.: Accessory corner cones as putative UV-sensitive photoreceptors in the retinas of seven adult nototheniid fishes. *Polar Biology*, 24, 628-632, 2001.

Watanabe, Y., Yukawa, M., Miyamoto, K., Takeda, H., Nishimura, Y., Akashi, M., Fujimoto, K., Fuma, S., Hirama, T., Ishigure, N., Joshima, H., Kouno, F.: International Symposium on the Criticality Accident in Tokaimura, Medical Aspects of Radiation Emergency. *NIRS-M-146*, 102-108, 2001.

Ishigure, N., Endo, A., Yamaguchi, Y. and Kawachi, K.: International Symposium on The Criticality Accident in Tokaimura, Medical Aspects of Radiation Emergency. *NIRS-M-146*,110-119,2001.

Environmental and Toxicological Sciences

Amachi, S., Kamagata, Y., Kanagawa, T. and Muramatsu, Y.: Bacteria mediate methylation of iodine in marine and terrestrial environments. Applied and Environmental Microbiology, 67, 2718-2722, 2001.

Doi, M., Nakamura, Y., Sakashita, T., Ogiu, N., Lagarde, F., Falk. R.: Lifetime risk of lung cancer due to radon exposure projected to Japanese and Swedish populations. Health Physics, 80, 552-562, 2001.

Fuma, S., Takeda, H., Miyamoto, K., Yanagisawa, K., Inoue, Y., Ishii, N., Sugai, C., Ishii, C. and Kawabata, Z.: Ecological evaluation of gadolinium toxicity compared with other heavy metals using an aquatic microcosm. Bull.Environ.Cont.Toxicol., 66, 231-238, 2001.

Furuya, K., Kudo, Y., Okinaga, K., Yamuki, M., Takahashi, S., Araki, Y. and Hisamatu, Y.: Seasonal variation and their characterization of suspended particulate matter in the air of subway stations. J. Trace Microprobe Tec., J. Trace Microprobe Tec., 19(4): 469-485.2001.

Ishii, N., Takeda, H., Doi, M., Fuma, S., Miyamoto, K., Yanagisawa, K. and Kawabata, Z.: A new method using enhanced green fluorescent protein (EGFP) to determine grazing rate on live bacterial cells by protests. Limnology, 3, 47-50, 2002.

Miyamoto, K., Inoue, Y., Iwakura, T., Takeda, H., Fuma, S., Yanagisawa, K. and Ishii, N.: An application of a transfer model to the drainage system of tritium in a river basin in the vicinity of a nuclear site. Fusion Science & Technology, 41, 483-487, 2002.

Miyamoto, K., Watanabe, Y., Yukawa, M., Takeda, H., Nishimura, Y., Ishigure, N., Hirama, T. and Akashi, M.: Reconstruction of two victims' posturing based on the induced radioactivies in their bones in the criticality accident in Tokai-mura, Japan.. Health Physics, 83, 19-25, 2002.

Muramatsu, Y., Yoshida, S., Tagami, K., Uchida, S. and Rühm, W.: ICP-MS analysis of environmental plutonium. Plutonium in the Enviroment, Radioactivity in the Environment. (Elsevier Science), 1, 63-77, 2001.

Muramatsu, Y., Hamilton, T., Uchida, S., Tagami, K. and Yoshida, S.: Measurement of ^{240}Pu/^{239}Pu isotopic ratios in soils from the Marshall Islands using ICP-MS. The Science of the Total Environment, 278, 151-159, 2001.

Muramatsu, Y., Noda, Y., Yonehara, H., Ishigure, N., Yoshida, S., Yukawa, M., Tagami, K., Ban-nai, T., Uchida, S., Akashi, M., Hirama, T. and Nakamura, Y.: Determination of radionuclides produced by neutrons in heavily exposed workers of the JCO criticality accident in Tokai-mura for estimating an individual's neutron fluence. J. Radiation Research, 42, S117-S128, 2001.

Muramatsu, Y., Fehn, U. and Yoshida, S.: Recycling of iodine in fore-arc areas: evidence from the iodine brines in Chiba, Japan. Earth and Planetary Science Letters, 192, 583-593, 2001.

Sakashita, T., Nakamura, Y. and Doi, M.: Test of wet scavenging parameterization schemes by simulation of monthly depositions of 7Be using normally available data on environmental monitoring and local meteorology. J. Nucl. Sci. Technol., 39, 180-186, 2002.

Sato, H., Takahashi, S. and Kubota, Y.: Effects of gadolinium on the retention and translocation of ^{239}Pu-hydroxide. Health Physics, 80, 164-169, 2001.

Shinonaga, T., Gerzabek, M. H., Strebl, F. and Muramatsu, Y.: Transfer of iodine from soil to cereal grains in agricultural areas of Austria. The Science of the Total Environment, 267, 33-40, 2001.

Steiner, M., Linkov, I. and Yoshida, S.: The role of fungi in the transfer and cycling of radionuclides in forest ecosystems. J. Environ. Radioact., 58, 217-241, 2002.

Takahashi, S., Okinaga, K., Kubota, Y., Furuya, K.: A new method to estimate the cytotoxic effects of suspended particulate matter on the cultured alveolar macrophages in vitro. Toxicology Method. (in presss)

Takeda, H., Miyamoto, K., Yukawa, M., Nishimura, Y., Watanabe, Y., Kim, H. S., Kuroda, N., Kouno, F., Joshima, H., Hirama, T. and Akashi, M.: Bioassay for neutron-dose estimations of three patients in the JCO criticality accident in Tokai-mura by measuring β-ray emitters. J. Radiation Res., 42, S129- S135, 2001.

Yanagisawa, K., Takeda, H., Miyamoto, K., Fuma, S. and Ishii, N.: Determination of ^{13}C concentration in biological materials using infrared absorption method. J. Radioanal. Nucl. Chem., 252, 277-280, 2002.

Yoshida, S., Muramatsu, Y., and Tagami, K.: Determination of uranium isotopes in soil core samples collected on the JCO grounds after the criticality accident. Environ. Sci. & Technol., 35, 4174-4179, 2001.

Sun, X-Z., Harada, Y., Takahashi, S., Shiomi, N. and Shiomi, T.: Purkinje cell degeneration in mice lacking the xeroderma pigmentosum group G gene. Journal of Neuroscience Research, 64, 348-354, 2001.

Sun, X-Z., Takahashi, S., Fukui, Y., Hisano, S., Kubota, Y., Sato, H. and Inouye, M.: Neurogenesis of heterotopic gray matter in the brain of the microcephalic mouse. Journal of Neuroscience Research, 66, 1083-1093, 2001.

Radon Research Group

Tokonami, S., Yang, M. and Sanada, T.: Contribution from thoron on the response of passive radon detectors. Health Phys., 80(6), 612-615, 2001

Zhuo, W., Iida, T. and Yang, X.: Occurrence of 222Rn, 226Ra, 228Ra and U in groundwater in Fujian Province, China. J. Environ. Radioactivity **53**(1), 111-120, 2001

Zhuo, W., Iida, T., Moriizumi, J., Aoyagi, T. and Takahashi, I.: Simulation of the concentrations and their distributions of indoor radon and thoron. Radiat. Prot. Dosim. **93**(4), 357-368, 2001

Ishikawa, T., Uchiyama, M., Hoshi, M., Takada, J., Endo, S., Sugiura, N., Kosato, T. and Shimizu, I.: New in-vivo calibration phantoms and their performance. Health Phys. **82**(3), 348-357, 2002

Redox Regulation Research Group

Ueda, J., Tsuchiya, Y.* and Ozawa, T.: Relationship between effects of phenolic compounds on the generation of free radicals from lactoperoxidase-catalyzed oxidation of NAD(P)H or GSH and their DPPH scavenging ability, *Chem. Pharm. Bull*., **49**, 299-304, 2001. (*Kyoritu College of Pharmacy)

Ueno, S.*, Kashimoto, T.*, Susa, N.*, Furukawa, Y.*, Ishii, M.*, Yokoi, K.*, Yasuno, M.*, Sasaki, Y.**, Ueda, J., Nishimura, Y. and Sugiyama, M.***: Detection of dichromate (VI)-induced DNA strand breaks and formation of paramagnetic chromium in multiple mouse organs, *Toxicol. Applied Pharmacol*., **170**, 56-62, 2001. (*Kitazato Univ., **Hachinohe Natl. Col. of Tec., ***Sugiyama Pharmacy)

Han, J.-Y.*, Takeshita, K. and Utsumi, H.*: Noninvasive detection of hydroxyl radical generation in lung by diesel exhaust particles, *Free Radic. Biol. Med*. **30**, 516-525, 2001. (*Kyushu University)

Shindo K.*, Shinozaki K.**, Kami, K.*, Anzai, K., Lee, S.***, Aoyagi, H.****, Kirino, Y.** and Shimada, I.*: Solution structure of micelle-bound H5 peptide (427- 452): A primary structure corresponding to the pore-forming region of the voltage dependent potassium channel, *Biochim. Biophys. Acta*. **1545**, 153-159, 2001. (*University of Tokyo, **Kyushu University,*** Fukuoka University, ****Nagasaki University)

Anzai, K., Ogawa, K.*, Ozawa, T. and Yamamoto, H.*: Quantitative comparison of two types of planar lipid bilayers - folded and painted - with respect to fusion with vesicles, *J. Biochem. Biophys. Methods*. **48**, 283-291, 2001. (*Kanagawa University)

Tanaka, I. and Ishihara, H.: Enhanced Expression of the Early Retrotransposon in C3H Mouse-Derived Myeloid Leukemia Cells. *Virology*, **280**, 107-114, 2001.

Inano, H. and Onoda, M.: Prevention of radiation-induced mammary tumors, Intl. *J. Radiat. Oncol. Biol. Phys*. **52** , 212-223, 2002

Nakagawa, H., Ohshima, Y., Takusagawa, M., Ikota, N., Takahashi, Y.*, Shimizu, S.**, and Ozawa, T.: Functional modification of cytochrome c by peroxynitrite in an electrontransfer reaction, *Chem. Pharm. Bull*., **49**, 1547-54, 2001. (*JEOL Ltd, ** Osaka University)

Nakagawa, H., Ikota, N., Ozawa, T., and Kotake, Y.*: Dose- and time-dependence of radiation-induced nitric oxide formation in mice as quantified with electron paramagnetic resonance. *Nitric Oxide, Biology and Chemistry*, **5**, 47-52, 2001. (*Oklahoma Medical Research Foundation)

Miura, Y., Anzai, K., Ueda, J., and Ozawa, T.: Pathophysiological significance of in vivo ESR signal decay in brain damage caused by X-irradiation. Radiation effect on nitroxyl decay of a lipophilic spin probe in the head region, *Biochim. Biophys. Acta*, **1525**, 167-172, 2001

Radiation Hazards Research Group

Hayata, I., Kanda, R., Minamihisamatsu, M., Furukawa, A., and Sasaki, M. M.: Cytogenetical dose estimation for 3 severely exposed cases in Tokai-mura criticality Accident. Journal of Radiation Research, 42 Suppl S149-S155. 2001.

Sasaki, M. M., Hayata, I., Kamada, N., Kodama, Y. and Kodama, S.: Chromosome aberration analysis in persons exposed to low-level radiation from the JCO criticality accident in Tokai-mura. Journal of Radiation Research, 42 Suppl S107-S116. 2001.

Kitagawa, M., Aizawa, S., Sado, T., Yamaguchi, S., Suzuki, T., Hirokawa, K., Ikeda, H.: A gene therapy model for retrovirus-induced disease with a viral env gene: expression-dependent resistance in immunosuppressed hosts. Leukemia, 15: 1779-1784, 2001.

Tanaka, K., Watanabe, K., Mori, M., Kamisaku, H., Tsuji, H., Hirabayashi, Y., Inoue, T., Yoshida, K., Aizawa, S.: Cytogenetic and cellular events during

radiation-induced thymic lymphomagenesisin p53 heterozygous (+/-) B10 mice. Int J Radiat Biol, 78: 165-172, 2002.

Yamaguchi, S., Kitagawa, M., Inoue, M., Tejima, Y., Kimura, M., Aizawa, S., Utsuyama, M., Hirokawa, K.: Role of lymphoid cells in age-related change of susceptibility to Friend leukemia virus-induced leukemia. Mech Ageing Dev 122: 219-232, 2001.

Suzuki, T., Aizawa, S., Ikeda, H.: Expression of receptor for ecotropic murine leukemia virus on hematopoietic cells. Arch Virol 146: 507-519, 2001.

Sakiyama, H., Masuda, R., Inoue, N., Yamamoto, K., Nakagawa, K., Yoshida, K.: Establishment and characterization of macrophage-like cell lines expressing ostoclast-specific markers. J Bone Miner Metab, 19-220-227, 2001.

Nose, M., Wang, B., Itsukaichi, H., Yukawa, O., Hayata, I., Yamada, T. and Ohyama, H.: Rescue of lethally irradiated mice from hematopoietic death by preexposure to 0.5 Gy X-rays without recovery of peripheral blood cell depletion and its modification by OK432. Radiat Res., 156, 195-204, 2001.

Nose, M., Uzawa, A., Ogiu, T. and Suzuki, G.: OK-432 Reduces mortality and bacterial translocation in irradiated and granulocyte-colony stimulating factor (G-CSF)-treated mice. J Radiat. Res., 42, 191-200, 2001.

Wang, B.: Involvement of p53-dependent apoptosis in radiation teratogenesis and in the radioadaptive response in the late period of organogenesis of mice. J. Radiat. Res., 42, 1-10, 2001.

Nenoi, M., Ichimura, S., Mita, K., Yukawa, O. and Cartwright, I. L.: Regulation of the catalase gene promoter by Spl, CCAAT-recognizing factors, and a WT1/Egr-related factor in hydrogen peroxide-resistant HP100 cells. Carcer Res., 61, 5885-5894, 2001.

Hama-Inaba, H., Choi, K. H., Wang, B., Haginoya, K., Yamada, T., Hayata, I. and Ohyama, H.: Fas-independent apoptpsis induced by UVC in p53-mutated human epithelial tumor A431 cells through activation of caspase-8 and JNK/SAPK. J. Radiat. Res., 42, 201-215, 2001.

Miyato, Y., Ibuki, Y., Ohyama, H., Yamada, T. and Goto, R.: Phosphatidylserine induces apoptosisi in CHO cells without mitochondrial dysfunction in a manner dependent on caspases other than caspases -1, -3, -8

and -9. FEBS letters, 594, 73-77, 2001.

Hirobe, T.: Endothelins are involved in regulating the proliferation and differentiation of mouse epidermal melanocytes in serum-free primary culture. J. Invest. Dermatol. Symp. Proc. 6: 25-31. 2001.

Mori, M., Itsukaichi, H., Nakamura, A. and Sato, K.: Molecular characterization of ionizing radiation-hypersensitive mutant M10 cells. Mut. Res. 487: 85-92. 2001.

Sugaya, K., Sasanuma, S., Cook, P. R. and Mita, K.: A mutation in the largest (catalytic) subunit of RNA polymerase II and its relation to the arrest of the cell cycle in the G_1 phase. Gene 274: 77-81. 2001.

Murakami, M., Minamihisamatsu, M., Sato, K. and Hayata, I.: Structural analysis of heavy ion radiation-induced chromosome aberrations by atomic force microscopy. J. Biophys. Meth. 48: 293-301. 2001.

Fujimaki, H., Nohara, K., Kobayashi, T., Suzuki, K., Eguchi-Kasai, K., Tsukumo, S., Kijima, M. and Tohyama, C.: Effect of a single oral dose of 2, 3, 7, 8-tetrachlorodibenzo-p-dioxin on immune function in Male NC/Nga mice. Toxicol. Sci. 66: 117-124. 2002.

Koike, M., Shiomi, T. and Koike, A.: Dimerization and Nuclear Localization of Ku Proteins. J. Biol. Chem. 276: 11167-11173. 2001.

Koike, M., Kuroiwa, A., Koike, A., Shiomi, T. and Matsuda, Y.: Expression and chromosome location of hamster Ku70 and ku80. Cytogenet. Cell Genet. 93: 52-56. 2001.

Transcriptome Profiling Research Group

Fukushima, T., Takata, M., Morrison, C., Araki, R., Fujimori, A., Abe, M., Tatsumi, K., Jasin, M., Dhar, P. K., Sonoda, E., Chiba, T., Takada, S.: Genetic analysis of the DNA-dependent protein kinase reveals an inhibitory role of Ku in late S-G2 phase DNA double-strand break repair. *J Biol Chem* 276, 44413-44418, 2001.

Hirai, Y., Hayashi, T., Kubo, Y., Hoki, Y., Arita, I., Tatsumi, K., Seyama, T.: X-irradiation induces up-regulation of ATM gene expression in wild-type lymphoblastoid cell lines,but not in their heterozygous or homozygous ataxia-telangiectasia counterparts. *Jpn J Cancer Res* 92, 710-717, 2001.

Kim, B. T., Kitagawa, H., Tamura, J., Saito, T., Kusche-Gullberg, M., Lindahl, U., Sugahara, K.: Human

tumor suppressor EXT gene family members EXTL1 and EXTL3 encode alpha 1, 4-acetylglucosaminyl-transferases that likely are involved in heparan sulfate/heparin biosynthesis. *Proc Natl Acad Sci USA* 98, 7176-7181, 2001.

Miura, M., Watanabe, H., Sasaki, T., Tatsumi, K., Muto, M.: Dynamic changes in subnuclear NP95 location during the cell cycle and its spatial relationship with DNA replication foci. *Exp Cell Res* 263, 202-208, 2001.

Ohhata, T., Araki, R., Fukumura, R., Kuroiwa, A., Matsuda, Y., Abe, M.: Cloning genomic structure and chromosomal localization of the gene encoding mouse DNA helicase RECQL5beta. *Gene* 280, 59-66, 2001.

Tachibana, A., Tatsumi, K., Furuno-Fukushi, I., Sasaki, M. S.: High frequency of deletions at the hypoxanthine-guanine phosphoribosyltransferase locus in an ataxia-telangiectasia lymphoblastoid cell line irradiated with gamma-rays. *Jpn J Cancer Res* 92, 1190-1198, 2001.

Laboratory Animal Development and Research Group
Ishikawa, Y., Yoshimoto, M.*, Yamamoto, N.*, Yasuda, T.*, Tokunaga, H.*, Iigou, M.*, Wakamatsu, Y.*, Ozato, K.*: Brain Structures of a Medaka Mutant, *el(eyeless)*, in Which Eye Vesicles Do Not Evaginate, Brain, Behavior and Evolution, 58, 173-184, 2001.

Internal Radiation Effects Research Group
Yamada, Y., Oghiso, Y., Enomoto, H. and Ishigure, N.: Induction of micronuclei in rat alveolar epithelial cell line by alpha particle irradiation. *Radiation Protection Dosimetry*, **99**, 219-221, 2002.

Research Center for Radiation Emergency Medicine
Akashi, M., Hirama, T., Tanosaki, S.*, Kuroiwa, N., Nakagawa, K., Tsuji, H., Katou, H., Yamada, S., Kamada, T., Kinugasa, T.*, Ariga, H.*, Maekawa, K.*, Suzuki, G.*, Tsujii, H.: Initial symptoms of acute radiation syndrome in the JCO criticality accident in Tokai-mura., Journal of Radiation Research, 42, 157-166, 2001

Hirama, T.: Case presentation of Worker C, Proceedings of International Symposium on the Criticality Accident in Tokaimura. Medical Aspects of Radiation Emergency, NIRS-M-146, 160-163, 2001

Akashi, M.: Dose estimation of victims severely exposed based on initial symptoms in the criticality accident in Tokaimura., Proceedings of International Symposium on the Criticality Accident in Tokaimura.

Medical Aspects of Radiation Emergency, NIRS-M-146, 72-80, 2001

Murata, H., Akashi, M.(Eds): The report of the criticality accident in a uranium conversion test plant in Tokai-mura. 2002

Hospital
Arai, K.*, Shibahara, T.*, Yamamoto, S., Yakushiji, T.*, Tanaka, C.*, Noma, H.*: Frequent allelic loss/imbalance on the short arm of chromosome 3 in tongue cancer., Bulletin of Tokyo Dental College, 42, 151-157, 2001

Yakushiji, T.*, Noma, H.*, Shibahara, T.*, Arai, K.*, Yamamoto, S., Tanaka, C.*, Uzawa, K.*, Tanzawa, H.*: Analysis of a role for p16/CDKN2 expression and methylation patterns in Human Oral squamous cell carcinoma., Bulletin of Tokyo Dental College, 42, 159-168, 2001

Yamamoto, S., Noma, H.*, Shibahara, T.*: Allelic imbalance on the long arm of chromosome 21 in human oral squamous cell carcinoma: Relationship between allelic imbalances (LOH and MSI) and clinicopathologic features., Bulletin of Tokyo Dental College, 42, 211-223, 2001

Nakagawa, H., Ooshima, Y., Takusagawa, M., Ikota, N., Takahashi, Y.*, Shimizu, S.*, Ozawa, T.: Functional Modification of Cytochrome c by Peroxynitrite in an Electron Transfer Reaction.,Chemical & Pharmaceutical Bulletin, 49, 1547-1554, 2001

Itani, Y.*, Watanabe, S.*, Masuda, Y.*, Hanamura, K.*, Asakura, K.*, Sone, S.*, Sunami, Y.*, Miyamoto, T.: Measurement of aortic diameters and detection of asymptomatic aortic aneurysms in a mass screening program using a mobile helical computed tomography unit, Heart and Vessels, 16, 42-45, 2002

Iseki, Y.*, Futami, Y., Tomitani, T., Koda, S.*, Nishio, Y., Kanai, T., Kanazawa, M., Kitagawa, A., Mizuno, H.*, Murakami, T., Shinbo, M.*, Suda, M., Urakabe, E.: Numerical Simulation Design Study of a Positron Camera for Heavy-Ion Radiotherapy, IEEE Transactions on Nuclear Science, Vol. 48 No. 4, 1550-1559, 2001

Iwadate, Y.*, Mizoe, J., Osaka, Y.*, Yamaura, A.*, Tsujii, H.: High Linear Energy Transfer Carbon Radiation Effectively Kills Cultured Glioma Cells with Either Mutant or Wild-type p53, International Journal of Radiation Oncology Biology Physics, 50, 803-808, 2001

Oono, T., Nakano, T.*, Abe, A.*, Sano, T.*, Niibe, Y.*, Oka, K.*: Mucinous adenocarcinoma of Bartholin gland treated with radiation therapy. Acase report., Japanese Journal of Clinical Oncology, 31, 226-230, 2001

Imai, R., Hayakawa, K.*, Sakurai, H.*, Nakayama, Y.*, Mitsuhashi, N.*, Niibe, H.*: Small Cell Lung Cancer with a Brain Metastasis Controlled for 5Years: a case Report, Japanese Journal of Clinical Oncology, 31(3), 116-118, 2001

Imai, R., Ito, K.*, Ishigami, N.*, Oba, N.*, Nakajima, N.*: Occlusion of the Left Superficial Femoral Artery During Hepatic Arterial Infusion of Chemotherapy for Liver Metastases from Colon Cancer 18 Months After the Implantation of a Port System:a Case Report, Japanese Journal of Clinical Oncology, 32(2), 68-70, 2002

Nagatsuka, S., Fukushi, K., Shinotoh, H., Namba, H., Iyo, M.*, Tanaka, N.*, Aotsuka, A.*, Ota, T.*, Tanada, S., Irie, T.: A kinetic analysisi of [11C] MP4A using high-radioactive region which represents an integrated function for measurment of cerebral acetylcholinesterase activity without arterial blood sampling., Journal of Cerebral Blood Flow and Metabolism, 21, 1354-1366, 2001

Tanaka, N.*, Fukushi, K., Shinotoh, H., Nagatsuka, S.*, Namba, H., Iyo, M.*, Aotsuka, A.*, Ota, T.*, Tanada, S., Irie, T.: Positron Emission Tomographic Measurement of Brain Acetylcholinesterase Activity Using N-[11C] methylpiperidin-4-yl Acetate Without Arterial blood Sampling: Methodology of Shape Analysis and its Diagnostic Power for Alzheimer s Disease, Journal of Cerebral Blood Flow and Metabolism, 21, 295-306, 2001

Oono, T., Nakayama, Y.*, Kurihara, T.*, Ichikawa, H.*, Tsuda, K.*, Ishida, T.*, Hirato, J.*, Suzuki, Y.*: Endobronchial metastasis of breast cancer 5years after breast conserving therapy, Journal of Clinical Oncology, 6, 101-104, 2001

Oya, N.*, Sasai, K.*, Shibata, T.*, Takagi, T.*, Shibuya, K.*, Koike, S., Nojima, K., Furusawa, Y., Ando, K., Hiraoka, M.*: Time course of reoxygenation in experimental murine tumors after carbon-beam and x-ray irradiation, Journal of Radiation Research, 42, 131-141, 2001

Inoue, M.*, Suhara, T., Sudo, Y.*, Okubo, Y.*, Yasuno, F.*, Kishimoto, R., Yoshikawa, K., Tanada, S.,: Age related reduction of extrastriatal dopamine D2 receptor measured by PET., Life Sciences, 69, 1079-1084, 2001

Girard, F.*, Suhara, T., Sassa, T.*, Okubo, Y.*, Obata, T., Ikehira, H., Sudo, Y.*, Koga, M.*, Yoshioka, H.*, Yoshida, K.: 7Li 2D CSI of human brain on a clinical scanner., MAGMA, 13, 1079-1084, 2001

Endo, M., Tsunoo, T., Kandatsu, S., Tanada, S., Aradate, H.*, Saito, Y.*, Nakamori, N.*, Yoshida, K.*: Effect of scattered radiation on image noise in cone beam CT, Medical Physics, 28(4), 469-474, 2001

Suhara, T., Yasuno, F.*, Sudo, Y.*, Yamamoto, M.*, Inoue, M.*, Okubo, Y.*, Suzuki, K.: Dopamine D2 receptor in insular cortex and personality trait of novelty seeking, NeuroImage, 13, 891-895, 2001

Yasuno, F.*, Suhara, T., Sudo, Y.*, Yamamoto, M.*, Inoue, M.*, Okubo, Y.*, Suzuki, K.: Relation among dopamine D2 receptor binding,obesity and personality., Neuroscience Letters, 300, 59-61, 2001

Sudo, Y.*, Suhara, T., Inoue, M.*, Ito, H.*, Suzuki, K., Saijo, T.*, Halldin, C.*, Farde, L.*, Tanada, S.: Reproducibility of [¹¹C]FLB 457 binding in extrastriatal regions., Nuclear Medicine Communications, 22, 1215-1221, 2001

Saijo, T.*, Abe, T.*, Someya, Y.*, Sassa, T.*, Sudo, Y.*, Suhara, T., Shuno, T.*, Asai, K.*, Okubo, Y.*: 10-year progressive brain structural change in schizophrenia: an MRI morphorogicalstudy, Psychiatry and clinical neurosciencis, 55, 41-47, 2001

Yasuno, F.*, Suhara, T., Okubo, Y.*, Sudo, Y.*, Inoue, M.*, Ichimiya, T.*, Tanada, S.: Dose reration of limbic-cortical D2-dopamine receptor occupancy with risperidone., Synapse, 154, 112-114, 2001

Dept. of Accelerator Physics and Engineering

Honma, T., Ogawa, H. Y., Sano, Y., Noda, K., Takada, E., Yamada, S.: Ionization beam-profile monitor at HIMAC; Nucl. Instru. Meth. **A459**(2001)390-397.

Takada, E. and Kondo, T.: Synchrotron control system of HIMAC; Nucl.Instrum Meth, in press.

Tanabe, T., Chiba, K., Noda, K. and Watanabe, I.: An Electrostatic Storage Ring for Atomic and Molecular Science; Nucl. Instru. Meth. **A482**(2002)595-605

Wang, J., Galonsky, A., Kruse, J. J., Tryggestad, E., White-Stevens, R. H., Zecher, P. D., Iwata, Y., Ieki, K., Horvath, A., Deak, F., Kiss, A., Seres, Z., Warner,

R. E. and Schelin, H.: Dissociation of 6He: Phys. Rev. C in press.

Horvath, A., Weiner, J., Galonsky, A., Deak, F., Higurashi, Y., Ieki, K., Iwata, Y., Kiss, A., Kolara, J. J., Seres, Z., von Schwartzenberg, J., Schelin, H., Takeuchi, S., Typel, S., and Warner, R. E.: Cross section for the astrophysical $^{14}C(n,\gamma)^{15}C$ reaction via the inverse reaction Astro. Phys. J in press.

Kruse, J. J., Galonsky, A., Snow, C., Tryggestad, E., Wang, J., Ieki, K., Iwata, Y. and Zecher, P. D.: Fragment detection system for studies of exotic,neutron-rich nucleei: Nucl. Instr. and Meth, A, (2001) in press.

Iwata, Y., Murakami, T., Sato, H., Iwase, H., Nakamura, T., Kurosawa, T., Heibronn, L., Ronningen, R. M., Ieki, K., Tozawa, Y. and Niita, K.: Double-differential cross sections for the neutron production from heavy-ion reactions at energies E/A=290-600 MeV: Phys. Rev. C **64**, 054609(2001).

Takeuchi, S., Shimoura, S., Motobayashi, T., Akiyoshi, H., Ando, Y., Aoi, N., Fulop, Zs., Gomi, T., Higurashi, Y., Hirai, M., Iwasa, N., Iwasaki, H., Iwata, Y., Kobayashi, H., Kurokawa, M., Liu, Z., Minemura, T., Ozawa, S., Sakurai, H., Serata, M., Teranishi, T., Yamada, K., Yanagisawa, Y. and Ishihara, M.: Isobaric analog state of 14Be: phys. Lett. B **515**,255(2001)

Zeitlin, B., Fukumura, A., Heilbronn, L., Iwata, Y., Miller, J. and Murakami, T.: Fragmentation cross section of 600 MeV/Nucleon 20Ne on elemental targets: Phys. Rev. C **64**, 024902(2001)

Kitagawa, A., Muramatsu, M., Sasaki, M., Yamada, S., Biri, S., Jincho, K., Okada, T., Sakuma, T., Takasugi, W. and Yamamoto, M.: Study of the Extracted Beam and the Radial Mgnetic Field of ECR ion source at HIMAC; Rev. Sci. Instrum., **73**, 604(2002).

Sasaki, M., Kitagawa, A., Muramatsu, M., Jincho, K., Sasaki, N., Sakuma, T., Takasugi, W. and Yamamoto, M.: Metallic Ion Beam Production at HIMAC; Rev. Sci. Instrum., **73**, 545(2002).

Sato, Y., Miyata, T., Miyoshi, T., Kitagawa, A., Muramatsu, M., Murakami, T., Honma, T., Yamamoto, M., Ogawa, H. and Yamada, S.: Effects of Ion-Pumping in a Pulsed Penning Source; Rev. Sci. Instrum., **73**, 720(2002).

Muramatsu, M., kitagawa, A., Sato, Y., Yamada, S., Hattori, T., Hanagasaki, M., Fukushima, T. and Ogawa, H.: Development of an ECR ion source for carbon therapy; Rev. Sci. Instrum., **73**, 573(2002).

Kumada, M., Fujisawa, T., Hirano, Y., Iwashita, Y., Endo, M., Aoki, M., Kohda, T., Bolshakova, I. and Holyaka, R.: Development of high field permanent magnets: IEEE Trans. Magnet, in press.

Torikoshi, M., Tsunoo, T., Endo, M., Noda, K., Kumada, M., Yamada, S., Soga, F., Hyodo, K.: Design of synchroeron light source and its beamline dedicated to dual-energy X-ray computed tomography, J. Biomed. Opt., **6**, 371-377, 2001.

Dept. of Medical Physics

Endo, M., Tsunoo, T., Nakamori, N.*, Yoshida, K.*: Effect of scattered radiation on image noise in cone beam CT, *Medical Physics*, 28(4), 469-474, 2001

Sasaki, M.*, Nakao, N.*, Nunomiya, T.*, Fukumura, A., Nakamura, T., Shibata, T.*: Development of self-TOF neutron detector and its application to concrete and iron shielding experiments, *Nuclear Instruments and Methods in Physics Research Section A*, 476, 327-331, 2002

Sasaki, M.*, Kim, E.*, Nunomiya, T.*, Nakamura, T., Nakao, N.*, Shibata, T.*, Uwamino, Y.*, Ito, S.*, Fukumura, A.: Measurements of high-energy neutrons penetrated through concrete shields using self-TOF, NE213 and activation detectors, *Nuclear Science and Engineering*, 141, 140-153,2002

Nishizawa, K., Uruma, T.*, Takiguchi, Y.*, Kuriyama, T.*, Yanagawa, N.*, Matsumoto, M., Iwai, K.*: Dose evaluation and effective dose estimation from CT fluoroscopy-guided lung biopsy, *Jpn J Med Phys*, 21, 215-226, 2001

Sasaki, M.*, Nakao, N.*, Nunomiya, T.*, Nakamura, T., Shibata, T.*, Fukumura, A.: Response function measurements of the self-TOF neutron detector for neutrons up to 800 MeV, *Journal of Nuclear Science and Technology*, 38, 8-14, 2001

Hasegawa, T., Michel, C.*, Murayama, H., Yamaya, T., Matsuura, H.*, Tanada, S.: Monte Carlo simulation for PET scanners and shields, *Jpn J Med Phys*, 21(3), 174-186, 2001

Iseki, Y.*, Futami, Y., Tomitani, T., Koda, S.*, Nishio, Y., Kanai, T., Kanazawa, M., Kitagawa, A., Mizuno, H.*, Murakami, T., Shinbo, M.*, Suda, M., Urakabe, E.: Numerical simulation design study of a positron camera for heavy-ion radiotherapy, *IEEE Transactions*

on Nuclear Science, 48 (4), 1550-1559, 2001

Zeitlin, C.*, Fukumura, A., Heilbronn, L.*, Iwata, Y., Miller, J.*, Murakami, T.: Fragmentation cross sections of 600 MeV/nucleon Ne-20 on elemental target, *Physical Review*, C64, 024902, 2001

Hayakawa, H.*, Kobayashi, N.*, Kuroyanagi, K.*, Nishizawa, K.: Technical Report: Pediatric absorbed doses from rotational panoramic radiography, *Dentomaxillofacial Radiology*, 30, 285-292, 2001

Haneishi, H.*, Yamada, A.*, Takagi, K.*, Murayama, H.: Monte Carlo simulation for depth endocing multicrystal detector for PET, *2001 IEEE Med Imag Conf Record*, M13A-15, 2001

Hasegawa, T., Tanaka, E., Yamashita, T.*, Watanabe, M.*, Yamaya, T., Murayama, H.: A Monte-Carlo simulation study on coarse septa for scatter correction in 3D PET, *2001 IEEE Med Imag Conf Record*, M13B-22, 2001

Inadama, N.*, Murayama, H., Omura, T.*, Yamashita, T.*, Yamamoto, S.*, Ishibashi, H.*, Kawai, H.*, Omi, K.*, Umehara, T.*, Kasahara, T.*: A depth of interaction detector for PET with DSO crystals doped with different amount of Ce, *2001 IEEE Med Imag Conf Record*, M2-3, 2001

Kitamura, K.*, Amano, M.*, Murayama, H.: Count rate analysis of PET scanner designs based on a GSO depth of interaction detector with a large area PS-PMT, *2001 IEEE Med Imag Conf Record*, M5A-7, 2001

Yamamoto, S.*, Murayama, H.: Development of a LGSO detector using a tapered fiber for a high-resolution animal PET, *2001 IEEE Med Imag Conf Record*, M9A-21, 2001

Nakamura, A., Takahashi, H.*, Zhang, L.*, Fukuda, D.*, Nakazawa, M.*, Misawa, M.*, Murayama, H.: Clustering algorithm with adaptive shaping method for CdZnTe detectors, *Proc IEEE 12th Int Workshop Room-temperature semiconductor X-and Gamma-ray Detectors*, R9-2, 2001

Hasegawa, T., Murayama, H., Matsuura, H.*, Yamaya, T.: A phantom and simulation study on body-shields to cope with radioactivity outside the field of view in 3D PET, *2001 IEEE Med Imag Conf Record*, M5A-22, 2001

Endo, M., Tsunoo, T., Kandatsu, S., Tanada, S., Aradate,

H.*, Saito, Y.*: 4-dimensional computed tomography-Its concepts and preliminary development, *2001 IEEE Med Imag Conf Record*, M7-6, 2001

Fukumura, A., Hiraoka, T., Noda, Y., Tomitani, T., Takeshita, M., Kanai, T., Murakami, T., Minohara, S., Matsufuji, N., Futami, Y.*, Kohno, T.*, Nakamura, T.*: Measurements of charge-changing cross sections for therapeutic ion beams, *American Institute of Physics Conference Proceedings*, 610, 281-284, 2002

Endo, M., Tsunoo, T., Kandatsu, S., Tanada, S., Aradate, H.*, Saito, Y.*: 4-dimensional computed tomography (4D CT) - Its concepts and design, *Proceedings of CARS2001*, 1098-1098, 2001

Endo, M., Tsunoo, T., Sato, K.*, Kusakabe, M.*, Fukuda, Y.*: Performance of cone beam CT using a flat-panel imager, *Proceedings of SPIE*, 4320, 815-821, 2001

Dept. of Medical Imaging

Haradahira, T., Zhang, M.-R., Maeda, J., Okauchi, T., Kida, T., Kawabe, K., Sasaki, S., Suhara, T., Suzuki K.: A prodrug of NMDA/Glycine Site Antagonist, L-703, 717, with Improved BBB Permeability: 4-Acetoxy Derivative And Its Positron-Emitter Labeled Analog. Chem. Pharm. Bull., 49(2), 147-150, 2001 (IF*HL=1.177*10.0=11.8)

Sasaki, S., Kanda, T., Ishibasi, N., Yamamoto, F., Haradahira, T., Okauchi, T., Maeda, J., Suzuki, K., Maeda, M.: 4, 5, 9, 10-Tetrhydro-1, 4-ethanobenz[b] quinolizine as a Prodrug for Its Quininolizinium Cation as a Ligand to the Open state of the TCP-Binding Site of NMDA Receptors. Bioorg. Med. Chem. Lett., 11, 519-521, 2001(IF*HL = 1.927*3.2 = 6.2)

Takei, M., Kida, T., Suzuki, K.: Sensitive measurement of positron emitters eluted from HPLC. Appl. Radiat. Isot., 55, 229-234, 2001(IF*HL = 0.716*5.3 = 3.8)

Noguchi, J., Suzuki, K.: Imaging Plate Characteristics of positron emitters:[11]C, ^{13}N, [15]0,[18]F and [38]K. Radiochim. Acta., 89,433-437,2001 (IF*HL = 0.775*6.6 = 5.2)

Hosoi, R., Kobayashi, K., Itoh, T., Gee, A., Suzuki, K., Inoue, O.: Different sensitivities to competitive inhibition of benzodiazepine receptor binding of ^{11}C-iomazenil and [11]C- flumazenil in rhesus monkey brain. Ann.Nucl. Med., 15(2), 137-139, 2001

Zhang, M.-R., Tuchiyma, A., Haradahira, T., Furutsuka, K., Yoshida, Y., Kida, T., Noguchi, J., Irie, T., Suzuki,

K.: Synthesis and Prelminary evaluation of [^{18}F] FEtP4A, a Promising PET tracer for mapping acetylcholinesterase in vivo. Nucl. Med. Biol.,29,463-468.2002(IF*HL = 1.58*4.8 = 7.54)

Szelecsenyi, F., Suzuki, K., Kovacs, Z., Takei, M., Okada, K.: Production possibility of 60, 61,62Cu radioisotopes by alpha induced reactions on cobalt for PET studies. Nucl. Instr. and Meth. B., 187,153-163,2002 (IF*HL = 0.955*5.6 = 5.4)

Szelecsenyi, F., Suzuki, K., Kovacs, Z., Takei, M., Okada, K.: Alpha beam monitoring via^{nat} Cu+alpha processes in the energy range from 40 to 60 Mev. Nucl. Instr.and Meth. B. 184, 589-596, 2001 (IF*HL = 0.955*5.6 = 5.4)

Haradahira, T., Okauchi, T., Maeda, J., Zhang, M.-R., Kida, T., Kawabe, K., Mishina, M., Watanabe, Y., Suzuki, K., Suhara, T.: A Positron-Emitter Labeled Glycine Site Antagonist, [^{11}C]L-703, 717, Preferentially Binds to a Cerebellar NMDA Receptor Subtype Consisting of GluR ε 3 Subunit In Vivo, But Not In Vitro. Synapse, 43,131- 133,2002 (IF*HL = 3.402*5.4 = 18.4)

Shinotoh, H., Aotsuka, A., Fukushi, K., Nagatsuka, S., Tanaka, N., Ota, T., Tanada, S. and Irie, T.: Effect of donepezil on brain acetylcholinesterase activity in patients with AD measured by PET. Neurology, 56, p408-410(2001) (IF*HL4.781*6.6 = 31.6)

Kikuchi, T., Fukushi, K., Ikota, N., Ueda, T., Nagatsuka, S., Arano, Y. and Irie, T.: Synthesis of Piperidinyl and Pyrrolidinyl Butyrates for Potential In Vivo Measurement of Cerebral Butyrylcholinesterase Activity. J. Labelled Cpd. Radiopharm. 44, p31-41(2001) (IF*HL0.756*5.8 = 4.4)

Tanaka, N., Fukushi, K., Shinotoh, H., Nagatsuka, S., Namba, H., Iyo, M., Aotsuka, A., Ota, T. Tanada, S. and Irie, T.: Positron Emission Tomographic Measurement of Brain Acetylcholinesterase Activity Using N-[^{11}C] methylpiperidin-4-yl Acetate Without Arterial Blood Sampling: Methodology of Shape Analysis and its Diagnostic Power for Alzeimer's Disease. Journal of Cerebral Blood Flow and Metabolism. 21, p295-306(2001) (IF*HL5.926*6.1 = 36.2)

Shinotoh, H., Namba, H., Yamaguchi, M., Fukushi, K., Nagatsuka, S., Iyo, M., Asahina, M., Hattori, T., Tanada, S. and Irie, T.: In Vivo Mapping of Brain Cholinergic Function in Parkinson's Disease and Progressive Supranuclear Palsy. Advances in Neurology. 86, p249-255(2001) (IF*HL0.968*8.8 = 8.6)

Nagatsuka, S., Fukushi, K., Shinotoh, H., Namba, H., Iyo, M. Tanaka, N. Aotsuka, A., Ota, T., Tanada, S. and Irie, T.: Kinetic Analysis of [^{11}C]MP4A Using a High- Radioactivity Brain Region That Represents an Integrated Input Function for Measurement of Cerebral Acetylcholinesterase Activity Without Arterial Blood Sampling. Journal of Cerebral Blood Flow and Metabolism. 21, p1354-1366(2001) (IF*HL5.926*6.1 = 36.2)

Yokoyama, A., Morimoto, S., Araki, H., Sanada, J., Baba, H., Shinohara, A., Shibata, S., Saito, T. and Ohkubo, Y.: Radiochemical study on the mechanism of target fragmentation of Cu, Nb, Pr and Au targets induced by ^{12}C and ^{40}Ar projectiles. Radiochim. Acta. 89, p703-706 2001) (IF*HL0.775*6.6 = 5.2)

Tomitani, T. and Hirasawa, M. Image reconstruction from limited angle Compton camera data. Phys. Med. Biol. 47, p2129-2145(2002) (IF*HL2.013*6.0 = 12.1)

Girard, F., Suhara, T., Sassa, T., Okubo, Y., Obata, T., Ikehira, H. Sudo, Y. Koga, M., Yoshioka, H. and Yoshida, K.: ^{7}Li 2D CSI of human brain on a clinical scanner. Magnetic Resonance Materials in Physics, Biology and Medicine, 13, p1-7(2001)

Sunaga, T., Ikehira, H., Furukawa, S., Shinkai, H., Kobayashi, H., Matsumoto, Y., Yoshitome, E., Obata, T., Tanada, S., Murata, H. and Sasaki, Y.: Measurement of the electrical properties of human skin and the variation among subjects with certain skin conditions. Phys. Med. Biol. 47, pN11-N15 (2002).(IF*HL2.013*6.0 = 12.1)

Takanashi, J., Inoue, K., Tomita, M., Kurihara, A., Morita, F., Ikehira, H., Tanada, S., Yoshitome, E. and Kohno, Y.: Brain N- acetylaspartate is elevated in Pelizaeus-Merzbacher disease with PLP1 duplication. Neurology. 58, p237-241(2002)(IF*HL4.781*6.6 = 31.6)

Ikehira, H., Obata, T. and Tanada, S.: Long-term assessment of posttansplant renal prognosis with 31P magnetic resonance spectroscopy. Transplantation. 72(4), p627-630(2001) (IF*4.035*5.3 = 21.4)

Heavy-Ion Radiobiology Research Group
Kawata, T., Durante, M., Furusawa, Y., George, K., Takai, N., Honglu, Wu., Cucinotta, F. A.: Dose-response of initial G2-chromatid breaks induced in normal human fibroblasts by heavy ions. *Int J Radiat*

Biol **77**, 165-174, 2001.2.

George, K., Honglu, Wu., Willingham, V., Furusawa, Y., Kawata, T., Cucinotta, F. A.: High- and low-LET induced chromosome damage in human lymphocytes: a time-course of aberrations in metaphase and interphase. *Int J Radiat Biol* **77**, 175-183, 2001.2.

Ando, K., Furusawa, Y., Suzuki, M., Nojima, K., Majima, H., Koike, S., Aoki, M., Shimizu, W., Futami, Y., Ogino, T., Murayama, S., Ikeda, H.: Relative biological effectiveness of the 235 MeV proton beams at the National Cancer Center Hospital East. *J Radiat Res* **42**, 79-89. 2001.3.

Shigematsu, N., Ihara, N., Kawata, T., Kawaguchi, O., Tekeda, A., Ishibashi, R., Kutsuki, S., Kubo, A., Kanai T., Furusawa Y., Isobe K., Uno T., Ito, H.: Cell killing and mutation induction by heavy ion beams. *Int J Mol Med* **7**, 509-513. 2001.5.

Oya, N., Sasai, K., Shibamoto, T., Takagi, T., Shibuya, K., Koike, S., Nojima, K., Furusawa, Y., Ando, K., Hiraoka, M.: Time Course of Reoxygenation in Experimental Murine Tumors after Carbon-beam and X-ray Irradiation. *J Radiat Res* **42**, 131-141. 2001.6.

Kawata, T., Durante, M., Furusawa, Y., George, K., Ito, H., Honglu, Wu., Cucinotta, F. A.: G2-Chromosome Aberarions Induced by High-LET Radiations. *Adv Space Res* **27**, 383-391. 2001.6.

Nose, M., Uzawa, A., Ogyu, T., Suzuki, G: OK-432 reduces mortality and bacterial translocation in irradiated and granulocyte-colony stimulating factor (G-CSF) - treated mice. *J Radiat Res* **42**, 191-200. 2001.6.

Chunlin, Shao., Aoki, M., Furusawa, Y.: Medium-mediated Bystander Effects on HSG Cells Co-cultivated with Cells Irradiated by X-rays or a 290 MeV/u Carbon Beam. *J Radiat Res* **42**, 305-316. 2001.9.

Takahashi, A., Ohnishi, K., Ota, I., Asakawa, I., Tamamoto, T., Furusawa, Y., Matsumoto, H., Ohnishi, T.: p53-dependent Thermal Enhancement of Cellular Sensitivity against Different LET Radiation in Human Squamous Cell Carcinomas. *Int J Radiat Biol* **77**, 1043-1051. 2001.10.

Kawata, T., Durante, M., Furusawa, Y., George, K., Ito, H., Honglu, Wu., Cucinotta, F. A.: Rejoining of isochromatid breaks induced by heavy ions in G2-phase normal human fibroblasts. *Radiat Res* **156**, 598-602. 2001.11.

Special Research on Bio-Emission

Yamamoto, M.: -Towards the Creation of New-Paradigm- What is 'Science and Technology Involved In Mind and Sprit'? Report of The Trans-disciplinary Forum, - Towards the Creation of New-Paradigm- Science and Technology Involved In Mind and Sprit, 11-19, Hayama, 2001.

Yamamoto, M.: Human Potential in Physics and Physiology. Report of The Trans-disciplinary Forum, - Towards the Creation of New-Paradigm- Science and Technology Involved In Mind and Sprit, 109-120, Hayama, 2001.

Yoichi, H., Kokubo, H., Yamamoto, M.: Development of a Measuring System for nT-order Magnetic Fields and Electrostatic Fields Generated Near a Human Body. J Int Soc Life Info Sci., 19:329-338, 2001.

Haraguchi, S., Kotake, J., Chen, W., Parkhomtchouk, D., Zhang, T., Yamamoto, M.: Biophoton Change by Mental Concentration. J Int Soc Life Info Sci, 19:373-380, 2001.

Kokubo, H.: A Consideration on Research for Anomalous Phenomena with Devices for Photon Detection-Studies in Japan and China-. J Int Soc Life Info Sci, 19:389-396, 2001.

Yamamoto, M., Kokubo, H., Kokado, T., Haraguchi, S., Zhang, T., Tanaka, M., Parkhomtchouk, D., Soma, T.[*1], Kawano, K.[*2]: An Experiment on Remote Action against Man in Sense Shielding Condition (Part 3). J Int Soc Life Info Sci, 19:437-452, 2001. ([*1]Tokyo Metropolitan College, [*2]Nippon Med sch.)

Kawano, K.[*1], Yamamoto, M., Kokubo, H., Tanaka, M., Zhang, T., Kokado, T., Soma, T.[*2]: EEG α waves of a Receiver in a Remote Action Experiment-Part 2. J Int Soc Life Info Sci, 19:453-457, 2001. ([*1]Nippon Med Sch., [*2]Tokyo Metropolitan College)

Zhang, T., Yamamoto, M., Kokubo, H., Kawano, K.,[*1] Tanaka, M., Kokado, T.: Analysis of the Receiver's EEG in Remote Perception Task. J Int Soc Life Info Sci, 19:458-465, 2001. ([*1]Nippon Med sch.)

Tanaka, M., Yamamoto, M., Kokubo, H., Kokado, T., Zhang, T., Parkhomtchouk, D., Kawano, K.[*1], Soma T[*2]: ECG Analysis in a Remote Action Experiment. J Int Soc Life Info Sci, 19:466-472, 2001. ([*1]Nippon Med Sch., [*2]Tokyo Metropolitan College)

Chen, W., Kokubo, H., Kokado, T., Zhang, T., Kawano, K.[*1], Yamamoto M: Skin Temperature Changes of Rwciber'sLaogong on the Left Hand. J Int Soc Life Info Sci, 19:473-479, 2001.

Kokubo, H., Yamamoto, M., Yamada, K.[*1], Kawano, K.[*2], Soma, T.[*3], Tanaka, M., Zhang, T., Fukuda, N.: Analysis of Electrodermal Activity (EDA) in Remote Perception Task. J Int Soc Life Info Sci, 19:480-487, 2001. ([*1]Morita Children's Clinic, [*2]Nippon Med Sch., [*3]Tokyo Metropolitan College)

Amemiya, K.[*1], Takahashi, H.[*1], Nakazawa, M.[*1], Nakagawa, Y.[*2], Shimizu, H.[*3], Majima, T.[*4], Nakaichi, T.[*5], Yasuda, N., Yamamoto, M.: Microdosimetry in BNCT using CR-39 and AFM. Extended Abstracts (The 62nd Autumn Meeting, 2001); The Japan Society of Applied Physics, No.1, 64, Aichi, 2001. ([*1]Univ. of Tokyo, [*2]National Kagawa Children's Hosp. [*3]Kagawa Univ., [*4]AIST [*5]Yamaguchi Univ.)

Yamamoto, M.: Status of Pilot Studies in Japan on "Human PotentioalScience". Science and Spiritual Healing III: Bridging Worlds and Filling Gaps", Kona, 2001.

Yamamoto, M., Kokubo, H., Kawano, K.[*1], Tanaka, M., Zhang, T., Chen, W.: DMILS -Are There Any Effects Other Than Suggestion in External Qi or KI? Science and Spiritual Healing III: Bridging Worlds and Filling Gaps", Kona, 2001. ([*1]Nippon Med Sch.)

Kokubo, H., Chen, W., Yamamoto, M., Kawano, K.[*1]: Electrodermal Activity (EDA) and Skin Temperature Changes in Remote Action "Toh-ate". Science and Spiritual Healing III: Bridging Worlds and Filling Gaps", Kona, 2001. ([*1]Nippon Med Sch.)

Kawano, K.[*1], Yamamoto, M., Kokubo, H.: Study of EEG in the Altered State of Consciousness. Science and Spiritual Healing III: Bridging Worlds and Filling Gaps", Kona, 2001. ([*1]Nippon Med Sch.)

Yasuda, N., Yamamoto, M., Skvarc, J Giacomelli, M.[*1], Ilic, R.[*1], Colovchenko, A.[*2], Tretykova, S.[*2], Wanatabe, N.[*3], Amema, K.[*3], Okura, K.[*4]: Measurement of the nuclear fragmentation in the reactions of therapeutic beams with tissue-like materials using CR-39 track detector. Reaction cross sections and detectors applied to the HIMAC beams, 30-34, Chiba, 2001. ([*1]J. Stefan Institute, [*2]Joint Institute for Nuclear Research, [*3]University of Tokyo, [*4]Nihon University)

Kokubo, H., Yoichi, H., Chen, W., Yamamoto, M., Kawano, K.[*1], Fukuda, N.: Receiver's EDA Transition of DMILS in Remote Action Experiments. Tokyo, 2001.12.23. ([*1]Nippon Med Sch.)

Yamamoto, M., Machi, Y., Ito, M.[*1], Kawano, K.[*2], Kido, M.[*3], Sugano, H.[*4], Kokubo, H., Yoichi, H., Liu, C.[*2] : Report on Attendance at the International conference "Bridging Worlds and Filling Gaps in the Science of Spiritual Healing", Hawaii, Nov.29-Dec.3, 2001. J Int Soc Life Info Sci, 20:61-69, 2002. ([*1]Tokyo Denki University, Kido, M.[*2], Tohoku University, [*3]Touhoku Gakuin University, [*4]MOA Health Science Foundation)

Chen, W., Kokubo, H., Kokado, T., Shang, T., Haraguchi, S., Kawano, K.[*1], Soma, T.[*2]: Skin Temperature Changes of Receiver's Laogong on the Left Hand in Remote Action Experiment （II）. J Int Soc Life Info Sci, 20:70-77, 2002. ([*1]Nippon Med Sch., [*2]Tokyo Metropolitan College)

Tanaka, M., Yamamoto, M., Kokubo, H., Kokado, T., Zhang, T., Parkhomtchouk, D., Chen, W., Haraguchi, S., Kawano, K.[*1], Soma, T.[*2]: EEG Analysis in Remote Action Experiment （II）. J Int Soc Life Info Sci, 20: 78-84, 2002.
([*1]Nippon Med Sch., [*2]Tokyo Metropolitan College)

Kawano, K.[*1], Yamamoto, M., Kokubo, H., Tanaka, M., Chen, W., Zhang, T., Kokado, T.: Chronological Change in EEGs of a Child while Concentrating on Tasks. J Int Soc Life Info Sci, 20: 85-90, 2002. ([*1]Nippon Med Sch.)

Kotake, J., Haraguchi, S., Parkhomtchouk, D., Yamamoto, M.: Change of Biophoton Emission By Mental Concentration Part -Trial of Detection of Healing Effect by Biophoton Change. J Int Soc Life Info Sci, 20: 132-147, 2002.

Parkhomtchouk, D., Kotake, J., Chen, W., Shang, T., Kokubo, H., Yamamoto, M.: An Attempt to Reproduce the Presentiment EDA Response. J Int Soc Life Info Sci, 20: 190-194, 2002.

Yoichi, H., Kokubo, H., Haraguchi, S., Yamamoto, M.: Anomaly of Random Number Generator Outputs Cumulative Deviation at a Meeting and New Year's Holiday -. J Int Soc Life Info Sci, 20: 195-201, 2002.

Frontier Research Center
Ban, S., Shinohara, T., Hirai, Y., Moritaku, Y., Cologne, JB., MacPhee, DG.: Chromosomal instability in BRCA1- or BRCA2-defective human cancer cells detected by pontaneous micronucleus assay. *Mutation Research*, **474**, 15-23, 2001

Bonassi, S., Fenech, M., Lando, C., Lin, Y-P., Ceppi, M., Chang, WP., Holland, N., Kirsh-Volders, M., Zeiger, E., Ban, S., et al.: Human MicroNucleus Project: International database comparison for results with the cytokinesis-block micronucleus assay in human lymphocytes. I: Effect of laboratory protocol, scoring criteria, and host factors on the frequency of micronuclei., *Environmental and Molecular Mutagenesis*, **37**, 31-45, 2001

Wang, Y., Michikawa, Y., Mallodos, C., Bai, Y., Woodhouse, L., Yarasheki, KE., Miller, CA., Askanas, V., Engel, WK., Bhasin, S., Attardi, G.: Muscle-specific mutations accumulate with aging in critical human mtDNA control sites for replication. *Proc Natl. Acad Sci USA*, **98**, 4022-4027, 2001

Michikawa, Y., Laderman, K., Richter, K. and Attardi, G.: Clonal distribution in vivo and after transfer into mtDNA-less cells of human fibroblast mtDNA carrying the aging-dependent specific T414G mutation revels its replicative advantage. *Nucleic Acid Research*, 2002

Matsui, Y., Tsuchida, Y., Keng, PC.: Effect of p53 mutations on cellular sensitivity to ionizing radiation. *Am J Clin Oncol*, **24**, 486-490, 2001

Matsui, Y., Asano, T., Kenmochi, T., Maruyama, M., Akutsu, N., Itoh, T., Saito, T. and Ochiai, T.: Cytoprotective Effect of Pretreatment of 15-deoxy-yspergualin (DSG) on Hepatic Cells to Prevent from Warm Isc hemic Reperfusion-Injury in Rats. Transplantation Proceedings, 34, 2002. (in press).

Michikawa, Y. and Attardi, G.: Screening for aging dependent mutations on human mitochondrial DNA., *Methods in Molecular Biology*, **197**, 75-92, 2002

List of Keywords

Author index

Organization and Staff

Status of March 31, 2002
Yasuhito Sasaki, M.D., PhD., President
Keiko Yumino, Secretary
Toshihiko Ozawa, PhD., Executive Director
Haruo Suzuki, Executive Director
Masaoki Terashima, Auditor
Takashi Murai, Advisory Auditor

Low Dose Radiation Effects Research Project
  Toshiaki Ogiu, M.D., Ph.D., Director
  Mitsuoki Morimyo Ph.D., Vice-Director*
  Yoshiya Shimada, Ph.D., Vice-Director
  Biological Effects of Neutrons
  Toshiaki Ogiu, M.D., Ph.D., Team Leader*
  Takeshi Hiraoka, Ph.D.
  Yasushi Ohmachi, D.V.M., Ph.D. (Sept. 2001～)
  Yukiko Nakata, Ph.D. (～Nov. 2001) ††
  Tsuyoshi Hamano, Ph.D. (May 2002～) ††
  Shinji Fushiki, M.D., Ph.D.****
  Radiation and Environmental Carcinogenesis
  Yoshiya Shimada, Ph.D., Team Leader*
  Mayumi Nishimura
  Shizuko Kakinuma, Ph.D.****
  Mie Murata, D.V.M., Ph.D.+++++
  Kyoko Ｙasumura, M.S.†††
  Atsushi Inoue, M.D.†††
  Masahiko Hatano, M.D., Ph.D.***
  Genetic Effects on Radiation Carcinogenesis
  Hideo Tsuji, Ph.D., Team Leader
  Hiroko Ishii, Ph.D.
  Takanori Katsube, Ph.D.
  Hideki Ukai, Ph.D.††
  Hereditary Effects of Radiation
  Masatake Yamauchi, Ph.D., Team Leader*
  Tomoyasu Higashi, M.S.
  Etsuko Hongo
  Satsuki Tsuji

---

*Dual Capacity
**Honorary Scientist
***Visiting Cooperative Researcher
****Visiting Researcher
†Visiting Technical Staff
††Post Doctorial Fellow
†††Post Graduate Fellow
††††Trainee
+Graduate Student of Cooperation Program
++Senior Consultant
+++Cooperative Researcher
++++HIMAC Machine Time Coordinator
+++++Staff Technologist of Priority

Wu Jian Yu, M.S.***
Mitsuoki Morimyo, Ph.D.*
Radiation Effects on Germ Cells
  Tadahiro Shiomi, Ph.D., Team Leader
  Masahiko Takahagi, Ph.D.
  Naoko Shiomi†

Nakaminoto Laboratory for Marine Radioecology
  Masashi Kusakabe, PhD.,Director
  Management Section
  Naokata Suzuki,Head and 7staffs

International Space Radiation Laboratory
  Kazunobu Fujitaka, Ph.D., Director
  Masahide Furukawa, Ph.D.*
  Masahiro Doi, Ph.D.*
  Etsuko Ito+++
  Satomi Onuma
  Radiation measurements in space
  Hiroshi Yamaguchi, Ph.D., Team leader
  Masashi Takada, Ph.D.
  Yukio Uchihori, Ph.D.
  Tatsumi Koi, Ph.D.+++
  Nakahiro Yasuda, Ph.D.+++
  Hisashi Kitamura, M.S.+++
  Takashi Nakamura, Ph.D.+
  Toshisuke Kashiwagi, Ph.D.+
  Mieko Kurano
  Dairo So
  Kazuko Kaiho
  Radiation protection in space.
  Kazunobu Fujitaka, Ph.D., Team leader*
  Hiroshi Yasuda, Ph.D.
  Susumu Kinpara, Ph.D.
  Cellular and molecular effects in Space
  Kazunobu Fujitaka, Ph.D., Team leader*
  Hideyuki Majima, D.D.S., Ph.D.&
  Kumie Nojima, B.S.
  Masao Suzuki, Ph.D.
  Sizuo Tomita***, &
  Chizuru Tsuruoka***
  Rekiko Bando
  Chikako Kizu

Keiko Sakita
Liu Chihua
Setsuko Kawai
Preventive medicine in space
Satoshi Fukuda, D.V.M., Ph.D.,Team leader
Haruo Iida
Shogo Hasegawa, D.D.S., Ph.D.+++
Takeo Ohnishi, Ph.D.+
Kuniyo Tarumi

Environmental Radiation Protection Research Group
Kenzo Fujimoto, Ph.D., Director
Teruhisa Watabe, M.S. Vice-Director
Radionuclide Behavior around the Living Environment
Kunio Shiraishi, Ph. D., Team Leader
Sarata Kumar Sahoo, Ph. D.
Shinzo Kimura, Ph. D.
Internal Exposure
Yoshikazu Nishimura, D. V. M., Ph. D., Team Leader
Yoshito Watanabe, Ph. D.
Radiation Protection Dosimetry
Nobuhito Ishigure, Ph. D., Team Leader
Takashi Nakano, Ph. D.
Masaki Matsumoto, M.S.
Hiroko Enomoto
Radiation Epidemiology and Risk Assessment
Yasuhiko Yoshimoto, Ph. D., Team Leader
Shinji Yoshinaga, Ph. D.
Radiation Exposure Mitigation
Katsumi Kurotaki, Ph. D., Team Leader
Distribution of Radionuclides in the Ocean
Masatoshi Yamada, Ph. D., Team Leader
Tatsuo Aono, Ph. D.
Mechanism of Accumulation of Radionuclides and Stable Isotopes by Marine Organisms
Toshiaki Ishii, B. S., Team Leader
Motokazu Nakahara, B. S.
Ryoichi Nakamura, B. S.
Taeko Miyazaki, Ph. D.
Mitsue Matsuba
Assessments of Radiological Impacts of Releases of Radioactive Substances into the Marine Environment
Shigeki Hirano, Ph. D., Team Leader
Teruhisa Watabe, M. S.
Setsuko Yokosuka
Guest Research Associate
Masafumi Uchiyama, Ph. D.
Toshiyuki Nakajima, Ph. D.
Masaharu Okano, Ph. D.
Atsuko Shinohara, Ph. D.
Masahito Wada, Ph. D.
Shiro Sakurai, Ph. D.

Izuru Kakuta, Ph. D.
Post Doctoral Fellow
Shino Homma-Takeda, Ph. D.Research Fellow
Hiroyuki Fukuda
Kazutoshi Suzuki
Miki Amaba
Hiromichi Oobu

Environmental and Toxicological Science Research Group
Ysuyuki Muramastu, Ph.D., Director
Environmental Toxicology
Yasuyuki Muramatsu, Ph.D., Head
Hiroshi Sato, Ph.D.
Yoshihisa Kubota, D.V.M.
X.Z.Sun,Ph.D.††
Model Ecosystem Studies
Hiroshi Takeda, Ph.D., Head
Kiriko Miymoto, Ph.D.
Kei Yanagisawa, Ph.D.
Shoichi Fuma, M.S.
Nobuyoshi Ishii, Ph.D††
Methodology Development
Masahiro Doi, Ph.D., Head
Tetsuya Sakashita, Ph.D.
Biogeochemical Research
Yasuyuki Muramatsu*,Ph.D., Head
Shigeo Uchida, Ph.D.
Satoshi Yoshida, Ph.D.
Keiko Tagami, Ph,D.
Tadaaki Ban-nai,M.S.

Radon Research Group
Yuji Yamada, Ph.D. Group Reader
Masahide Furukawa, Ph.D Team Reader.
Shinji Tokonami, Ph.D.
Tetsuo Ishikawa, Ph.D.
Kumiko Fukutsu, B.S.
Takeko Odaka
Hirokazu Ichitsubo, Ph.D.
Weihai Zhuo, Ph.D.
Hidenori Yonehara*, Ph.D.
Akira Koizumi, B.S.
Suminori Akiba, Ph.D.
Quanfu Sun, Ph.D.
Atsuto Ohashi, M.S.
Koji Ishikawa
Masato Sugino, Ph.D.
Masahiro Hosoda

Redox Regulation Research Group
Nobuo Ikota, Ph.D.Director
1st Team
Jun-ichi Ueda, Ph.D.,Team Leader
Keizo Tkeshita, Ph.D.

Megumi Ueno, M.S.,+++++
Kaori Fujii,+++++
Keita Saito+
Kinya Yazaki,†††
Chino Nisizawa,†††
2nd Team
  Kazunori Anzai,Ph.D.Team Leader
  Masako Furuse,
  Hiroshi Ishihara, Ph.D.
  Izumi Tanaka,
  Masaaki Sato, Ph.D.††
  Mandal Badal, Ph.D.#
  Takashi Moritake†††
  Khoroljav Ragchaa, Ph.D†††
3rd Team
  Hiroshi Inano, Ph.D.Team Leader
  Makoto Onoda, Ph.D.
4th Team
  Nobuo Ikota*, Ph.D.Team Leader
  Kiyoko Imai, Ph.D.
  Keiko Suzuki, Ph.D.
  Hidehiko Nakagawa, Ph.D.
  Akira Hanaki, Ph.D.***

Radiation Hazards Research Group
  Isamu Hayata, Ph.D.,Director
1st Team
  Isamu Hayata, Ph.D.Team leader
  Masako Minamihisamatsu, B.S.
  Reiko Kanda, Ph.D.
  Akira Furukawa, Ph.D.
  Wang Chunyan***
  Zhang Wei, B.M.***
2ndTeam
  Shiro Aizawa, Ph.D.Team Leader
  Kazuko Yoshida, Ph.D.
  Kaoru Tanaka, B.S.
  Yoko Hirabayashi, M.D.,Ph.D.***
  Tohru Inoue,M.D.,Ph.D.***
  Keiko Watanabe, B.S.††
  Masanobu Kitagawa, M.D.,Ph.D††
3rdTeam
  Osami Yukawa, Ph.D.,Team Leader
  Masako Nose,B.S.
  Mitsuru Nenoi, Ph.D.
  Wang Bing, Ph.D.
  Tetsuo Nakajima,Ph.D.
  Kazuhiro Daino,M.S.††
  Takeshi Yamada, Ph.D***
  Harumi Ohyama, Ph.D***
  Sachiko Ichimura,Ph.D***
  Hiroko Hama-Inaba, Ph.D***
  Chihiro Azuma,B.S.††††
4thTeam
  Tomohisa Hirobe, Ph.D,Team Leader

Hiromi Itsukaichi
Kiyomi Eguchi-Kasai, Ph.D
Masahiko Mori, Ph.D.
Masahiro Murakami, Ph.D.
Manabu Koike, Ph.D.
Kimihiko Sugaya, Ph.D.
Yasuharu Ninomiya, Ph.D.
Motoi Ohba, Ph.D.***
Haruki Ootaka, B.S.††
Kori Ohno, M.S.

Transcriptome Profiling Research Group
  Kouichi Tatsumi, M.D., Ph.D., Director
  Masumi Abe, Ph.D., Team Leader
  Toshiyuki Saito, Ph.D., Team Leader
  Ikuko Furuno-Fukushi, Ph.D.,
  Yuko Noda,
  Eiko Kubo,
  Ryoko Araki, M.D., Ph.D., ††
  Ryutaro Fukumura, Ph.D.,***
  Hirakazu Takahashi, Ph.D.,***
  Akira Fujimori, M.D., Ph.D.,****
  Masahiro Muto, Ph.D.,**
  Yuko Houki-Fujimori, B.Ph.,†
  Akiko Hayashi, B.S.,†
  Tatsuya Ohhata,#
  Yoko Tsutsumi,Ph.D.,+
  Yuki Miyamoto,†††
  Atushi Hattori,†††
  Takeshi Furuse, Ph.D.,***
  Hiroshi Tanooka, Ph.D.,***
  Takayuki Kurihara, Ph.D.,***
  Yasuko Taguchi, Ph.D.,***
  Yasuyoshi Kanari, Ph.D.,***
  Tamiko Iwasaki, Ph.D.,***
  Ken Morita, M.S.,***
  Naokazu Sasaki, B.S.,***
  Maki Nakahara, M.S.,***
  Charles A. Waldren, Ph.D.,**
  Akiko Ueno, Ph.D.,**
  Diane B. Vannais, B.S.,**

Laboratory Animal Development and Research Group
  Satoru Matsushita, D.V.M.,Ph.D., Director
  Yuji Ishikawa, Ph.D., Team Leader
  Masanori Okamoto, Ph.D.*
  Akihiro Kawano, D.V.M., M.S.*
  Seiji Kito, Ph.D.*
  Hiromi Omoe, D.V.M., Ph.D.*
  Kazuko Aoki, Ph.D.,***

Internal Radiation Effects Research Group
  Yoichi Oghiso, D.V.M., Ph.D., Director
  Yutaka Yamada, D.V.M., Ph.D., Team Leader

The Research center for Radiation Emergency Medicine
Yasuhiro Takeuchi, M.D., Ph.D,Director
Makoto Aakshi, M.D.,Ph.D.,Project Leader
Pathophysiological Study on Tissue Injury due to Acute High dose Irradiation
Toshiyasu Hirama, M.D., Ph.D.,Head
Naoyuki Anzai, M.D., Ph.D.
Misao Hachiya, Ph.D.
Hisayoshi Kondo,M.D.
Saori Kawamura,M.D.
Daisaku Takai,Ph.D.***
Sang-Hee Park,Ph.D.***
Rika Kawaguchi,M.S.***
Yasunari Takada††
Kazumi Harada†††
Manabu Koike, Ph.D.
Yasuharu Ninomiya, Ph.D.
Kaori Ohno, M.S.
Tomoe Yamauchi
Aki Koike
Motoi Ohba, Ph.D.***
Development of Chelating Agents for Internal Contaminations
Satoshi Fukuda,D.V.M.,Ph.D.,Head.
Haruzo Iida
Yan Yueming****
Makoto Akashi,M.D.,Ph.D.
Development Program of a System for dose Assessment and Evaluation in Radiation Emergency
Yutaka Noda,B.S.,Head
Makoto Akashi*,M.D.,Ph.D.
Shinji Sato
Yoshikazu Kumamoto,Ph.D.
Isamu Hayata*,Ph.D.
Masako Minamihisamatsu,B.S.
Reiko Kanda*,Ph.D.
Akira Furukawa*,M.S.
Study for Reduction of Detriment Induced by Ionizing Irradiation
Makoto Akashi*,M.D.,Ph.D.,Head
Yoshiko Kawase,B.S.
Reina Kondo††††
Nobuo Ikota*,Ph.D.
Kazuki Anzai*,Ph.D.
Hiroshi Ishihara*,Ph.D.
Masako Furuse*
Hiroshi Inano* ,Ph.D.
Shiro Aizawa*,Ph.D.
Kazuko Yoshida*,Ph.D.
Kaoru Tanaka*,B.S.
Emergency Response on Accidental Environmental Contamination
Kenzo Fujimoto*,Ph.D.,Head

Hiroshi Takeda*,Ph.D.
Shinzo Kimura*,Ph.D.
Katsumi Kurotaki*,Ph.D.
Masae Yukawa*,Ph.D.
Yoshikazu Nishimura*,D.V.M.,Ph.D.
Nobuhito Ishigure*,Ph.D.
Kiriko Miyamoto*,Ph.D.
Yasuyuki Muramatsu*,Ph.D.
Takashi Nakano*,Ph.D.
Reiko Kanda*,Ph.D.
Sarata Kumar Sahoo*,Ph.D.
Yoshito Watanabe*,Ph.D.
Masaki Matsumoto*,B.S.
Kunio Shiraishi*,Ph.D.

Hospital
Hirohiko Tsujii, M.D.,Director
Section of Clinical Oncology
Shinroku Morita, M.D.,Section Head
1st Room
Tadaaki Miyamoto, M.D.
Hiroshi Kato, M.D.
Shigeru Yamada,M.D.
Naoyoshi Yamamoto, M.D.
3Resident Doctors
2nd Room
Junetsu Mizoe, M.D.
Takeshi Yanagi,M.D.
Hiroshi Tsuji, M.D.
Tatsuya Ohno , M.D.
3Resident Doctors
Clinical Radio-Technology
Kunio Sakashita and 10 Staff Members
Section of Clinical Diagnosis
Susumi Kandatsu, M.D., Section Head
Laboratory Examinations
Hidehumi Ezawa, M.D.
Hiroko Moriya and 3 Staff Members
Imaging Diagnosis
Tadashi Kamada, M.D.
Tkayuki Obata, M.D.
Kyosan Yoshikawa, M.D.
Ryuuichi Yoneyama, M.D.
And 2 Resident Doctors
Section of Nursing
Mitsuko Matsuda, Section Head
Tamiko Satoh
Fusako Kitane
Chiemi Murakami, Noriko Tokuyama
30 Staff Members and 4 Assistants
Pharmacy
Shin Watanabe, Kazuo Seki and Takashi Nakano

Department of Accelerator Physics and Engineering
Fuminori Soga, Ph. D., Director

Cyclotron Operation Section
  Toshihiro Honma, Ph. D., Section Head
  Koji Kono*
  Satoru Hojo
  Yukio Sakamoto
HIMAC Operation Section
  Eiichi Takada, Ph. D., Section Head
  Koji Kono
  Mitsuru Suda
  Masayuki Muramatsu
  Mitsuo Yoshimoto
  Technical Management Section
  Takeshi Murakami, Ph. D., Section Head
  Akinori Sugiura
Low Energy Beam Research Section
  Yukio Sato, Ph. D., Section Head
  Atsushi Kitagawa, Ph. D.
  Valeri Kapin, Ph. D.(JSPS Fellow)
  Takashi Fujisawa, Ph. D.#####
High Energy Beam Research Section
  Satoru Yamada, Ph. D., Section Head
  Masayuki Kumada, Ph. D.
  Mitsutaka Kanazawa, Ph. D.
  Masami Torikoshi, Ph. D
  Koji Noda, Ph. D.
  Yoshiyuki Iwata, Ph. D.(JISTEC Fellow))
  Makoto Sasaki, Ph. D. ††
  Toshiyuki Misu, Ph. D.††
  Takuji Furukawa, M. S.†
  Tetsumi Tanabe, Ph. D.****
  Shinji Shibuya, Ph. D.†††
Medical Physics Research Section
  Tatsuaki Kanai, Ph. D., Section Head
  Shinichi Minohara, Ph. D.
  Naruhiro Matsufuji, Ph. D.
  Kazuyuki Hyodo, Ph. D.****

Department of Medical Physics
  Masahiro Endo, Ph.D., Director
  Mitsue Takeshita, Secretary
  Therapy Biophysics Section
  Tatsuaki Kanai, Ph.D., Section Head
  Akifumi Fukumura, Ph.D.
  Nobuyuki Kanematsu, Ph.D.
  Masaaki Hirai, Ph.D. 1
  Masataka Komori, Ph.D.1
  Eriko Urakabe, Ph.D.1
  Ken Yusa, Ph.D.***
  Haruo Yamashita, Ph.D.***
  Yasuyuki Futami, Ph.D.***
  Teiji Nishio, Ph.D.***
  Takashi Akagi, Ph.D.***
  Munefumi Shinbo, Ph.D.***
  Akio Higashi, Ph.D.***
  Hiroki Otani, Ph.D.††††

Therapy System Section
  Masahiro Endo, Ph.D., Section Head*
  Hiroko Koyama-Ito, Ph.D.
  Nobuyuki Miyahara, Ph.D.
  Takanori Tsnoo, Ph.D. 1
  Akira Ito, Ph.D.****
  Katsuyuki Nishimura, Ph.D.****
  Shigeo Furukawa***
  Yuzuru Nakamura, Ph.D.††††
  Kazumasa Satoh, B.S.††††
  Satoshi Matsusita, M.S.††††
Imaging Physics Section
  Hideo Murayama, Ph.D., Section Head
  Toru Matsumoto, Ph.D.
  Taiga Yamaya, Ph.D. 1
  Tomoyuki Hasegawa, Ph.D.****
  Keishi Kitamura, Ph.D.****
  Takeshi Iinuma, Ph.D.****
  Norimasa Nohara, Ph.D.****
  Eiichi Tanaka, Ph.D.****
  Hideharu Yoshida, M.S.†
  Sigenori Shimizu, M.S.†
  Naoko Inadama, M.S.†
  Hiroyuki Takahashi, Ph.D.***
  Hideaki Haneishi, Ph.D.***
  Hideyuki Kawai, Ph.D.***
  Yoshihisa Akiyama, Ph.D.††††
Medical Exposure Assessment Section
  Kanae Nishizawa, Ph.D.
  Yutaka Ito, Ph.D.
  Takashi Maruyama, Ph.D.
  Kazuo Iwai, Ph.D., D.D.S††††

Department of Medical Imaging
  Shuji Tanada, M.D., Director
  Taiko Joshima, Secretary
  Radiopharmaceutical Chemistry Section
  Kazutoshi Suzuki, Ph.D.,Head
  Terushi Haradahira, Ph.D.
  Kazuyosyi Nemoto
  Masayuki Suzuki
  Ryuji Nakao
  Osamu Inoue, Ph.D.++++
  Ren Iwata, Ph.D.***
  Tomoko Nakanishi, Ph.D.***
  Kiyoshi Matsumura, Ph,D.***
  Toshimitu Fukumura, M.S.†††
  Keitarou Tanoi, M.S.†††
  Keiko Kawahara, Secretary
  Radiotracer and Radiopharmacology Section
  Toshiaki Irie, Ph.D., Head
  Sadao Shibata, B.S.
  Kiyoshi Fukushi, M.S.
  Hitoshi Shinotoh, M.D.****
  Masahiko Hirasawa, M.S.****

Hiromi Omoe, D.V.M., Ph.D. and 6 Staff Members
Kazuaki Ichinohe, B.S.††
Mikio Saito, Ph.D.††
Fumiaki Sato, Ph.D. ***

Office of Planning and Coordination
 Yuji Nakamura, PhD., Director
 Yasuhiro Yukimatsu, Head
 Masahiro Yamauchi, PhD., Planning Manager
 Kazunori Anzai, PhD., Evaluation Manager and 5
 staff.

Office of Public Relation
 Yuji Nakamura*, PhD,. Director and 2 staff.

Department of Management
 Masakazu Murakami, Director
 Personnel and General Affairs Section
 Toshio Tanabe, Head and 12 staff
 Budget and Accounting Section
 Akio Kawamata, Head and 8 staff
 Contract and Property Management Section
 Yukio Sakurai, Head and 9 staff
 Facility Management S4ecytion
 Masakichi Sakai, Head and 8 staff

Department of International Co-operation, Research Exchange and Training
 Yoshiklazu Inoue, Director
 International Co-operation Section
 Yoshikazu Inoue*, head and 2 staff
 Research and Scientific Information Exchange Section
 Yukio Kamakura, Head and 2 staff
 Training School
 Hsamasa Joshima, PhD, Head
 Yoshiyuki Shirakawa, PhD.
 Itsuro Tamanoi, PhD.**
 Kazuo Watari, PhD.** and 2 staff

Audit Office
 Katsutoshi Bito, Head

Department of Radiation Protection and Safety
 Shigeaki Kiuchi, Director
 Radiation Safety Section
 Noriyuki Yoshida, Head and 9 staff
 Emergency Preparedness and Monotoring Office
 Mitsuhiro Kuchigi, Head and 3 staff

 Safety Control Section
 Tsuneo Komaya, Head and 2 staff
 Radiotoxicology Building Operation Office
 Akira Koizumi, Head and 3 staff
 Radiation Safety Technology Developement Sec-

tion
 Noriyoshi Yoshida*, Head